



**UNIVERSITY OF
KWAZULU-NATAL**

**INYUVESI
YAKWAZULU-NATALI**

**The Methyltransferase and Helicase Enzymes as
Therapeutic Targets of Zika Virus: A Bio-
Computational Analysis of Interactions with
Potential Inhibitors**

Miss Nikita Devnarain

2019

A thesis submitted to the School of Health Science, University of Kwa-Zulu Natal, Westville, in
fulfilment for the degree of Doctor of Philosophy

The Methyltransferase and Helicase Enzymes as Therapeutic Targets of Zika Virus: A Bio-Computational Analysis of Interactions with Potential Inhibitors

Miss N Devnarain

211531113

2019

A thesis submitted to the School of Pharmacy and Pharmacology, Faculty of Health Sciences, University of KwaZulu-Natal, Westville, for the degree of Doctor of Philosophy.

This is the thesis in which the chapters are written as a set of discrete research publications, with an overall introduction and final summary. Typically, these chapters will have been published in internationally recognized, peer-reviewed journals.

This is to clarify that the contents of this thesis are the original research work of Miss N Devnarain. As the candidate's supervisor, I agree to the submission of this thesis.

Supervisor:

Signed: _____

Name: Professor Mahmoud E. S. Soliman

Date:

PREFACE

This thesis is divided into **seven chapters**, including this one:

Chapter 1:

The preliminary chapter of this thesis provides a coherent background and rationale, the aim and objectives of this study, as well as the subject's novelty and relevance. Chapter 1 presents the structure of the thesis, according to UKZN's guidelines, and is concluded with the outline of the thesis.

Chapter 2:

This subsequent chapter is a literature review on what is known about the rampant Zika virus (ZIKV), as well as what is not known. Included in this chapter are information regarding ZIKV epidemiology and transmission, life cycle, pathogenesis and clinical manifestation, diagnosis of ZIKV, and therapeutic targets of the virus and host. Additionally, an overview of the up-to-date research and advancements on drug design and development against ZIKV is provided.

Chapter 3:

This chapter introduces computer-aided drug design and includes an in-depth description into the computational methodologies that were applied to carry out analyses, as well as the conceptual understanding behind molecular dynamics, modelling and drug design.

Chapter 4: (Published article)

This chapter features an article titled, "Brain Grants Permission of Access to Zika Virus but Denies Entry to Drugs: A Molecular Modeling Perspective to Infiltrate the Boundary.", which integrates a review, proposed strategies for drug design and the application of computational tools. This material will assist researchers in designing and developing effective and potent drugs to treat ZIKV. This article has been published in the journal of *RSC Advances* and is the final version of the published manuscript. This chapter is presented in the required format of the journal.

Chapter 5: (Published article)

This chapter includes an article titled, “A Panoptic Uncovering of the Dynamical Evolution of the Zika Virus NS5 Methyltransferase Binding Site Loops–Zeroing in on the Molecular Landscape.”, which addresses another objective of this thesis, covering the molecular dynamics of the ZIKV NS5 methyltransferase enzyme, particularly upon binding to two potential inhibitors, sinefungin and compound 5. This is a comparative study showing the interactions that occur between the two inhibitors and the methyltransferase, respectively, to demonstrate which inhibitor is a more potent inhibitor in terms of binding to the viral enzyme. This information is key in the drug development process toward finding anti-ZIKV drugs. This article has been published in the journal of *Chemical Biology and Drug Design* and is the final version of the published manuscript. This chapter is presented in the required format of the journal.

Chapter 6: (Published article)

This chapter comprises an article titled, “Molecular Mechanism of Resveratrol Inhibition of Zika Virus NS3 Helicase - Behind the Scenes”, which examines the structural dynamics of the ZIKV NS3 helicase enzyme upon binding of resveratrol, an ATPase inhibitor. Molecular dynamics were carried out on bound and unbound enzymes to determine the binding mechanism and binding interactions, which is key in determining the efficiency of this potential ZIKV inhibitor in drug development. This article has been published in the journal of *Future Virology* and is the final version of the published manuscript. This chapter is presented in the required format of the journal.

Chapter 7:

This chapter concludes the thesis and recommends future work.

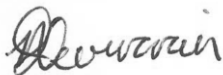
DECLARATION I - PLAGIARISM

I, Nikita Devnarain, declare that

1. The research project in this thesis, except where otherwise indicated, is my original research.
2. This thesis has not been submitted for any degree or examination at any other university.
3. This thesis does not contain other person's data, pictures, graphs or other information, unless specifically acknowledged as being sourced from other persons.
4. This thesis does not contain other persons' writing, unless specifically acknowledged as being sourced from other researchers. Where other written sources have been quoted, then:
 - a. Their words have been re-written, but the general information attributed to them has been referenced.
 - b. Where their exact words have been used, then their writing has been placed in italics and inside quotation marks and referenced.
5. This thesis does not contain text, graphics or tables copied and pasted from the internet, unless specifically acknowledged, and the source being detailed in the thesis and in the References sections.

A detailed contribution to publications that form part and/or include research presented in this thesis is stated (include publications submitted, accepted, in press and published).

Signed:



Nikita Devnarain

DECLARATION II – PUBLICATIONS

1. Nikita Devnarain, Charlette Tiloke, Savania Nagiah and Anil Amichand Chuturgoon. (2017). Fusaric acid induces oxidative stress and apoptosis in human cancerous oesophageal SNO cells. *Toxicon*, 126: 4-11. (Published)

Contribution:

Nikita Devnarain: contributed to the project by performing all the experimental work and manuscript preparation and writing.

Charlette Tiloke: Co-supervisor

Savania Nagiah: Co-supervisor

Anil Amichand Chuturgoon: Supervisor

2. Nikita Devnarain, Pritika Ramharack and Mahmoud E. S. Soliman. (2017). Brain Grants Permission of Access to Zika Virus but Denies Entry to Drugs: A Molecular Modeling Perspective to Infiltrate the Boundary. *Royal Society of Chemistry RSC Advances*. 7 (75): 47416-47424.

Contribution:

Nikita Devnarain: contributed to the project by performing all the experimental work and manuscript preparation, writing and image construction.

Pritika Ramharack: Co-supervisor

Mahmoud E. S. Soliman: Supervisor

3. Nikita Devnarain and Mahmoud E. S. Soliman. (2018). A Panoptic Uncovering of the Dynamical Evolution of the Zika Virus NS5 Methyltransferase Binding Site Loops – Zeroing in on the Molecular Landscape. *Chemical Biology and Drug Design*. 92(5): 1838-1850

Contribution:

Nikita Devnarain: contributed to the project by performing all the experimental work and manuscript preparation, writing and image construction.

Mahmoud E. S. Soliman: Supervisor

4. Nikita Devnarain and Mahmoud E. S. Soliman. (2018). Molecular Mechanism of Resveratrol Inhibition of Zika Virus NS3 Helicase - Behind the Scenes. *Future Virology*.

Contribution:

Nikita Devnarain: contributed to the project by performing all the experimental work and manuscript preparation, writing and image construction.

Mahmoud E. S. Soliman: Supervisor

ABSTRACT

The rampant Zika virus has received worldwide attention after becoming a global crisis following the Brazilian epidemic in 2015. From an obscure and neglected pathogen, Zika virus is now a notorious virus associated with neurological disorders in infants and adults. Since 2016, the rapid research response from the global scientific community have led to the discovery of numerous potential small molecule inhibitors and vaccines against the Zika virus. Although, in spite of this massive research initiative, there is still no effective antiviral nor vaccine that has made it out of clinical trials.

The design and development of new chemical entities demands excessive cost, time and resources. Therefore, this study applies computer-aided drug design techniques, which accelerates the rational drug design process. Computational approaches including molecular docking, virtual screening, molecular modeling and molecular dynamics facilitate the filtration of large databases of compounds to sift out potential lead compounds.

Furthermore, research has dedicated several resources toward FDA-approved drug repurposing. Generally, drugs have similar effects on viruses of the same family; hence drugs that have previously been effective in treating other *flaviviruses*, such as Dengue virus and West Nile virus, are being tested for its potential inhibition of Zika virus. However, the ability of these drugs to pass the blood-brain barrier to treat infected neurons poses a challenge to anti-Zika virus drug discovery. This study proposes innovative strategies to design drugs that are capable of passing the blood-brain barrier, and to be able to use drugs that are impermeable via drug delivery mechanisms. This study also assesses the bioavailability and blood-brain barrier permeability of screened drugs to scrutinize the list of potential Zika virus inhibitors.

Apart from identifying potential inhibitors, understanding the structural dynamics of viral targets and molecular mechanisms underlying potential inhibition of the virus is imperative. This study explores the structural and molecular dynamics of key targets of the Zika virus, the NS3 helicase and the NS5 methyltransferase enzymes, using computational approaches mentioned above and several others elaborated in this thesis. These computational methods also allowed the identification of precise interactions, amino acid residues, inhibitory mechanisms and pharmacophoric features involved in binding of lead compounds to these enzymes.

Chapter 4 represents the first study of this thesis, which presents a concise literature background of Zika virus and identifies blood-brain barrier permeability as a core challenge in anti-Zika virus drug development. This study also provides approaches that may enable researchers to create effective anti-Zika virus drugs.

Chapter 5 is the subsequent study of this thesis, which applies molecular dynamics to comparatively investigate the mechanism of inhibition and binding mode of two potential inhibitors, sinefungin and compound 5, to the NS5 methyltransferase. The specific pharmacophoric moieties of the most stable inhibitor are also identified in this study.

Chapter 6 is the final study of this thesis, which examines the structural dynamics of the Zika virus NS3 helicase enzyme upon binding of ATPase inhibitor and flavivirus lead compound, resveratrol, and reports the key interactions and amino acid residues of the NS3 helicase that contribute highly to binding of resveratrol.

This thesis presents an all-inclusive *in silico* assessment to advance research in drug design and development of Zika virus inhibitors, thus providing a greater understanding of the structural dynamics that occur in unbound and inhibitor-bound Zika virus target enzymes. Therefore, the constituents of this thesis are considered an essential platform in the progression of research toward anti-ZIKV drug design, discovery and delivery against Zika virus.

RESEARCH OUTPUT

A. List of Publications

1. Nikita Devnarain, Pritika Ramharack and Mahmoud E. S. Soliman. (2017). Brain Grants Permission of Access to Zika Virus but Denies Entry to Drugs: A Molecular Modeling Perspective to Infiltrate the Boundary. *Royal Society of Chemistry RSC Advances*. 7 (75): 47416-47424.
2. Nikita Devnarain and Mahmoud E. S. Soliman. (2018). A Panoptic Uncovering of the Dynamical Evolution of the Zika Virus NS5 Methyltransferase Binding Site Loops – Zeroing in on the Molecular Landscape. *Chemical Biology and Drug Design*. 92(5): 1838-1850
3. Nikita Devnarain and Mahmoud E. S. Soliman. (2018). Molecular Mechanism of Resveratrol Inhibition of Zika Virus NS3 Helicase - Behind the Scenes. *Future Virology*.

B. Submitted

1. Nikita Devnarain, Letitia Shunmugam and Mahmoud E. S. Soliman. (2018). Chronicles of viperin: Are we using the most of this broad-spectrum human weapon to counteract viruses? *Drug Discovery Today*.
2. Pritika Ramharack, Nikita Devnarain, Letitia Shunmugam and Mahmoud E. S. Soliman. (2018). Navigating research toward the re-emerging nipah virus- a new piece to the puzzle. *Expert Opinion on Drug Discovery*.
3. Nikita Devnarain, Letitia Shunmugam and Mahmoud E. S. Soliman. (2018). Computational scaffolding and screening approach using pharmacophoric fingerprints: identifying potential inhibitors of Zika virus. *Drug Designing: Open Access*.
4. Letitia Shunmugam, Nikita Devnarain and Mahmoud E. S. Soliman. (2018). Enhanced pharmacophore-based virtual screening approach in the discovery of potential inhibitors of HCV NS3 helicase. *Future Virology*.

Conferences

1. 8th CHPC Introductory Programming Conference, Potchefstroom, South Africa.
2. 8th DAAD South Africa Conference, Durban, South Africa.
3. 2018 CHPC National Conference, Cape town, South Africa – Poster presentation.

TABLE OF CONTENTS

Preface.....	III
Declaration I - Plagiarism	V
Declaration II – Publications.....	VI
Abstract	VIII
Research Output.....	X
List of Figures	XV
List of Tables.....	XX
List of Abbreviations.....	XXI
List of Amino Acids.....	XXIV
Chapter 1: Introduction	1
1 Background & Rationale.....	1
2 Aims & Objectives.....	2
3 Novelty & Significance.....	4
4 References.....	5
Chapter 2: Literature Review	9
1 Introduction to Zika Virus.....	9
2 Epidemiology & Distribution.....	9
3 The Zika Virus Life Cycle.....	11

4	Clinical Manifestation of Zika Virus.....	12
5	Diagnosis of Zika Virus	13
6	Components of Zika Virus	14
7	Zika Virus Pathogenesis.....	17
8	Pharmacological Targets of Zika Virus.....	19
8.1	The NS3 Helicase.....	21
8.2	The NS5 Methyltransferase.....	22
9	Therapeutic targets of Host	23
10	Advances in Design & Development of Anti-Zika Virus Drugs & Therapies.....	24
10.1	Small Molecule Inhibitors	24
10.2	Prophylactic Antibodies and Vaccines.....	28
11	References	30
Chapter 3: Computational Methodology		44
1	Introduction	44
2	Quantum Mechanics.....	45
2.1	The Schrödinger Equation.....	46
2.2	The Born-Oppenheimer Approximation Theory	48
2.3	Potential Energy Surface	49
3	Molecular Mechanics	49

3.1	Potential Energy Function	50
4	Molecular Dynamics	52
4.1	Molecular Dynamics Post Analyses.....	53
5	Other Computer-Aided Drug Design Techniques Utilized in the Study.....	59
5.1	Molecular Docking.....	59
5.2	Virtual Screening.....	59
6	References	60
Chapter 4	67
	Brain Grants Permission of Access to Zika Virus but Denies Entry to Drugs: A Molecular Modeling Perspective to Infiltrate the Boundary.....	67
Chapter 5	88
	A Panoptic Uncovering of the Dynamical Evolution of the Zika Virus NS5 Methyltransferase Binding Site Loops–Zeroing in on the Molecular Landscape.....	88
Chapter 6	121
	Molecular Mechanism of Resveratrol Inhibition of Zika Virus NS3 Helicase - Behind the Scenes	121
6	Conclusion.....	141
Chapter 7: Synthesis	148
1	Conclusion.....	148
2	Future Perspectives	149

3	References	149
	Appendices	150

LIST OF FIGURES

Chapter 2

Figure 2.1 Global distribution of Zika virus in humans and animals since 1947. Autochthonous vector-borne human cases were documented in colored countries, while countered labeled with using animal profiles and years have documented Zika virus in naturally infected animals (Bueno *et al.*, 2016).

Figure 2.2 The life cycle of Zika virus in blood and in organisms. A key role player in the viral life cycle is the vector, which in this case is the *Aedes* mosquito (Adapted from Sreedharan, 2015).

Figure 2.3 The Zika virion above segments of Zika virus genome with corresponding available crystal structures of encoded proteins (PDB: 4I31, 5GJB, 5H4I, 5IY3, 5U4W and 5YGH) (Prepared by Author).

Figure 2.4 Phylogenetic analysis of Zika virus genomes based on region. Phylogenetic analysis of existing genomes was categorized by lineage and then continent of isolation. Asian strains (America) were grouped in blue, African strains in red, and strains from Asia and Oceania in green (Beaver *et al.*, 2018).

Figure 2.5 The NS3 helicase of Zika virus. The three domains of comparable size are demonstrated in orange (Domain 1), blue (Domain 2) and green (Domain 3). The P-loop of Domain 1 is represented in yellow, which surrounds the binding site of ATP. The RNA-binding loop whose flexibility influences RNA replication is shown in pink (Prepared by Author).

Figure 2.6 Diagram represents the methyltransferase enzyme of the Zika virus NS5 protein on the left, showing the three different binding-pockets, and the four-step process of capping by the methyltransferase on the right (Prepared by Author).

Figure 2.7 Drugs that target different stages of the Zika virus life cycle (Saiz *et al.*, 2018).

Chapter 3

Figure 3.1 The Niels Bohr Model (1913) demonstrating the absorption and emission of photons as electron move to higher/lower energy levels (n) (Prepared by Author).

Figure 3.2 Schrödinger's Quantum Mechanical Model (1926) demonstrating orbitals as differently shaped "lobes" where electrons are probably found (Prepared by Author).

Figure 3.3 Graphical representation of "ball and spring" model describing potential energy function and corresponding potential energy diagram (Prepared by Author).

Figure 3.4 Illustration of the thermodynamic cycle in MM/PBSA or MM/GBSA calculations. The addition of the gas-phase configurational entropy and energy and the difference in solvation free energies between the ligand and complex results in the FBE results. The blue surface signifies the solvent (Prepared by Author).

Chapter 4

Figure 1: A schematic representation of the blood-brain barrier and pathways across this barrier.

Figure 2: Hydrophobic footprints (highlighted in yellow) in chemical structures of potential anti-ZIKV compounds which have the ability to permeate the BBB.

Figure 3: Phases involved in the suggested approach to improve the BBB-permeability profile of the inhibitor.

Chapter 5

Figure 4: A schematic representation of the Zika virus NS5 enzyme. The structural protein of zika virus NS5 is divided into its two major subunits, the methyltransferase (bound to its natural substrate) and the RNA-dependent RNA-polymerase.

Figure 2: **A.** Superimposed crystal structures of DENV and ZIKV NS5 MTases showing similarities and differences in coils, β -sheets and α -helices. **B.** Structures of ZIKV and DENV MTases illustrating similar binding pockets and solvent accessible surface areas. **C.** Sequence similarities and differences between ZIKV and DENV.

Figure 3: Implications of lack of SAM binding to MTase. Illustration of SAM-binding to the MTase as a prerequisite for viral RNA methylation and viral replication (left), and the consequence of an alternative molecule binding in the SAM-binding pocket and inhibiting viral RNA methylation and replication (right).

Figure 4: Potential ZIKV inhibitors. Chemical structure of SFG and Compound 5 (left), as well as the chemical formula and functional groups of SFG (top right) and Compound 5 (bottom right).

Figure 5: Fluctuations in rigidity of SFG-bound and Compound 5-bound complexes compared to apo are shown in **A** and **B**, respectively, with emphasis on loop movements during the 52ns, 122ns and 173ns periods of the simulation. **C** shows that SFG reached convergence and was less flexible toward the latter period of the simulation, as compared to that of the apo and Compound 5-bound systems.

Figure S1: Graphs illustrating the radius of gyration (RoG) showing the variation of MTase compactness of the apo vs SFG-bound system (left) and the apo vs Compound 5-bound system (right) throughout a 200ns molecular dynamic simulation.

Figure 6: (Top left) Graph depicts hydrogen-bonding analysis of the apo and bound systems. (Top right) Bond and non-bond interactions that exist between each inhibitor and their binding site residues, as well as the interacting areas of the ligand which are hydrogen donors and acceptors. (Bottom) Surface areas of each inhibitor in the MTase pocket describing the hydrogen bonding capacity of each ligand during parts of the simulation that correspond to fluctuations in energy, along with the solvent accessible surface areas of the MTase at those points which correspond to ligand movement in the SAM-binding pocket.

Figure 7: The average energy interpretation of each residue throughout the simulation of the apo MTase vs SFG-bound MTase. Highly fluctuating residues in the system are also illustrated in the crystal structure of the MTase and correlated with the peaks in the graph.

Figure 8: The average energy interpretation of each residue throughout the simulation of the apo MTase vs Compound 5-bound MTase. Highly fluctuating residues in the system are also illustrated in the crystal structure of the MTase and correlated with the peaks in the graph.

Figure S2: Dynamic cross correlation of the α -carbon atoms of the apo MTase (**A**), SFG-bound MTase complex (**B**) and Compound 5-bound-MTase complex (**C**).

Figure 9: MTase residues that interact with SFG (left) and energy contributions of the highest interacting residues at the SAM-binding site (right).

Figure 10: MTase residues that interact with Compound 5 (left) and energy contributions of the highest interacting residues at the SAM-binding site (right).

Figure 11: Schematic representation of the key chemical, structural and pharmacophoric fingerprints of SFG.

Chapter 6

Figure 5: Superimposition of the Zika virus and Dengue virus NS3 helicases as well as their corresponding overlapping sequences showing the similarities and differences in their amino acid residues.

Figure 6: Chemical structure of resveratrol.

Figure 7: Protein sequences of the different domains of Zika virus NS3 helicase, as well as the major binding sites and loops. ATP: adenosine triphosphate; ssRNA: single-stranded RNA

Figure 8: Multiple sequence alignment of three strains of helicase sequences (strains: H/PF/2013, BRA/2016 and MR766).

Figure 9: Resveratrol binding to ZIKV NS3 helicase stabilizes the enzyme. Snapshots at 10 ns intervals from 150-200 ns show the spontaneous behavior of the RNA-binding loop (green) in the

apo enzyme (grey), while the same loop (blue) in the bound enzyme (red) becomes stable via formation of a 3_{10} -helix.

Figure 10: Resveratrol binding to the NS3 helicase (red) induces compactness of the enzyme, as compared to the apo (grey).

Figure 11: Residues of the apo helicase (grey) fluctuate more than residues of the resveratrol-bound helicase (red)

Figure 12: Exploration of the interactions that exist between resveratrol and residues of the ZIKV NS3 helicase. A. Resveratrol within binding pocket of helicase zooming into the hydrophobic interactions and hydrogen bonds between ligand binding residues and resveratrol. B. Per-residue decomposition analysis of ligand binding residues. C. Hydrogen bonding in ligand binding pocket. EEL: electrostatic energy; vdW: van der Waals.

LIST OF TABLES

Chapter 2

Table 2.1 Compounds that represent potential antiviral compounds against the Zika virus (Devnarain, Ramharack and Soliman, 2017; Munjal et al., 2017; Saiz and Martín-Acebes, 2017; da Silva, Martins and Jardim, 2018).

Table 2.2 Stages of Zika virus vaccines that entered clinical trials (Adapted from Garg, Mehmetoglu-Gurbuz and Joshi, 2018).

Chapter 4

Table 1: Predicted Bioavailability Features of Prospective Anti-ZIKV Inhibitors.

Table 2: Pre-existing drug delivery systems and their principle roles in disease and virus therapies

Chapter 5

Table 1: An outline of the MM/PBSA binding free energy contributions to the SFG-MTase system and the Compound 5-MTase system.

Chapter 6

Table 1: A representation of the binding free energy contributions to the Resveratrol-bound system.

Table 2: Druglikeness of Resveratrol

LIST OF ABBREVIATIONS

Abbreviation	Definition
ΔG_{bind}	Change in free binding energy
3D-QSAR	Three-dimensional quantitative structure-activity relationship
Ab	Antibody
AMBER	Assisted Model Building with Energy Refinement
ATP	Adenosine triphosphate
BBB	Blood-brain barrier
CADD	Computer-aided drug design
CHARRM	Chemistry at HARvard Macromolecular Mechanics
CSF	Cerebrospinal fluid
DCCM	Dynamic Cross Correlation Matrices
DENV	Dengue virus
ds	Double-stranded
ELISA	Enzyme-linked immunosorbent assay
ENCAD	Energy Calculation and Dynamics
ER	Endoplasmic reticulum
FBE	Free binding energy
FDA	Food and Drug Administration
GROMOS	GRoningen Molecular Simulation
GTP	Guanosine triphosphate
HCV	Hepatitis C virus
hTERT	Human telomerase reverse transcriptase
IFN	Interferon
IRF7	IFN regulatory factor 7
IgG/IgM	Immunoglobulin G/M

JEV	Japanese Encephalitis virus
MC	Monte Carlo
MD	Molecular Dynamics
MIA	Multiplex microsphere immunoassay
MM	Molecular mechanics
MM/PBSA and MM/GBSA)	MM energies integrated with Poisson–Boltzmann or generalized Born surface area
MTase	Methyltransferase
NMR	Nuclear magnetic resonance
ns	Nanoseconds
NS	Non-structural
NSC	Neural stem cell
OPLS-AA	All-atom Optimized Potentials for Liquid Simulations
ORF	Open reading frame
PEF	Potential energy function
PES	Potential energy surface
PRNT	Plaque-reduction neutralization test
QM	Quantum mechanics
RdRp	RNA-dependent RNA-polymerase
RMSD	Root-mean-square deviation
RMSF	Root-mean-square fluctuation
RNA	Ribonucleic acid
RoG	Radius of gyration
RPE	Retinal pigment
RT-qPCR	Quantitative reverse transcription polymerase chain reaction
SAM	S-adenosyl-L-methionine
siRNA	Small interfering RNA
TLR	Toll-like receptor

UTR	Untranslated region
VS	Virtual Screening
WHO	World Health Organization
WNV	West Nile virus
YFV	Yellow Fever virus
ZIKV	Zika virus

LIST OF AMINO ACIDS

Three Letter Code	Amino Acid
Ala	Alanine
Arg	Arginine
Asn	Asparagine
Asp	Aspartic Acid
Cys	Cysteine
Gln	Glutamine
Glu	Glutamic Acid
Gly	Glycine
His	Histidine
Ile	Isoleucine
Leu	Leucine
Lys	Lysine
Met	Methionine
Phe	Phenylalanine
Pro	Proline
Ser	Serine
Thr	Threonine
Trp	Tryptophan
Tyr	Tyrosine
Val	Valine

CHAPTER 1: INTRODUCTION

1 Background & Rationale

Zika virus is an arthropod-borne *flavivirus* that belongs to the *Flaviviridae* family (White *et al.*, 2016). Despite the reduced rate of ZIKV infections since early 2017, ZIKV remains a universal problem (Depoux *et al.*, 2018). Some of the underlying concerns include the possibility of re-emergence and distribution of ZIKV in parts of the world with high prevalence of *Aedes* mosquitoes, the gap in literature surrounding modes of transmission not yet determined, the enduring risk for women that want to have children and other susceptible women residing or traveling in endemic countries, and the devastating congenital anomalies associated with ZIKV (Hajra, Bandyopadhyay and Hajra, 2016). Over and above these concerns, the biggest problem is the current lack of an approved, effective antiviral treatment that will also pass the blood-brain barrier (BBB) (Munjal *et al.*, 2017).

Over the last few years, there have been many endeavors to assess potential anti-ZIKV drugs targeting viral and host proteins (Pascoalino *et al.*, 2016; Munjal *et al.*, 2017; Yuan *et al.*, 2017; Zhang *et al.*, 2017; Xia *et al.*, 2018). Directing drugs toward key viral proteins in the ZIKV life cycle may inhibit replication of the virus with minimal harm to the host (Saiz and Martín-Acebes, 2017). A typical ZIKV particle consists of structural proteins (capsid, precursor membrane, membrane and envelope) and non-structural proteins (NS1, NS2A, NS2B, NS3, NS4A, NS4B, NS5) (Weaver *et al.*, 2016). All proteins are important in the ZIKV life cycle, but the NS3 and NS5 are the most fundamental proteins in ZIKV maturation and replication (Saw *et al.*, 2017). The NS3 protein is composed of the C-terminal helicase involved in ATP hydrolysis and RNA binding, and the N-terminal protease associated with maturation of ZIKV NS proteins (Jain *et al.*, 2016; Y. Li *et al.*, 2018). The NS5 protein constitutes an N-terminal methyltransferase (MTase) involved in RNA capping and a C-terminal RNA-dependent RNA-polymerase (RdRp) responsible for RNA synthesis (Duan *et al.*, 2017; Zhang *et al.*, 2017).

The usual symptoms of ZIKV infection include mild fever, rash, conjunctivitis and arthralgia (Beaver *et al.*, 2018). Although, since 2016, ZIKV infection was discovered to be associated with secondary complications including neurological disorder Guillain–Barré syndrome and congenital brain aberrations such as microcephaly, ventriculomegaly, cerebral atrophy, diffuse calcifications, ocular anomalies and cortical development (Baud *et al.*, 2017; Krauer *et al.*, 2017; Agrawal *et al.*, 2018; Lee *et al.*, 2018; Mier-Y-Teran-Romero *et al.*, 2018).

A great deal of research effort has been put into preventative measures such as vaccines, and therapeutic approaches such as antivirals, however, effective treatment regimens are yet to pass clinical trials (Pascoalino *et al.*, 2016; Xu *et al.*, 2016; Xie *et al.*, 2017; Garg, Mehmetoglu-Gurbuz and Joshi, 2018). Considerable factors that pose as challenges in the drug design and discovery process of ZIKV inhibitors include BBB permeation, target-specificity, drug efficacy and minimal host toxicity (Saiz and Martín-Acebes, 2017; Alimonti *et al.*, 2018). Developing a new chemical entity that agrees with all these factors, also taking into consideration progressing viral mutations and unknown ZIKV pathogenicity, requires extensive time, effort and money. A more rapid and economical approach involves computer-aided drug design (CADD) (Goldbeck, 2012; Das, Saha and Abdul, 2017), which applies molecular dynamics simulations, molecular docking, virtual screening and pharmacophore modelling to filter out lead compounds from large databases to be experimentally tested (Trott and Olson, 2010; Lionta *et al.*, 2014; Munir, Azam and Mehmood, 2016; Raabe, 2017). So instead of starting from scratch, computational methods allow for certain steps in the rational drug design process to be avoided.

As a result of a lack of effective inhibitors of ZIKV infection, the study herein applies fundamental computational approaches for research into anti-ZIKV therapy, thus providing an improved understanding of drug targets and potential inhibitors of ZIKV.

2 Aims & Objectives

The main goals of this thesis are:

- a) To identify challenges associated with drug design and discovery of potent ZIKV inhibitors and provide computational approaches to overcome those challenges,
- b) To classify the ZIKV NS3 and NS5 major target proteins, and apply computational methods to identify potential small molecules that inhibit them, and
- c) To analyze the intra- and intermolecular interactions between those potential inhibitors and target proteins.

Objectives:

1. To generate systematic strategies describing the steps taken toward designing compounds and identifying potential inhibitors of drug targets with improved BBB permeability by:
 - 1.1. Providing a coherent introduction to ZIKV and identifying core challenges in ZIKV therapy.
 - 1.2. Assessing bioavailability of screened drugs as potential ZIKV inhibitors.
 - 1.3. Presenting strategies to assist with the design of compounds with improved BBB permeability profile and to deliver those that are impermeable.

2. To explore the structural dynamics and mechanism of inhibition of the ZIKV NS5 MTase enzyme when bound to competitive inhibitors of the natural substrate, S-adenosyl-L-methionine (SAM), namely, sinefungin and compound 5. This imparts knowledge of the binding mode at the SAM-binding site, thus contributing to effective anti-ZIKV drug design and discovery. This will also give us a better understanding of which inhibitor binds with greater affinity to the MTase by:
 - 2.1. Incorporating molecular docking with 200 ns of molecular dynamic simulations for the apo enzyme and inhibitor-bound complexes.
 - 2.2. Implementing various post-dynamic analyses to describe the binding landscape of the MTase and to reveal structural modifications in ZIKV NS5 MTase following inhibitor binding.

3. To study the binding landscape of the ATPase pocket in the ZIKV NS3 helicase by presenting the chemical features of *flavivirus* lead drug, resveratrol, at the ATP-binding pocket by:
 - 3.1. Applying molecular docking to obtain conformations of resveratrol that bind with highest affinity to the helicase pocket.
 - 3.2. Employing 200 ns of molecular dynamics simulations of the unbound and resveratrol-bound enzymes, identifying the precise residues and interactions involved in binding of resveratrol to the helicase.

3 Novelty & Significance

Before the Brazilian outbreak in 2015, ZIKV was much-neglected in terms of research and very little was understood about the virus or the mechanism of infection (Campos, Bandeira and Sardi, 2015; Saiz and Martín-Acebes, 2017). Since then, there have been numerous attempts to discover effective drugs that can cure the virus, as well as preventative vaccines and antibodies (Barrows *et al.*, 2016; Byler, Ogungbe and Setzer, 2016; Larocca *et al.*, 2016; Xu *et al.*, 2016; Richner *et al.*, 2017; Shan, Muruato, *et al.*, 2017; Xie *et al.*, 2017; Garg, Mehmetoglu-Gurbuz and Joshi, 2018), however, none have been successful in providing an effective, approved anti-ZIKV treatment till date.

The urge for a cure is driven by a number of factors, particularly the devastating effects of ZIKV on pregnant women and their infants as ZIKV has been associated with neurological complications in babies as well as adults (Brasil *et al.*, 2016; Chan *et al.*, 2016; Krauer *et al.*, 2017; Agrawal *et al.*, 2018; Mier-Y-Teran-Romero *et al.*, 2018). The danger associated with ZIKV infection persists also because of the increasing mutation rate, modes of ZIKV transmission that are still unknown and travelers from countries where ZIKV is still rife.

We decided to identify challenges associated with the design and discovery of ZIKV inhibitors. A major requirement for an effective drug is its ability to pass the BBB, so we created novel approaches to design BBB-permeable drugs as well as transport BBB-impermeable drugs to the brain. A potent antiviral drug must also have minimal adverse effects toward its host, therefore, we undertook studies to investigate mechanisms of inhibition of compounds on viral targets instead of host targets. Using CADD, we investigated the structural dynamics and binding mechanisms of the two major viral targets that are key role players in ZIKV infection, the NS3 and NS5 proteins. This was the first study to investigate the binding landscapes of the potential inhibitors Sinefungin, Compound 5 and Resveratrol to ZIKV enzymes. Characterization of the structural and functional nature of the binding pockets within these enzymes will favor the development of potential unique and selective small molecule inhibitors of ZIKV. Understanding the interactions that occur between the inhibitors and enzymes, as well as the amino acid residues that highly contribute to binding and enzyme activity, will assist in improving inhibition by modification of those residues and in treating possible mutations that may occur in future.

Therefore, the composition of this thesis is regarded as an essential platform in the progression of research toward anti-ZIKV drug design, discovery and delivery.

The structure of the thesis is according to UKZN guidelines.

4 References

Agrawal, R. et al. (2018) 'Zika Virus and the Eye', *Ocular Immunology and Inflammation*, 26(5), pp. 654–659. doi: 10.1080/09273948.2017.1294184.

Alimonti, J. B. et al. (2018) 'Zika virus crosses an in vitro human blood brain barrier model.', *Fluids and barriers of the CNS*. BioMed Central, 15(1), p. 15. doi: 10.1186/s12987-018-0100-y.

Barrows, N. J. et al. (2016) 'A Screen of FDA-Approved Drugs for Inhibitors of Zika Virus Infection', *Cell Host and Microbe*, 20(2), pp. 259–270. doi: 10.1016/j.chom.2016.07.004.

Baud, D. et al. (2017) 'An update on Zika virus infection', *The Lancet*. Elsevier, 390(10107), pp. 2099–2109. doi: 10.1016/S0140-6736(17)31450-2.

Beaver, J. T. et al. (2018) 'Evolution of Two Major Zika Virus Lineages: Implications for Pathology, Immune Response, and Vaccine Development', *Frontiers in Immunology*. Frontiers, 9, p. 1640. doi: 10.3389/fimmu.2018.01640.

Brasil, P. et al. (2016) 'Guillain-Barre syndrome associated with Zika virus infection', *Lancet*, 387(1), p. 1482. doi: 10.1016/S0140-6736(16)30058-7.

Byler, K. G., Ogungbe, I. V. and Setzer, W. N. (2016) 'In-silico screening for anti-Zika virus phytochemicals', *Journal of Molecular Graphics and Modelling*, 69, pp. 78–91. doi: 10.1016/j.jmgm.2016.08.011.

Campos, G. S., Bandeira, A. C. and Sardi, S. I. (2015) 'Zika Virus Outbreak, Bahia Brazil', *Emerging Infectious Diseases*, 21(10), pp. 1885–1886. doi: 10.32301/eid2110.150847.

Chan, J. et al. (2016) 'Zika fever and congenital Zika syndrome: An unexpected emerging arboviral disease', *Journal of Infection*, 72, pp. 507–524. doi: <http://linkinghub.elsevier.com/retrieve/pii/S016344531600061X>.

Das, P. S., Saha, P. and Abdul, A. P. J. (2017) 'A Review on Computer Aided Drug Design In Drug Discovery', *World Journal of Pharmacy and Pharmaceutical Sciences*, 6(7), pp. 279–291. doi: 10.20959/wjpps20177-9450.

Depoux, A. et al. (2018) 'A multi-faceted pandemic: a review of the state of knowledge on the Zika virus', *Public Health Reviews. BioMed Central*, 39(10), pp. 1–12. doi: 10.1186/s40985-018-0087-6.

Duan, W. et al. (2017) 'The crystal structure of Zika virus NS5 reveals conserved drug targets', *The EMBO Journal*, 36(7), pp. 919–933. doi: 10.15252/embj.201696241.

Garg, H., Mehmetoglu-Gurbuz, T. and Joshi, A. (2018) 'Recent Advances in Zika Virus Vaccines', *Viruses*, 10(11), p. E631. doi: 10.3390/v10110631.

Goldbeck, G. (2012) *The Economic Impact of Molecular Modelling*, Goldbeck Consulting Report. doi: 10.5281/zenodo.44359.

Hajra, A., Bandyopadhyay, D. and Hajra, S. K. (2016) 'Zika Virus: A Global Threat to Humanity: A Comprehensive Review and Current Developments.', *North American journal of medical sciences. Wolters Kluwer -- Medknow Publications*, 8(3), pp. 123–8. doi: 10.4103/1947-2714.179112.

Jain, R. et al. (2016) 'Structure of the NS3 helicase from Zika virus', *Nature Structural and Molecular Biology. Nature Publishing Group*, 23(8), pp. 752–754. doi: 10.1038/nsmb.3258.

Krauer, F. et al. (2017) 'Zika Virus Infection as a Cause of Congenital Brain Abnormalities and Guillain–Barré Syndrome: Systematic Review', *PLOS Medicine*, 14(1), pp. 1–27. doi: 10.1371/journal.pmed.1002203.

Larocca, R. A. et al. (2016) 'Vaccine protection against Zika virus from Brazil.', *Nature. NIH Public Access*, 536(7617), pp. 474–8. doi: 10.1038/nature18952.

Lee, I. et al. (2018) 'Probing Molecular Insights into Zika Virus–Host Interactions.', *Viruses. Multidisciplinary Digital Publishing Institute (MDPI)*, 10(5). doi: 10.3390/v10050233.

Li, Y. et al. (2018) 'Structural Insights into the Inhibition of Zika Virus NS2B-NS3 Protease by a Small-Molecule Inhibitor', *Structure*, 26(4), p. 555–564.e3. doi: 10.1016/j.str.2018.02.005.

Lionta, E. et al. (2014) 'Structure-based virtual screening for drug discovery: principles, applications and recent advances.', *Current Topics in Medicinal Chemistry*, 14(16), pp. 1923–1938. doi: 10.2174/1568026614666140929124445.

- Mier-Y-Teran-Romero, L. et al. (2018) 'Guillain-Barré syndrome risk among individuals infected with Zika virus: a multi-country assessment.', *BMC medicine*. BioMed Central, 16(1), p. 67. doi: 10.1186/s12916-018-1052-4.
- Munir, A., Azam, S. and Mehmood, A. (2016) 'Structure-Based Pharmacophore Modeling, Virtual Screening and Molecular docking for the Treatment of ESR1 Mutations in Breast Cancer', *Drug Designing: Open Access*, 5(137), pp. 2169-0138. doi: 10.4172/2169-0138.1000137.
- Munjal, A. et al. (2017) 'Advances in Developing Therapies to Combat Zika Virus: Current Knowledge and Future Perspectives', *Frontiers in Microbiology*, 8(1469), pp. 1–19. doi: 10.3389/fmicb.2017.01469.
- Pascoalino, B. S. et al. (2016) 'Zika antiviral chemotherapy: identification of drugs and promising starting points for drug discovery from an FDA-approved library.', *F1000Research*. Faculty of 1000 Ltd, 5, p. 2523. doi: 10.12688/f1000research.9648.1.
- Raabe, G. (2017) 'Molecular Dynamics Simulations', in *Molecular Modeling and Simulation*. Springer, Singapore, pp. 83–113. doi: 10.1007/978-981-10-3545-6_4.
- Richner, J. M. et al. (2017) 'Vaccine Mediated Protection Against Zika Virus-Induced Congenital Disease.', *Cell*. NIH Public Access, 170(2), p. 273–283.e12. doi: 10.1016/j.cell.2017.06.040.
- Saiz, J.-C. and Martín-Acebes, M. A. (2017) 'The Race To Find Antivirals for Zika Virus', *Antimicrobial Agents and Chemotherapy*. American Society for Microbiology Journals, 61(6), pp. e00411-17. doi: 10.1128/AAC.00411-17.
- Saw, W. G. et al. (2017) 'Structural features of Zika virus non-structural proteins 3 and -5 and its individual domains in solution as well as insights into NS3 inhibition', *Antiviral Research*. Elsevier, 141(1), pp. 73–90. doi: 10.1016/J.ANTIVIRAL.2017.02.005.
- Shan, C. et al. (2017) 'A live-attenuated Zika virus vaccine candidate induces sterilizing immunity in mouse models.', *Nature medicine*. NIH Public Access, 23(6), pp. 763–767. doi: 10.1038/nm.4322.
- Trott, O. and Olson, A. J. (2010) 'AutoDock Vina: improving the speed and accuracy of docking with a new scoring function, efficient optimization and multithreading', *Journal of Computational Chemistry*, 31(1), pp. 445–461. doi: 10.1002/jcc.21334.
- Weaver, S. C. et al. (2016) 'Zika virus: History, emergence, biology, and prospects for control', *Antiviral Research*. Elsevier B.V., 130, pp. 69–80. doi: 10.1016/j.antiviral.2016.03.010.
- White, M. K. et al. (2016) 'Zika virus: An emergent neuropathological agent', *Annals of Neurology*, 80(4), pp. 479–489. doi: 10.1002/ana.24748.

Xia, H. et al. (2018) ‘An evolutionary NS1 mutation enhances Zika virus evasion of host interferon induction.’, *Nature communications*. Nature Publishing Group, 9(1), p. 414. doi: 10.1038/s41467-017-02816-2.

Xie, X. et al. (2017) ‘Small Molecules and Antibodies for Zika Therapy’, *The Journal of Infectious Diseases*. Oxford University Press, 216(suppl_10), pp. S945–S950. doi: 10.1093/infdis/jix406.

Xu, M. et al. (2016) ‘Identification of small-molecule inhibitors of Zika virus infection and induced neural cell death via a drug repurposing screen.’, *Nature medicine*. NIH Public Access, 22(10), pp. 1101–1107. doi: 10.1038/nm.4184.

Yuan, S. et al. (2017) ‘Structure-based discovery of clinically approved drugs as Zika virus NS2B-NS3 protease inhibitors that potently inhibit Zika virus infection in vitro and in vivo’, *Antiviral Research*. Elsevier B.V., 145, pp. 33–43. doi: 10.1016/j.antiviral.2017.07.007.

Zhang, C. et al. (2017) ‘Structure of the NS5 methyltransferase from Zika virus and implications in inhibitor design’, *Biochemical and Biophysical Research Communications*. Academic Press, 492(4), pp. 624–630. doi: 10.1016/J.BBRC.2016.11.098.

CHAPTER 2: LITERATURE REVIEW

1 Introduction to Zika Virus

The ZIKV is a mosquito-borne virus at the center of the continuing pandemic and public health crisis (Plourde and Bloch, 2016). In 1947, ZIKV was originally isolated from a sentinel rhesus macaque monkey and afterwards in *Aedes africanus* mosquitoes. The virus was named after the place where it had been first isolated, i.e. within the Ugandan Zika forest (Dick, Kitchen and Haddock, 1952a). The ZIKV belongs to the *flavivirus* genus and is akin to other *flaviviruses*, including Dengue virus (DENV), West Nile virus (WNV), Yellow Fever virus (YFV) and Japanese Encephalitis virus (JEV) (Devnarain, Ramharack and Soliman, 2017). The similarity of the *flaviviruses* also give reason to them having the same vector, which is the *Aedes aegypti* mosquito (Muktar, Tamerat and Shewafera, 2016). Infection by ZIKV seems to show mild illness, however, persistent infection can lead to severe manifestations that include congenital brain abnormalities and Guillain-Barré syndrome (Lazear and Diamond, 2016).

The chapter herein has pertinent and up-to-date literature that is relevant to the aims and objectives of this study, and brings into context the known facts about ZIKV, as well as what has not yet been established. The viral structure itself will be elaborated to provide insight into the pharmacological targets of ZIKV that will advance the drug design and development of anti-ZIKV drugs.

2 Epidemiology & Distribution

The primary mode of transmission of ZIKV is through the bite of an infected *Aedes* mosquito (*Stegomyia subgenus*) (Muktar, Tamerat and Shewafera, 2016). Other known methods include sexual transmission, perinatal, blood transfusion, intrauterine, and laboratory exposure (Filipe, Martins and Rocha, 1973; Besnard *et al.*, 2014; Musso *et al.*, 2014; Musso, Roche, Robin, *et al.*, 2015; Tabata *et al.*, 2016; Turmel *et al.*, 2016; Sharma and Lal, 2017; Winkler *et al.*, 2017).

Only occasional ZIKV cases had been documented prior to 2007, after the initial outbreak in 1947 (MacNamara, 1954; Filipe, Martins and Rocha, 1973; Olson *et al.*, 1981; Petersen *et al.*, 2016). After these sporadic cases, in 2007, the Micronesian Yap state had reported the first ZIKV outbreak

(Lanciotti *et al.*, 2008; Duffy *et al.*, 2009). The ZIKV was later massively identified in October 2013 in French Polynesia and other islands of the Pacific (Cao-Lormeau and Musso, 2014; Cao-Lormeau *et al.*, 2014). The virus then moved to South America in May 2015 when infections were reported in Brazil, which were found to be associated with Guillain-Barré syndrome and later with microcephaly (Campos, Bandeira and Sardi, 2015). From 2015 till 2017, over 20 countries in Europe documented 2133 cases of ZIKV infection (Spiteri *et al.*, 2017). The World Health Organization (WHO) has declared three areas in Europe as high risk, which include Georgia, south of the Russian Federation and the Madeira island in Portugal (Gulland, 2016). Up till now, mosquito-borne ZIKV has infected 86 countries and lands worldwide (Figure 2.1) (Hills, Fischer and Petersen, 2017).

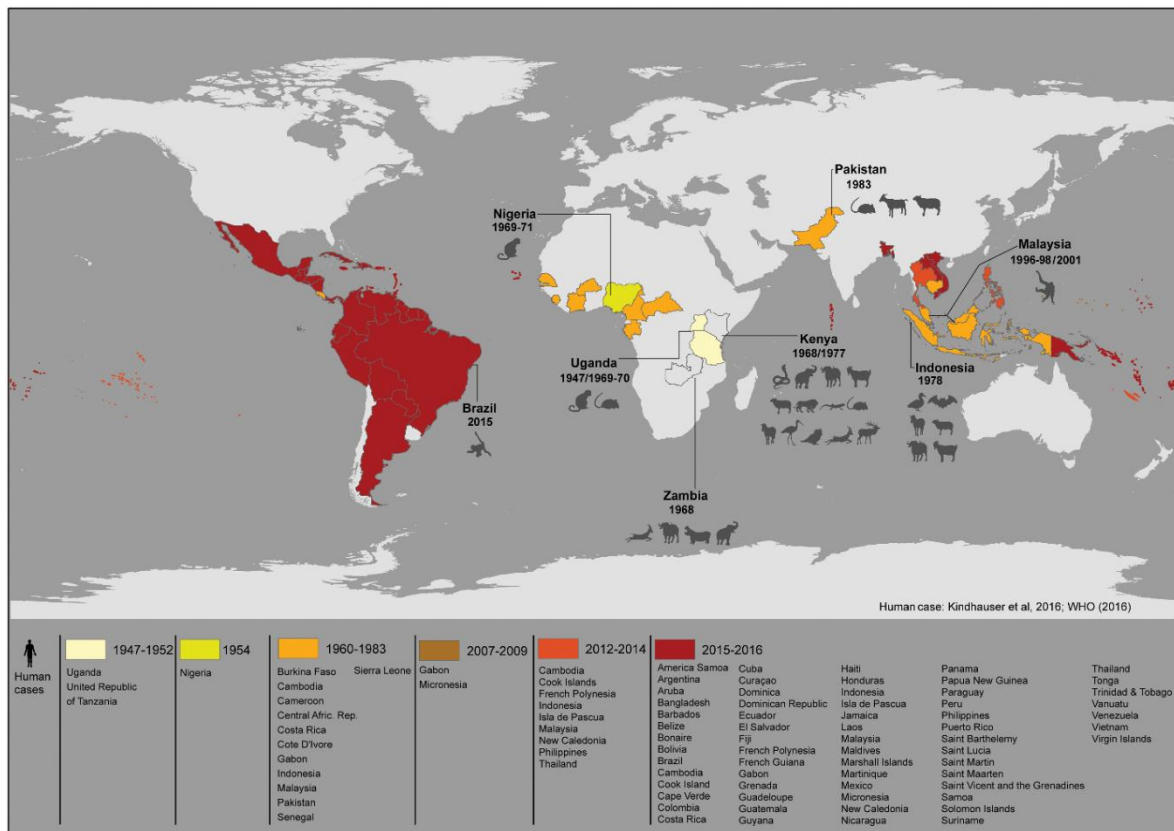


Figure 2.1 Global distribution of Zika virus in humans and animals since 1947. Autochthonous vector-borne human cases were documented in colored countries, while countered labeled with using animal profiles and years have documented Zika virus in naturally infected animals (Bueno *et al.*, 2016).

The most effective way to prevent ZIKV infection is to avoid being bitten by mosquitoes. This is accomplished by using mosquito repellent that is EPA-registered, being protected by door and window screens, removing standing water surrounding residences and using long-sleeved clothing (Hennessey, Fischer and Staples, 2016). In Africa, ZIKV was detected in *Aedes aegypti*, *Aedes africanus*, *Aedes apicoargenteus*, *Aedes luteocephalus*, *Aedes albopictus*, *Aedes vitattus*, *Aedes dalzieli*, *Aedes taylori*, *Aedes hirsutus*, *Aedes unilinaetus*, *Aedes metallicus*, *Aedes furcifer* and *Aedes opok*. The ZIKV has also been isolated from *Anopheles coustani*, *Culex perfuscus* and *Mansonia uniformis* mosquitoes (Shehu *et al.*, 2018).

3 The Zika Virus Life Cycle

The ZIKV particle enters an animal cell via clathrin-dependent endocytosis through cellular receptors on the cell surface. Upon fusion of the cell membrane and the viral particle, viral components are released into the cell, the viral RNA strand is translated for polyprotein formation. The new polyproteins are cleaved, forming NS and structural proteins, and assemble in the endoplasmic reticulum (ER) to form new virions. Viral replication via the polymerase occurs on the surface of the ER to produce double-stranded (ds) RNA, which is transcribed and replicated. The assembled virions enter the Golgi apparatus to mature into viral particles via cleavage by Furin-like protease and dock onto the inner cell membrane to exit the cell through exocytosis where they set off to infectious life cycles (Sreedharan, 2015; Lee *et al.*, 2018). Replicated viral particles in the blood of monkeys infected with ZIKV are transmitted to other monkeys through mosquito bites. Mosquitoes carrying infected blood also transmit the virus to people, and their infected blood are passed on to other people through mosquito bites, sexual transmission and other modes of distribution. Finally, when the virus is transmitted to a pregnant mother, it is passed on to her baby perinatally (Figure 2.2) (Besnard *et al.*, 2014).

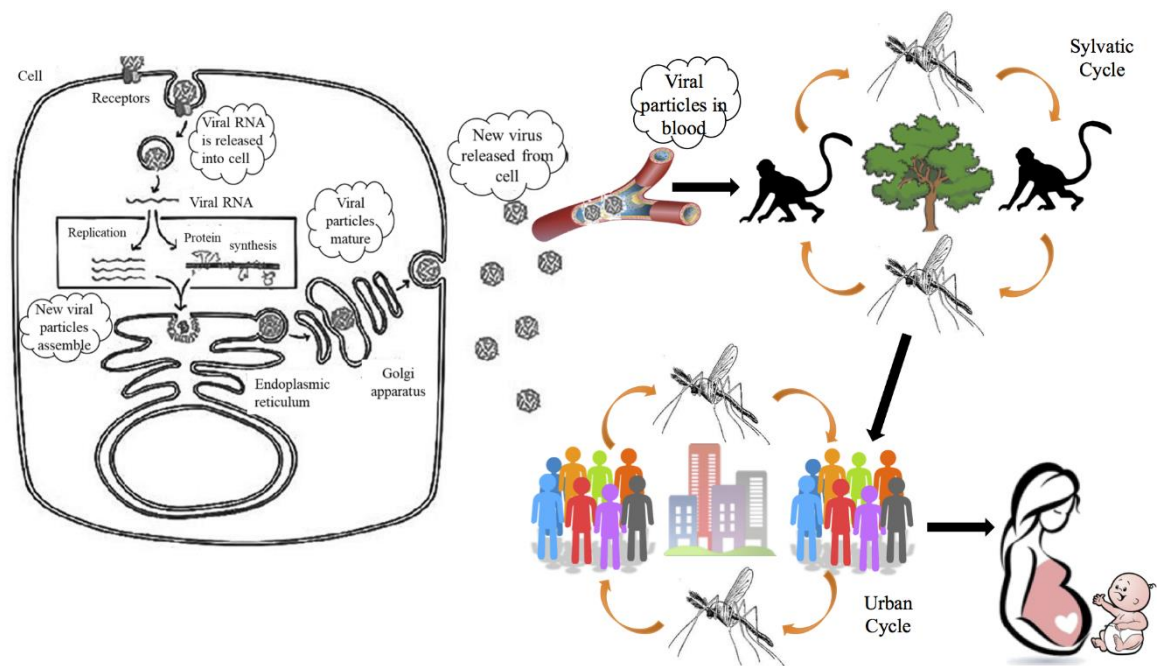


Figure 2.2 The life cycle of Zika virus in blood and in organisms. A key role player in the viral life cycle is the vector, which in this case is the *Aedes* mosquito (Adapted from (Sreedharan, 2015)).

4 Clinical Manifestation of Zika Virus

Since 2015, the distribution of ZIKV throughout the Western Hemisphere has been associated with congenital abnormalities, microcephaly and Guillain-Barré syndrome (Lazear and Diamond, 2016). Surprisingly, there is a broad range of cell types and body fluids in which ZIKV manifests. This is consistent with the incidences, modes of transmission and clinical manifestations that were documented during the current epidemic (Calvet *et al.*, 2018).

The general symptoms of ZIKV infection include mild flu-like symptoms, such as cutaneous rashes, arthralgia, low-grade fever, conjunctivitis and myalgia, which typically clear up within a week (A. Wang *et al.*, 2017). Although lately severe disease has affected people who have been infected with ZIKV. Associated diseases include thrombocytopenic purpura, thrombocytopenia and multiple organ failure (Brent *et al.*, 2016; Sharp *et al.*, 2016; Boyer Chammard *et al.*, 2017; Hersh, Gundacker and Boltax, 2017). It may be noted that infection of ZIKV has a preference to neural progenitor cells as

opposed adult neural cells, as seen by the rare occurrence of encephalitis and meningitis. This is also consistent with the ability of the virus to cause damage to the neonatal brain, resulting in impaired neurodevelopment and microcephaly in babies (Miner and Diamond, 2017). ZIKV infection has also manifested in eye tissue, leading to uveitis and conjunctivitis in adults (Furtado *et al.*, 2016; Agrawal *et al.*, 2018).

The most pressing concerns of the American ZIKV outbreak are the associated congenital abnormalities and number of stillborn babies. These inconsistent abnormalities include corpus callosum abnormalities, microcephaly, brainstem and cerebellum hypoplasia, cerebral calcifications, cortical deformities, intrauterine growth limitation, ventriculomegaly, enlarged cisterna magna and impeded myelination (Miner and Diamond, 2017). ZIKV infection of infants may also cause loss of hearing and vision, and more consequently optic neuritis, dislocation of the lens and mottling of retinal pigment epithelium (Vinhaes *et al.*, 2016; Singh *et al.*, 2017; Manangeeswaran *et al.*, 2018; Zaidi *et al.*, 2018).

A few cases of ZIKV infection are associated with autoimmunity, however, the mechanism of induction is unknown (Anaya *et al.*, 2016; Monsalve *et al.*, 2017; Acosta-Ampudia *et al.*, 2018). Guillain-Barré syndrome was associated with ZIKV infection during the French Polynesian, Brazilian and Colombian outbreaks, which presents as peripheral nerve degeneration and ascending paralysis (Brasil *et al.*, 2016). It either occurs simultaneously with ZIKV infection or as a repercussion, which implies that polyneuropathy occurs as a result of either direct infection, and/or autoimmunity (Mier-Y-Teran-Romero *et al.*, 2018).

5 Diagnosis of Zika Virus

The early symptoms of ZIKV infection present itself rather ambiguously, as they are indicative of several other illnesses and diseases. Therefore, verification of ZIKV infection requires laboratory evidence, such as tissue or fluid samples with detected ZIKV antigen or RNA (Baud *et al.*, 2017). Generally, diagnostic strategies used to detect other arboviruses are used to diagnose ZIKV infection. Acute-phase samples are tested for the ZIKV genome using quantitative reverse transcription PCR (RT-qPCR) and to detect specific anti-ZIKV IgG and IgM antibodies, serology assays such as enzyme-linked immunosorbent assay (ELISA) and immunofluorescence are used (Calvet, Dos Santos

and Sequeira, 2016). Clinical specimens such as amniotic fluid, placenta, saliva, cerebrospinal fluid (CSF), blood (serum and plasma) including cord blood, urine, semen, breast milk, tissues and vaginal secretion can be used to detect ZIKV (Gourinat *et al.*, 2015; Calvet *et al.*, 2016a, 2018; Calvet, Dos Santos and Sequeira, 2016; Mansuy *et al.*, 2016; Carod-Artal, 2018). Should a doctor detect microcephalic features of a fetus after an ultrasound, RT-qPCR and viral metagenomics can be used to identify ZIKV in the amniotic fluid of the pregnant woman and sequence the ZIKV genome (Khandia, Munjal and Dhama, 2017). Due to the transient nature of viremia, molecular techniques used, like RT-qPCR ought to be implemented soon after the onset of the infection, typically within a week, when ZIKV nucleic acids are present (Lanciotti *et al.*, 2008).

The plaque-reduction neutralization test (PRNT) is used to verify test results that are negative ZIKV nucleic acid tests, non-negative serology tests or presumed equivocal, positive or inconclusive. However, PRNT is labor intensive, strenuous, time consuming, cost-ineffective, demands specialized infrastructure and produces low yield (Shan, Ortiz, *et al.*, 2017). An improved diagnostic assay, called the multiplex microsphere immunoassay (MIA) is used to detect antibodies against ZIKV envelope (E) protein and NS proteins NS1 and NS5 (Wong *et al.*, 2017). Antigens of ZIKV may also be detected in tissue samples via immunohistochemistry. It is recommended that both serological and molecular tests be performed for a reliable and accurate diagnosis (Calvet, Dos Santos and Sequeira, 2016).

Despite having the knowledge of how to diagnose ZIKV, routine lab diagnosis is still lacking in resource-limited countries, such as Nigeria. Well-equipped labs for thorough diagnosis of ZIKV is still scarce, therefore, the reinforcement of health systems and workforce is crucial (Shehu *et al.*, 2018).

6 Components of Zika Virus

The enveloped ZIKV encloses an 11 kilobase viral genome made up of positive-sense, single stranded RNA, or (+)ssRNA. The genome of an individual ZIKV particle constitutes 3,419 amino acid residues and 10,794 nucleotide base pairs. Included is the open reading frame (ORF) comprising a 106 nucleotide long 5'-untranslated region (UTR) containing an m⁷gpppAmpN₂ and a 428 nucleotide long 3'-UTR that lacks a poly-A tail. A strand not too far from the 3' end that is crucial for viral replication

is a 90-120 nucleotide long strand that translates into a hairpin loop. Host cell furin-like proteases and viral serine proteases cleave the genome to produce segments that translate into functional domains of the virus. The polyprotein encoded by the ORF is cleaved into three structural proteins, Precursor of Membrane (PrM), Envelope (E) and Capsid (C). The rest of the genome encodes seven NS proteins, NS1, NS2A, NS2B, NS3, NS4A, NS4B and NS5 (van Hemert and Berkhout, 2016). The NS1, NS3 and NS5 proteins are highly conserved while the NS2a, NS2b, NS4a and NS4b are not. The arrangement of the genomic protein is as follows: 5'-C-PrM-E-NS1-NS2a-NS2b-NS3-NS4a-NS4b-NS5-3'. A vital step for virion maturation is the cleavage of PrM to form Pr and M by proteases located in the Golgi apparatus during particle release (Figure 2.3) (Li *et al.*, 2008; Nambala and Su, 2018).

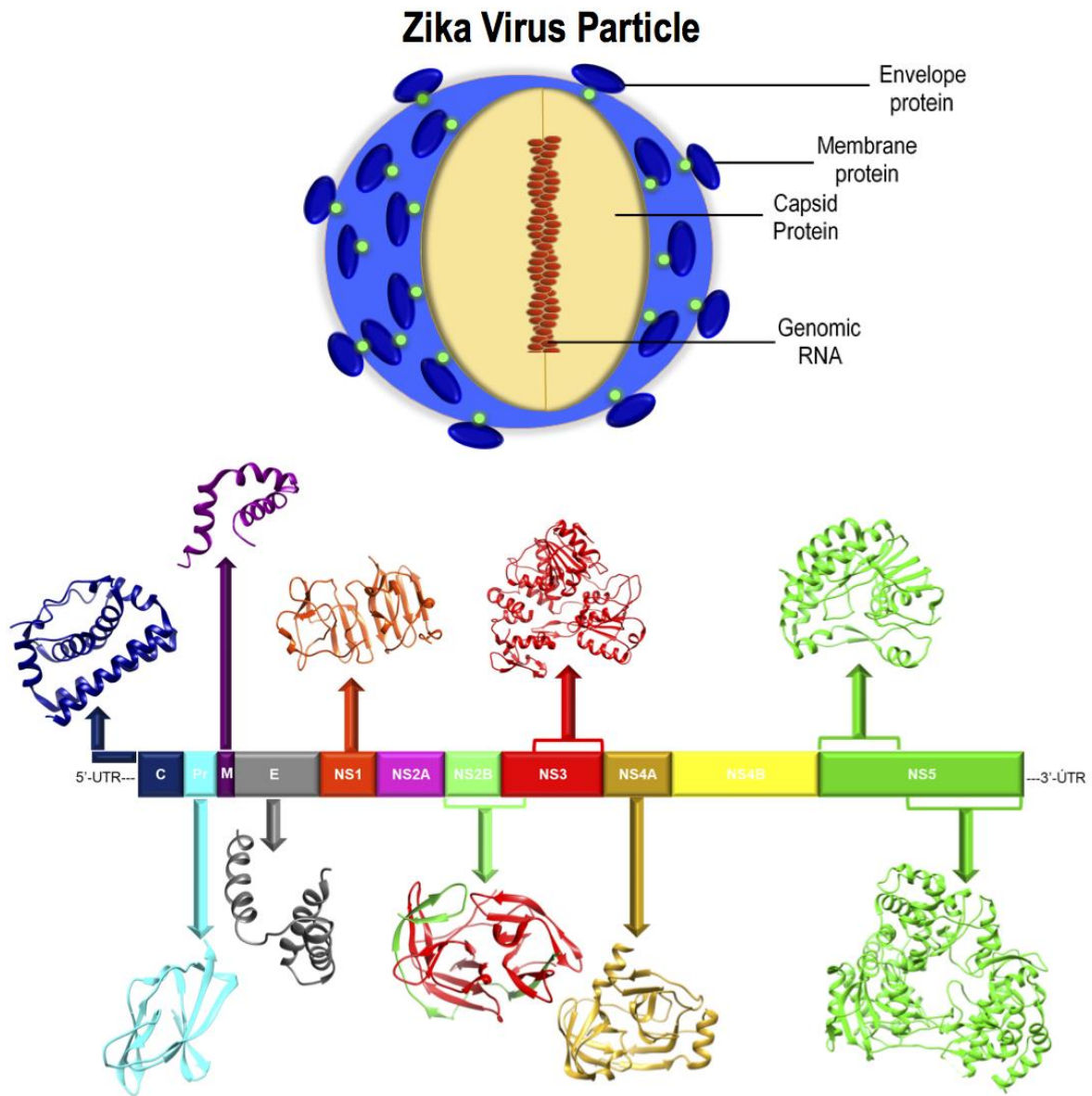


Figure 2.3 The Zika virion above segments of Zika virus genome with corresponding available crystal structures of encoded proteins (PDB: 4I31, 5GJB, 5H4I, 5IY3, 5U4W and 5YGH) (Prepared by Author).

7 Zika Virus Pathogenesis

In the mosquito vector, the virus replicates in salivary cells and the epithelial cell layer of central alimentary canal and small intestine (Guedes *et al.*, 2017; Lim *et al.*, 2018). The infectious ZIKV appears in the saliva of the mosquito after approximately five days. Upon biting, the mosquito cutaneously inoculates ZIKV into the host (Dudley *et al.*, 2017). Thereafter, fibroblasts, Langerhans cells and epidermal keratinocytes become infected (Olagnier *et al.*, 2016). It has been observed in African and Asian strains that when ZIKV enters the bloodstream, it mainly targets monocytes (Foo *et al.*, 2017). Monocytes have the ability to permeate the placenta, testes and brain, which are immune privileged sites (Benhar, London and Schwartz, 2012). Once the virus is transmitted, the ZIKV E protein contains the main epitope that mediates viral attachment to the host cell receptor, which is followed by endocytosis of the virus particles, nucleocapsid uncoating, and release of viral RNA into the host cell. The E protein has also been observed to enter the nucleus of the host cell upon ZIKV infection (Shehu *et al.*, 2018). This could justify the range of developmental complications that arise from ZIKV infection.

There is more than one way that ZIKV can be transmitted perinatally. It can occur via trophoblastic plug leakage, through the placenta, vertical transmission of the virus during delivery, or viral diffusion into the amniotic sac during its development (Boeuf *et al.*, 2016; Tabata *et al.*, 2016; Sarwar and Saqib, 2017; Winkler *et al.*, 2017). Infection of ZIKV through the placenta may compromise its ability to supply enough oxygen and nutrients to the growing foetus, contributing to microcephaly (Miner *et al.*, 2016). In 2016, a hypothesis was proposed that liver injury due to ZIKV infection leads to metabolite accumulation, including vitamin A, which may lead to the pathogenesis of microcephaly (Mawson, 2016). Buildup of vitamin A is toxic and has previously caused embryopathies such as microcephaly (Dibley and Jeacocke, 2001).

The virus is transmitted sexually during acute viral infection. Due to the potential neurological complications that may occur, this has special significance when the subjected partner is pregnant. The ZIKV tends to attack the nervous system by permeating the foetal blood-brain barrier. Upon attachment to neuronal cells, ZIKV RNA is released and induces apoptosis, which ultimately causes impediment of neuronal growth, proliferation and differentiation (Musso, Roche, Robin, *et al.*, 2015; Mansuy *et al.*, 2016; Turmel *et al.*, 2016; Devhare *et al.*, 2017; Winkler *et al.*, 2017).

In 2017, Simonin *et al.* found genetic pathogenic differences between the Asian and African ZIKV strains (Figure 2.4) *in vivo* and *ex vivo*, where African strains are more virulent. Asian strains of ZIKV may contribute to the ability to initiate persistent infections within foetal nervous systems, but African strains can cause more acute infections (Simonin *et al.*, 2017). Should the African strain infect a pregnant mother in her early stages of pregnancy, it could lead to natural abortion, but infection of the same woman by the Asian strain may only cause chronic effects without foetal demise (Shehu *et al.*, 2018).

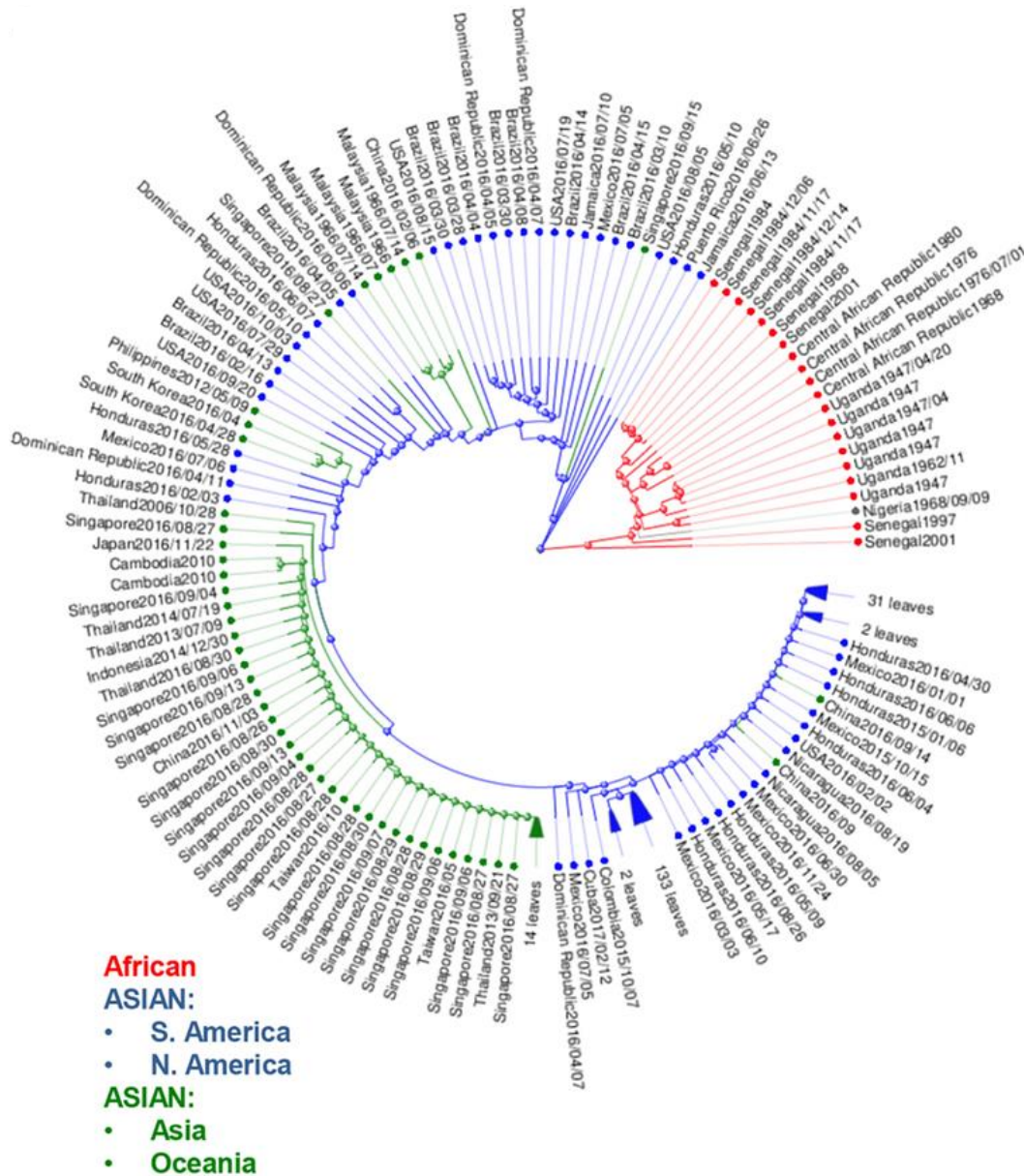


Figure 2.4 Phylogenetic analysis of Zika virus genomes based on region. Phylogenetic analysis of existing genomes was categorized by lineage and then continent of isolation. Asian strains (America) were grouped in blue, African strains in red, and strains from Asia and Oceania in green (Beaver *et al.*, 2018).

Upon onset of ZIKV infection, the immune system reacts by developing IgM, which persists in the blood stream for approximately three months. This is followed by the development of IgG, which persists in the blood stream for years (Calvet *et al.*, 2018). Upon viral attack, a cell releases interferon (IFN) to warn other cells to enhance their defenses. The NS5 protein of ZIKV antagonizes the IFN-I response to stimulate E3 ubiquitin ligase UBR4-independent degradation of STAT2 in humans (Grant *et al.*, 2016; Miner and Diamond, 2017).

8 Pharmacological Targets of Zika Virus

Identifying and understanding viral targets are important in the drug design and discovery process. Among the NS proteins of ZIKV, the NS3 and NS5 proteins are lead targets for the design of anti-ZIKV drugs, while the NS1, E and PrM proteins can be used for prophylactic antibody and vaccine development (Barzon *et al.*, 2016).

The ZIKV C protein is a symmetric, icosahedral homodimer that is essential for enclosure of viral RNA during assembly of the ZIKV particle. The C protein has a sphere-shaped lipid bilayer membrane that stems from the host cell (A. Wang *et al.*, 2017). It constitutes a hydrophobic region involved in interaction and dimerization with the membrane, and an RNA-binding region (Fontaine *et al.*, 2018).

The ZIKV PrM protein constitutes a C-terminal transmembrane domain, a central ectodomain and the Pr N-terminal domain. For assembly and release of virions that are capable of fusion, furin-like proteases of the host cell cleave the Pr domain (Nambala and Su, 2018).

The E protein is the key target for neutralizing antibodies as it comprises of immunogenic epitopes – ectodomains E-DI, E-DII and E-DIII. It functions in the recognition of entry cofactors and host cell receptors (Barzon *et al.*, 2016). The DII domain has a fusion loop in its apex, which is hydrophobic

in nature and responsible for penetration into the cellular membrane (Bressanelli *et al.*, 2004). This domain is identified by cross-reactive antibodies with low neutralizing efficiency, while the DIII domain is identified by protective neutralizing antibodies. The DIII domain resembles an immunoglobulin and comprises of the receptor-binding site (J. Wang *et al.*, 2017). The ZIKV E protein contains a glycosylation site at Asparagine residue 154 and a five-residue insertion, as compared to DENV E protein, which is glycosylated at Asparagine residues 67 and 153. Alteration of these glycosylation sites will influence neurovirulence and transmission of ZIKV (Fontes-Garfias *et al.*, 2017; Wen *et al.*, 2018).

The glycosylated NS1 protein plays a major role in immune evasion and ZIKV maturation and replication (Muller and Young, 2013). The NS1 interacts with the E and PrM proteins and forms intracellular homodimers and extracellular hexameric lipoproteins (Edeling, Diamond and Fremont, 2014). It also exhibits various electrostatic characteristics involved in host interactions that may influence immunogenicity and pathogenesis (Song *et al.*, 2016). The NS1 gene of the Asian ZIKV strain that causes majority of the recent epidemics contains a mutation that augments mosquito infection and is responsible for the inhibition of IFN- β induction (Xia *et al.*, 2018).

Information regarding the NS2A protein lacking in literature. It is a hydrophobic constituent of the replication complex and regulates host cellular defenses against viruses (Leung *et al.*, 2008). Yoon *et al.* (2017) have shown that the ZIKV NS2A protein expression decreases proliferation, causes radial glial cells to differentiate early and leads to abnormal neuronal positioning in infants (Yoon *et al.*, 2017). A mutation of amino acid residue 175 (A \rightarrow V) in the NS2A protein impairs synthesis of ZIKV RNA *in vivo* (Márquez-Jurado *et al.*, 2018). There is a current lack of an experimentally-derived crystal structure of the NS2A protein.

Like the NS2A protein, the ZIKV NS2B cofactor is a small protein situated within the membrane. It interacts with and chaperones the NS3 protease by means of a central hydrophilic region, whereas the hydrophobic regions secure the NS2B–NS3 complex to the membrane of the ER (Barzon *et al.*, 2016). the NS2B cofactor region from Zika virus protease is essential for recognition of host cell substrates (Hill *et al.*, 2018).

The ZIKV NS3 protein is made up of two connected domains that are globular in shape (Jain *et al.*, 2016). The helicase occupies the C-terminal end, while the protease is situated at the N-terminal end.

The helicase is a monomer associated with viral RNA unwinding for replication, while the protease binds to the NS2B cofactor and is involved in polyprotein cleavage (Saw *et al.*, 2017).

Like the NS2A, the ZIKV NS4A and NS4B are integral membrane proteins and components of the replication complex, also associated with the NS3 protein. The NS4A and NS4B proteins are responsible for inhibiting the Akt-mTOR pathway and cellular dysregulation during ZIKV infection, causing defective productions of neurons from neural stem cells (NSCs) and abnormal stimulation of autophagy in NSCs of fetuses (Liang *et al.*, 2016). The ZIKV NS4A protein also inhibits the interaction of the RLR-mitochondrial antiviral-signaling protein that induces immune responses upon viral attack. Therefore, the NS4A plays a role in immune evasion (Ma *et al.*, 2018). Till date, there has been no experimentally-determined crystal structure of the ZIKV NS4B enzyme.

The ZIKV NS5 protein represents the largest protein that is conserved among *flaviviruses* (Duan *et al.*, 2017). The C-terminal RdRp is responsible for viral RNA synthesis, while the N-terminal MTase is responsible for methylation and capping the 5' end of the viral RNA (Coutard *et al.*, 2017; Zhang *et al.*, 2017).

8.1 The NS3 Helicase

The ZIKV NS3 helicase belongs to the SF2 superfamily of helicases (Singleton, Dillingham and Wigley, 2007). The helicase domain occupies amino acid residues 168-617 of the entire NS3 enzyme and contains three domains that are similar to each other based on size (Figure 2.5). Residues 182–327 that make up Domain 1 and residues 328-480 that form Domain 2 constitute α/β RecA-like folds arranged one behind the other, which are conserved in Superfamily 1 and 2 helicases (Jain *et al.*, 2016). Domain 1 comprises motifs I (Walker A or P loop), Ia, II (Walker B) and III, which are divided from motifs IV, IVa, V and VI of domain 2. Motifs I, II and VI are fundamental in ATP binding and hydrolysis, while motifs Ia, IV and V are involved in interdomain communication and RNA binding. The helicase of ZIKV and DENV4 bind ATP at the lower end of the fissure at the border of domains 1 and 2, while the RNA-binding pocket separates domains 1 and 2 from domain 3. Domain 2 connects with Domain 3 through a β -hairpin strand of domain 2, which serves to enable unwinding of ds RNA. Domain 3 mainly contain α -helical structures that interact with RNA in addition to the NS5 RdRp (Saw *et al.*, 2017).

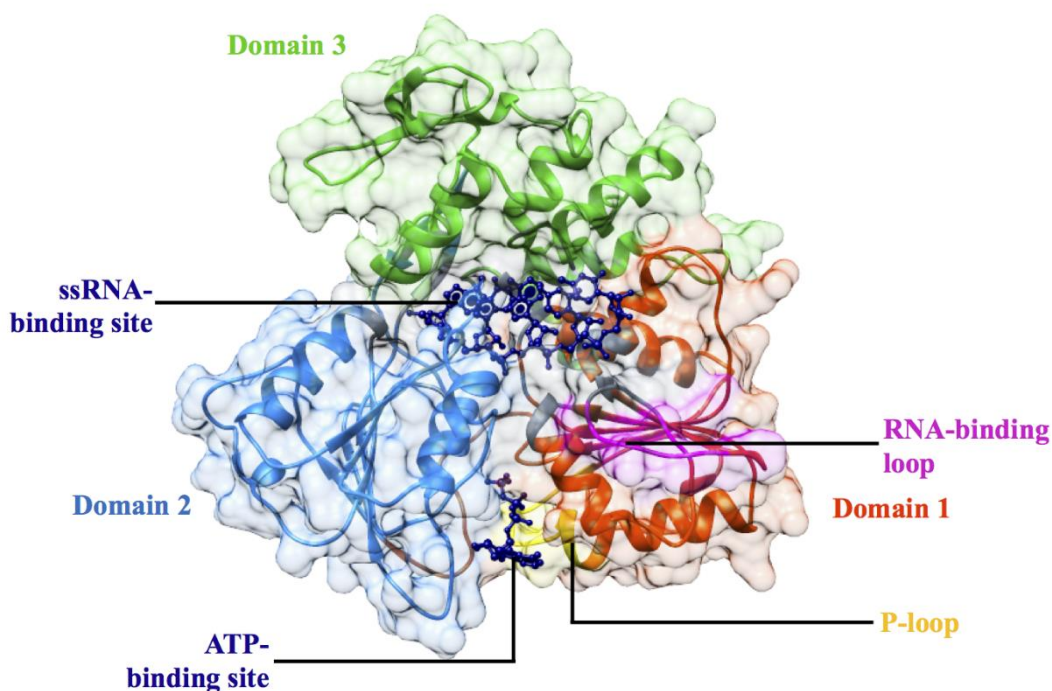


Figure 2.5 The NS3 helicase of Zika virus. The three domains of comparable size are demonstrated in orange (Domain 1), blue (Domain 2) and green (Domain 3). The P-loop of Domain 1 is represented in yellow, which surrounds the binding site of ATP. The RNA-binding loop whose flexibility influences RNA replication is shown in pink (Prepared by Author).

8.2 The NS5 Methyltransferase

The first 260 amino acid residues of the ZIKV NS5 protein makes up the MTase enzyme. The 33kDa enzyme has three binding sites that bind ssRNA, SAM (a methyl donor and natural substrate) and guanosine triphosphate (GTP) (Coloma *et al.*, 2016). The MTase consists of four α -helices in the center of seven β -sheets. The MTase consists of a K-D-K-E catalytic tetrad that is conserved among *flaviviruses*. The N-terminal end, especially residue (D146) of the MTase is the functional end that serves to methylate the 5' cap at positions N-7 and ribose 2'-OH, which is essential for viral RNA replication. (Stephen *et al.*, 2016). Capping includes four stages (Figure 2.6) (Chatrin *et al.*, 2018). Apart from methylation, the MTase is also involved in the initiation and elongation of RNA polymerization by the RdRp (Coutard *et al.*, 2017).

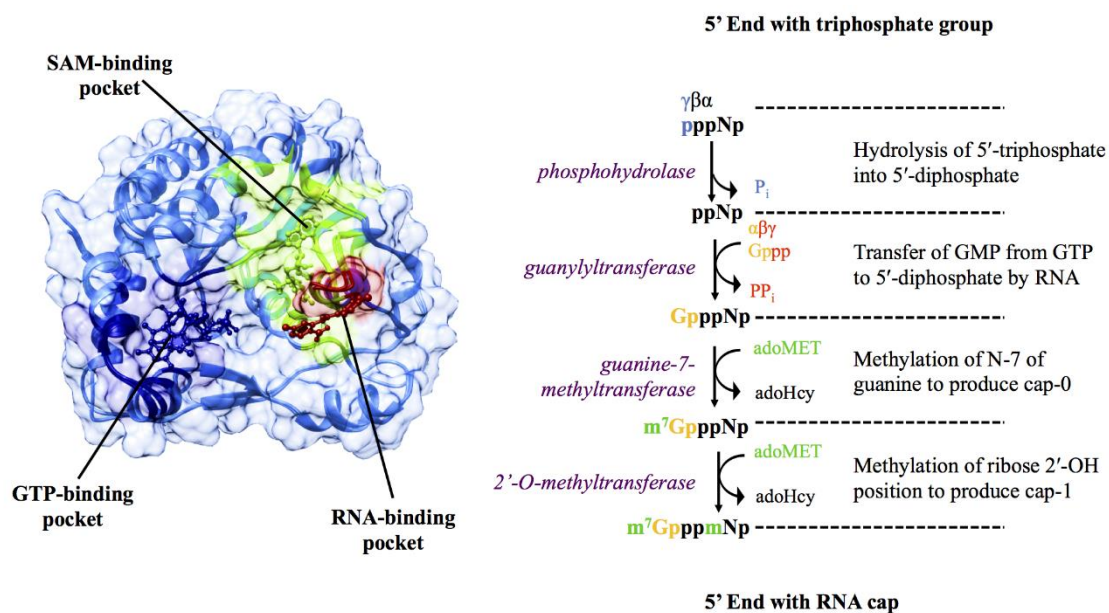


Figure 2.6 Diagram represents the methyltransferase enzyme of the Zika virus NS5 protein on the left, showing the three different binding-pockets, and the four-step process of capping by the methyltransferase on the right (Prepared by Author).

9 Therapeutic targets of Host

Apart from the viral targets, identifying the host factors associated with viral inhibition and activation of immune response against viral attack are especially important aspects of research. Host proteins that are established as promoters of ZIKV infection include AXL, Tyro-3, DC-SIGN, TIM-1 and TIM-4 (Barzon *et al.*, 2016).

In cells of the human placenta, the most expressed ZIKV entry factor is TIM-1 (Tabata *et al.*, 2016). In radial glia of the developing human cortex, AXL is expressed abundantly during neurogenesis (Nowakowski *et al.*, 2016; Retallack *et al.*, 2016). In mammalian cells, ZIKV infects foetal endothelial cells via AXL tyrosine kinase receptors, allowing passage of the virus into the foetal bloodstream and tissues (Olagnier *et al.*, 2016; Meertens *et al.*, 2017; Richard *et al.*, 2017).

Both innate and inflammatory immune responses are activated when ZIKV infects a host cell, inducing cellular expression of IFN- α , IFN- β , CCL5, IFN regulatory factor 7 (IRF7), MDA5, RIG-I and TLR3 (Barzon *et al.*, 2016). Increased expression and activation of TLR3 due to ZIKV infection caused shrinkage of organelles, erratic neuron production and apoptosis (Dang *et al.*, 2016), while TLR3 inhibition via small interfering RNA (siRNA) augmented ZIKV replication (Hamel *et al.*, 2015). Therefore, TLR3 is a major factor in the activation of host antiviral response against ZIKV.

Replication of ZIKV can be reduced via regulating the innate immune response of the host through treatment with IFN-I and IFN-II (Lazear *et al.*, 2016; Chaudhary *et al.*, 2017; Lee and Ng, 2018). Other host restriction proteins in ZIKV inhibition include IFN-induced transmembrane proteins, which may be promising therapeutic targets for drug design (Saiz *et al.*, 2018). The *SPCSI* gene is essential for selective cleavage of *flavivirus* proteins (Zhang *et al.*, 2016).

10 Advances in Design & Development of Anti-Zika Virus Drugs & Therapies

There is no effective antiviral treatment currently available for ZIKV. Although recently, much effort has been put into the hunt for potential antivirals using various approaches, from drug-based to target-based. The identified potential antiviral compounds include those that target the host as well as the virus (Saiz and Martín-Acebes, 2017). The following up-to-date information will promote design and development of more potent drugs to curb ZIKV.

10.1 Small Molecule Inhibitors

Specific anti-ZIKV drugs are currently lacking. Patients infected with ZIKV are treated for their symptoms, such as anti-histamines to treat itchy rashes, fluids for dehydration and acetaminophen for pain and fever (Centers for Disease Control and Prevention, 2018). Several compounds have been shown to inhibit different stages of the ZIKV life cycle (Figure 2.7).

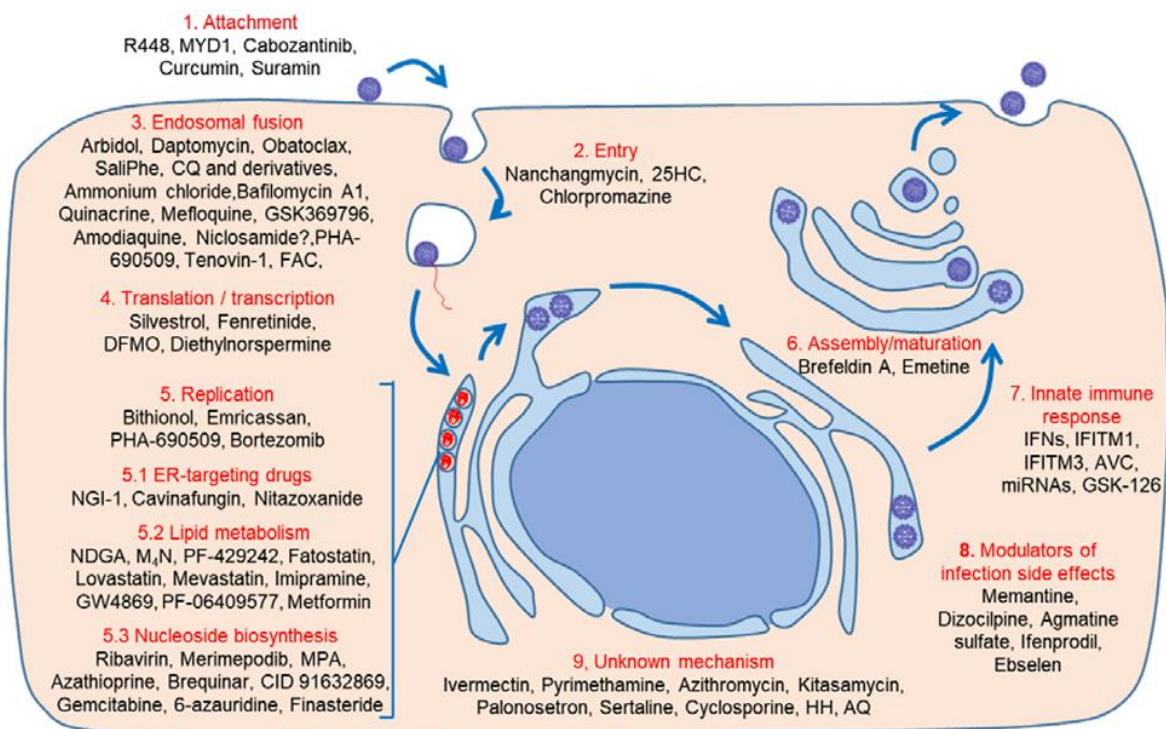


Figure 2.7 Drugs that target different stages of the Zika virus life cycle (Saiz *et al.*, 2018).

Two main classes of small molecule inhibitors of ZIKV are nucleoside/nucleotide inhibitors and non-nucleoside inhibitors. In the nucleoside/nucleotide group, NITD008, sofosbuvir, BCX4430 and MK-0608 have presented moderate *in vitro* and *in vivo* potency, although none of them totally prevent demise of mice infected with ZIKV (Xie *et al.*, 2017). Sofosbuvir is an FDA-approved treatment for Hepatitis C virus (HCV) with low efficacy against ZIKV (Reznik and Ashby, 2017). Nucleoside/nucleotide inhibitors are the basis of antiviral drugs due to its broad-spectrum inhibition of viruses from a single lineage.

Non-nucleoside inhibitors have been identified through cell-based screening in an effort to repurpose drugs, which concentrated on pharmacologically active compounds, FDA-approved compounds and compounds already in clinical trial. This led to the identification of daptomycin, palonosetron, emricasan, brequinar, mefloquine, ivermectin, mycophenolate mofetil, niclosamide, and antimalarial compounds. Of these, drugs approved for pregnancy B category include palonosetron, niclosamide and daptomycin. However, these drugs have presented low potency *in vitro* and no potency *in vivo* (Barrows *et al.*, 2016; Kmietowicz, 2016; Pascoalino *et al.*, 2016; Xu *et al.*, 2016; Adcock *et al.*,

2017). Table 2.1 represents compounds that have demonstrated anti-ZIKV activity in different cell types.

Table 2.1 Compounds that represent potential antiviral compounds against the Zika virus (Devnarain, Ramharack and Soliman, 2017; Munjal *et al.*, 2017; Saiz and Martín-Acebes, 2017; da Silva, Martins and Jardim, 2018).

Compound	Description	Tested cell/assay	Reference
Emricasan	Pan-caspase inhibitor	Glioblastoma SBN-19, hNPCS and human astrocytes cells	(Xu <i>et al.</i> , 2016)
Palonosetron*	Nausea/vomiting drug	<i>In silico</i>	(Barrows <i>et al.</i> , 2016)
Bortezomib	20S proteasome inhibitor	C6/36, vero cells, C57BL/6 mice	(Xin <i>et al.</i> , 2017)
Bromocriptine	Ergoline derivative and dopamine agonist	Vero cells	(Chan <i>et al.</i> , 2017)
Brequinar	Pyrimidine synthesis inhibitor	<i>In silico</i>	(Adcock <i>et al.</i> , 2017)
Chloroquine[#]	Antimalarial agent	Vero, hNSC and hBMEC cells	(Shiryaev <i>et al.</i> , 2017)
Niclosamide*, PHA-690509	Antiparasitic drugs	Glioblastoma SBN-19, hNPCS and human astrocytes	(Xu <i>et al.</i> , 2016)
Ivermectin[#]	Antiparasitic drugs	HuH7 cells	(Kmietowicz, 2016)
Daptomycin*	Lipopeptide antibiotic	HuH7 cells	(Barrows <i>et al.</i> , 2016)
Mycophenolic acid	Immune-suppressant drug	HuH7 cells	(Barrows <i>et al.</i> , 2016)
Sertraline[#]	Antidepressant	HuH7 cells	(Barrows <i>et al.</i> , 2016)
Pyrimethamine	Antimalarial agent	HuH7 cells	(Barrows <i>et al.</i> , 2016)
Cyclosporine A	Immunosuppressant	HuH7 cells	(Barrows <i>et al.</i> , 2016)
Azathioprine*	Immunosuppressant	HuH7 cells	(Barrows <i>et al.</i> , 2016)

Mefloquine*	Antimalaria drug	HuH7 cells	(Barrows <i>et al.</i> , 2016)
Sofosbuvir*	Adenosine analog	HNPCs, Huh-7, SH-5YSY, Vero cells, neurosphere, <i>in silico</i>	(Reznik and Ashby, 2017)
Curcumin	Antioxidant and anti-inflammatory agent	HeLa cells	(Mounce <i>et al.</i> , 2017)
25-Hydroxycholesterol	Regulates cholesterol and immunity	BHKK-21	(Li <i>et al.</i> , 2017)
Epigallocatechin gallate	Phenolic antioxidant	Vero cells	(Carneiro <i>et al.</i> , 2016)
Saliphenylhalamide	Immuno-modulatory agent	Human telomerase reverse transcriptase (hTERT)-immortalized retinal pigment (RPE)	(Kuivanen <i>et al.</i> , 2017)
GSK126	EZH2 MTase inhibitor	TERT-immortalized HFF cells	(Arbuckle <i>et al.</i> , 2017)
Pentagalloylglucose	Phenolic antioxidant	Vero B4	(Behrendt <i>et al.</i> , 2017)
Heparin	Anticoagulant	Human neural progenitor cells	(Ghezzi <i>et al.</i> , 2017)
Suramin	Anti-parasitic drug	Vero cells	(Tan <i>et al.</i> , 2017)
Obatoclox	Pro-apoptotic protein	hTERT-RPE	(Kuivanen <i>et al.</i> , 2017)
Nanchangmycin	Antibiotic	U2OS cells	(Rausch <i>et al.</i> , 2017)
Novobiocin, lopinavir-ritonavir	Antibiotic, HIV antiviral	Vero/Huh-7/ <i>in silico</i>	(Yuan <i>et al.</i> , 2017)
Aprotinin	Competitive serine protease inhibitor	<i>In silico</i>	(Chen <i>et al.</i> , 2016)
N-(4-hydroxyphenyl) retinamide	Pro-apoptotic agent	Vero cells	(C. Wang <i>et al.</i> , 2017)
Merimepodib	Antiproliferative agent	Huh7	(Tong <i>et al.</i> , 2018)
Gemcitabine	Cytidine analog	hTERT-RPE	(Kuivanen <i>et al.</i> , 2017)
Cimiracemate B, Rosemarinic acid	Phenylpropanoid, antioxidant.	<i>In silico</i>	(Byler, Ogungbe and Setzer, 2016)

6-methylmercaptopurine riboside	Thiopurine nucleoside analogue	Vero and SII—SY5Y neuronal cells	(de Carvalho <i>et al.</i> , 2017)
4',7-digalloylecatechin, prenylated chalcone, 2',4,4'-trihydroxy-3,3'-diprenylchalcone, bis-indole alkaloid flinderole, lignan di-O-demethylisoguaiacin	ZIKV NS5 RdRp inhibitors	<i>In silico</i>	(Byler, Ogungbe and Setzer, 2016)
Nordihydroguaiaretic Acid	Hypolipidemic drug	Vero cells	(Merino-Ramos <i>et al.</i> , 2017)
7-deaza-2'-C-methyladenosine (CMA), 2'-C-methylcytidine, 2'-C-methylguanosine, 2'-C-methyluridine	Nucleoside analogues	Vero, Human nUKF-NB-4 and PS cells	(Zmurko <i>et al.</i> , 2016)

10.2 Prophylactic Antibodies and Vaccines

The overwhelming effects of ZIKV have called on the urgency of effective therapeutic agents and a vaccine. Developmental stage vaccines against ZIKV include nucleic acid-based vaccines, inactivated virus, subunit vaccines, live vector vaccines, recombinant ZIKV, and virus-like particles (Alam *et al.*, 2017; Ali *et al.*, 2017).

Epitopes of B and T cells have been identified, which are crucial in the development of vaccines. These include HLA-B7 (B cells), QTLTPVGRL (T cells) and IRCIGVSNRDFV (T cells) (Ali *et al.*, 2017). In 2016, researchers published work of DNA vaccines that express ZIKV E and PrM, and a sequence of deletion mutants, which prevented viraemia in mice (Larocca *et al.*, 2016). In 2017, a live-attenuated vaccine containing a 3'-UTR deletion of 10 nucleotides prevented viraemia and induced protective immunity and a strong T cell response (Shan, Muruato, *et al.*, 2017). An RNA vaccine encoding ZIKV PrM-E and modified using 1-methylpseudouridine, also known as mRNA-LNP, showed safe and effective moderate immunization in mice and macaques (Pardi *et al.*, 2017). Two immunizations using this vaccine decreased foetal mice infection and totally rescued a viability defect (Richner *et al.*, 2017). This vaccine entered combined phase I/II clinical trial. In 2018, an attenuated vaccine based on recombinant vesicular stomatitis virus was developed, which expressed

PrM-E-NS1 ZIKV polyprotein. It stimulated T cell immune response, ZIKV antibodies (Abs) and conferred protection against ZIKV in mice (A. Li *et al.*, 2018). Potential vaccines that are currently in clinical trials are listed in Table 2.2 below.

Table 2.2 Stages of Zika virus vaccines that entered clinical trials (Adapted from Garg, Mehmetoglu-Gurbuz and Joshi, 2018).

Vaccine Name	Antigen	Platform	Phase	Clinical Trial No.	Anticipated End Date
VRC 319	PrM-E	DNA vaccine	I	NCT02840487	Dec 2018
VRC 320	PrM-E	DNA vaccine	I	NCT02996461	Dec 2018
VRC 705	PrM-E	DNA vaccine	II	NCT03110770	Jan 2020
GLS 5700	PrM-E	DNA vaccine	I	NCT02887482	Jun 2018
GLS 5700	PrM-E	DNA vaccine	I	NCT02809443	Nov 2017
ZPIV	Whole virus	Purified inactivated virus	I	NCT02963909	Feb 2019
ZPIV	Whole virus	Purified inactivated virus	I	NCT02952833	Jun 2019
ZPIV	Whole virus	Purified inactivated virus	I	NCT02937233	Jun 2018
ZPIV	Whole virus	Purified inactivated virus	I	NCT03008122	Jan 2020
VLA1601	Whole virus	Purified inactivated virus	I	NCT03425149	Nov 2018
MV-ZIKA	PrM-E in measles vector	Live attenuated recombinant vaccine	I	NCT02996890	Apr 2018
mRNA-1325	PrM-E	mRNA vaccine	I/II	NCT03014089	Sep 2018
TAK-426	Whole virus	Purified inactivated virus	I	NCT03343626	Sep 2020
rZIKV/D4D30-713	Whole genome	Live attenuated virus	I	NCT03611946	Sep 2019
MR 766	Whole virus	Purified inactivated virus	I	N/A	N/A

The third domain of ZIKV E protein was inhibited by ZKA64 human monoclonal Ab, and prevented death in mice (Stettler *et al.*, 2016). However, they do not support Ab-dependent enhancement and certain mutations must be engineered, *flaviviruses* often develop resistance to Abs and the cost of development still limits its use especially in third-world countries (Xie *et al.*, 2017). The development of EDE1 class of Abs have shown to regulate fatal ZIKV infection (Ali *et al.*, 2017). An effective human monoclonal Ab ZIKV-117 inhibited E protein from different Asian-American and African strains *in vitro* and *in vivo*, by significantly decreasing foetal and placental infection, tissue pathology and demise (Hasan *et al.*, 2017).

The considerable development that has been made regarding discovery of anti-ZIKV therapeutics remains at an initial phase of discovery. It will be several years until ZIKV therapy is approved by the FDA.

11 References

Acosta-Ampudia, Y. *et al.* (2018) 'Autoimmune Neurological Conditions Associated With Zika Virus Infection.', *Frontiers in molecular neuroscience*. Frontiers Media SA, 11, p. 116. doi: 10.3389/fnmol.2018.00116.

Adcock, R. S. *et al.* (2017) 'Evaluation of anti-Zika virus activities of broad-spectrum antivirals and NIH clinical collection compounds using a cell-based, high-throughput screen assay', *Antiviral Research*, 138, pp. 47–56. doi: 10.1016/j.antiviral.2016.11.018.

Agrawal, R. *et al.* (2018) 'Zika Virus and the Eye', *Ocular Immunology and Inflammation*, 26(5), pp. 654–659. doi: 10.1080/09273948.2017.1294184.

Alam, A. *et al.* (2017) 'Recent trends in ZikV research: A step away from cure', *Biomedicine & Pharmacotherapy*, 91(1), pp. 1152–1159. doi: 10.1016/j.biopha.2017.05.045.

Ali, A. *et al.* (2017) 'Advances in research on Zika virus', *Asian Pacific Journal of Tropical Medicine*. No longer published by Elsevier, 10(4), pp. 321–331. doi: 10.1016/J.APJTM.2017.03.020.

Anaya, J.-M. *et al.* (2016) 'Zika virus and neurologic autoimmunity: the putative role of gangliosides.', *BMC medicine*. BioMed Central, 14, p. 49. doi: 10.1186/s12916-016-0601-y.

Arbuckle, J. H. *et al.* (2017) 'Inhibitors of the Histone Methyltransferases EZH2/1 Induce a Potent

Antiviral State and Suppress Infection by Diverse Viral Pathogens.’, *mBio*. American Society for Microbiology (ASM), 8(4), pp. 01141-17. doi: 10.1128/mBio.01141-17.

Barrows, N. J. *et al.* (2016) ‘A Screen of FDA-Approved Drugs for Inhibitors of Zika Virus Infection’, *Cell Host and Microbe*, 20(2), pp. 259–270. doi: 10.1016/j.chom.2016.07.004.

Barzon, L. *et al.* (2016) ‘Zika virus: from pathogenesis to disease control’, *FEMS Microbiology Letters*. Edited by A. van Vliet. Oxford University Press, 363(18), p. fnw202. doi: 10.1093/femsle/fnw202.

Baud, D. *et al.* (2017) ‘An update on Zika virus infection’, *The Lancet*. Elsevier, 390(10107), pp. 2099–2109. doi: 10.1016/S0140-6736(17)31450-2.

Beaver, J. T. *et al.* (2018) ‘Evolution of Two Major Zika Virus Lineages: Implications for Pathology, Immune Response, and Vaccine Development’, *Frontiers in Immunology*. Frontiers, 9, p. 1640. doi: 10.3389/fimmu.2018.01640.

Behrendt, P. *et al.* (2017) ‘Pentagalloylglucose, a highly bioavailable polyphenolic compound present in Cortex moutan, efficiently blocks hepatitis C virus entry’, *Antiviral Research*, 147, pp. 19–28. doi: 10.1016/j.antiviral.2017.09.006.

Benhar, I., London, A. and Schwartz, M. (2012) ‘The privileged immunity of immune privileged organs: the case of the eye.’, *Frontiers in immunology*. Frontiers Media SA, 3, p. 296. doi: 10.3389/fimmu.2012.00296.

Besnard, M. *et al.* (2014) ‘Evidence of perinatal transmission of zika virus, French Polynesia, December 2013 and February 2014’, *Eurosurveillance*, 19(13), pp. 8–11. doi: 10.2807/1560-7917.ES2014.19.13.20751.

Boeuf, P. *et al.* (2016) ‘The global threat of Zika virus to pregnancy: epidemiology, clinical perspectives, mechanisms, and impact.’, *BMC medicine*. BioMed Central, 14(1), pp. 112–120. doi: 10.1186/s12916-016-0660-0.

Boyer Chammard, T. *et al.* (2017) ‘Severe Thrombocytopenia after Zika Virus Infection, Guadeloupe, 2016.’, *Emerging infectious diseases*. Centers for Disease Control and Prevention, 23(4), pp. 696–698. doi: 10.3201/eid2304.161967.

Brasil, P. *et al.* (2016) ‘Guillain-Barre syndrome associated with Zika virus infection’, *Lancet*, 387(1), p. 1482. doi: 10.1016/S0140-6736(16)30058-7.

Brent, C. *et al.* (2016) ‘Preliminary Findings from an Investigation of Zika Virus Infection in a Patient with No Known Risk Factors — Utah, 2016’, *MMWR. Morbidity and Mortality Weekly Report*,

65(36), pp. 981–982. doi: 10.15585/mmwr.mm6536e4.

Bressanelli, S. *et al.* (2004) ‘Structure of a flavivirus envelope glycoprotein in its low-pH-induced membrane fusion conformation.’, *The EMBO journal*. European Molecular Biology Organization, 23(4), pp. 728–38. doi: 10.1038/sj.emboj.7600064.

Bueno, M. G. *et al.* (2016) ‘Animals in the Zika Virus Life Cycle: What to Expect from Megadiverse Latin American Countries’, *PLOS Neglected Tropical Diseases*. Edited by A. C. A. Clements. Public Library of Science, 10(12), p. e0005073. doi: 10.1371/journal.pntd.0005073.

Byler, K. G., Ogungbe, I. V. and Setzer, W. N. (2016) ‘In-silico screening for anti-Zika virus phytochemicals’, *Journal of Molecular Graphics and Modelling*, 69, pp. 78–91. doi: 10.1016/j.jmgm.2016.08.011.

Calvet, G. *et al.* (2016) ‘Detection and sequencing of Zika virus from amniotic fluid of fetuses with microcephaly in Brazil: a case study’, *The Lancet Infectious Diseases*. Elsevier, 16(6), pp. 653–660. doi: 10.1016/S1473-3099(16)00095-5.

Calvet, G. A. *et al.* (2018) ‘Study on the persistence of Zika virus (ZIKV) in body fluids of patients with ZIKV infection in Brazil.’, *BMC infectious diseases*. BioMed Central, 18(1), p. 49. doi: 10.1186/s12879-018-2965-4.

Calvet, G. A., Dos Santos, F. B. and Sequeira, P. C. (2016) ‘Zika virus infection: Epidemiology, clinical manifestations and diagnosis’, *Current Opinion in Infectious Diseases*, 29(5), pp. 459–466. doi: 10.1097/QCO.0000000000000301.

Campos, G. S., Bandeira, A. C. and Sardi, S. I. (2015) ‘Zika Virus Outbreak, Bahia Brazil’, *Emerging Infectious Diseases*, 21(10), pp. 1885–1886. doi: 10.32301/eid2110.150847.

Cao-Lormeau, V.-M. *et al.* (2014) ‘Zika virus, French polynesia, South pacific, 2013.’, *Emerging infectious diseases*. Centers for Disease Control and Prevention, 20(6), pp. 1085–6. doi: 10.3201/eid2006.140138.

Cao-Lormeau, V.-M. and Musso, D. (2014) ‘Emerging arboviruses in the Pacific.’, *Lancet*. Elsevier, 384(9954), pp. 1571–2. doi: 10.1016/S0140-6736(14)61977-2.

Carneiro, B. M. *et al.* (2016) ‘The green tea molecule EGCG inhibits Zika virus entry’, *Virology*. Academic Press, 496(1), pp. 215–218. doi: 10.1016/J.VIROL.2016.06.012.

Carod-Artal, F. J. (2018) ‘Neurological complications of Zika virus infection’, *Expert Review of Anti-Infective Therapy*, 16(5), pp. 399–410. doi: 10.1080/14787210.2018.1466702.

de Carvalho, O. V. *et al.* (2017) 'The thiopurine nucleoside analogue 6-methylmercaptapurine riboside (6MMPr) effectively blocks Zika virus replication', *International Journal of Antimicrobial Agents*, 50(6), pp. 718–725. doi: 10.1016/j.ijantimicag.2017.08.016.

Centers for Disease Control and Prevention (2018). Available at: <https://www.cdc.gov/zika/symptoms/treatment.html> (Accessed: 15 January 2019).

Chan, J. F.-W. *et al.* (2017) 'Novel antiviral activity and mechanism of bromocriptine as a Zika virus NS2B-NS3 protease inhibitor', *Antiviral Research*. Elsevier, 141(1), pp. 29–37. doi: 10.1016/J.ANTIVIRAL.2017.02.002.

Chatrin, C. *et al.* (2018) 'The structure of the binary methyltransferase-SAH complex from Zika virus reveals a novel conformation for the mechanism of mRNA capping', *Oncotarget*. Impact Journals, 9(3), pp. 3160–3171. doi: 10.18632/oncotarget.23223.

Chaudhary, V. *et al.* (2017) 'Selective Activation of Type II Interferon Signaling by Zika Virus NS5 Protein', *Journal of Virology*. Edited by B. R. G. Williams, 91(14), pp. e00163-17. doi: 10.1128/JVI.00163-17.

Chen, X. *et al.* (2016) 'Mechanisms of activation and inhibition of Zika virus NS2B-NS3 protease.', *Cell research*. Nature Publishing Group, 26(11), pp. 1260–1263. doi: 10.1038/cr.2016.116.

Coloma, J. *et al.* (2016) 'Structures of NS5 Methyltransferase from Zika Virus', *Cell Rep*, 16(12), pp. 3097–3102. doi: 10.1016/j.celrep.2016.08.091.

Coutard, B. *et al.* (2017) 'Zika Virus Methyltransferase: Structure and Functions for Drug Design Perspectives', *Journal of Virology*, 91(5), pp. e02202-16. doi: 10.1128/JVI.02202-16.

Dang, J. *et al.* (2016) 'Zika Virus Depletes Neural Progenitors in Human Cerebral Organoids through Activation of the Innate Immune Receptor TLR3.', *Cell stem cell*. NIH Public Access, 19(2), pp. 258–265. doi: 10.1016/j.stem.2016.04.014.

Devhare, P. *et al.* (2017) 'Zika virus infection dysregulates human neural stem cell growth and inhibits differentiation into neuroprogenitor cells', *Cell Death and Disease*. Nature Publishing Group, 8(10), p. e3106. doi: 10.1038/cddis.2017.517.

Devnarain, N., Ramharack, P. and Soliman, M. E. (2017) 'Brain grants permission of access to Zika virus but denies entry to drugs: a molecular modeling perspective to infiltrate the boundary', *RSC Advances*. Royal Society of Chemistry, 7(75), pp. 47416–47424. doi: 10.1039/C7RA05918C.

Dibley, M. J. and Jeacocke, D. A. (2001) 'Safety and Toxicity of Vitamin A Supplements in Pregnancy', *Food and Nutrition Bulletin*. SAGE PublicationsSage CA: Los Angeles, CA, 22(3), pp.

248–266. doi: 10.1177/156482650102200304.

Dick, G. W. A., Kitchen, S. F. and Haddock, A. J. (1952) ‘Zika Virus (I). Isolations and serological specificity’, *Transactions of the Royal Society of Tropical Medicine and Hygiene*, 46(5), pp. 509–520. doi: 10.1016/0035-9203(52)90042-4.

Duan, W. *et al.* (2017) ‘The crystal structure of Zika virus NS5 reveals conserved drug targets’, *The EMBO Journal*, 36(7), pp. 919–933. doi: 10.15252/embj.201696241.

Dudley, D. M. *et al.* (2017) ‘Infection via mosquito bite alters Zika virus tissue tropism and replication kinetics in rhesus macaques’, *Nature Communications*. Nature Publishing Group, 8(1), p. 2096. doi: 10.1038/s41467-017-02222-8.

Duffy, M. R. *et al.* (2009) ‘Zika virus outbreak on Yap Island, Federated States of Micronesia’, *The New England Journal of Medicine*, 360(1), pp. 2536–2543.

Edeling, M. A., Diamond, M. S. and Fremont, D. H. (2014) ‘Structural basis of Flavivirus NS1 assembly and antibody recognition.’, *Proceedings of the National Academy of Sciences of the United States of America*. National Academy of Sciences, 111(11), pp. 4285–90. doi: 10.1073/pnas.1322036111.

Filipe, A. R., Martins, C. M. V. and Rocha, H. (1973) ‘Laboratory infection with Zika virus after vaccination against yellow fever’, *Archiv für die gesamte Virusforschung*, 43(4), pp. 315–319. doi: 10.1007/BF01556147.

Fontaine, K. A. *et al.* (2018) ‘The Cellular NMD Pathway Restricts Zika Virus Infection and Is Targeted by the Viral Capsid Protein.’, *mBio*. American Society for Microbiology, 9(6), pp. e02126-18. doi: 10.1128/mBio.02126-18.

Fontes-Garfias, C. R. *et al.* (2017) ‘Functional Analysis of Glycosylation of Zika Virus Envelope Protein.’, *Cell reports*. NIH Public Access, 21(5), pp. 1180–1190. doi: 10.1016/j.celrep.2017.10.016.

Foo, S.-S. *et al.* (2017) ‘Asian Zika virus strains target CD14+ blood monocytes and induce M2-skewed immunosuppression during pregnancy.’, *Nature microbiology*. NIH Public Access, 2(11), pp. 1558–1570. doi: 10.1038/s41564-017-0016-3.

Furtado, J. M. *et al.* (2016) ‘Uveitis Associated with Zika Virus Infection’, *New England Journal of Medicine*, 375(4), pp. 394–396. doi: 10.1056/NEJMc1603618.

Garg, H., Mehmetoglu-Gurbuz, T. and Joshi, A. (2018) ‘Recent Advances in Zika Virus Vaccines’, *Viruses*, 10(11), p. E631. doi: 10.3390/v10110631.

- Ghezzi, S. *et al.* (2017) 'Heparin prevents Zika virus induced-cytopathic effects in human neural progenitor cells', *Antiviral Research*, 140, pp. 13–17. doi: 10.1016/j.antiviral.2016.12.023.
- Gourinat, A. C. *et al.* (2015) 'Detection of zika virus in urine', *Emerging Infectious Diseases*, 21(1), pp. 84–86. doi: 10.3201/eid2101.140894.
- Grant, A. *et al.* (2016) 'Zika Virus Targets Human STAT2 to Inhibit Type I Interferon Signaling', *Cell Host & Microbe*. Cell Press, 19(6), pp. 882–890. doi: 10.1016/J.CHOM.2016.05.009.
- Guedes, D. R. *et al.* (2017) 'Zika virus replication in the mosquito *Culex quinquefasciatus* in Brazil.', *Emerging microbes & infections*. Nature Publishing Group, 6(8), p. e69. doi: 10.1038/emi.2017.59.
- Gulland, A. (2016) 'WHO warns of risk of Zika virus in Europe.', *BMJ (Clinical research ed.)*. British Medical Journal Publishing Group, 353, p. i2887. doi: 10.1136/bmj.i2887.
- Hamel, R. *et al.* (2015) 'Biology of Zika Virus Infection in Human Skin Cells', *Journal of Virology*, 89(17), pp. 8880–8896. doi: 10.1128/jvi.00354-15.
- Hasan, S. S. *et al.* (2017) 'A human antibody against Zika virus crosslinks the E protein to prevent infection', *Nature Communications*. Nature Publishing Group, 8(14722), pp. 1–6. doi: 10.1038/ncomms14722.
- van Hemert, F. and Berkhout, B. (2016) 'Nucleotide composition of the Zika virus RNA genome and its codon usage.', *Virology journal*. BioMed Central, 13(1), pp. 95–103. doi: 10.1186/s12985-016-0551-1.
- Hennessey, M., Fischer, M. and Staples, J. E. (2016) 'Zika Virus Spreads to New Areas - Region of the Americas, May 2015-January 2016', *American Journal of Transplantation*. John Wiley & Sons, Ltd, 16(3), pp. 1031–1034. doi: 10.1111/ajt.13743.
- Hersh, A. M., Gundacker, N. D. and Boltax, J. (2017) 'Zika-associated Shock and Multi-Organ Dysfunction', *Annals of the American Thoracic Society*. American Thoracic Society, 14(11), pp. 1706–1708. doi: 10.1513/AnnalsATS.201612-988CC.
- Hill, M. E. *et al.* (2018) 'The Unique Cofactor Region of Zika Virus NS2B–NS3 Protease Facilitates Cleavage of Key Host Proteins', *ACS Chemical Biology*, 13(9), pp. 2398–2405. doi: 10.1021/acscchembio.8b00508.
- Hills, S. L., Fischer, M. and Petersen, L. R. (2017) 'Epidemiology of Zika Virus Infection', *The Journal of Infectious Diseases*, 216(suppl_10), pp. S868–S874. doi: 10.1093/infdis/jix434.
- Jain, R. *et al.* (2016) 'Structure of the NS3 helicase from Zika virus', *Nature Structural and Molecular*

Biology. Nature Publishing Group, 23(8), pp. 752–754. doi: 10.1038/nsmb.3258.

Khandia, R., Munjal, A. and Dhama, K. (2017) ‘Consequences of Zika Virus Infection During Fetal Stage and Pregnancy Safe Drugs: An Update’, *International Journal of Pharmacology*, 13(4), pp. 370–377. doi: 10.3923/ijp.2017.370.377.

Kmietowicz, Z. (2016) ‘Questions your patients may have about Zika virus’, *BMJ*, p. i649. doi: 10.1136/bmj.i649.

Kuivanen, S. *et al.* (2017) ‘Obatoclox, saliphenylhalamide and gemcitabine inhibit Zika virus infection in vitro and differentially affect cellular signaling, transcription and metabolism’, *Antiviral Research*, 139, pp. 117–128. doi: 10.1016/j.antiviral.2016.12.022.

Lanciotti, R. S. *et al.* (2008) ‘Genetic and serologic properties of Zika virus associated with an epidemic, Yap State, Micronesia, 2007.’, *Emerging infectious diseases*. Centers for Disease Control and Prevention, 14(8), pp. 1232–9. doi: 10.3201/eid1408.080287.

Larocca, R. A. *et al.* (2016) ‘Vaccine protection against Zika virus from Brazil.’, *Nature*. NIH Public Access, 536(7617), pp. 474–8. doi: 10.1038/nature18952.

Lazear, H. and Diamond, M. (2016) ‘Zika Virus : New Clinical Syndromes and Its Emergence in the Western Hemisphere’, *Journal of Virology*, 90(10), pp. 4864–4875. doi: 10.1128/JVI.00252-16.Editor.

Lazear, H. M. *et al.* (2016) ‘A Mouse Model of Zika Virus Pathogenesis’, *Cell Host & Microbe*, 19(5), pp. 720–730. doi: 10.1016/j.chom.2016.03.010.

Lee, C. Y.-P. and Ng, L. F. P. (2018) ‘Zika virus: from an obscurity to a priority’, *Microbes and Infection*. Elsevier Masson, 20(11–12), pp. 635–645. doi: 10.1016/J.MICINF.2018.02.009.

Lee, I. *et al.* (2018) ‘Probing Molecular Insights into Zika Virus–Host Interactions.’, *Viruses*. Multidisciplinary Digital Publishing Institute (MDPI), 10(5). doi: 10.3390/v10050233.

Leung, J. Y. *et al.* (2008) ‘Role of Nonstructural Protein NS2A in Flavivirus Assembly’, *Journal of virology*. American Society for Microbiology Journals, 82(10), pp. 4731–4741. doi: 10.1128/jvi.00002-08.

Li, A. *et al.* (2018) ‘A Zika virus vaccine expressing premembrane-envelope-NS1 polyprotein.’, *Nature communications*. Nature Publishing Group, 9(1), p. 3067. doi: 10.1038/s41467-018-05276-4.

Li, C. *et al.* (2017) ‘25-Hydroxycholesterol Protects Host against Zika Virus Infection and Its Associated Microcephaly in a Mouse Model.’, *Immunity*. Elsevier, 46(3), pp. 446–456. doi:

10.1016/j.immuni.2017.02.012.

Li, L. *et al.* (2008) 'The Flavivirus Precursor Membrane-Envelope Protein Complex: Structure and Maturation', *Science*, 319(5871), pp. 1830–1834. doi: 10.1126/science.1153263.

Liang, Q. *et al.* (2016) 'Zika Virus NS4A and NS4B Proteins Deregulate Akt-mTOR Signaling in Human Fetal Neural Stem Cells to Inhibit Neurogenesis and Induce Autophagy', *Cell Stem Cell*, 19(5), pp. 663–671. doi: 10.1016/j.stem.2016.07.019.

Lim, E. X. Y. *et al.* (2018) 'Mosquitoes as Suitable Vectors for Alphaviruses.', *Viruses*. Multidisciplinary Digital Publishing Institute (MDPI), 10(2), pp. 84–100. doi: 10.3390/v10020084.

Ma, J. *et al.* (2018) 'Zika Virus Non-structural Protein 4A Blocks the RLR-MAVS Signaling', *Frontiers in Microbiology*. Frontiers, 9(1350), pp. 1–10. doi: 10.3389/fmicb.2018.01350.

MacNamara, F. . (1954) 'Zika virus : A report on three cases of human infection during an epidemic of jaundice in Nigeria', *Transactions of the Royal Society of Tropical Medicine and Hygiene*. No longer published by Elsevier, 48(2), pp. 139–145. doi: 10.1016/0035-9203(54)90006-1.

Manangeeswaran, M. *et al.* (2018) 'ZIKA virus infection causes persistent chorioretinal lesions', *Emerging Microbes & Infections*. Nature Publishing Group, 7(1), p. 96. doi: 10.1038/s41426-018-0096-z.

Mansuy, J. M. *et al.* (2016) 'Zika virus: high infectious viral load in semen, a new sexually transmitted pathogen?', *The Lancet Infectious Diseases*. Elsevier Ltd, 16(4), p. 405. doi: 10.1016/S1473-3099(16)00122-5.

Márquez-Jurado, S. *et al.* (2018) 'An Alanine-to-Valine Substitution in the Residue 175 of Zika Virus NS2A Protein Affects Viral RNA Synthesis and Attenuates the Virus In Vivo', *Viruses*. Multidisciplinary Digital Publishing Institute, 10(10), p. 547. doi: 10.3390/v10100547.

Mawson, A. R. (2016) 'Pathogenesis of Zika Virus-Associated Embryopathy.', *BioResearch open access*. Mary Ann Liebert, Inc., 5(1), pp. 171–6. doi: 10.1089/biores.2016.0004.

Meertens, L. *et al.* (2017) 'Axl Mediates ZIKA Virus Entry in Human Glial Cells and Modulates Innate Immune Responses', *Cell Reports*, 18(2), pp. 324–333. doi: 10.1016/j.celrep.2016.12.045.

Merino-Ramos, T. *et al.* (2017) 'Antiviral Activity of Nordihydroguaiaretic Acid and Its Derivative Tetra-O-Methyl Nordihydroguaiaretic Acid against West Nile Virus and Zika Virus.', *Antimicrobial agents and chemotherapy*. American Society for Microbiology (ASM), 61(8), pp. e00376-17. doi: 10.1128/AAC.00376-17.

- Mier-Y-Teran-Romero, L. *et al.* (2018) ‘Guillain-Barré syndrome risk among individuals infected with Zika virus: a multi-country assessment.’, *BMC medicine*. BioMed Central, 16(1), p. 67. doi: 10.1186/s12916-018-1052-4.
- Miner, J. J. *et al.* (2016) ‘Zika Virus Infection during Pregnancy in Mice Causes Placental Damage and Fetal Demise’, *Cell*, 165(5), pp. 1081–1091. doi: 10.1016/j.cell.2016.05.008.
- Miner, J. J. and Diamond, M. S. (2017) ‘Zika Virus Pathogenesis and Tissue Tropism’, *Cell Host & Microbe*, 21(2), pp. 134–142. doi: 10.1016/j.chom.2017.01.004.
- Monsalve, D. M. *et al.* (2017) ‘Zika virus and autoimmunity. One-step forward’, *Autoimmunity Reviews*, 16(12), pp. 1237–1245. doi: 10.1016/j.autrev.2017.10.008.
- Mounce, B. C. *et al.* (2017) ‘Curcumin inhibits Zika and chikungunya virus infection by inhibiting cell binding’, *Antiviral Research*, 142(1), pp. 148–157. doi: 10.1016/j.antiviral.2017.03.014.
- Muktar, Y., Tamerat, N. and Shewafera, A. (2016) ‘Aedes aegypti as a Vector of Flavivirus’, *Journal of Tropical Diseases*. OMICS International, 04(05), pp. 1–7. doi: 10.4172/2329-891X.1000223.
- Muller, D. A. and Young, P. R. (2013) ‘The flavivirus NS1 protein: Molecular and structural biology, immunology, role in pathogenesis and application as a diagnostic biomarker’, *Antiviral Research*. Elsevier, 98(2), pp. 192–208. doi: 10.1016/J.ANTIVIRAL.2013.03.008.
- Munjal, A. *et al.* (2017) ‘Advances in Developing Therapies to Combat Zika Virus: Current Knowledge and Future Perspectives’, *Frontiers in Microbiology*, 8(1469), pp. 1–19. doi: 10.3389/fmicb.2017.01469.
- Musso, D. *et al.* (2014) ‘Potential for Zika virus transmission through blood transfusion demonstrated during an outbreak in French Polynesia, November 2013 to February 2014’, *Eurosurveillance*, 19(14), pp. 14–16. doi: 10.2807/1560-7917.ES2014.19.14.20761.
- Musso, D. *et al.* (2015) ‘Potential sexual transmission of zika virus’, *Emerging Infectious Diseases*, 21(2), pp. 359–361. doi: 10.3201/eid2102.141363.
- Nambala, P. and Su, W.-C. (2018) ‘Role of Zika Virus prM Protein in Viral Pathogenicity and Use in Vaccine Development.’, *Frontiers in microbiology*. Frontiers Media SA, 9, p. 1797. doi: 10.3389/fmicb.2018.01797.
- Nowakowski, T. J. *et al.* (2016) ‘Expression analysis highlights AXL as a candidate zika virus entry receptor in neural stem cells’, *Cell Stem Cell*. Elsevier Inc., 18(5), pp. 591–596. doi: 10.1016/j.stem.2016.03.012.

Olagnier, D. *et al.* (2016) 'Mechanisms of Zika Virus Infection and Neuropathogenesis.', *DNA and cell biology*. Mary Ann Liebert, Inc., 35(8), pp. 367–72. doi: 10.1089/dna.2016.3404.

Olson, J. G. *et al.* (1981) 'Zika virus, a cause of fever in Central Java, Indonesia', *Transactions of the Royal Society of Tropical Medicine and Hygiene*. No longer published by Elsevier, 75(3), pp. 389–393. doi: 10.1016/0035-9203(81)90100-0.

Pardi, N. *et al.* (2017) 'Zika virus protection by a single low-dose nucleoside-modified mRNA vaccination.', *Nature*. NIH Public Access, 543(7644), pp. 248–251. doi: 10.1038/nature21428.

Pascoalino, B. S. *et al.* (2016) 'Zika antiviral chemotherapy: identification of drugs and promising starting points for drug discovery from an FDA-approved library.', *F1000Research*. Faculty of 1000 Ltd, 5, p. 2523. doi: 10.12688/f1000research.9648.1.

Petersen, L. R. *et al.* (2016) 'Zika Virus', *New England Journal of Medicine*. Edited by L. R. Baden, 374(16), pp. 1552–1563. doi: 10.1056/NEJMra1602113.

Plourde, A. R. and Bloch, E. M. (2016) 'A Literature Review of Zika Virus', *Emerging Infectious Diseases*, 22(7), pp. 1185–1192. doi: 10.3201/eid2207.151990.

Rausch, K. *et al.* (2017) 'Screening Bioactives Reveals Nanchangmycin as a Broad Spectrum Antiviral Active against Zika Virus.', *Cell reports*. NIH Public Access, 18(3), pp. 804–815. doi: 10.1016/j.celrep.2016.12.068.

Retallack, H. *et al.* (2016) 'Zika virus cell tropism in the developing human brain and inhibition by azithromycin', *Proceedings of the National Academy of Sciences*, 113(50), pp. 14408–14413. doi: 10.1073/pnas.1618029113.

Reznik, S. E. and Ashby, J. C. R. (2017) 'Sofosbuvir: an antiviral drug with potential efficacy against Zika infection.', *International journal of infectious diseases*. The Author(s), 55, pp. 29–30. doi: 10.1016/j.ijid.2016.12.011.

Richard, A. S. *et al.* (2017) 'AXL-dependent infection of human fetal endothelial cells distinguishes Zika virus from other pathogenic flaviviruses.', *Proceedings of the National Academy of Sciences of the United States of America*. National Academy of Sciences, 114(8), pp. 2024–2029. doi: 10.1073/pnas.1620558114.

Richner, J. M. *et al.* (2017) 'Vaccine Mediated Protection Against Zika Virus-Induced Congenital Disease.', *Cell*. NIH Public Access, 170(2), p. 273–283.e12. doi: 10.1016/j.cell.2017.06.040.

Saiz, J.-C. *et al.* (2018) 'Host-Directed Antivirals: A Realistic Alternative to Fight Zika Virus.', *Viruses*. Multidisciplinary Digital Publishing Institute (MDPI), 10(9), p. E453. doi:

10.3390/v10090453.

Saiz, J.-C. and Martín-Acebes, M. A. (2017) 'The Race To Find Antivirals for Zika Virus', *Antimicrobial Agents and Chemotherapy*. American Society for Microbiology Journals, 61(6), pp. e00411-17. doi: 10.1128/AAC.00411-17.

Sarwar, M. R. and Saqib, A. (2017) 'Zika Virus Infection during Pregnancy and its Management', *Journal of MPE Molecular Pathological Epidemiology*. iMedPub, 2(S1), pp. 1–6. Available at: <http://molecular-pathological-epidemiology.imedpub.com/zika-virus-infection-during-pregnancy-and-its-management.php?aid=17709> (Accessed: 9 January 2019).

Saw, W. G. *et al.* (2017) 'Structural features of Zika virus non-structural proteins 3 and -5 and its individual domains in solution as well as insights into NS3 inhibition', *Antiviral Research*. Elsevier, 141(1), pp. 73–90. doi: 10.1016/J.ANTIVIRAL.2017.02.005.

Shan, C., Muruato, A. E., *et al.* (2017) 'A live-attenuated Zika virus vaccine candidate induces sterilizing immunity in mouse models.', *Nature medicine*. NIH Public Access, 23(6), pp. 763–767. doi: 10.1038/nm.4322.

Shan, C., Ortiz, D. A., *et al.* (2017) 'Evaluation of a Novel Reporter Virus Neutralization Test for Serological Diagnosis of Zika and Dengue Virus Infection.', *Journal of clinical microbiology*. American Society for Microbiology Journals, 55(10), pp. 3028–3036. doi: 10.1128/JCM.00975-17.

Sharma, A. and Lal, S. K. (2017) 'Zika Virus: Transmission, Detection, Control, and Prevention.', *Frontiers in microbiology*. Frontiers Media SA, 8, p. 110. doi: 10.3389/fmicb.2017.00110.

Sharp, T. M. *et al.* (2016) 'Zika Virus Infection Associated With Severe Thrombocytopenia.', *Clinical infectious diseases : an official publication of the Infectious Diseases Society of America*. NIH Public Access, 63(9), pp. 1198–1201. doi: 10.1093/cid/ciw476.

Shehu, N. Y. *et al.* (2018) 'Pathogenesis, Diagnostic Challenges and Treatment of Zika Virus Disease in Resource-limited Settings', *Nigerian Postgraduate Medical Journal*, 25(2), pp. 67–72. doi: 10.4103/npmj.npmj_36_18.

Shiryayev, S. A. *et al.* (2017) 'Repurposing of the anti-malaria drug chloroquine for Zika Virus treatment and prophylaxis', *Scientific Reports*. Nature Publishing Group, 7(15771), pp. 1–9. doi: 10.1038/s41598-017-15467-6.

da Silva, S., Martins, D. O. S. and Jardim, A. C. G. (2018) 'A Review of the Ongoing Research on Zika Virus Treatment.', *Viruses*. Multidisciplinary Digital Publishing Institute (MDPI), 10(255), pp. 1–18. doi: 10.3390/v10050255.

- Simonin, Y. *et al.* (2017) ‘Differential virulence between Asian and African lineages of Zika virus’, *PLOS Neglected Tropical Diseases*. Edited by R. Rico-Hesse. Public Library of Science, 11(9), p. e0005821. doi: 10.1371/journal.pntd.0005821.
- Singh, P. K. *et al.* (2017) ‘Zika virus infects cells lining the blood-retinal barrier and causes chorioretinal atrophy in mouse eyes’, 2(4). doi: 10.1172/jci.insight.92340.
- Singleton, M. R., Dillingham, M. S. and Wigley, D. B. (2007) ‘Structure and Mechanism of Helicases and Nucleic Acid Translocases’, *Annual Review of Biochemistry*, 76(1), pp. 23–50. doi: 10.1146/annurev.biochem.76.052305.115300.
- Song, H. *et al.* (2016) ‘Zika virus NS1 structure reveals diversity of electrostatic surfaces among flaviviruses’, *Nature Structural and Molecular Biology*, 23(5), pp. 456–458. doi: 10.1038/nsmb.3213.
- Spiteri, G. *et al.* (2017) ‘Surveillance of Zika virus infection in the EU/EEA, June 2015 to January 2017.’, *Euro surveillance: bulletin Europeen sur les maladies transmissibles = European communicable disease bulletin*. European Centre for Disease Prevention and Control, 22(41). doi: 10.2807/1560-7917.ES.2017.22.41.17-00254.
- Sreedharan, J. (2015) ‘The Zika Virus: A new Threat from mosquito’, *Scientia*, 11(1), pp. 9–17. Available at: https://www.researchgate.net/publication/304058803_The_Zika_Virus_A_new_Threat_from_mosquito (Accessed: 4 January 2019).
- Stephen, P. *et al.* (2016) ‘Structural Insight into NS5 of Zika Virus Leading to the Discovery of MTase Inhibitors’, *Journal of the American Chemical Society*, 138(50), pp. 16212–16215. doi: 10.1021/jacs.6b10399.
- Stettler, K. *et al.* (2016) ‘Specificity, cross-reactivity, and function of antibodies elicited by Zika virus infection.’, *Science (New York, N.Y.)*, 353(6301), pp. 823–6. doi: 10.1126/science.aaf8505.
- Tabata, T. *et al.* (2016) ‘Zika Virus Targets Different Primary Human Placental Cells, Suggesting Two Routes for Vertical Transmission’, *Cell Host and Microbe*. Elsevier Inc, 20(10), pp. 155–166. doi: 10.1016/j.chom.2016.07.002.
- Tan, C. W. *et al.* (2017) ‘Polysulfonate suramin inhibits Zika virus infection’, *Antiviral Research*, 143, pp. 186–194. doi: 10.1016/j.antiviral.2017.04.017.
- Tong, X. *et al.* (2018) ‘Merimepodib, an IMPDH inhibitor, suppresses replication of Zika virus and other emerging viral pathogens’, *Antiviral Research*, 149, pp. 34–40. doi: 10.1016/j.antiviral.2017.11.004.

- Turmel, J. M. *et al.* (2016) 'Late sexual transmission of Zika virus related to persistence in the semen', *The Lancet*, 387(10037), p. 2501. doi: 10.1016/S0140-6736(16)30775-9.
- Vinhaes, E. S. *et al.* (2016) 'Transient Hearing Loss in Adults Associated with Zika Virus Infection', *Clinical Infectious Diseases*. Oxford University Press, 64(5), p. ciw770. doi: 10.1093/cid/ciw770.
- Wang, A. *et al.* (2017) 'Zika virus genome biology and molecular pathogenesis', *Emerging Microbes & Infections*. Nature Publishing Group, 6(3), p. e13. doi: 10.1038/emi.2016.141.
- Wang, C. *et al.* (2017) 'Nuclear import inhibitor N-(4-hydroxyphenyl) retinamide targets Zika virus (ZIKV) nonstructural protein 5 to inhibit ZIKV infection', *Biochemical and Biophysical Research Communications*, 493(4), pp. 1555–1559. doi: 10.1016/j.bbrc.2017.10.016.
- Wang, J. *et al.* (2017) 'A Human Bi-specific Antibody against Zika Virus with High Therapeutic Potential.', *Cell*. NIH Public Access, 171(1), p. 229–241.e15. doi: 10.1016/j.cell.2017.09.002.
- Wen, D. *et al.* (2018) 'N-glycosylation of Viral E Protein Is the Determinant for Vector Midgut Invasion by Flaviviruses.', *mBio*. American Society for Microbiology (ASM), 9(1), pp. e00046-18. doi: 10.1128/mBio.00046-18.
- Winkler, C. W. *et al.* (2017) 'Sexual and Vertical Transmission of Zika Virus in anti-interferon receptor-treated Rag1-deficient mice', *Scientific reports*, 7(7176), pp. 1–13. doi: 10.1038/s41598-017-07099-7.
- Wong, S. J. *et al.* (2017) 'A Multiplex Microsphere Immunoassay for Zika Virus Diagnosis', *EBioMedicine*. Elsevier, 16(1), pp. 136–140. doi: 10.1016/J.EBIOM.2017.01.008.
- Xia, H. *et al.* (2018) 'An evolutionary NS1 mutation enhances Zika virus evasion of host interferon induction.', *Nature communications*. Nature Publishing Group, 9(1), p. 414. doi: 10.1038/s41467-017-02816-2.
- Xie, X. *et al.* (2017) 'Small Molecules and Antibodies for Zika Therapy', *The Journal of Infectious Diseases*. Oxford University Press, 216(suppl_10), pp. S945–S950. doi: 10.1093/infdis/jix406.
- Xin, Q.-L. *et al.* (2017) 'Quantitative Proteomic Analysis of Mosquito C6/36 Cells Reveals Host Proteins Involved in Zika Virus Infection.', *Journal of virology*. American Society for Microbiology Journals, 91(12), pp. e00554-17. doi: 10.1128/JVI.00554-17.
- Xu, M. *et al.* (2016) 'Identification of small-molecule inhibitors of Zika virus infection and induced neural cell death via a drug repurposing screen.', *Nature medicine*. NIH Public Access, 22(10), pp. 1101–1107. doi: 10.1038/nm.4184.

Yoon, K.-J. *et al.* (2017) 'Zika-Virus-Encoded NS2A Disrupts Mammalian Cortical Neurogenesis by Degrading Adherens Junction Proteins', *Cell Stem Cell*, 21(3), p. 349–358.e6. doi: 10.1016/j.stem.2017.07.014.

Yuan, S. *et al.* (2017) 'Structure-based discovery of clinically approved drugs as Zika virus NS2B-NS3 protease inhibitors that potently inhibit Zika virus infection in vitro and in vivo', *Antiviral Research*. Elsevier B.V., 145, pp. 33–43. doi: 10.1016/j.antiviral.2017.07.007.

Zaidi, M. B. *et al.* (2018) 'Non-congenital severe ocular complications of Zika virus infection.', *JMM case reports*. Microbiology Society, 5(6), p. e005152. doi: 10.1099/jmmcr.0.005152.

Zhang, C. *et al.* (2017) 'Structure of the NS5 methyltransferase from Zika virus and implications in inhibitor design', *Biochemical and Biophysical Research Communications*. Academic Press, 492(4), pp. 624–630. doi: 10.1016/J.BBRC.2016.11.098.

Zhang, R. *et al.* (2016) 'A CRISPR screen defines a signal peptide processing pathway required by flaviviruses.', *Nature*. NIH Public Access, 535(7610), pp. 164–8. doi: 10.1038/nature18625.

Zmurko, J. *et al.* (2016) 'The Viral Polymerase Inhibitor 7-Deaza-2'-C-Methyladenosine Is a Potent Inhibitor of In Vitro Zika Virus Replication and Delays Disease Progression in a Robust Mouse Infection Model.', *PLoS neglected tropical diseases*. Public Library of Science, 10(5), p. e0004695. doi: 10.1371/journal.pntd.0004695.

CHAPTER 3: COMPUTATIONAL METHODOLOGY

1 Introduction

Molecular modelling is the science that explores chemical and biological phenomena in terms of the properties of the constituent atoms and molecules (Schmidt, Bergner and Schwede, 2014). It connects the living world of biology with the inanimate world of chemistry and physics by analyzing the structure and properties of atoms and molecules based on universal laws of physics (Hinsen, 2000). Molecular modelling has immense practical use particularly in the fields of materials research, drug design and discovery, computational chemistry and computational biology by studying biological and chemical systems of various sizes (Redhu and Jindal, 2013).

Experimentation can appropriately provide the biochemical interactions through which a drug substance triggers its pharmacological effect in a biological system, however, an afternoon on the computer can save six months in the lab and labor costs. At present, molecular modelling is an integral component of pharmaceutical lead discovery (Goldbeck, 2012).

Rational drug design is a multidisciplinary approach pertaining to the process of using knowledge of a biological target to discover novel pharmaceutical compounds (Y. Wang *et al.*, 2015). Usually, the compound is a small molecule that influences the biomolecule it binds to, either via activation or inhibition, causing a therapeutic effect. These small molecules are designed to be complimentary in charge and shape to the pocket of the biological target it binds to, to ensure it binds with high affinity (Yu and MacKerell, 2017). The rational drug design approach comprises of three main disciplines: computational chemistry, information technology and structural biology; and may be split into two main categories, namely, the lead discovery and optimization method, and the compounds' druggability prediction method (Y. Wang *et al.*, 2015). Computational methods that correspond to these approaches include virtual screening, drug target prediction, molecular docking, three-dimensional quantitative structure-activity relationship (3D-QSAR) analyses, active vs allosteric site modification and scaffold hopping (Zheng *et al.*, 2013).

Molecular modelling may be described as a three-step process. The first step involves the selection of a model to define a system's inter- and intra- molecular interactions (Redhu and Jindal, 2013). Molecular modelling techniques can broadly be divided into two groups, namely, classical and quantum mechanics (QM) (Sutcliffe and Woolley, 2012). Classical mechanics, or Newtonian

mechanics, consider molecules rather crudely, like atoms as balls and bonds as springs, and describes the motions of macroscopic objects (Chow, 2013). Conversely, QM considers the probability of an electron being at a location without having a precise position of atoms or bonds (Quesne, Borowski and De Visser, 2016). Quantum mechanical techniques can be broadly divided into two categories, namely, semi-empirical and ab initio methods (Ballentine, 2014). Semi-empirical methods involve a significant amount of parameterization using parameters extracted from experimental data (Christensen *et al.*, 2016). Ab initio methods on the other hand are considered theoretically “pure” in the sense that they do not depend solely on experimental measurements (Pokluda *et al.*, 2015).

The second step involves the application of molecular dynamics to calculate the energies of atoms and molecules within the system. The final step involves the analysis of the calculation, as well as the verification of the calculation (Redhu and Jindal, 2013).

The chapter herein appropriately expands on the techniques of molecular modelling/computational chemistry utilized in this study.

2 Quantum Mechanics

In the 1920s, QM was pioneered by physics experts Werner Karl Heisenberg, Max Born and Wolfgang Ernst Pauli at a German university (Born, Elsasser and Anderson, 1981). Quantum mechanics is a basic physical theory that defines the electrons, atoms and photons of nature at a microscale. It also expresses the behavior of these minute units much differently from that seen at greater scales (Aerts, 2014).

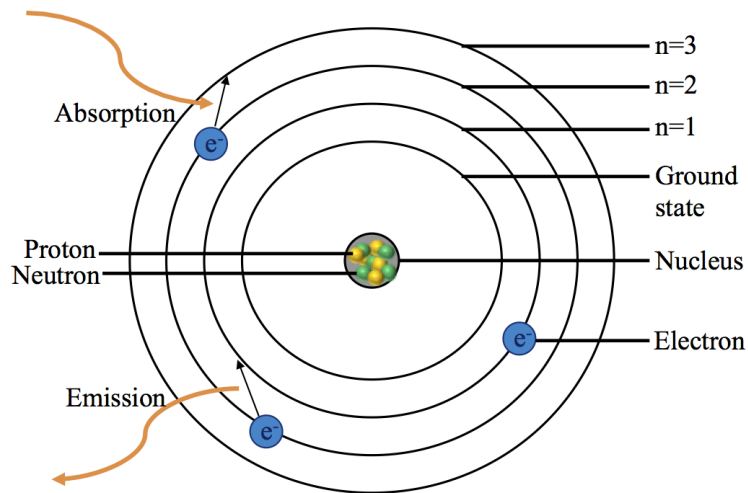
Theoretical chemistry and QM can be applied to biological entities and challenges, to provide new understandings into the electronic nature of biological systems (Merz, 2014). Various biological processes involve energy conversion that are naturally quantum mechanical, including proton and electron transfer, light absorption, excitation energy transfer and chemical reactions (McConnell, Li and Brudvig, 2010; Sjulstok, Olsen and Solov’Yov, 2015; Brookes, 2017).

Analysis of biological systems using QM involves mapping the electrons that constitute molecules in a 3D space (Sjulstok, Olsen and Solov’Yov, 2015; Shen, Wu and Yang, 2016). The Schrödinger

equation is a fundamental mathematical model in QM, as is the Born-Oppenheimer approximation theory in molecular systems (Schrödinger, 1926; Nelson, 1966; Brambilla *et al.*, 2018).

2.1 The Schrödinger Equation

In 1913, the Danish physicist Niels Bohr proposed that the electron can circle the nucleus only in permitted circular paths, called orbitals (Bohr, 1913). A photon is emitted when an electron falls to a lower energy level (closer to the nucleus) and a photon is absorbed when an electron jumps to a higher energy level (Figure 3.1). However, his model could not explain the thousands of atoms existing with more than one electron, nor did it explain the chemical behaviors of atoms (Kragh, 2012).



The Bohr Model (1913)

Figure 3.1 The Niels Bohr Model (1913) demonstrating the absorption and emission of photons as electron move to higher/lower energy levels (n) (Prepared by Author).

In 1926, Austrian expert in physics, Erwin Schrödinger, built on Bohr's model by presenting the quantum theory that describes the model in a mathematical sense based on probability, as it is impossible to know the exact position and momentum of an electron simultaneously (Figure 3.2) (Schrödinger, 1926).

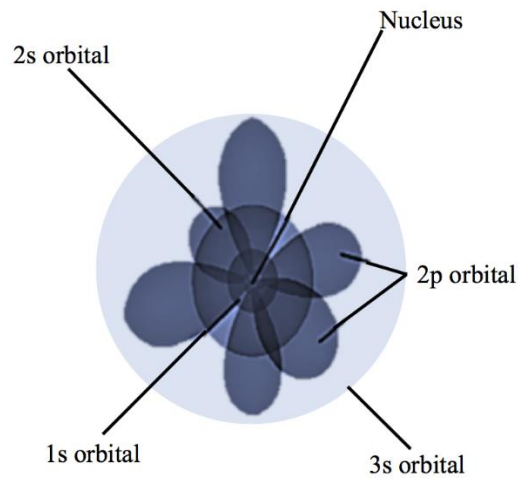


Figure 3.2 Schrödinger’s Quantum Mechanical Model (1926) demonstrating orbitals as differently shaped “lobes” where electrons are probably found (Prepared by Author).

Schrödinger’s wave equation considers all matter, including electrons, as waves and contains quantum numbers that specify the properties of atomic orbitals and properties of electrons in orbitals.

The Schrödinger equation is as follows:

$$\mathbf{H}\Psi = \mathbf{E}\Psi \quad (1)$$

Where,

- H Hamiltonian operator (includes derivatives regarding atom location)
- E System’s energy “eigenvalues”
- Ψ Wave function (normalized, continuous, anti-symmetric and single valued)

$$\mathbf{H} = \mathbf{T} + \mathbf{V} \quad (2)$$

Where,

$$\mathbf{H} = \left[-\frac{\hbar^2}{8\pi^2} \sum_i \frac{1}{m_j} \left(\frac{\partial^2}{\partial x^2} + \frac{\partial^2}{\partial y^2} + \frac{\partial^2}{\partial z^2} \right) \right] + \sum_i \sum_{<j} \left(\frac{e_i e_j}{r_{ij}} \right) \quad (3)$$

- T Kinetic energy of atom
- V Total potential energy of atom

The height of complexity of the Schrödinger equation is simplified by the Born-Oppenheimer approximation theory due to the immense number of atoms in molecular systems (Sherrill, 2005; Barde *et al.*, 2015).

2.2 The Born-Oppenheimer Approximation Theory

A year after Schrödinger proposed the quantum theory, the physicists, Julius Robert Oppenheimer and Max Born presented the Born-Oppenheimer approximation that assumes that the motion of electrons and atomic nuclei in a molecule can be separated (Born and Oppenheimer, 1927). The theory considers a constant kinetic energy of the nucleus while solving for that of electrons. Nuclei weigh more than electrons, thus the difference in their velocities make them applicable for using the Born-Oppenheimer approximation theory (Brambilla *et al.*, 2018).

The wave function is as follows:

$$\Psi(\mathbf{r}_{\text{elec}}) = \Psi(\mathbf{r}_{\text{elec}}) (\Psi(\mathbf{r}_{\text{nucl}})) \quad (4)$$

Eq 3.2.1 is converted:

$$H_{EN}\Psi(\mathbf{r}_{\text{elec}}) = E_{EN}\Psi(\mathbf{r}_{\text{elec}}) \quad (5)$$

Where,

H_{EN} Difference between terms based activity to fixed nuclear positions (V_{NN}) or their activity to the non-fixed electron positions.

$$(\mathbf{H}_{\text{el}} + \mathbf{V}_{\text{NN}}) \Psi(\mathbf{r}_{\text{el}}) = E_{\text{EN}}\Psi(\mathbf{r}_{\text{el}}) \quad (6)$$

Where,

E_{EN} Fixed nuclear and fluctuating electron co-ordinates.

The electronic movements within a molecule is explained by the Schrödinger equation, while ground electronic states are more accurate using the Born-Oppenheimer approximation. Fixed positions of electrons can be analyzed once the equation is solved to construct a potential energy surface (PES) and curve (Lewars, 2011).

2.3 *Potential Energy Surface*

The PES can be calculated using clamped-nuclei electronic structure calculations that arise from the Schrödinger equation and Born-Oppenheimer approximation. Since an electron's position varies according to that of the nucleus, the PES is considered as the probability of collision of an atom's motion within a molecule. Nuclear clusters of high energy are indicated by high potential energy regions, while nuclear arrangements of low energy are shown by low energy regions. This becomes useful in the applications of computational chemistry when classifying conformations of the lowest energy state (Sutcliffe and Woolley, 2013).

3 **Molecular Mechanics**

Molecular mechanics (MM), also known as force field methods, are used for modelling of molecular systems by assuming the validity of the Born-Oppenheimer approximation theory. Force fields are applied to analyze a system's potential energy as a function of nuclear arrangements (Cornell, Howard and Kollman, 1991). Molecular mechanics, which applies classical Newtonian mechanics, is applicable for the analysis of complex and large biological systems containing more than thousands of atoms (Kostal, 2016). Protein-ligand complexes that are simulated using MM techniques yield free energy estimates, which are efficient, precise, consider solvation effects, as well as ligand and protein flexibility (Huang *et al.*, 2006).

Computer aided drug design makes use of 3D models of biological targets, such as proteins. Even though QM is suitable for restrained studies on straightforward models of binding sites within proteins and for analyzing the properties of isolated drug-like molecules, it is generally required to likewise run simulations on the entire protein solvated in water when utilizing CADD (Vanommeslaeghe *et al.*, 2014). Despite innovative attempts to apply semi-empirical methods to achieve this (Liu *et al.*, 2001), there are weaknesses of semi-empirical energy functions that place strict constraints on the timescale of the simulation.

For these reasons, MM force fields are the preferred approaches for protein dynamics, which resemble the QM energy surface with a model of classical mechanics, thus making it inexpensive with respect to molecular systems that have thousands of atoms. Moreover, a fairly precise description of

dispersion forces is provided by MM potential energy functions, which present QM approaches only begin improving at higher theoretical levels (Lu *et al.*, 2016).

3.1 Potential Energy Function

The potential energy of a system is calculated using the potential energy function (PEF) of MM. The PEF is described as the energy of a force field used to parameterize a molecular system, which is governed by a set of equations that also provide constituent atom types of a molecule (Golden and Olsen, 2008).

The total potential energy consists of the extended sum of each potential intra- and inter- molecular constituents, which include:

1. Bond stretching (between directly bonded atoms)

$$E_r = \sum K_r (r - r_0)^2 \quad (7)$$

2. Angle bending (atoms bounded to same central atoms)

$$E_\theta = \sum K_\theta (\theta - \theta_0)^2 \quad (8)$$

3. Bond torsion

$$E_\phi = \sum K_\phi [1 + \cos(n\phi - \phi_0)] \quad (9)$$

4. Non-bonded interactions (van der Waals and electrostatic)

$$E_{nb} = \left[\sum \sum \left(\frac{A_{ij}}{r_{ij}^{12}} - \frac{B_{ij}}{r_{ij}^6} \right) \right] + \left[\sum \sum \left(\frac{q_i q_j}{D r_{ij}} \right) \right] \quad (10)$$

Where,

K_r	Bond force constant
K_θ	Angle force constant
K_ϕ	Dihedral angle force constant
r_0	Equilibrium distance

- θ_0 Equilibrium angle
- ϕ_0 Equilibrium phase angle
- r_{ij} Distance
- A_{ij}, B_{ij} van der Waal parameters
- D Molecular dielectric constant
- q_i, q_j : Charge points

According to the “ball and spring” model, atoms are considered balls or spheres with radii and bonds are considered springs (Figure 3.3). Therefore, the final potential energy function equation is:

$$\mathbf{E_{total} = E_r + E_\theta + E_\phi + E_{nb}} \quad (11)$$

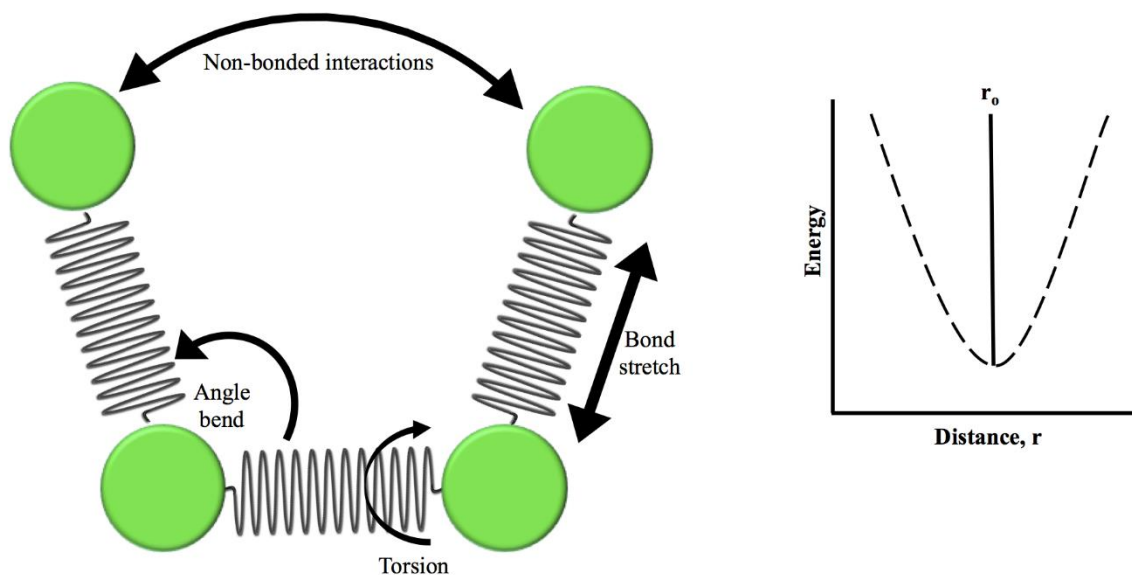


Figure 3.3 Graphical representation of “ball and spring” model describing potential energy function and corresponding potential energy diagram (Prepared by Author).

Force fields are mathematical equations that explain the reliance of a system’s energy on the coordinates of its particles. It contains a set of parameters achieved from QM calculations or

experimental data and an analytical form of potential energy between atoms. Various force fields of different complexities for different systems exist in literature (González, 2011).

Some of the most popular force fields include Chemistry at HARvard Macromolecular Mechanics (CHARMM) (Brooks *et al.*, 1983), Assisted Model Building with Energy Refinement (AMBER) (Sprenger, Jaeger and Pfandtner, 2015), Energy Calculation and Dynamics (ENCAD) (González, 2011), GRONingen Molecular Simulation (GROMOS) (Vlachakis *et al.*, 2014) and All-atom Optimized Potentials for Liquid Simulations (OPLS-AA) (Siu, Pluhackova and Böckmann, 2012). Studies carried out in the following chapters of this thesis utilized the harmonic AMBER force field to parameterize molecular systems since AMBER was designed for nucleic acids and proteins calculation (Case *et al.*, 2014).

4 Molecular Dynamics

The principal simulation techniques that exist include molecular dynamics and Monte Carlo. Monte Carlo (MC) simulations that use computational algorithms to yield results that depend on replicated randomized sampling, which was initially developed in 1955 by Enrico Fermi, John Pasta, Stanislaw Ulam and Mary Tsingou (Fermi *et al.*, 1955). Then in 1957, Berni Julian Alder and Tom Everett Wainwright developed a liquid dynamic simulation method that analyzed interactions between hard spheres (Alder and Wainwright, 1959), followed by J. B. Gibson, A. N. Goland, M. Milgram, and G. H. Vineyard in 1960 who simulated radiation damage (Gibson *et al.*, 1960). Aneesur Rahman then went on to publishing milestone simulations atoms of liquid argon in 1964 (Rahman, 1964).

Molecular dynamics (MD) simulations are more useful than MC simulations in the sense that MD provides dynamical features of the system. These include rheological properties, transport coefficients, spectra and time-based reactions to perturbations (Allen, 2004). Moreover, incomparable properties of biological phenomena from atom to organism level can be explained by MD simulations. The essential insight of living organisms are being improved by MD simulations, from drug development to treat diseases to creation of innovative materials that interact with biological systems and naturally replenishable energy sources (Perilla *et al.*, 2015). This simulation technique is extensively applied in experimental approaches such as the determination of nuclear magnetic resonance (NMR) structure and X-ray crystallography (Karplus and McCammon, 2002).

The Newtonian equation of motion of atoms is integrated and determined in the mathematical algorithms of MD simulations, which allow both kinetic energy and thermodynamic properties to be analyzed (González, 2011). Molecular dynamics simulations are implemented to identify the properties and motions of groups of atoms and molecules with respect to the interatomic/intermolecular interactions and their structures (Hollingsworth and Dror, 2018). The prerequisite initial conditions of atoms include the positions and velocities of every atom, a suitable force field to characterize interatomic forces, and applied boundary conditions.

The equation of motion may be solved:

$$\mathbf{F}_i = \mathbf{m}_i \frac{d^2 \mathbf{r}_i(t)}{dt^2} \quad (12)$$

Where,

$\mathbf{r}_i(t)$	Atomic position vector of i^{th} atom
t	Time
m_i	Mass of i^{th} atom
F_i	Interacting force on i^{th} atom

Basically, MD simulations comprise of four continuous stages that are reiterated to produce a trajectory. The first stage involves defining the co-ordinates of each atom, interatomic bond characteristics and atom acceleration. The second stage is the calculation of potential energy of each atom. The third stage solves the equation of motion by applying the energy calculations from stage 2, and the fourth stage involves capturing the altered atomic co-ordinates and the new state of the system, for the cycle to restart from stage one. Upon generation of a complete trajectory, the time-evolution of the system can be analyzed quantitatively (Jakobsson, 2001).

4.1 Molecular Dynamics Post Analyses

The MD trajectories are a sequence of snap shots or system coordinates over the simulation period, characterized by velocity vectors and position. Trajectories describe the time evolution of the system in phase space (Devadoss and Raj, 2014). Certain conditions must be met before selecting analytical software. A program ought to have diverse analysis options, rapid processing software should be built-in to hold large quantities of data, and visualization software must be able to generate high

quality video clips and snapshots of trajectories (Likhachev, Balabaev and Galzitskaya, 2016). The type of the MD study will determine post-analyses that should be carried out, although, the creation of new graphical systems must be substantiated by quantifiable assessment.

For the study herein, post analyses are fundamental in the determination of the dynamic structural arrangements, flexibility, energetics and stability of the biomolecular system, the characteristics of the ligand binding interactions of the system and the thermodynamic energy fluctuations throughout the trajectory of the system.

4.1.1 *Systems Stability*

Convergence – The acquisition of a sufficient number of phase points may be defined as convergence. Protein unfolding involves dynamic changes of bond types and vibration of bond angles, which may be described by convergence. When a molecular system reaches equilibrium and illustrates a final dynamic and conformational plateau, the MD trajectory is considered accurate and reproducible. The protein-ligand system shows energetically constant conformations in this area of stability (De Simone, Mote and Veglia, 2014).

Root-mean-square deviation (RMSD) – To compare findings from different MD trajectories on the same molecule, the RMSD between the combined averaged structures of the trajectories must be determined (Dixit, Ponomarev and Beveridge, 2006). The deviation of two static structures of a single trajectory with spatial differences can be measured using RMSD, whose trajectory is defined as:

$$\mathbf{RMSD} = \left(\frac{\sum_N (\mathbf{R}_i - \mathbf{R}_i^0)^2}{N} \right)^{\frac{1}{2}} \quad (13)$$

Where,

- N Total number of atoms in the system
- R_i Vector position of the C α atom of the ith atom in the reference conformation-calculated after aligning the structure to the initial conformation (O) using the least square fitting

The mean RMSD is determined by dividing the average by the number of frames in each trajectory, which can be calculated for the receptor, ligand and complex of a system (Kufareva and Abagyan, 2011; Schreiner *et al.*, 2012).

Radius of gyration (RoG) – A protein's RoG is described as the root-mean-square distance between atoms and their collective gravitational center, which estimates compactness of a protein along a trajectory. The RoG of a system is defined by the following reaction:

$$\mathbf{r}^2_{\text{gyr}} = \frac{\sum_{i=1}^n w_i (\mathbf{r}_i - \mathbf{r}^-)^2}{\sum_{i=1}^n w_i} \quad (14)$$

Where,

- r_i Position of the i^{th} atom
- r Center weight of the i^{th} atom

The mean RoG is calculated by dividing the average by the number of frames in a trajectory (Stepto *et al.*, 2015).

4.1.2 *Thermodynamic Free Binding Energy Calculations*

Free binding energy (FBE) calculations that incorporate entropic and enthalpic contributions substantiate protein-ligand binding mechanisms. Estimation of FBE allows for the generation of more approaches and algorithms. Some include molecular docking calculations, thermodynamic integration, linear integration energy and free energy perturbation (Du *et al.*, 2016).

The MM energies integrated with Poisson–Boltzmann or generalized Born surface area (MM/PBSA and MM/GBSA) continuum solvation approaches are common techniques to evaluate the FBE of small molecules or ligands to large biological molecules. The MM/GBSA and MM/PBSA approaches are established on MD simulations of protein–ligand complexes (Figure 3.4), therefore, they are transitional in computational effort and precision between severe alchemical perturbation methods and empirical scoring (Genheden and Ryde, 2015).

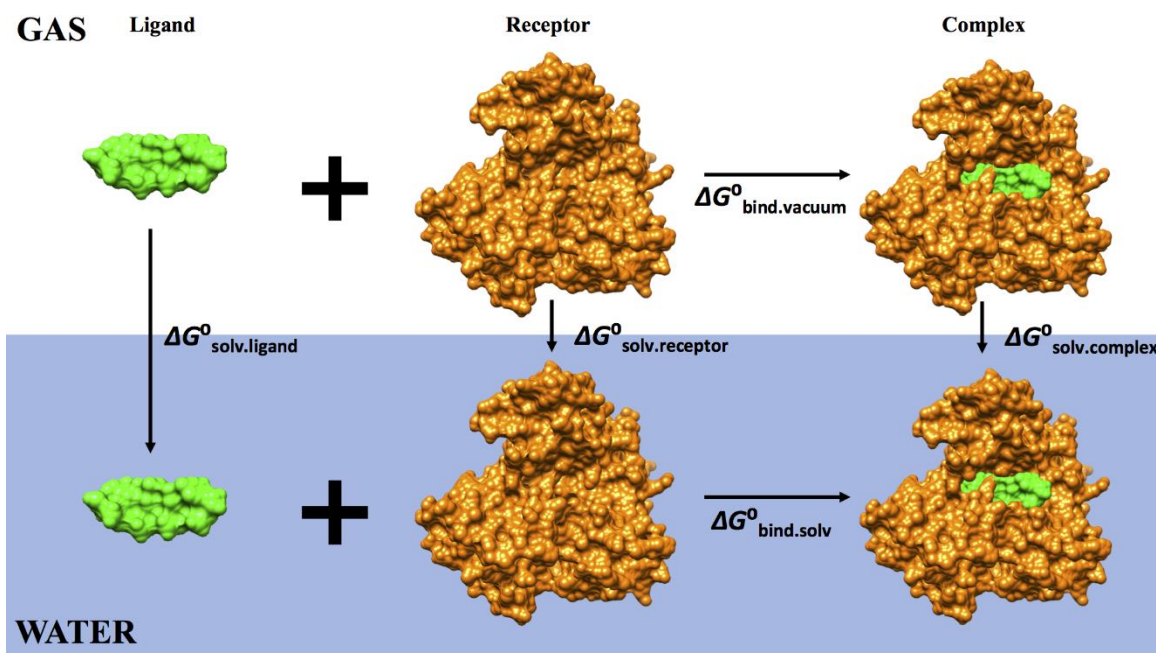


Figure 3.4 Illustration of the thermodynamic cycle in MM/PBSA or MM/GBSA calculations. The addition of the gas-phase configurational entropy and energy and the difference in solvation free energies between the ligand and complex results in the FBE results. The blue surface signifies the solvent (Prepared by Author).

The ultimate goal of drug design is to discover novel compounds that bind to a molecular receptor (Genheden and Ryde, 2015). Basically, binding may be described as:



Where,

- L Ligand
- R Receptor (protein or other biomacromolecule)

The affinity with which the ligand binds to the receptor is known as the FBE or ΔG_{bind} , which is calculated using the MM/GBSA and MM/PBSA approaches for a protein system (ligand, receptor and complex) is represented as:

$$\Delta G_{\text{bind}} = G_{\text{complex}} - G_{\text{receptor}} - G_{\text{ligand}} \quad (15)$$

$$\Delta G_{\text{bind}} = E_{\text{gas}} + G_{\text{sol}} - TS \quad (16)$$

$$E_{\text{gas}} = E_{\text{int}} + E_{\text{vdW}} + E_{\text{ele}} \quad (17)$$

$$G_{\text{sol}} = G_{\text{GB}} + G_{\text{SA}} \quad (18)$$

$$G_{\text{SA}} = \gamma \text{SASA} \quad (19)$$

Where,

E_{ele}	Electrostatic potential energy from Coulomb forces
E_{gas}	Gas-phase energy (based on FF14SB force field terms)
E_{int}	Internal energy
E_{vdW}	Van der Waals energy
G_{sol}	Solvation free energy
G_{GB}	Polar solvation energy
G_{SA}	Non-polar solvation energy
S	Total entropy of solute
SASA	Solvent accessible surface area (water probe radius of 1.4 Å)
T	Total entropy of temperature

The MM/GBSA and MM/PBSA methods are quantifiable analyses of ligand-protein binding affinity and thus can improve docked molecular structures (Chen *et al.*, 2018).

4.1.3 Conformational Fluctuations of the System

Root-mean-square fluctuation (RMSF) – Calculates alpha-carbon atomic fluctuations of a protein's constituent amino acid residues based on the changes in the structure of the protein along the trajectory of the system. This allows for the determination of protein flexibility based on calculations (Bornot, Etchebest and de Brevern, 2011). Standardized RMSF is calculated using the following equation:

$$sRMSF = \frac{(RMSF_i - \overline{RMSF})}{\sigma(RMSF)} \quad (20)$$

Where,

RMSF_i RMSF of the ith residue
 σ (RMSF) RMSF's standard deviation

4.1.4 *Dynamic Cross Correlation Matrices*

Dynamic Cross Correlation Matrices (DCCM) can quantifies the correlation coefficients of interatomic motions. The correlation coefficient ranges from -1 (negative/anti-correlated motion) to +1 (positively correlated motion) (Kasahara, Fukuda and Nakamura, 2014). The equation below is used to describe DCCM:

$$C_{ij} = \frac{\langle \Delta r_i \cdot \Delta r_j \rangle}{(\langle \Delta r_i^2 \rangle \langle \Delta r_j^2 \rangle)^{\frac{1}{2}}} \quad (21)$$

Where,

C_{ij} Cross-correlation coefficient (-1 to +1)
i ith residue
j jth residue
 Δr_i ith displacement vector
 Δr_j jth displacement vector

Protein-ligand binding results in movements of amino acids within proteins, making DCCM a useful tool (Kasahara, Fukuda and Nakamura, 2014; Devnarain and Soliman, 2018).

5 Other Computer-Aided Drug Design Techniques Utilized in the Study

5.1 *Molecular Docking*

Molecular docking is one of the most well-known computational methods in drug design. It applies several techniques to predict the conformation of a complex and binding affinity between a ligand and receptor, which demonstrate the most common application of docking (Alonso, Bliznyuk and Gready, 2006; Meng *et al.*, 2011). Several studies have also presented drug delivery/protein-protein complexes such as aptamers and nanoparticles (de Ruyck *et al.*, 2016).

Molecular docking encompasses two key steps. The first step involves evaluating different ligand conformations in a protein's binding pocket using different algorithms. The "lock and key" analogy regards the ligand as a rigid key and receptor as a rigid enzyme, where only the appropriately sized key (ligand) fits into the key hole (binding site) of the lock (enzyme) to open it (elicit a reaction). The ligand can also be regarded as flexible either via simulation-based or random techniques. The flexible ligand technique is the preferred approach since the ligand fits more accurately into the protein. The second step involves the use of a scoring function to rank the different ligand-enzyme configurations. The scoring algorithm may be based on MM force fields, previous binding affinities or statistically chosen contacts (Du *et al.*, 2016)

For the purpose of this study, docked complex were substantiated with MD simulations to show that all ligands were stable in the binding pockets of the enzymes.

5.2 *Virtual Screening*

Virtual screening (VS) is an indispensable tool in drug design and discovery since it allows researchers to explore through small molecule databases using knowledge of biological targets it may bind to (Pyzer-Knapp *et al.*, 2015). The VS method enables sorting of large databases of small molecules to a more realistic figure and provides hits that are most likely to qualify lead compounds. This approach applies multiple filters to classify biologically active alternatives to existing drugs on the basis that molecules of comparable structural are likely to have similar characteristics and features (Lionta *et al.*, 2014; Cele, Ramesh and Soliman, 2016).

There are two sub-categories of VS, namely the ligand-based and structure-based VS approaches. Ligand-based VS works with compounds that are known to interact with a biological target to generate libraries of small molecules (Ripphausen, Nisius and Bajorath, 2011). Structure-based VS recognizes dynamically favorable ligand binding affinities to a binding site of a biological target, allowing for an improved understanding of the binding site and interactions between the ligand and enzyme. This category of VS filters compounds from a massive library for molecular docking (Lionta *et al.*, 2014).

In this study, pharmacophore-based VS is applied since it has shown to have various advantages in the identification and optimization of lead compounds. The method utilizes pharmacophoric moieties based on functional groups of an existing inhibitor, such as aromatics, cations, hydrogen bond acceptors and donor, and cations. These pharmacophoric moieties are set as the standards or templates to identify a few hit compounds in extensive libraries (Cele, Ramesh and Soliman, 2016; Munir, Azam and Mehmood, 2016).

6 References

Aerts, D. (2014) ‘Quantum theory and human perception of the macro-world’, *Frontiers in Psychology*, 5(554), pp. 1–19. doi: 10.3389/fpsyg.2014.00554.

Alder, B. J. and Wainwright, T. E. (1959) ‘Studies in Molecular Dynamics. I. General Method’, *The Journal of Chemical Physics*. American Institute of Physics, 31(2), pp. 459–466. doi: 10.1063/1.1730376.

Allen, M. P. (2004) ‘Introduction to Molecular Dynamics Simulation’, *Computational Soft Matter: From Synthetic Polymers to Proteins*, 23(1), pp. 1–28.

Alonso, H., Bliznyuk, A. A. and Gready, J. E. (2006) ‘Combining Docking and Molecular Dynamic Simulations in Drug Design’, *Medicinal Research Reviews*. Wiley Periodicals, Inc, 26(5), pp. 531–568. doi: 10.1002/med.20067.

Ballentine, L. E. (2014) *Quantum Mechanics: A Modern Development Second Edition*. 2nd edn. World Scientific Publishing Company. doi: <https://doi.org/10.1142/9038>.

Barde, N. P. *et al.* (2015) ‘Deriving time dependent Schrödinger equation from Wave-Mechanics, Schrödinger time independent equation, classical and Hamilton-Jacobi equations.’, *Leonardo*

Electronic Journal of Practices and Technologies, 14(26), pp. 31–48.

Bohr, N. (1913) ‘On the constitution of atoms and molecules’, *The London, Edinburgh, and Dublin Philosophical Magazine and Journal of Science*, 26(1), pp. 1–25.

Born, M., Elsasser, W. M. and Anderson, D. L. (1981) ‘My Life: Recollections of a Nobel Laureate and Memoirs of a Physicist in the Atomic Age.’, *American Journal of Physics*, 49(1), pp. 94–95. doi: 10.1119/1.12605.

Born, M. and Oppenheimer, R. (1927) ‘Zur Quantentheorie der Molekeln’, *Annalen der Physik*, 389(20), pp. 457–484. doi: 10.1002/andp.19273892002.

Bornot, A., Etchebest, C. and de Brevern, A. G. (2011) ‘Predicting protein flexibility through the prediction of local structures.’, *Proteins*. Inserm, 79(3), pp. 839–52. doi: 10.1002/prot.22922.

Brambilla, N. *et al.* (2018) ‘Born-Oppenheimer approximation in an effective field theory language’, *Physical Review D*, 97(1), pp. 1–16. doi: 10.1103/PhysRevD.97.016016.

Brookes, J. C. (2017) ‘Quantum effects in biology: golden rule in enzymes, olfaction, photosynthesis and magnetodetection’, *Proceedings of the Royal Society A: Mathematical, Physical and Engineering Science*, 473(2201), p. 20160822. doi: 10.1098/rspa.2016.0822.

Brooks, B. R. *et al.* (1983) ‘CHARMM: A program for macromolecular energy, minimization, and dynamics calculations’, *Journal of computational chemistry*, 4(2), pp. 187–217. Available at: <http://karin.fq.uh.edu/charmm/ref/charmm0.pdf> (Accessed: 28 March 2017).

Case, D. A. *et al.* (2014) ‘Amber 14’. doi: <http://www.ambermd.org>.

Cele, F. N., Ramesh, M. and Soliman, M. E. S. (2016) ‘Per-residue energy decomposition pharmacophore model to enhance virtual screening in drug discovery: A study for identification of reverse transcriptase inhibitors as potential anti-HIV agents’, *Drug Design, Development and Therapy*, 10, pp. 1365–1377. doi: 10.2147/DDDT.S95533.

Chen, F. *et al.* (2018) ‘Assessing the performance of MM/PBSA and MM/GBSA methods. 8. Predicting binding free energies and poses of protein-RNA complexes.’, *RNA*, p. rna-065896. doi: 10.1261/rna.065896.118.

Chow, T. L. (2013) *Classical Mechanics*. 2nd Editio. CRC Press.

Christensen, A. S. *et al.* (2016) ‘Semiempirical Quantum Mechanical Methods for Noncovalent Interactions for Chemical and Biochemical Applications’, *Chemical Reviews*, 116(9), pp. 5301–5337. doi: 10.1021/acs.chemrev.5b00584.

Cornell, W. D., Howard, A. E. and Kollman, P. (1991) ‘Molecular mechanical potential functions and their application to study molecular systems: Current Opinion in Structural Biology 1991, 1:201–212’, *Current Opinion in Structural Biology*. Elsevier Current Trends, 1(2), pp. 201–212. doi: 10.1016/0959-440X(91)90062-X.

Devadoss, F. R. and Raj, V. P. (2014) *Analysis and Visual Summarization of Molecular Dynamics Simulation*. Universitat Konstanz. Available at: <https://pdfs.semanticscholar.org/318f/525f314fb38e0d03e26f008e7f06d050924e.pdf>.

Devnarain, N. and Soliman, M. E. S. (2018) ‘A Panoptic Uncovering of the Dynamical Evolution of the Zika Virus NS5 Methyltransferase Binding Site Loops- Zeroing in on the Molecular Landscape’, *Chemical Biology & Drug Design*, 92(5), pp. 1838–1850. doi: 10.1111/cbdd.13353.

Dixit, S. B., Ponomarev, S. Y. and Beveridge, D. L. (2006) ‘Root Mean Square Deviation Probability Analysis of Molecular Dynamics Trajectories on DNA’, *Journal of Chemical Information and Modeling*, 46(3), pp. 1084–1093. doi: 10.1021/ci0504925.

Du, X. *et al.* (2016) ‘Insights into Protein-Ligand Interactions: Mechanisms, Models, and Methods.’, *International journal of molecular sciences*. Multidisciplinary Digital Publishing Institute (MDPI), 17(2), p. 144. doi: 10.3390/ijms17020144.

Fermi, E. *et al.* (1955) *Studies of Nonlinear Problems (Los Alamos Report LA-1940)*.

Genheden, S. and Ryde, U. (2015) ‘The MM/PBSA and MM/GBSA methods to estimate ligand-binding affinities’, *Expert Opinion on Drug Discovery*, 10(5), pp. 449–461. doi: 10.1517/17460441.2015.1032936.

Gibson, J. B. *et al.* (1960) ‘Dynamics of Radiation Damage’, *Physical Review*. American Physical Society, 120(4), pp. 1229–1253. doi: 10.1103/PhysRev.120.1229.

Goldbeck, G. (2012) *The Economic Impact of Molecular Modelling, Goldbeck Consulting Report*. doi: 10.5281/zenodo.44359.

Golden, S. D. and Olsen, K. W. (2008) ‘Use of the Conjugate Peak Refinement Algorithm for Identification of Ligand-Binding Pathways in Globins’, in *Methods in Enzymology*. Academic Press, pp. 417–437. doi: 10.1016/S0076-6879(07)37021-3.

González, M. A. (2011) ‘Force fields and molecular dynamics simulations’, *Collection SFN*, 12, pp. 169–200. doi: 10.1051/sfn/201112009.

Hinsen, K. (2000) ‘The Molecular Modeling Toolkit: A New Approach to Molecular Simulations’, *Journal of Computational Chemistry*, 21(2), pp. 79–85. doi: 10.1002/(SICI)1096-

987X(20000130)21:2<79::AID-JCC1>3.0.CO;2-B.

Hollingsworth, S. A. and Dror, R. O. (2018) 'Molecular Dynamics Simulation for All.', *Neuron*. Elsevier, 99(6), pp. 1129–1143. doi: 10.1016/j.neuron.2018.08.011.

Huang, N. *et al.* (2006) 'Molecular mechanics methods for predicting protein–ligand binding', *Phys. Chem. Chem. Phys.* The Royal Society of Chemistry, 8(44), pp. 5166–5177. doi: 10.1039/B608269F.

Jakobsson, E. (2001) 'Computational Biochemistry and Biophysics', *Journal of the American Chemical Society*. American Chemical Society, 123(50), p. 12745. doi: 10.1021/JA015256Z.

Karplus, M. and McCammon, J. A. (2002) 'Molecular dynamics simulations of biomolecules', *Nature Structural Biology*. Nature Publishing Group, 9(9), pp. 646–652. doi: 10.1038/nsb0902-646.

Kasahara, K., Fukuda, I. and Nakamura, H. (2014) 'A novel approach of dynamic cross correlation analysis on molecular dynamics simulations and its application to Ets1 dimer-DNA complex', *PLoS ONE*, 9(11), p. e112419. doi: 10.1371/journal.pone.0112419.

Kostal, J. (2016) 'Computational Chemistry in Predictive Toxicology: status quo et quo vadis?', in *Advances in Molecular Toxicology*. Elsevier, pp. 139–186. doi: 10.1016/B978-0-12-804700-2.00004-0.

Kragh, H. (2012) *Niels Bohr and the quantum atom: The Bohr model of atomic structure*. Oxford University Press. doi: 10.1093/acprof:oso/9780199654987.001.0001.

Kufareva, I. and Abagyan, R. (2011) 'Methods of Protein Structure Comparison', in *Methods in molecular biology (Clifton, N.J.)*, pp. 231–257. doi: 10.1007/978-1-61779-588-6_10.

Lewars, E. G. (2011) 'The Concept of the Potential Energy Surface', in *Computational Chemistry*, pp. 9–41. doi: 10.1007/978-90-481-3862-3_2.

Likhachev, I. V, Balabaev, N. K. and Galzitskaya, O. V (2016) 'Available Instruments for Analyzing Molecular Dynamics Trajectories.', *The open biochemistry journal*. Bentham Science Publishers, 10(1), pp. 1–11. doi: 10.2174/1874091X01610010001.

Lionta, E. *et al.* (2014) 'Structure-based virtual screening for drug discovery: principles, applications and recent advances.', *Current Topics in Medicinal Chemistry*, 14(16), pp. 1923–1938. doi: 10.2174/1568026614666140929124445.

Liu, H. *et al.* (2001) 'Quantum mechanics simulation of protein dynamics on long timescale', *Proteins: Structure, Function, and Genetics*. John Wiley & Sons, Ltd, 44(4), pp. 484–489. doi: 10.1002/prot.1114.

- Lu, X. *et al.* (2016) ‘QM/MM free energy simulations: recent progress and challenges.’, *Molecular simulation*. NIH Public Access, 42(13), pp. 1056–1078. doi: 10.1080/08927022.2015.1132317.
- McConnell, I., Li, G. and Brudvig, G. W. (2010) ‘Energy conversion in natural and artificial photosynthesis’, *Chemistry and Biology*. Elsevier Ltd, 17(5), pp. 434–447. doi: 10.1016/j.chembiol.2010.05.005.
- Meng, X.-Y. *et al.* (2011) ‘Molecular Docking: A powerful approach for structure-based drug discovery’, *Current Computational-Aided Drug Design*, 7(2), pp. 146–157. doi: <https://doi.org/10.2174/157340911795677602>.
- Merz, K. M. (2014) ‘Using quantum mechanical approaches to study biological systems’, *Accounts of Chemical Research*, 47(9), pp. 2804–2811. doi: 10.1021/ar5001023.
- Munir, A., Azam, S. and Mehmood, A. (2016) ‘Structure-Based Pharmacophore Modeling, Virtual Screening and Molecular docking for the Treatment of ESR1 Mutations in Breast Cancer’, *Drug Designing: Open Access*, 5(137), pp. 2169-0138. doi: 10.4172/2169-0138.1000137.
- Nelson, E. (1966) ‘Derivation of the schrödinger equation from newtonian mechanics’, *Physical Review*, 150(4), pp. 1079–1085. doi: 10.1103/PhysRevD.10.1358.
- Perilla, J. R. *et al.* (2015) ‘Molecular dynamics simulations of large macromolecular complexes’, *Current Opinion in Structural Biology*. Elsevier Current Trends, 31, pp. 64–74. doi: 10.1016/J.SBI.2015.03.007.
- Pokluda, J. *et al.* (2015) ‘Ab initio calculations of mechanical properties: Methods and applications’, *Progress in Materials Science*, 73(1), pp. 127–158. doi: 10.1016/j.pmatsci.2015.04.001.
- Pyzer-Knapp, E. O. *et al.* (2015) ‘What Is High-Throughput Virtual Screening? A Perspective from Organic Materials Discovery’, *Annual Review of Materials Research*, 45(1), pp. 195–216. doi: 10.1146/)).
- Quesne, M. G., Borowski, T. and De Visser, S. P. (2016) ‘Quantum Mechanics/Molecular Mechanics Modeling of Enzymatic Processes: Caveats and Breakthroughs’, *Chemistry - A European Journal*, 22(8), pp. 2562–2581. doi: 10.1002/chem.201503802.
- Rahman, A. (1964) ‘Correlations in the Motion of Atoms in Liquid Argon’, *Physical Review*. American Physical Society, 136(2A), pp. A405–A411. doi: 10.1103/PhysRev.136.A405.
- Redhu, S. and Jindal, A. (2013) ‘Molecular modelling: A new scaffold for drug design’, *International Journal of Pharmacy and Pharmaceutical Sciences*, 5(Suppl.1), pp. 5–8. doi: 10.1016/j.tet.2017.04.015.

Ripphausen, P., Nisius, B. and Bajorath, J. (2011) 'State-of-the-art in ligand-based virtual screening', *Drug Discovery Today*. Elsevier Current Trends, 16(9–10), pp. 372–376. doi: 10.1016/J.DRUDIS.2011.02.011.

de Ruyck, J. *et al.* (2016) 'Molecular docking as a popular tool in drug design, an in silico travel', *Advances and Applications in Bioinformatics and Chemistry*, 9(1), pp. 1–11. doi: 10.2147/AABC.S105289.

Schmidt, T., Bergner, A. and Schwede, T. (2014) 'Modelling three-dimensional protein structures for applications in drug design', *Drug Discovery Today*. Elsevier Ltd, 19(7), pp. 890–897. doi: 10.1016/j.drudis.2013.10.027.

Schreiner, W. *et al.* (2012) 'Relaxation estimation of RMSD in molecular dynamics immunosimulations.', *Computational and mathematical methods in medicine*. Hindawi Limited, 2012, p. 173521. doi: 10.1155/2012/173521.

Schrödinger, E. (1926) 'An Undulatory Theory of the Mechanics of Atoms and Molecules', *Physical Review*, 28(6), pp. 1049–1070. doi: 10.1103/PhysRev.28.1049.

Shen, L., Wu, J. and Yang, W. (2016) 'Multiscale quantum mechanics/molecular mechanics simulations with neural networks.', *Journal of chemical theory and computation*, 12(10), pp. 4934–4946. doi: 10.1021/acs.jctc.6b00663.

Sherrill, C. D. (2005) *C. David Sherrill - The Born-Oppenheimer Approximation.pdf*.

De Simone, A., Mote, K. R. and Veglia, G. (2014) 'Structural dynamics and conformational equilibria of SERCA regulatory proteins in membranes by solid-state NMR restrained simulations.', *Biophysical journal*. The Biophysical Society, 106(12), pp. 2566–76. doi: 10.1016/j.bpj.2014.03.026.

Siu, S. W. I., Pluhackova, K. and Böckmann, R. A. (2012) 'Optimization of the OPLS-AA Force Field for Long Hydrocarbons', *Journal of Chemical Theory and Computation*, 8(4), pp. 1459–1470. doi: 10.1021/ct200908r.

Sjulstok, E., Olsen, J. M. H. and Solov'Yov, I. A. (2015) 'Quantifying electron transfer reactions in biological systems: What interactions play the major role?', *Scientific Reports*. Nature Publishing Group, 5(18446), pp. 1–11. doi: 10.1038/srep18446.

Sprenger, K. G., Jaeger, V. W. and Pfaendtner, J. (2015) 'The general AMBER force field (GAFF) can accurately predict thermodynamic and transport properties of many ionic liquids', *Journal of Physical Chemistry B*, 119(18), pp. 5882–5895. doi: 10.1021/acs.jpbc.5b00689.

Stepito, R. *et al.* (2015) 'Definitions of terms relating to individual macromolecules, macromolecular

assemblies, polymer solutions, and amorphous bulk polymers (IUPAC Recommendations 2014)', *Pure and Applied Chemistry*. De Gruyter, 87(1), pp. 71–120. doi: 10.1515/pac-2013-0201.

Sutcliffe, B. T. and Woolley, R. G. (2012) 'Atoms and Molecules in Classical Chemistry and Quantum Mechanics', in *Philosophy of Chemistry*. North-Holland, pp. 387–426. doi: 10.1016/B978-0-444-51675-6.50028-1.

Sutcliffe, B. and Woolley, R. G. (2013) 'The Potential Energy Surface in Molecular Quantum Mechanics', *Advances in Quantum Methods and Applications in Chemistry, Physics, and Biology*, 23(1), pp. 3–40. doi: 10.1007/978-3-319-01529-3_1.

Vanommeslaeghe, K. *et al.* (2014) 'Molecular mechanics.', *Current pharmaceutical design*. NIH Public Access, 20(20), pp. 3281–92. Available at: <http://www.ncbi.nlm.nih.gov/pubmed/23947650> (Accessed: 6 January 2019).

Vlachakis, D. *et al.* (2014) 'Current State-of-the-Art Molecular Dynamics Methods and Applications', in *Advances in Protein Chemistry and Structural Biology*. Academic Press, pp. 269–313. doi: 10.1016/B978-0-12-800168-4.00007-X.

Wang, Y. *et al.* (2015) 'In silico ADME/T modelling for rational drug design', *Quarterly Reviews of Biophysics*, 48(4), pp. 488–515. doi: 10.1017/S0033583515000190.

Yu, W. and MacKerell, A. D. J. (2017) 'Computer-Aided Drug Design Methods.', *Methods in molecular biology*. NIH Public Access, 1520(1), pp. 85–106. doi: 10.1007/978-1-4939-6634-9_5.

Zheng, M. *et al.* (2013) 'Computational methods for drug design and discovery: Focus on China', *Trends in Pharmacological Sciences*. Elsevier Ltd, 34(10), pp. 549–559. doi: 10.1016/j.tips.2013.08.004.

CHAPTER 4

Brain Grants Permission of Access to Zika Virus but Denies Entry to Drugs: A Molecular Modeling Perspective to Infiltrate the Boundary

Brain Grants Permission of Access to Zika Virus but Denies Entry to Drugs: A Molecular Modeling Perspective to Infiltrate the Boundary

Nikita Devnarain, Pritika Ramharack and Mahmoud E. Soliman

Molecular Bio-computation and Drug Design Laboratory, School of Health Sciences,
University of KwaZulu-Natal, Westville Campus, Durban 4001, South Africa. E-mail:
soliman@ukzn.ac.za; Fax: +27 31 260 7872; Tel: +27 31 260 8048

Abstract

The magnetism of the Zika virus to neuronal cells proves to be one of the major concerns in the development of effective inhibitors. Although the blood-brain barrier limits the entry of most drugs, tailored small molecule inhibitors and drug delivery systems are currently being designed to overcome this obstacle. We have identified the core challenge to be addressed - blood-brain barrier permeability - and provided insight into strategies that can be used to improve drug delivery to the brain. We have compiled drugs that have previously been proposed as potential Zika virus inhibitors and classified chemical features of those drugs, which influence blood-brain barrier permeability. Thereafter, we created a route map to design drugs with improved blood-brain barrier permeability. An alternative approach using drug delivery systems to transport membrane-impermeable Zika virus inhibitors to the brain is also proposed, along with descriptions of known drug carriers. This review provides information for further research toward inhibitors of Zika virus.

The Tale of Zika Virus

The Zika virus (ZIKV), a mosquito-borne virus, belongs to the *Flaviviridae* family and has similar characteristics to other flaviviruses such as Dengue virus, West Nile virus and Japanese Encephalitis virus.¹ The rapid disseminating potential and repercussion in humans are attributed to the various modes of transmission, primarily through the bite of an infected *Aedes aegypti* mosquito.² The ZIKV is also transmitted through sexual intercourse³, blood transfusions⁴ and from a mother to child perinatally.⁵

The ZIKV was originally isolated in Uganda in the Zika forest in 1947.⁶ For nearly 7 decades thenceforth, sporadic infections caused by ZIKV were reported in several countries worldwide. These include more equatorial countries of Africa such as Tanzania, Egypt, Kenya, Nigeria, Central African Republic, and Gabon; some Asian countries including Pakistan, India, Malaysia, Thailand, the Philippines and Indonesia; and many islands in the Pacific Ocean.⁷⁻¹⁰ The most devastating and highly publicized outbreak that captured the world's attention occurred in Brazil in 2015, which triggered global panic as it rapidly spread across America.¹¹ In 2016, the ZIKV broadened its geographic spectrum to North American Florida and Texas where the infection was locally transmitted.¹⁰

There has been prior ambiguity regarding the diagnosis of ZIKV, as its infection manifests similarly to common colds and other *flavivirus* infections.¹² These symptoms include fever, headaches, conjunctivitis, joint pain, muscle pain and skin rash.^{13,14} The speculation of ZIKV infection depends on its manifestation and history of mosquito bites.¹² The ZIKV is detectable in bodily fluids such as saliva¹⁵, semen^{16,17}, urine¹⁸ and amniotic fluid¹⁹, which can be verified in the laboratory.²⁰ The various modes of transmission of ZIKV make the human body highly susceptible to infection. When ZIKV enters the body through an infected female mosquito bite, the infection manifests as a rash in the vicinity of the bite.⁹ This occurs due to the release of virions into dermal and epidermal layers of

the skin, where ZIKV is introduced to the bloodstream and advances to the lymph nodes to replicate and cause viremia.²¹

The ZIKV is an enveloped icosahedral virus that is made up of a single-stranded, positive-sense genome. The enveloped virion comprises of an 11 kilobase genome consisting of 10,794 nucleotides encoding 3,419 amino acids.²² The open reading frame (ORF) of the 5' and 3' untranslated region (UTR) encodes a polyprotein that is cleaved into three structural proteins, being the capsid (C), precursor membrane (prM), and envelope (E).²³ Seven non-structural (NS) proteins are also found in this assembly, namely, NS1, NS2a, NS2b, NS3, NS4a, NS4b, and NS5 (largest viral protein).²⁴ The genomic protein organization is 5'-C-prM-E-NS1-NS2a-NS2b-NS3-NS4a-NS4b-NS5-3' ²⁵ and contains an m⁷gpppAmpN₂ at the 5' end and lacks a poly-A tail at the 3' end.²⁶ A highly conserved 90-120-nucleotide strand is situated close to the 3' end that develops into a hairpin loop and is vital for replication.^{26,27} Of the non-structural proteins, NS1, NS3 and NS5 are highly conserved whereas the NS2a, NS2b, NS4a and NS4b are small and hydrophobic.²⁴ Of critical importance is the proteolytic cleavage of prM to produce the pr and M protein by furin-like protease located in the trans-Golgi network during the egress of the particles as this promotes maturation of virions.²⁸

The ramifications of ZIKV infections have heavily impacted thousands worldwide, particularly in newborns, since ZIKV-infected pregnant women have given birth to babies with congenital brain abnormalities, predominantly microcephaly and intracranial calcification.¹³ The ZIKV infection has also been shown to elicit Guillain–Barré Syndrome, which ultimately advances to paralysis and death.²⁹

Studies have shown tropism of the ZIKV for cells of the nervous system, whereby entry into neuronal and endothelial cells occur via AXL receptors situated on the cell surface.^{30–32} The ZIKV has also

affected retinal cells that line the blood-retinal barrier (i.e. retinal pigment epithelium and retinal endothelium) in mice, which also express AXL receptors. This presents as conjunctivitis.³³

Blood-Brain Barrier Permeability as a Core Challenge in ZIKV Therapy

Treating the symptoms of ZIKV will not yield permanent results; hence nipping the cause at the bud may be the best route to a solution. The blood-brain barrier (BBB) and placental barrier are surrounded by lipophilic membranes and junctions, through which only certain compounds can permeate.³⁴ It has been shown that the placenta is permissive to most drugs as it serves to allow for the exchange of nutrients for its biological purpose.³⁵ The ZIKV can penetrate these membranes, which is evident by its downstream pathogenic effects in fetal nervous systems.^{13,26,29,30}

The specific characteristics of a compound govern the method by which it is transported across the BBB, or whether or not it is transported at all. Compounds that have surface hydrogen bonds (hydrophilic compounds) are only permissive through tight junctions of the BBB, which ultimately serve to prevent the passage of molecules between cells of the endothelium. These hydrophilic compounds are impermeable through the lipophilic endothelium and require lipid-mediated transport in order to permeate transcellularly. Large molecules, such as insulin and transferrin, require receptors, whereas small molecules require carrier-mediated transport to move across the barrier. There is also active efflux transport for endogenous BBB transporters (Figure 1- BBB).^{34,36-38}

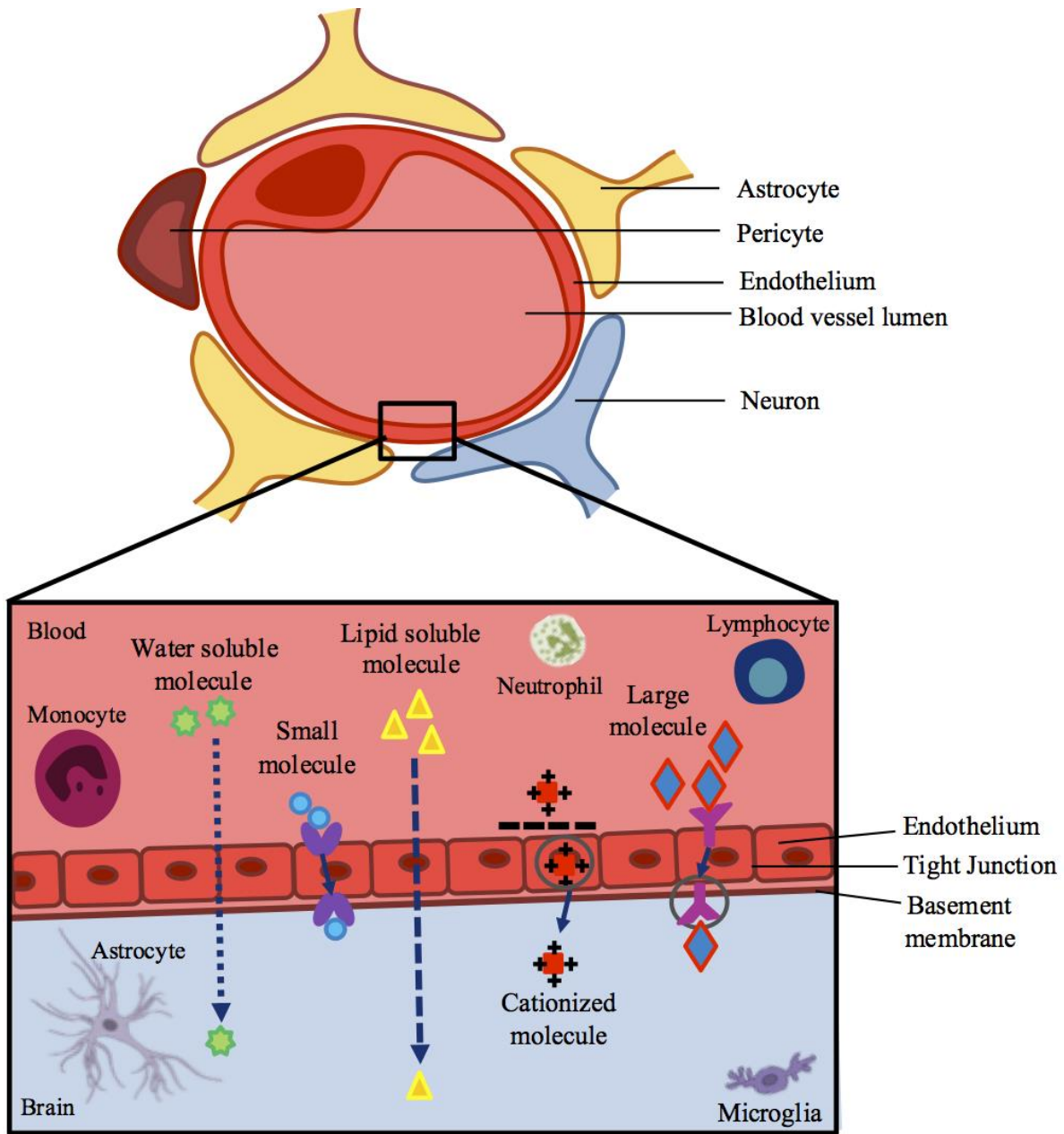


Figure 13: A schematic representation of the blood-brain barrier and pathways across this barrier.

Bioavailability Features of Screened Drugs as Prospective ZIKV Inhibitors

There are FDA-approved drugs that have been proposed as anti-ZIKV drugs based on their diverse antiviral/antimicrobial/antibacterial activities in diseases other than ZIKV ³⁹, however, the ability of those drugs to pass the BBB, their properties as hydrophilic/lipophilic compounds, and their ability to be absorbed by the gastrointestinal tract (GIT) have not yet been clearly elucidated. To this effect, we have taken a step further and utilized a chemical data base, PubChem, along with ADME prediction tools, Swiss ADME ⁴⁰ to predict specific characteristics of these candidate anti-ZIKV drugs and to verify whether or not the proposed compounds by Barrows *et al.* (2016) could be potential anti-ZIKV drugs with BBB-permeable profiles. The proposed compounds are listed in Table 1.

Table 1: Predicted Bioavailability Features of Prospective Anti-ZIKV Inhibitors.

Drug name	Lipid solubility (logp)	Bbb permeation	Git absorption
Auranofin	0.00	No	High
Azathioprine	0.72	No	Low
Bortezomib	0.00	No	High
Clofazimine	4.72	No	Low
Cyclosporine a	6.16	No	Low
Dactinomycin	5.33	No	Low
Daptomycin	0.79	No	Low
Deferasirox	2.48	No	High
Digoxin	4.69	No	Low
Fingolimod	3.76	Yes	High
Gemcitabine hcl	0.00	No	High
Ivermectin	6.31	No	Low
Mebendazole	1.27	No	High
Mefloquine hcl	0.00	No	Low
Mercaptopurine hydrate	0.47	No	High
Methoxsalen	2.22	Yes	High
Micafungin	-0.72	No	Low
Mycophenolate mofetil	3.67	No	High
Mycophenolic acid	2.38	No	High

Nitd008	1.30	No	Low
Palonosetron hcl	0.00	Yes	High
Pyrimethamine	2.15	Yes	High
Sertraline	3.40	Yes	High
Sofosbuvir	3.05	No	Low
Sorafenib tosylate	3.84	No	Low
Thioguanine	0.14	No	High

The partition coefficient (LogP) measures how hydrophilic or hydrophobic a molecule is. The desired LogP value of a molecule likely to permeate lipophilic membranes should lie between 0-5.⁴¹ The ability of a drug to pass through the BBB is influenced by their unique but varying properties.³⁶ In Table 1, ~80% of the drugs described have the ability to pass through lipophilic membranes, however, less than 20% of those drugs can penetrate the BBB⁴⁰. Efficient GIT absorption of orally administered drugs is required for entry into the bloodstream and sufficient drug delivery⁴², although, just half the drugs mentioned are highly absorbed via the GIT. The results of this table suggest that the ability of a compound to pass through the BBB depends on factors additional to lipophilicity. From this exercise we highlight 5 compounds that are predicted to pass the BBB and the hydrophobic spots of each compound are shadowed in yellow in Figure 2.

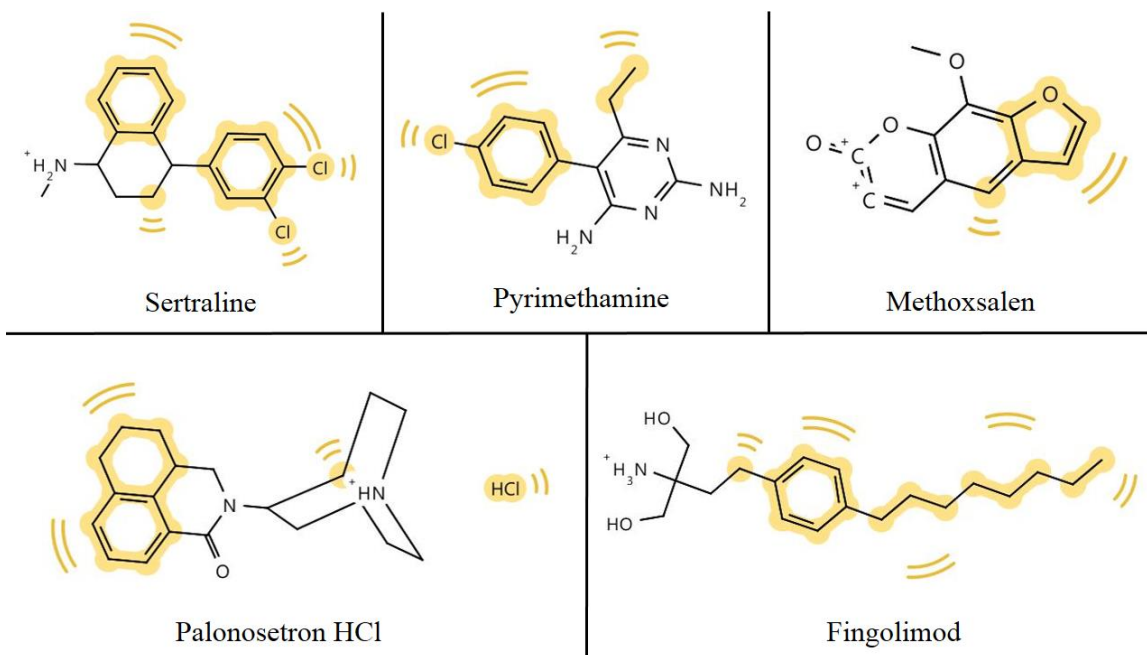


Figure 14: Hydrophobic footprints (highlighted in yellow) in chemical structures of potential anti-ZIKV compounds which have the ability to permeate the BBB.

Hydrophobic groups of compounds are required for hydrophobic interactions with target molecules. Hydrophobic interactions are comparably stronger than some weak intermolecular forces, such as Hydrogen bonds or Van der Waals interactions, and ensure protein-ligand complexes remain stable and biologically active.⁴³ As depicted in Figure 2, all five compounds from Table 1 that have the ability to pass the BBB bear hydrophobic groups and therefore, possess the potential to form hydrophobic interactions with target molecules. Although, fingomolid and sertraline have more hydrophobic spots than the other compounds in Figure 2, and therefore, are more likely to form stronger hydrophobic interactions.

Systematic Approach to Tackle the Challenge

To overcome the hurdle faced by most drug therapies, we are presenting two main strategies that could potentially assist with the design and bioavailability of compounds with an improved BBB permeability profile. Furthermore, we include an approach that relies on the pre-existing BBB-impermeable drugs conjugated to drug delivery systems. These strategies are: (1) improve the inhibitor and (2) carry the cargo.

Improve the Inhibitor

In this approach, *in silico* tools may be used to model and optimize potential compounds (Figure 3), followed by compound synthesis and biological testing. Phase 1 includes targeted selection of potential anti-ZIKV compounds. This incorporates screening for potential compounds with specific physicochemical properties and antiviral activities using chemical databases, and the use of absorption, distribution, metabolism, excretion (ADME) prediction tools such as Swiss ADME, in order to filter out compounds that encompass the ability to pass the BBB. The ability of a compound to pass through the BBB is governed by a function of lipophilicity, the molecular characteristics of charged and hydrophobic residues of the compound as well as molecular weight.³⁷ The main lipophilic properties that must be considered include the Hansch constant (π), hydrophobic fragmental constant (f), LogP, capacity factor values from RP-HPLC (Logkw), calculated log P values (CLOGP) and molecular lipophilic potential (MLP).⁴⁴ With regard to the charge of the compound, only uncharged molecules can diffuse across the membrane to become reprotonated once it leaves the membrane and enters the brain fluid.³⁷ As the size of a compound gets larger, its ability to permeate the BBB decreases.⁴⁵

Phase 2 involves the prediction of lipid permeability of the potential anti-ZIKV compounds using molecular dynamic simulations and 3D-modelled lipid bilayer simulations. Due to the surrounding

lipid membrane in the BBB, it is necessary to assess compound interactions with the target enzyme within lipid membrane.⁴⁶

Phase 3 involves the estimation of binding affinities between potential compounds, which pass through the BBB, and viral enzymes. This may be achieved via binding free energy calculations or molecular docking of the compound of interest into the active site of the target enzyme.⁴⁷

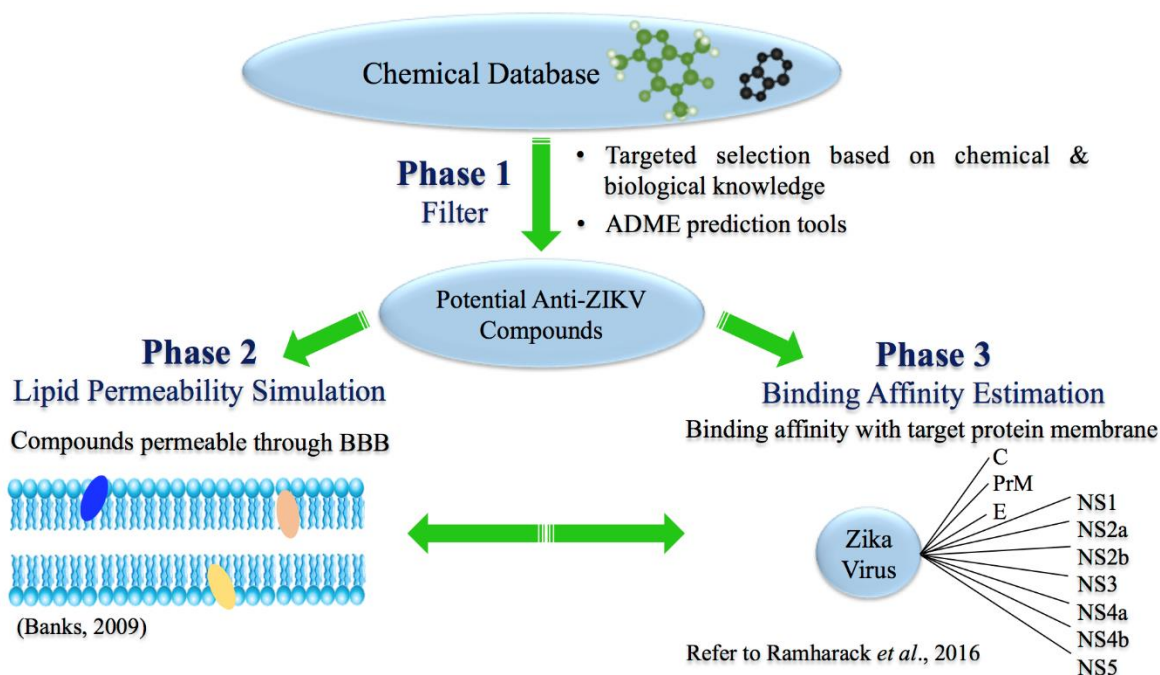


Figure 15: Phases involved in the suggested approach to improve the BBB-permeability profile of the inhibitor.

Following the design process, the compounds must be synthesized for further testing. Synthesis of the compound involves construction of the carbon framework and the addition/deletion/transformation of functional groups for functionality of compound. Validation of synthesis is carried out by ligand-binding assays which involves placing the target enzyme and compound of interest into a solvent (e.g. water) to allow the compound to interact with the active site

residues of the enzyme.⁴⁸ Binding studies provide reliable assessments of binding affinities, errors and binding mode.⁴⁸ Further studies including biological testing will investigate toxicity and efficacy of the compound, including *in vitro* studies (cellular level), *in vivo* studies (organism level) and ultimately clinical trials. Microscale thermophoresis (MST) may also be used in order to analyze the interaction between the inhibitors and receptors, experimentally, which is established on the controlled movement of particles along a temperature gradient.⁴⁹

Carry the Cargo

An alternate to creating new BBB-permeable drugs will involve the utilization of drug carriers that have already been successful in delivering drugs to the brain. This approach eliminates the additional time and expense required to design and formulate new drugs and drug delivery systems. A drug carrier could be used to transport a BBB-impermeable drug to the brain and allow for the drug to carry out its function against ZIKV.

There are existing drugs that have been proven to inhibit ZIKV replication in isolated ZIKV infected cells, such as NITD008⁵⁰ and sofosbuvir⁵¹, however the drugs cannot pass the BBB to counteract the virus (Table 1). With half the battle won due to their ability to inhibit ZIKV, ultimate triumph over ZIKV would entail overcoming impermeability, which requires the potential ZIKV inhibitors to be transported across the BBB.

Previously utilized membrane-permeable drug delivery approaches have been successful in transporting membrane-impermeable drugs across the BBB for other infections and diseases, such as

Parkinson's disease and Alzheimer's disease.⁵²⁻⁵⁵ Some known drug delivery systems used in various disease cases include polymers and polymeric nanoparticles such as micro/nanospheres, micro/nanocapsules, dendrimers, liposomes, hydrogels, gold nanoparticles, micelles; others include lipoproteins and aptamers (Table 2).^{54,56}

Table 2: Pre-existing drug delivery systems and their principle roles in disease and virus therapies

Drug delivery system	Description	Disease/viral target	References
Dendrimer	<ul style="list-style-type: none"> • Hyperbranched, monodispersed, water soluble (1-100 nm) macromolecule • Encapsulated drug in its interior or adsorbs drug on and conjugates to its surface groups • Releases free 5-fluorouracil upon hydrolysis • Intracellular delivery of poorly soluble drugs • Carriers in gene therapy 	<ul style="list-style-type: none"> • Inhibitors of haemagglutinin of human erythrocytes by Influenza virus • Amino groups of dendrimer react with nucleic acid phosphate groups to form transfection complexes 	56,57
Microsphere & nanocapsule	<ul style="list-style-type: none"> • Microsphere –drug is dispersed within polymer throughout particle • Nanocapsule- cavity contains drug surrounded by polymer membrane • Drug release through diffusion through polymer or degradation of polymer 	<ul style="list-style-type: none"> • Entraps luteinizing hormone-releasing hormone in prostate cancer 	57,58

Liposomes	<ul style="list-style-type: none"> • Amphiphilic vesicular structures made up of cholesterol & phospholipids • Core suited for hydrophilic drug delivery • Phospholipid membrane encapsulate hydrophobic drugs 	<ul style="list-style-type: none"> • Facultative intracellular bacteria-mediated infections • Parasites (e.g. Leishmania) • Viruses • Systemic fungal diseases in cancer • Melanomas 	56,59,60
Micelles	<ul style="list-style-type: none"> • Core comprised of hydrophobic polymers • Shell comprised of hydrophilic polymers • Suitable for drugs with poor solubility • Nanosize; <i>in vivo</i> endurance; remains stable in plasma • Delivery of drugs & small interfering RNA 	<ul style="list-style-type: none"> • Targets tumour sites in cancer by active/passive mechanisms 	56,61,62
Hydrogel	<ul style="list-style-type: none"> • Network of natural/synthetic hydrophilic polymers that are cross-linked • Highly absorbent, biodegradable, high porosity, biocompatible • Swell rapidly in aqueous solution • Used in oral & topical drug delivery 	<ul style="list-style-type: none"> • Local & systemic diseases • Oral delivery of insulin in diabetes; salmon calcitonin for postmenopausal osteoporosis; growth hormone for decelerated/stunted growth-associated diseases 	56,63,64
Gold/silver nanoparticle	<ul style="list-style-type: none"> • Low toxicity; high specificity & selectivity • Easily controlled & modifiable • High ratio of surface area:amount 	<ul style="list-style-type: none"> • Selective damage of tumour cells • Certain infectious & dermal diseases • H1N1, H3N2, H5N1 Influenza A virus • Herpes Simplex Virus 	65-68

	<ul style="list-style-type: none"> • Conjugation of proteins on colloidal gold nanoparticles occurs via electrostatic interactions between citrate(-) on surfaces of gold nanoparticles & groups(+) on proteins • Effortless cellular penetration 	<ul style="list-style-type: none"> • Human Immunodeficiency Virus • Hepatitis B Virus • Metapneumovirus • Respiratory syncytial virus 	
Lipid nanoparticle	<ul style="list-style-type: none"> • 10-1000 nm • Carriers with dispersed melted lipid in surfactant • Colloidal system with hydrophobic core that encloses drug & surface coated with hydrophilic polymers 	<ul style="list-style-type: none"> • Humoral immunity against Ebola infection. • Silencing of hepatitis C virus replication • Gene therapy 	56,69-72
Aptamer	<ul style="list-style-type: none"> • Short, single-stranded (ss) DNA or RNA that have definitive 2° & 3° structures that strongly bind to specific target proteins • Low immunogenicity & toxicity • Variety of targets & modifiable chemical structure 	<ul style="list-style-type: none"> • α-Thrombin in thrombosis • PTK7 and nucleolin in cancer • IGHM in lymphoma • VEGF in age-related macular degeneration • A1 domain of vWF in thrombotic microangiopathies & carotid artery disease • Neutralizes r5 strains of HIV-1 • Blocks gp120-CCR5 interaction 	73-77

The inhibitor-carrier approach will involve techniques similar to the previous suggested approach. The first step would be to create an inhibitor-carrier complex by binding the known ZIKV inhibitor to the carrier. The complex must then be simulated to analyze the trajectory of the complex as well

as the potential energy of the entire complex through a lipid bilayer. Once there is computational evidence to show that the inhibitor can theoretically bind to the carrier and move through a lipid membrane, the inhibitor-carrier complex must be synthesized to test it biologically (e.g. *in vivo* testing), which will be used to confirm drug delivery through the BBB to the brain. Technical guidance related to the *in silico* tools involved in these approaches and examples of computationally docking a compound-polymer complex is provided in the supplementary information.

Conclusion

The various challenges associated with ZIKV treatment has led to the ongoing search for a cure - one of the major problems being drug delivery across the BBB. The approaches described in this review serve to provide information that can be used for further research into the design of drugs with improved BBB-permeability profile that may have a greater ability to inhibit ZIKV. Though experimental validation is necessary, this is not the scope of the current study. Instead, this study serves as a cornerstone that will open doors to further experimental and molecular validation regarding ZIKV therapy.

Conflicts of interest

Authors declare no potential conflicts of interest.

Acknowledgements

The authors acknowledge the College of Health Sciences, UKZN.

References

- 1 I. Briguglio, S. Piras, P. Corona and A. Carta, *Int. J. Med. Chem.*, 2011, **2011**, 1–22.
- 2 R. K. Singh, K. Dhama, Y. S. Malik, M. A. Ramakrishnan, K. Karthik, R. Tiwari, S. Saurabh, S. Sachan and S. K. Joshi, *Vet. Q.*, 2016, **36**, 150–175.
- 3 D. Musso, C. Roche, E. Robin, T. Nhan, A. Teissier and V. M. Cao-Lormeau, *Emerg. Infect. Dis.*, 2015, **21**, 359–361.
- 4 D. Musso, T. Nhan, E. Robin, C. Roche, D. Bierlaire, K. Zisou, A. Shan Yan, V. M. Cao-Lormeau and J. Broult, *Eurosurveillance*, 2014, **19**, 14–16.
- 5 M. Besnard, S. Lastère, A. Teissier, V. M. Cao-Lormeau and D. Musso, *Eurosurveillance*, 2014, **19**, 8–11.
- 6 G. W. A. Dick, S. F. Kitchen and A. J. Haddow, *Trans. R. Soc. Trop. Med. Hyg.*, 1952, **55**, 509–520.
- 7 M. R. Duffy, C. Tai-Ho, T. Hancock, A. M. Powers, J. L. Kool, R. S. Lanciotti, M. Pretrick, C. Dubray, L. Guillaumot, A. Griggs, M. Bel, A. J. Lambert, J. Laven, O. Kosoy, A. Panella, B. J. Biggerstaff, M. Fischer and E. B. Hayes, *N. Engl. J. Med.*, 2009, **360**, 2536–2543.
- 8 D. Musso, E. J. Nilles and V. M. Cao-Lormeau, *Clin. Microbiol. Infect.*, 2014, **20**, O595–O596.
- 9 V. Sikka, V. K. Chattu, R. K. Popli and T. J. Galwankar, Sagar C, Kelkar, Dhanashree, Sawicki, Stanley G, Stawicki, Stanislaw P, Papadimos, *J. Glob. Infect. Dis.*, 2016, **8**, 3–15.
- 10 S.-I. Yun and Y.-M. Lee, *J. Microbiol.*, 2017, **55**, 204–219.
- 11 G. S. Campos, A. C. Bandeira and S. I. Sardi, *Emerg. Infect. Dis.*, 2015, **21**, 1885–1886.
- 12 D. Musso and D. J. Gubler, *Nature*, 2016, **11**, 10–20.
- 13 F. Krauer, M. Riesen, L. Reveiz, O. T. Oladapo, R. Martínez-Vega, T. V Porgo, A. Haefliger, N. J. Broutet and N. Low, *PLOS Med.*, 2017, **14**, 1–27.
- 14 P. Ramharack and M. E. S. Soliman, *R. Soc. Chem.*, 2016, **6**, 68719 – 68731.
- 15 D. Musso, C. Roche, T. X. Nhan, E. Robin, A. Teissier and V. M. Cao-Lormeau, *J. Clin. Virol.*, 2015, **68**, 53–55.
- 16 J. M. Mansuy, M. Dutertre, C. Mengelle, C. Fourcade, B. Marchou, P. Delobel, J. Izopet and G. Martin-Blondel, *Lancet Infect. Dis.*, 2016, **16**, 405.

- 17 J. M. Turmel, P. Abgueguen, B. Hubert, Y. M. Vandamme, M. Maquart, H. Le Guillou-Guillemette and I. Leparç-Goffart, *Lancet*, 2016, **387**, 2501.
- 18 A. C. Gourinat, O. O'Connor, E. Calvez, C. Goarant and M. Dupont-Rouzeyrol, *Emerg. Infect. Dis.*, 2015, **21**, 84–86.
- 19 G. Calvet, R. S. Aguiar, A. S. O. Melo, S. A. Sampaio, I. de Filippis, A. Fabri, E. S. M. Araujo, P. C. de Sequeira, M. C. L. de Mendonça, L. de Oliveira, D. A. Tschoeke, C. G. Schrago, F. L. Thompson, P. Brasil, F. B. dos Santos, R. M. R. Nogueira, A. Tanuri and A. M. B. de Filippis, *Lancet Infect. Dis.*, 2016, **16**, 653–660.
- 20 O. Faye, O. Faye, A. Dupressoir, M. Weidmann, M. Ndiaye and A. Alpha Sall, *J. Clin. Virol.*, 2008, **43**, 96–101.
- 21 R. Hamel, O. Dejarnac, S. Wichit, P. Ekchariyawat, A. Neyret, N. Luplertlop, M. Perera-Lecoin, P. Surasombatpattana, L. Talignani, F. Thomas, V. M. Cao-Lormeau, V. Choumet, L. Briant, P. Despres, A. Amara, H. Yssel and D. Misse, *J. Virol.*, 2015, **89**, 8880–8896.
- 22 O. Faye, C. C. M. Freire, A. Iamarino, O. Faye, J. Velasco, C. De Oliveira, M. Diallo, P. M. A. Zanotto and A. A. Sall, *PLoS Negl Trop Dis*, 2014, **8**, 1–10.
- 23 H. Tian, X. Ji, X. Yang, W. Xie, K. Yang, C. Chen, C. Wu, H. Chi, Z. Mu, Z. Wang and H. Yang, *Protein Cell*, 2016, **7**, 450–454.
- 24 H. Tian, X. Ji, X. Yang, Z. Zhang, Z. Lu, K. Yang, C. Chen, Q. Zhao, H. Chi, Z. Mu, W. Xie, Z. Wang, H. Lou, H. Yang and Z. Rao, *Protein Cell*, 2016, **7**, 562–570.
- 25 B. Ganguly and E. Ganguly, *bioRxiv*, 2016, 54486.
- 26 M. K. White, H. S. Wollebo, J. David Beckham, K. L. Tyler and K. Khalili, *Ann. Neurol.*, 2016, **80**, 479–489.
- 27 N. J. da Fonseca, M. Q. Lima Afonso, N. G. Pedersolli, L. C. de Oliveira, D. S. Andrade and L. Bleicher, *Biochem. Biophys. Res. Commun.*, DOI:10.1016/j.bbrc.2017.01.041.
- 28 G. Li, M. Poulsen, C. Fenyvuesvolgyi, Y. Yashiroda, M. Yoshida and J. M. Simard, *Proc. Natl. Acad. Sci.*, 2016, **114**, 201619735.
- 29 P. Brasil, P. C. Sequeira, A. D. Freitas, H. E. Zogbi, G. A. Calvet, R. V de Souza, A. M. Siqueira, M. C. de Mendonca, R. M. Nogueira, A. M. de Filippis and T. Solomon, *Lancet*, 2016, **387**, 1482.
- 30 J. J. Miner and M. S. Diamond, *Cell Stem Cell*, 2016, **18**, 559–560.
- 31 T. J. Nowakowski, A. A. Pollen, E. Di Lullo, C. Sandoval-Espinosa, M. Bershteyn and A. R. Kriegstein, *Cell Stem Cell*, 2016, **18**, 591–596.

- 32 H. Retallack, E. Di Lullo, C. Arias, K. A. Knopp, M. T. Laurie, C. Sandoval-Espinosa, W. R. M. Leon, R. Krencik, E. M. Ullian, J. Spatazza, A. A. Pollen, C. Mandel-Brehm, T. J. Nowakowski, A. R. Kriegstein, J. L. Derisi, N. Sestan and P.-Y. Shi, *Proc. Natl. Acad. Sci.*, 2016, **113**, 14408–14413.
- 33 P. K. Singh, J.-M. Guest, M. Kanwar, J. Boss, N. Gao, M. S. Juzych, G. W. Abrams, F.-S. Yu and A. Kumar, , DOI:10.1172/jci.insight.92340.
- 34 N. R. Saunders, M. D. Habgood, K. Møllgård and K. M. Dziegielewska, *FI000Research*, 2016, **5**, 1–15.
- 35 M. R. Syme, J. W. Paxton and J. a Keelan, *Clin. Pharmacokinet.*, 2004, **43**, 487–514.
- 36 W. A. Banks, *BMC Neurol.*, 2009, **9**, S3.
- 37 A. Seelig, R. Gottschlich and R. M. Devant, *Proc. Natl. Acad. Sci.*, 2016, **91**, 68–72.
- 38 J. M. Tarbell and M. Y. Pahakis, *J. Intern. Med.*, 2006, **259**, 339–350.
- 39 N. J. Barrows, R. K. Campos, S. T. Powell, K. R. Prasanth, G. Schott-Lerner, R. Soto-Acosta, G. Galarza-Muñoz, E. L. McGrath, R. Urrabaz-Garza, J. Gao, P. Wu, R. Menon, G. Saade, I. Fernandez-Salas, S. L. Rossi, N. Vasilakis, A. Routh, S. S. Bradrick and M. A. Garcia-Blanco, *Cell Host Microbe*, 2016, **20**, 259–270.
- 40 A. Daina, O. Michielin and V. Zoete, *Sci. Rep.*, 2017, **7**, 1–13.
- 41 A. Daina, O. Michielin and V. Zoete, *Journal Chem. Inf. Model.*, 2014, **54**, 3284–3301.
- 42 Y. N. Gavhane and A. V. Yadav, *Saudi Pharm. J.*, 2012, **20**, 331–344.
- 43 P. Atkins and J. De Paula, *Physical chemistry for the life sciences*, 2011.
- 44 P. P. Kore, M. M. Mutha, R. V. Antre, R. J. Oswal and S. S. Kshirsagar, *J. Med. Chem.*, 2012, **2**, 139–148.
- 45 J. A. Arnott and S. L. Planey, *Expert Opin. Drug Discov.*, 2012, **7**, 863–875.
- 46 R. Guixà-González, I. Rodríguez-Espigares, J. M. Ramírez-Anguita, P. Carrió-Gaspar, H. Martínez-Seara, T. Giorgino and J. Selent, 2014, **30**, 1478–1480.
- 47 X.-Y. Meng, H.-X. Zhang, M. Mezei and M. Cui, *Curr. Comput. Drug Des.*, 2011, **7**, 146–157.
- 48 E. C. Hulme and M. A. Trevethick, *Br. J. Pharmacol.*, 2010, **161**, 1219–1237.
- 49 Duhr, S., Baaske, P. and Bigus, H., 2016. Nanotemper Technologies GmbH, Hirschmann

Laborgerate Gmbh & Co. Kg. Patent no.: US9389211 B2.

- 50 Y. Q. Deng, N. N. Zhang, C. F. Li, M. Tian, J. N. Hao, X. P. Xie, P. Y. Shi and C. F. Qin, *Open Forum Infect. Dis.*, 2016, **3**, 6–9.
- 51 S. E. Reznik and J. C. R. Ashby, *Int. J. Infect. Dis.*, 2016, **55**, In press.
- 52 C. Roney, P. Kulkarni, V. Arora, P. Antich, F. Bonte, A. Wu, N. N. Mallikarjuana, S. Manohar, H.-F. Liang, A. R. Kulkarni, H.-W. Sung, M. Sairam and T. M. Aminabhavi, *J. Control. Release*, 2005, **108**, 193–214.
- 53 C. Spuch and C. Navarro, *J. Drug Deliv.*, 2011, **2011**, 1–12.
- 54 M. S. Gunay, A. Y. Ozer and S. Chalon, *Curr Neuropharmacol*, 2016, **14**, 376–391.
- 55 E. Blanco, H. Shen and M. Ferrari, *Nat. Biotechnol.*, 2015, **33**, 941–951.
- 56 A. Srivastava, T. Yadav, S. Sharma, A. Nayak, A. Kumari and N. Mishra, *J. Biosci. Med.*, 2016, **4**, 69–84.
- 57 N. A. Liechty, W. B., Kryscio, D.R., Slaughter, B. V. and Peppas, *Annu. Rev. Chem. Biomol. Eng.*, 2010, **1**, 149–173.
- 58 Z. Abouelfadel and D. Crawford, *Ther. Clin. Risk Manag.*, 2008, **4**, 513–526.
- 59 A. Coune, *Infection*, 1988, **16**, 141–147.
- 60 M. A. Tran, R. J. Watts and G. P. Robertson, *Pigment Cell Melanoma Res.*, 2009, **22**, 388–399.
- 61 U. Kedar, P. Phutane, S. Shidhaye and V. Kadam, *Nanomedicine Nanotechnology, Biol. Med.*, 2010, **6**, 714–729.
- 62 X.-B. Xiong, H. Uludağ and A. Lavasanifar, *Biomaterials*, 2010, **31**, 5886–5893.
- 63 D. Bhowmik, H. Gopinath, B. Pragati Kumar, S. Duraivel and K. P. Sampath Kumar, *Pharma Innov.*, 2012, **1**, 12–31.
- 64 L. A. Sharpe, A. M. Daily, S. D. Horava and N. A. Peppas, *Expert Opin. Drug Deliv.*, 2014, **11**, 901–915.
- 65 X. Yu, I. Trase, M. Ren, K. Duval, X. Guo and Z. Chen, *J. Nanomater.*, , DOI:10.1155/2016/1087250.Design.
- 66 H. Daraee, A. Eatemadi, E. Abbasi, S. Fekri Aval, M. Kouhi and A. Akbarzadeh, *Artif. cells, nanomedicine, Biotechnol.*, 2014, **1401**, 1–13.

- 67 W. Tao, B. L. Hurst, A. K. Shakya, M. J. Uddin, R. S. J. Ingrole, M. Hernandez-Sanabria, R. P. Arya, L. Bimler, S. Paust, E. B. Tarbet and H. S. Gill, *Antiviral Res.*, 2017, **141**, 62–72.
- 68 M. Rai, S. D. Deshmukh, A. P. Ingle, I. R. Gupta, M. Galdiero and S. Galdiero, *Crit. Rev. Microbiol.*, 2014, **42**, 46–56.
- 69 S. Mukherjee, S. Ray and R. S. Thakur, *Indian J Pharm Sci*, 2009, **71**, 349–358.
- 70 J. D. Bazzill, C. L. Cooper, Y. Fan, S. Bavari and J. J. Moon, *J. Immunol.*
- 71 J. Torrecilla, A. del Pozo-Rodríguez, M. yñgeles Solinís, P. S. Apaolaza, B. Berzal-Herranz, C. Romero-López, A. Berzal-Herranz and A. Rodríguez-Gascón, *Colloids Surfaces B Biointerfaces*, 2016, **146**, 808–817.
- 72 A. del Pozo-Rodríguez, M. Á. Solinís and A. Rodríguez-Gascón, *Eur. J. Pharm. Biopharm.*, 2016, **109**, 184–193.
- 73 A. K. Dey, M. Khati, M. Tang, R. Wyatt, S. M. Lea and W. James, *J. Virol.*, 2005, **79**, 13806–10.
- 74 F. Jiang, B. Liu, J. Lu, F. Li, D. Li, C. Liang, L. Dang, J. Liu, B. He, S. A. Badshah, C. Lu, X. He, B. Guo, X. B. Zhang, W. Tan, A. Lu and G. Zhang, *Int. J. Mol. Sci.*, 2015, **16**, 23784–23822.
- 75 S. D. Jayasena, *Clin. Chem.*, 1999, **45**, 1628–1650.
- 76 P. Ray and R. R. White, *Pharmaceuticals*, 2010, **3**, 1761–1778.
- 77 M. Blind and M. Blank, *Mol. Ther. - Nucleic Acids*, 2015, **4**, e223.

CHAPTER 5

A Panoptic Uncovering of the Dynamical Evolution of the Zika Virus NS5 Methyltransferase Binding Site Loops—Zeroing in on the Molecular Landscape

**A Panoptic Uncovering of the Dynamical Evolution of the Zika
Virus NS5 Methyltransferase Binding Site Loops– Zeroing in on
the Molecular Landscape**

Short running title: **The Dynamical Evolution of Zika Virus
Methyltransferase**

Nikita Devnarain¹ and Mahmoud E. S. Soliman^{1*}

¹Molecular Bio-computation and Drug Design Laboratory, School of Health Sciences,
University of KwaZulu-Natal, Westville, Durban 4001, South Africa

*Mahmoud E. S. Soliman; Email: soliman@ukzn.ac.za; Tel: 0312607413

Abstract

The global threat of the Zika virus to humanity is real. Innovative and potent anti-Zika virus drugs are still at large, due to the lack of anti-Zika virus drugs that have passed phase 1 trials. Experimental research has revealed novel inhibitors of Zika virus NS5 methyltransferase enzyme. This study has taken a step further to provide insight into the molecular dynamics of Zika virus and inhibitor binding, which have not been established experimentally. Movements of the methyltransferase binding site loops have a large role to play in the methylation of the viral mRNA cap, which is essential for Zika virus replication. Here we pinpoint the binding interactions between each potential inhibitor and the methyltransferase, residues that are responsible for binding, as well as which inhibitor-bound complex renders the methyltransferase more stable. We also highlight the conformational changes that occur within the methyltransferase to accommodate binding of inhibitors and consequences of those changes upon the RNA- and cap-binding sites in the methyltransferase. This research will improve the understanding of the Zika virus NS5 methyltransferase enzyme, and will be beneficial in driving the development of anti-Zika virus drugs.

Keywords

Zika virus inhibitors, NS5, Methyltransferase, Molecular dynamics

1 Introduction

In the beginning of 2016, the World Health Organization declared the escalating Zika virus (ZIKV) a public health crisis due to its association with neonatal microcephaly and Guillain-Barré syndrome ^[1]. ZIKV, the rapidly disseminating pathogen, which belongs to the *flavivirus* genus of the *Flaviviridae* family, is related to other *flaviviruses*, including West Nile virus (WNV), Yellow fever virus (YFV), Japanese encephalitis virus (JEV) and Dengue virus (DENV) ^[2]. ZIKV has revealed a tropism for a broad range of tissues including sensory organs and organs of the gastrointestinal tract, respiratory system and reproductive system ^[3–6].

The preeminent mode of transmission of ZIKV is through the bite of a previously infected *Aedes aegypti* mosquito, which acts as a viral vector. ZIKV may also be distributed via sexual intercourse, blood transfusion, maternal transmission and physical contact ^[7]. Control measures have been put in place to curb the spread of the virus, however, ultimate success is yet to be attained ^[8]. Vaccine development is still several years away since vaccine candidates are still in pre-clinical trials ^[9]. Additionally, due to the erratic and spontaneous temperament of *flavivirus* outbreaks, vaccine development against *flaviviruses* is restricted ^[10].

As a result of the extensive period involved in establishing a ZIKV vaccine, there are current endeavors toward developing antiviral therapeutics ^[11]. To date, *flavivirus* infections prevail with no approved antiviral treatment. Present-day treatment of ZIKV is based on the symptoms of infection ^[12]. There is also the question of whether or not novel inhibitors will pass the blood-brain barrier ^[13]. Generally, research is turned toward drugs that inhibit

enzymes involved in critical steps in the life cycle of the virus [14-16]. There has been a compelling amount of research in the last ten years, which had been directed toward the establishment of inhibitors of targeted enzymes of other *flaviviruses* including DENV, WNV and YFV [17,18].

There may be no elixir for treating ZIKV, but recognizing the targets that provide optimal therapy will aid science in establishing the most effective therapeutics. The *flavivirus* NS5 methyltransferase (MTase) enzyme is an attractive target for the development of inhibitors due to its fundamental roles in viral replication via formation of the viral mRNA cap as well as modulation of immune response [16]. We illustrate in Figure 1, the ZIKV NS5 MTase responsible for methylation of the viral mRNA cap, as well as the RNA-dependent RNA-polymerase (RdRp) responsible for viral RNA replication [17]. Together, these subunits work in harmony to ensure viral replication [19].

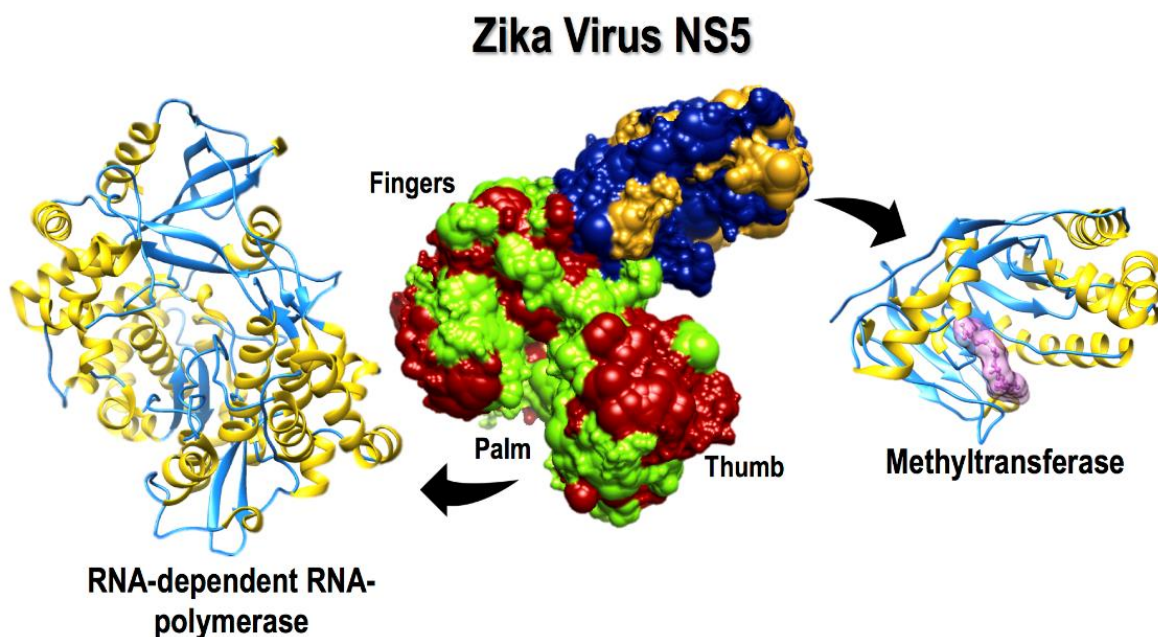


Figure 16: A schematic representation of the Zika virus NS5 enzyme. The structural protein of zika virus NS5 is divided into its two major subunits, the methyltransferase (bound to its natural substrate) and the RNA-dependent RNA-polymerase.

By virtue of the resemblance between *flaviviruses*, particularly between DENV and ZIKV, as we have presented in Figure 2, a great deal of the information regarding the drug discovery of DENV may possibly be enforced toward the establishment of ZIKV inhibitors [7,20]. Inhibitors that have been shown to suppress the MTase of DENV have also been potent in the inhibition of ZIKV MTase [14,21,22].

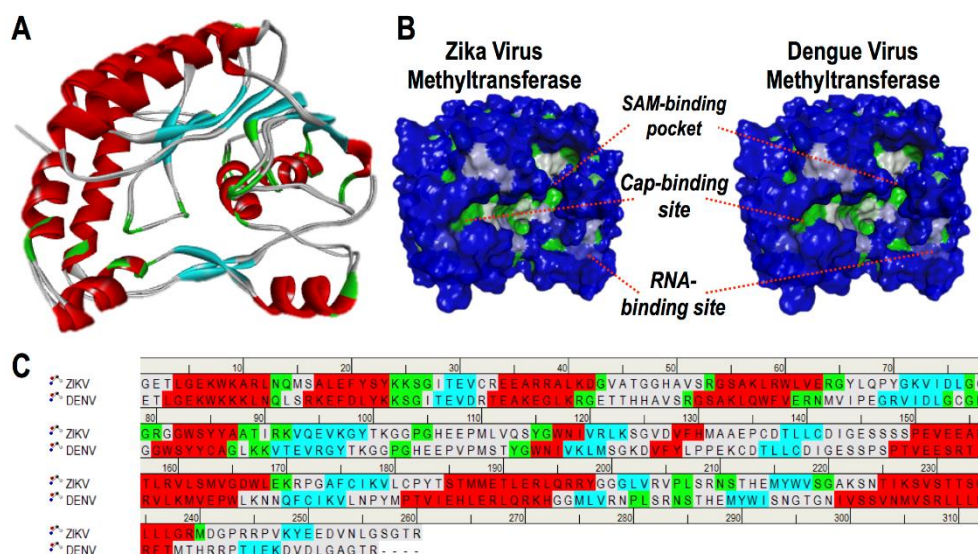


Figure 2: **A.** Superimposed crystal structures of DENV and ZIKV NS5 MTases showing similarities and differences in coils, β -sheets and α -helices. **B.** Structures of ZIKV and DENV MTases illustrating similar binding pockets and solvent accessible surface areas. **C.** Sequence similarities and differences between ZIKV and DENV.

A profoundly essential molecule for both DENV and ZIKV replication, particularly regarding the MTase component, includes S-adenosyl-L-methionine (SAM) [21]. Being the natural substrate of the

MTase, SAM serves as a methyl donor and allows for methylation of the mRNA cap, which is imperative for viral replication [23]. We demonstrate in Figure 3, that an absence of SAM-binding, as a result of displacement by an alternative compound, causes avoidance of viral replication since methylation of RNA does not occur.

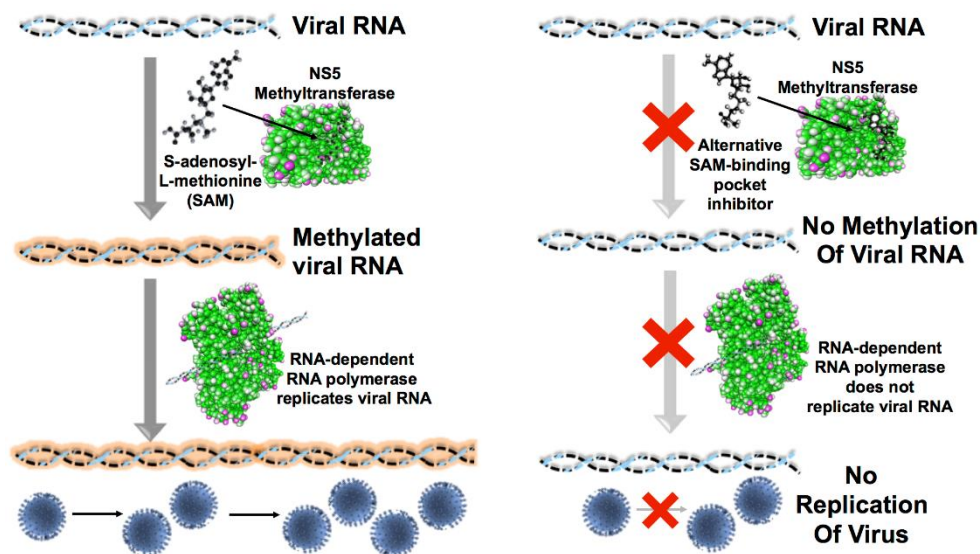


Figure 3: Implications of lack of SAM binding to MTase. Illustration of SAM-binding to the MTase as a prerequisite for viral RNA methylation and viral replication (left), and the consequence of an alternative molecule binding in the SAM-binding pocket and inhibiting viral RNA methylation and replication (right).

The adenosine derivative, sinefungin (SFG), was initially isolated as an antifungal antibiotic from *Streptomyces griseolus*, and accomplishes its inhibition by competitively binding to the SAM-binding pocket in the MTase [24]. Previously, SFG demonstrated inhibitory effects on MTases of DENV, WNV and YFV [17], and thus presented as a potential inhibitor of ZIKV [25]. Experimental evidence shows that even low concentrations of SFG inhibit ZIKV MTase and terminates internal methylation *in vitro* [21]. Coutard *et al* (2017) also demonstrates ZIKV suppression by another DENV inhibitor, Compound 5, which inhibits ZIKV MTase activity and is more potent against ZIKV MTase compared

to MTases of DENV and WNV [14,21,22]. In Figure 4, we illustrate the structures of SFG and Compound 5.

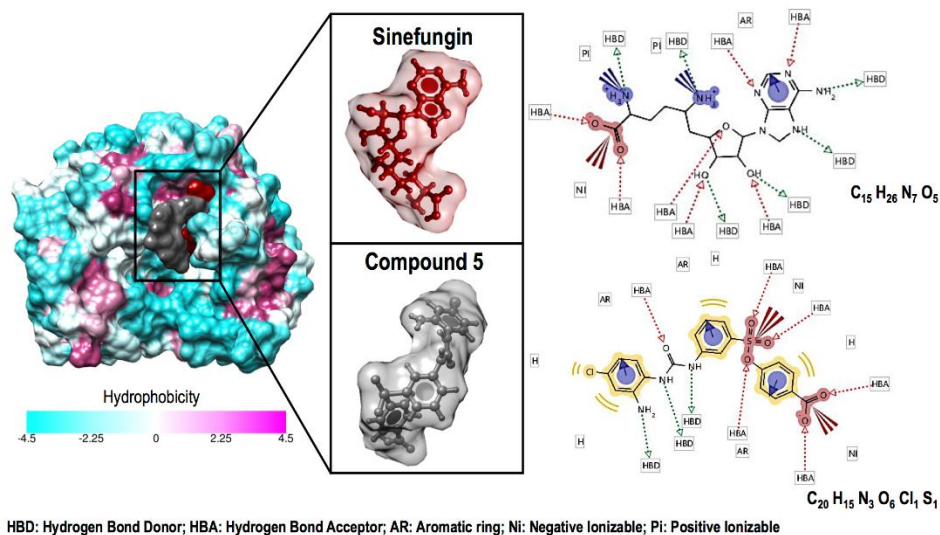


Figure 4: Potential ZIKV inhibitors. Chemical structure of SFG and Compound 5 (left), as well as the chemical formula and functional groups of SFG (top right) and Compound 5 (bottom right).

Based on preliminary viral inhibition and structural novelty, we considered further exploring the structural dynamics that take place at a molecular level within the independent ZIKV MTase (Apo), as well as ZIKV MTase bound to SFG and Compound 5, distinctly. We also compare the binding affinity, binding mode and stability of the bound complex of SFG to that of Compound 5. Two major loops in the MTase were focused on more than the rest, as one of the loops surrounds the SAM-binding pocket and the other surround the RNA-binding site. To our knowledge, this is the first study that utilizes integrated computational methods to analyze how binding of inhibitors, SFG and Compound 5, impact the conformational changes that occur within the ZIKV NS5 MTase.

Furthermore, we speculate that this study will improve the understanding of the structural information of the inhibitors and the ZIKV NS5 MTase, and will be valuable in anti-ZIKV drug design.

2 Computational Methods

2.1 System Preparation

The crystal structure of the NS5 MTase of ZIKV in complex with SFG was accessed from RCSB Protein Data Bank (PDB code: 5MRK) [25]. The protein (MTase) and ligands (SFG and Compound 5) were prepared using Molegro Molecular Viewer software (Molegro-a CLC bio company, Aarhus, Denmark) and UCSF Chimera software package [12]. The crystal structure of the MTase protein consists of chains A and B, however, in order to save computational time and expense, the distinct ligands conjugated to the singular chain A was utilized. Compound 5 was modeled using Avodagro [26]. Three systems including the Apo MTase, SFG-bound MTase and Compound 5-bound MTase were subjected to a 200 ns molecular dynamic simulation (described in section 2.3).

2.2 Molecular Docking

Molecular docking was used to predict optimized conformations and binding affinities of SFG and Compound 5 within the SAM-binding pocket of ZIKV NS5 MTase.[27] Docking software that was used in this study include UCSF Chimera [12,27] and AutoDock Vina [28]. SFG and Compound 5 were docked into the SAM-binding pocket of the NS5 MTase (grid box spacing of 0.375 Å and x, y, z dimensions of 28 x 32 x 34). The complex with the most negative binding energy (kcal.mol⁻¹) was subjected to molecular dynamic simulations. A greater expansion of molecular docking can be found in the referenced articles [29-31].

2.3 Molecular Dynamic Simulation

Molecular dynamic simulations were implemented using AMBER PMEMD dynamics engine with GPU acceleration and the protein was parameterized with the AMBER force field, FF14SB [32–35]. Hydrogen atoms were removed from the MTase protein, while SFG and Compound 5 were hydrogenated and charged with Gasteiger charges preceding the simulation. Antechamber created atomic partial charges for SFG and Compound 5 using the general AMBER force field (GAFF) and restrained electrostatic potential (RESP) methods [36–38]. The LEAP module implemented in AMBER 14 was used to combine, neutralize and solvate the systems by adding hydrogen atoms, chloride and sodium ions and suspending them in an orthorhombic box of TIP3P water molecules such that all atoms were within 10 Å of the box edges. The amino acid residues of the protein were renumbered due to missing residues in the initial crystal structure; therefore, all residue numbers reported from these findings are in fact four residues less than stated. An initial energy minimization of 2500 steps was performed with a restraint potential of 10 kcal.mol⁻¹ Å⁻² applied to the solutes, for 1000 steps of steepest descent followed by 1000 steps of conjugate gradient minimization. An additional unrestrained full minimization of 200 steps was performed by conjugate gradient algorithm.

A canonical ensemble (NVT) simulation was carried out for 50 ps from 0 K to 300 K, so that a fixed volume and number of atoms in each system was maintained. The systems' solutes were enforced with Langevin thermostat collision frequency of 1.0 ps⁻¹ and a potential harmonic restraint of 10 kcal.mol⁻¹ Å⁻². Thereafter, each system was equilibrated for 500 ps with a constant operating temperature of 300 K, as well as a constant pressure of 1 bar using the Berendsen barostat and number of atoms resembling an isobaric-isothermal ensemble. The overall simulation was conducted for 200 ns, where each simulation incorporated the shake algorithm to restrain hydrogen bonds. An SPFP precision model was utilized.

2.4 Post-dynamic Analysis

2.4.1 Computation of Thermodynamic Binding Free Energy & Per-Residue Decomposition Analysis

A well-known method utilized to determine the binding free energy (ΔG_{bind}) of small ligands to biological macromolecules includes molecular mechanics incorporated with the Poisson-Boltzmann or generalized Born and surface area continuum solvation (MM/PBSA and MM/GBSA) approach [39]. These methods are generally established on molecular dynamics simulations of the protein-ligand complex and are thus transitional in precision between empirical scoring and strict enzymatic perturbation methods [40].

ΔG_{bind} was averaged over 50 000 snapshots derived from the 200 ns trajectory. The binding strength estimated using this method for the MTase, SFG- and Compound 5-complexes could be represented as:

$$\begin{aligned} (1) \quad \Delta G_{\text{bind}} &= G_{\text{complex}} - G_{\text{receptor}} - G_{\text{ligand}} \\ (2) \quad \Delta G_{\text{bind}} &= E_{\text{gas}} + G_{\text{sol}} - TS \\ (3) \quad E_{\text{gas}} &= E_{\text{int}} + E_{\text{vdW}} + E_{\text{ele}} \\ (4) \quad G_{\text{sol}} &= G_{\text{GB}} + G_{\text{SA}} \\ (5) \quad G_{\text{SA}} &= \gamma \text{SASA} \end{aligned}$$

where:

E_{ele}	Electrostatic potential energy from Coulomb forces
E_{gas}	Gas-phase energy (based on FF14SB force field terms)
E_{int}	Internal energy
E_{vdW}	van der Waals energy
G_{sol}	Solvation free energy
G_{GB}	Polar solvation energy
G_{SA}	non-polar solvation energy

S	Total entropy of solute
SASA	Solvent accessible surface area (water probe radius of 1.4 Å)
T	Total entropy of temperature

To determine the per-residue contribution of SFG and compound 5 to the total ΔG_{bind} at the SAM-binding site, atomic level per-residue free energy decomposition was implemented for significant residues of each ligand using the AMBER14 MM/GBSA approach. The SFG- and Compound 5-bound complexes were subjected to further analysis.

2.4.2 Dynamic Cross-Correlation

Dynamic Cross-Correlation (DCC) is a well-known approach that may be utilized in the interpretation of molecular dynamic simulation-derived trajectories, by quantifying the correlation coefficients of motions between atoms ^[41]. The analysis of fluctuations between residues within the Apo MTase, SFG-bound MTase and Compound 5-bound Mtase were calculated using the CPPTRAJ module in the AMBER 14 suite. The equation that defines DCC is provided below:

$$C_{ij} = \frac{\langle \Delta r_i \Delta r_j \rangle}{(\langle \Delta r_i^2 \rangle \langle \Delta r_j^2 \rangle)^{\frac{1}{2}}}$$

where:

C_{ij} Cross-correlation coefficient (-1 [fully correlated] to +1 [anti-correlated])

i i^{th} residue

j j^{th} residue

Δr_i displacement vectors correspond to i^{th}

Δr_j displacement vectors correspond to j^{th}

The DCC matrix produced from each simulated system was constructed using Origin software.

2.5 Pharmacophore Model Generation and Structure-based Screening

The creation and analysis of a pharmacophore model is established as a vital part of drug design, as it is a beneficial tool for detection and development of new chemical entities (NCEs) ^[42]. LigandScout ^[43] tool was used to generate a pharmacophore model from the simulation of SFG.

3 Results & Discussion

3.1 Molecular dynamic simulations & Systems Stability

Trajectories of the Apo MTase system, as well as the SFG- and Compound 5-bound MTase systems were monitored during a 200 ns simulation to confirm the systems' stability, together with the precision of ensuing post-dynamic analyses.

3.1.1 Deviation of α -carbons within NS5 MTase

The stability of the 200 ns molecular dynamic simulations of the Apo MTase vs. SFG-bound MTase vs. Compound 5-bound MTase systems were explored by calculating the RMSD. In Figure 5, we demonstrate that during the simulation, the two inhibitor-bound complexes showed various RMSD patterns.

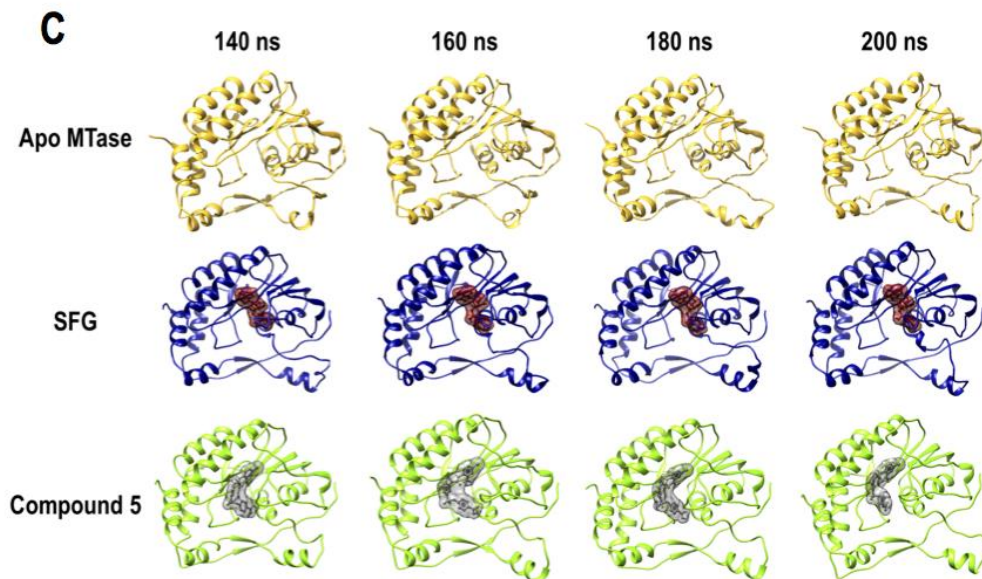
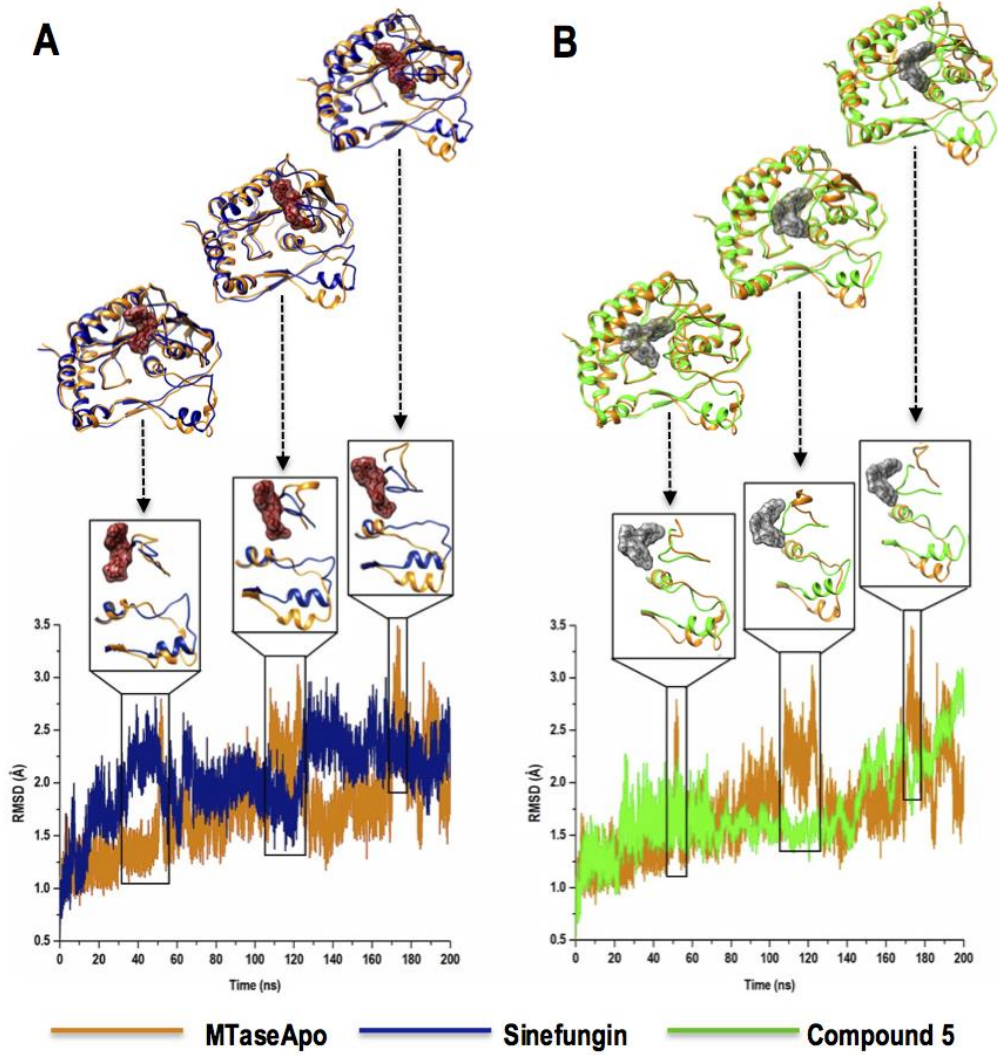


Figure 5: Fluctuations in rigidity of SFG-bound and Compound 5-bound complexes compared to apo are shown in **A** and **B**, respectively, with emphasis on loop movements during the 52ns, 122ns and 173ns periods of the simulation. **C** shows that SFG reached convergence and was less flexible toward the latter period of the simulation, as compared to that of the apo and Compound 5-bound systems.

The Compound 5-bound complex had reached convergence after 20 ns; however, the system began to fluctuate after 143 ns, although remaining within a 2.0 Å range until the end of the simulation. The SFG-MTase complex reached convergence after 169 ns, with fluctuations less than 1.5 Å. Indeed, both bound systems demonstrate stability; however, binding of SFG to the NS5 MTase renders the enzyme more stable than that of Compound 5, as convergence was maintained upon SFG-binding.

It was also noticed that binding of SFG to the MTase not only causes the SAM-binding site to become closed by the surround binding site loop (residues 100-110), but the MTase also conforms to close the RNA-binding site as the surrounding loop (residues 30-60) moves to prevent RNA from binding. Should RNA not bind to the MTase, replication of viral RNA by the RdRp will most likely not occur, preventing viral replication from occurring.

The fluctuation in rigidity in the Apo MTase (greater than 2 Å) prevented the system from reaching convergence, even toward the latter period of the simulation, indicating instability of the Apo MTase. These major rigorous fluctuations, as well as the fact that the bound systems had reached convergence whilst the unbound system had not, suggest that the MTase only stabilized upon binding of inhibitors, SFG and Compound 5.

3.1.2 Atomic Distribution of NS5 MTase Backbone

The radius of gyration (RoG) is an indicator of a structure's stability during a molecular dynamic simulation, as is associated with the compactness of secondary protein structures into 3D structures [44]. To assess the conformations of the Apo MTase, SFG- and Compound 5-bound MTase complexes, RoG was analyzed and plotted (Figure S1).

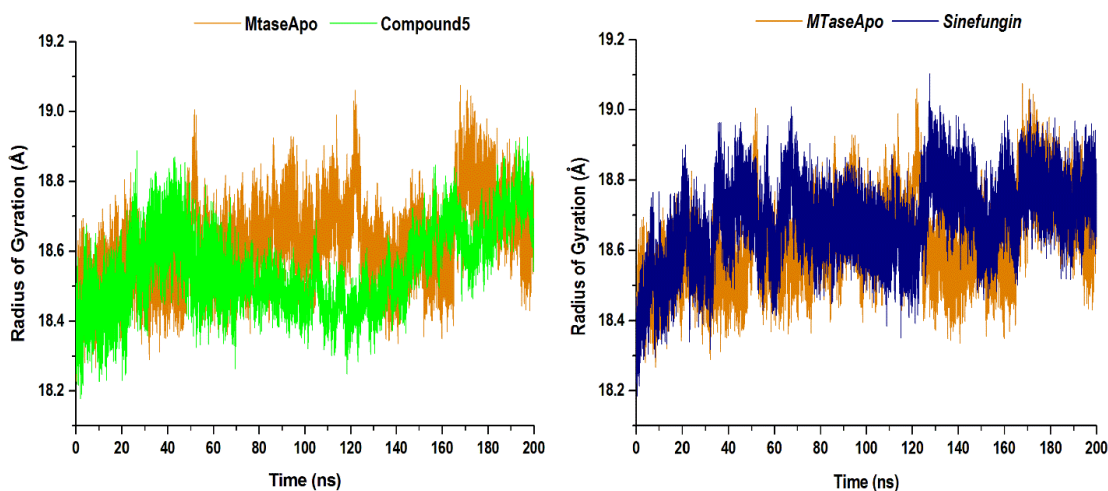


Figure S1: Graphs illustrating the radius of gyration (RoG) showing the variation of MTase compactness of the apo vs SFG-bound system (left) and the apo vs Compound 5-bound system (right) throughout a 200ns molecular dynamic simulation.

It was noticed that in the RMSD plot (Figure 6), at 52 ns, 122 ns and 173 ns the Apo MTase fluctuated significantly, whilst binding of both inhibitors, SFG and Compound 5, had stabilized the enzyme at those points in the simulation. Correspondingly, the RoG plots showed similar trends at 52 ns, 122 ns and 173 ns, as both inhibitors caused the MTase to become more compact to accommodate binding. The Apo MTase had a greater atomic distribution than the inhibitor-bound complexes and is therefore, more flexible and less compact than when bound.

3.2 Intra- and Intermolecular Interactions in ZIKV NS5 MTase

3.2.1 Intermolecular Hydrogen Bond Patterns

Hydrogen bonding between amino acid residues is subject to the spatial arrangement of the associated atoms, and is a major driving force in structural changes that occur within proteins. To further analyze the forces that drive the conformational changes within the enzyme, we evaluated the hydrogen bonding pattern of the apo, SFG-bound and Compound 5-bound MTase systems throughout the simulation.

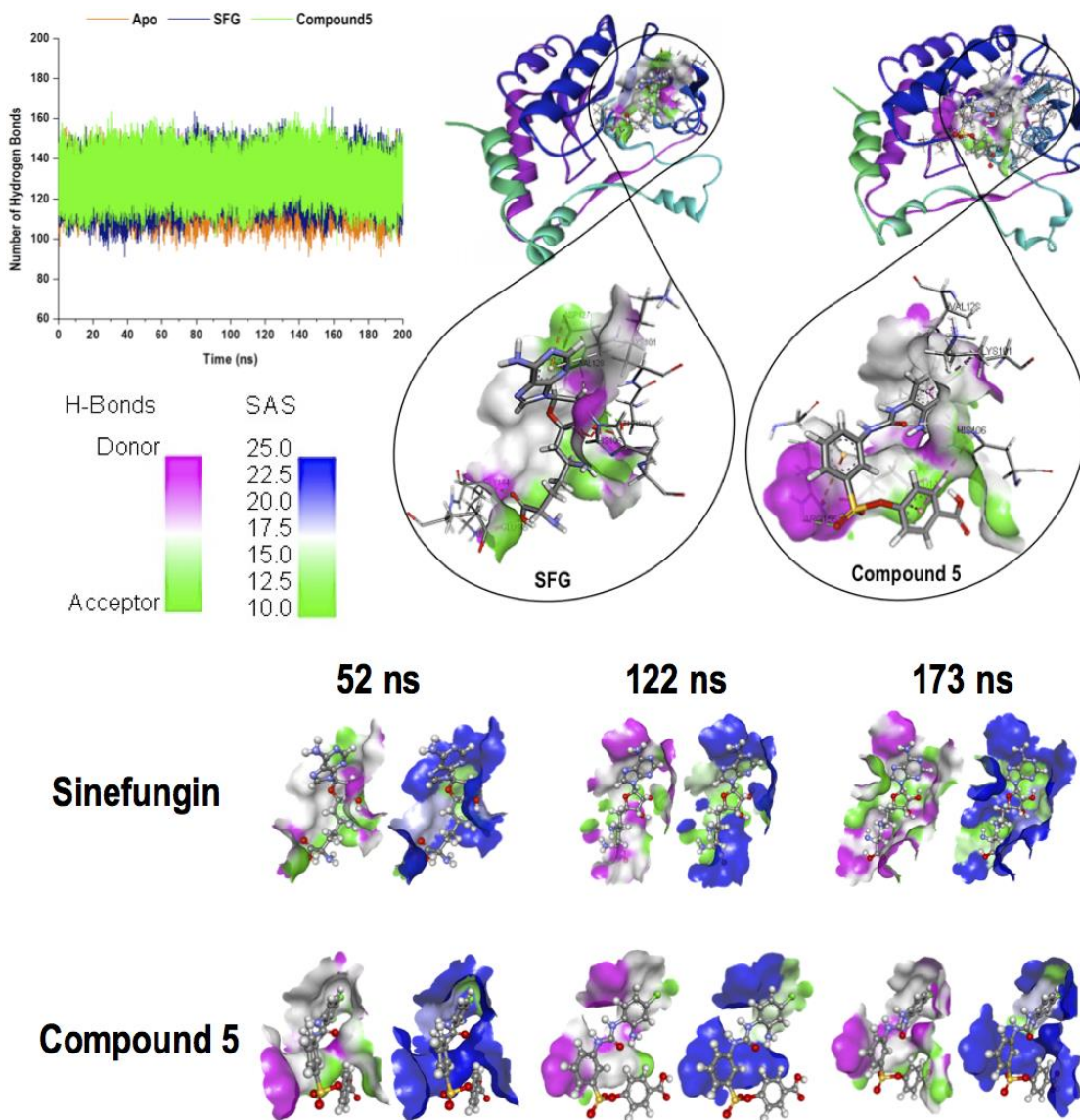


Figure 6: (Top left) Graph depicts hydrogen-bonding analysis of the apo and bound systems. (Top right) Bond and non-bond interactions that exist between each inhibitor and their binding site residues, as well as the interacting areas of the ligand which are hydrogen donors and acceptors. (Bottom) Surface areas of each inhibitor in the MTase pocket describing the hydrogen bonding capacity of each ligand during parts of the simulation that correspond to fluctuations in energy, along with the solvent accessible surface areas of the MTase at those points which correspond to ligand movement in the SAM-binding pocket.

We present in Figure 6 very similar hydrogen bonding patterns between the SFG-bound and Compound 5-bound MTase complexes. The SFG-bound MTase exhibited a slightly lesser number of hydrogen bonds than the Compound 5-bound MTase, during 25-75 ns and 130-155 ns, which correspond with the flexibility of the protein during that period of the simulation. Nonetheless, toward the latter period of the simulation, i.e. between 170-200 ns, the number of hydrogen bonds were approximately consistent in both inhibitor-bound MTase complexes. Although, the apo MTase displayed a reduced number of hydrogen bonds than both inhibitor-bound complexes, indicating that the apo system was less stable than bound systems.

3.2.2 Residual Variations within the NS5 MTase

To determine the flexibility of amino acid residues in the Apo and bound systems, root of mean square fluctuation (RMSF) of the residue α -carbons were calculated. In Figures 7 and 8, we illustrate that the MTase is more flexible when unbound, as compared to SFG- and Compound 5-bound enzymes, respectively. Binding of SFG and Compound 5 lower the systems' energy fluctuations making them more stable.

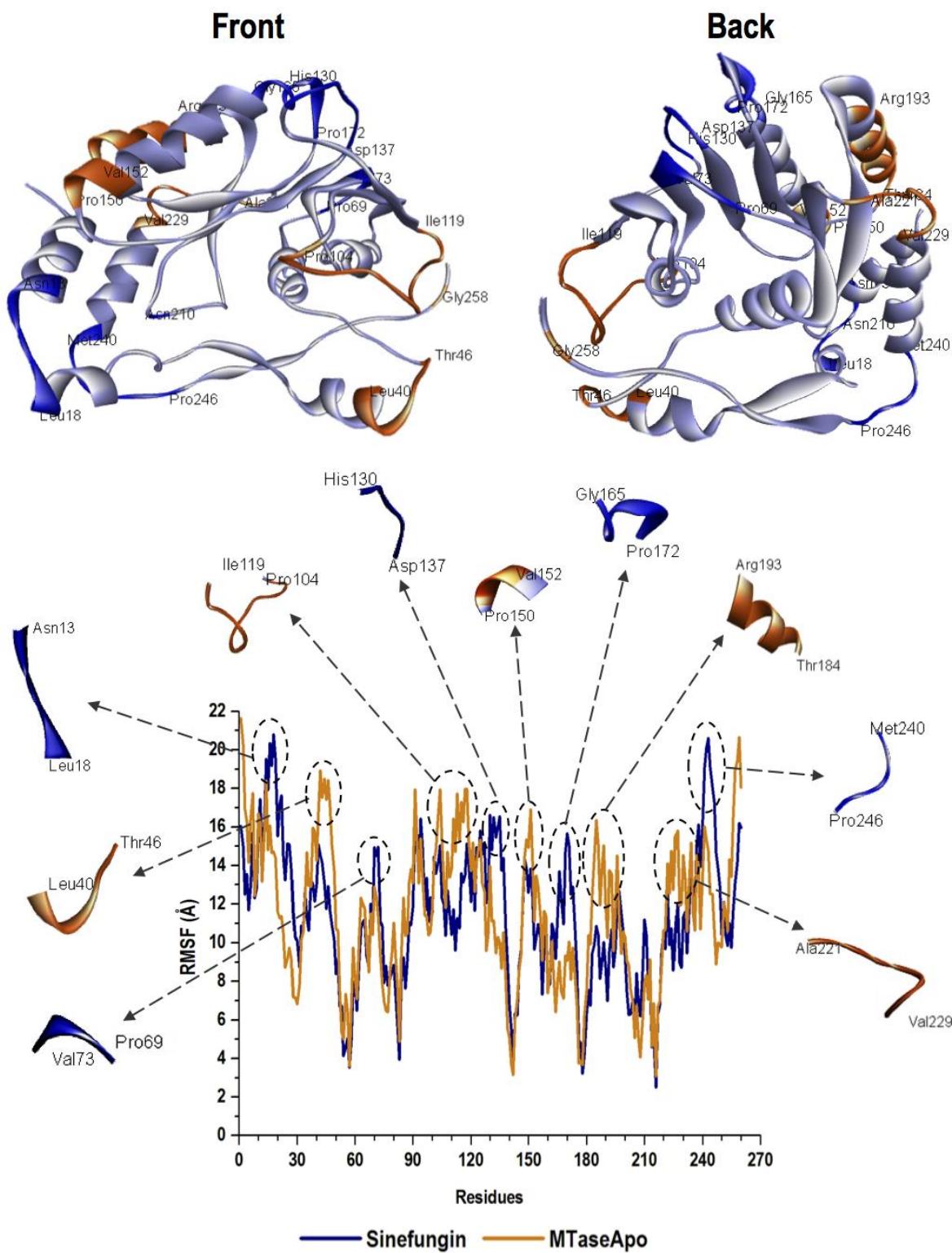


Figure 7: The average energy interpretation of each residue throughout the simulation of the apo MTase vs SFG-bound MTase. Highly fluctuating residues in the system are also illustrated in the crystal structure of the MTase and correlated with the peaks in the graph.

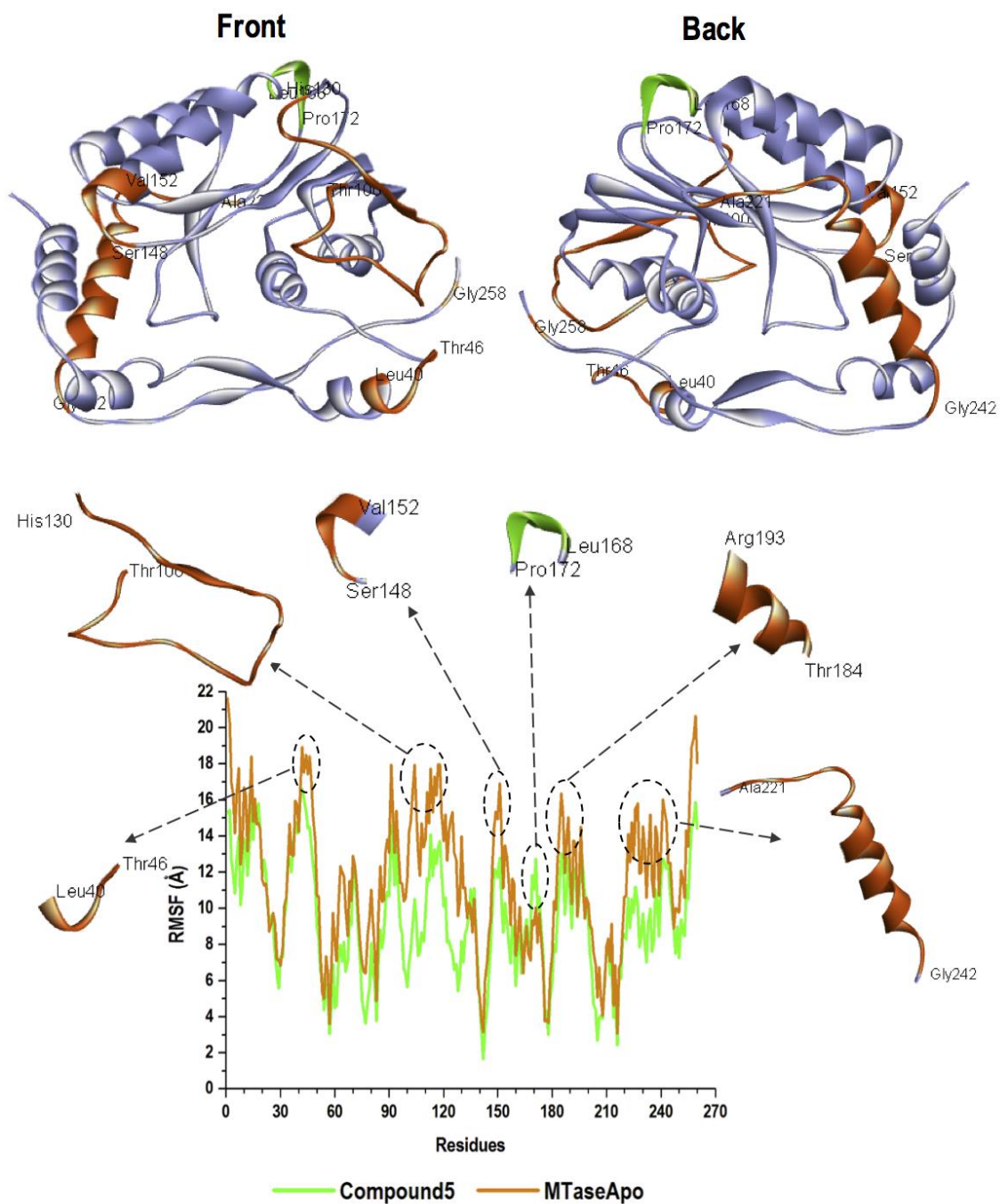


Figure 8: The average energy interpretation of each residue throughout the simulation of the apo MTase vs Compound 5-bound MTase. Highly fluctuating residues in the system are also illustrated in the crystal structure of the MTase and correlated with the peaks in the graph.

Most binding site residues displayed resemblance in energy patterns in both inhibitor-bound and unbound conformations (binding site residues of SFG: Ser52, Gly54, Ser55, Asp75, Gly77, Cys78, Gly79, Gly82, Trp83, Tyr99, Thr100, Lys101, Gly102, His106, Glu107, Val126, Asp127, Val128, Phe129, Asp142, Ile143 and Lys178; binding site residues of Compound 5: Lys57, Gly77, Cys78, Gly79, Arg80, Gly81, Gly82, Thr100, Lys101, His106, Glu107, Asp127, Val128, Phe129, Asp142, Ile143, Gly144, Glu145, Ser146, Arg159, and Lys178), while others fluctuated significantly. Those binding site residues that altered in motion greatly throughout the simulation include 106 and 107 upon SFG binding, as well as 100, 101, 102, 127, 128 and 129 upon Compound 5 binding. An intriguing observation is that although the residues that form a loop at the binding site (residues 100-107) altered in conformation majorly throughout the simulation, the residues that form a loop beneath the SAM-binding site (residues 34-53) fluctuated more. This finding was observed in the SFG-MTase complex (Figure 7), but quite the opposite in the Compound 5-MTase complex (Figure 8), where more fluctuation occurred at the binding site loop rather than the loop below the binding site. Binding of inhibitors rendered the MTase more stable as the flexibility of those residues decreased and the enzyme became more compact to accommodate inhibitor binding. The presence of these inhibitors in the SAM-binding site strongly affected the global dynamics of most loops and helices in the MTase enzyme.

These results are concurrent to those of DCC, which was utilized in the analysis of fluctuations of atoms within the NS5 MTase backbone, as well as domain motions, focusing specifically on the α -

carbons. Variations of colors represent residue distance analysis plots, where red to yellow areas signify positive/strong-correlated movements between α -carbons of residues and blue to black areas signify negative/anti-correlated movements. In Figure S2, it can be noticed that the Apo MTase fluctuates more than when bound. It is evident that highly fluctuating residues that are shown in RMSF graphs are parallel to the anti-correlative residual movements in the DCC plots of each system. Likewise, residues that follow similar trends in movement throughout the simulation show strong correlation patterns.

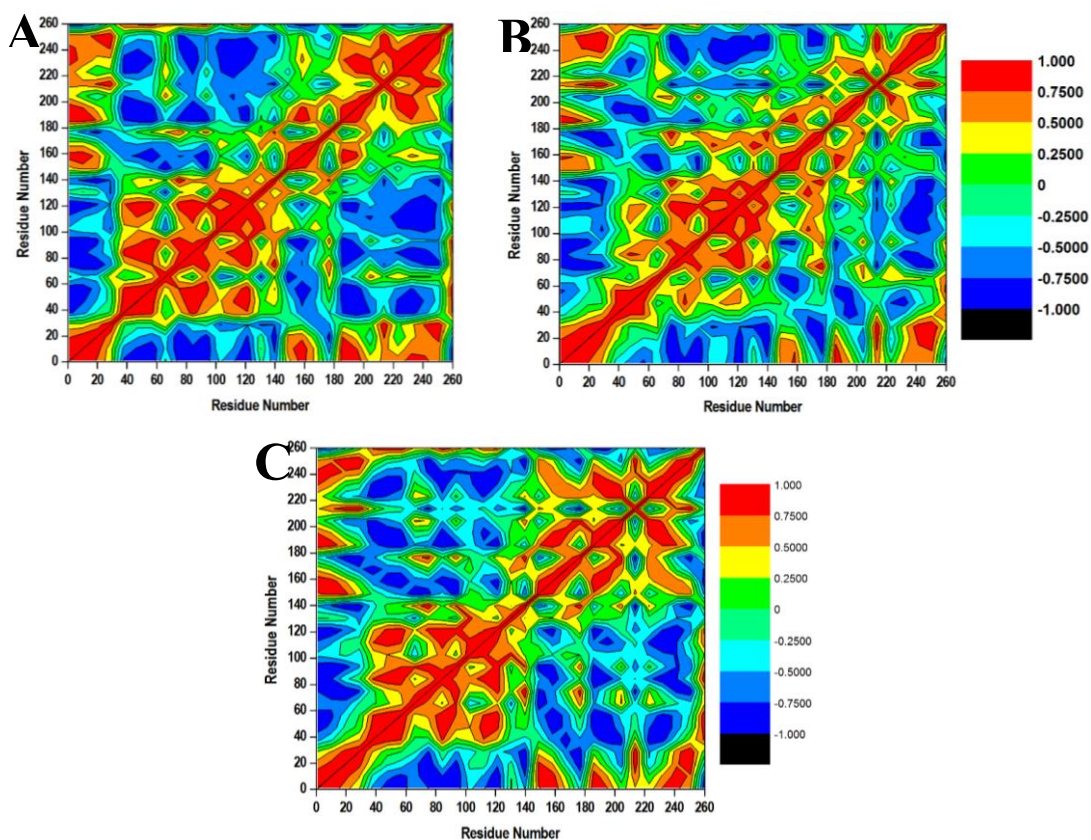


Figure S2: Dynamic cross correlation of the α -carbon atoms of the apo MTase (A), SFG-bound MTase complex (B) and Compound 5-bound-MTase complex (C).

3.2.3 Binding Free Energy Calculations

Average measures of the all factors of molecular mechanics computed over the 200 ns molecular dynamic simulation of the SFG-MTase and the Compound 5-MTase systems are tabulated below (Table 1).

Table 1: An outline of the MM/PBSA binding free energy contributions to the SFG-MTase system and the Compound 5-MTase system.

		<i>Energy Components (kcal.mol⁻¹)</i>				
		ΔE_{vdW}	ΔE_{elec}	ΔG_{gas}	ΔG_{solv}	ΔG_{bind}
<i>SFG-MTase System</i>	<i>MTase</i>	-2047.42 ± 20.73	-16727.67 ± 113.43	-18775.10 ± 111.10	-3474.49 ± 96.04	-22249.58 ± 52.82
	<i>SFG</i>	-4.37 ± 1.59	-93.06 ± 7.97	-97.43 ± 7.75	-42.69 ± 3.32	-140.12 ± 6.51
	<i>Complex</i>	-41.73 ± 4.86	-60.32 ± 23.63	-102.04 ± 26.13	67.05 ± 19.46	-34.99 ± 8.02
<i>Compound 5-MTase System</i>	<i>MTase</i>	-2041.29 ± 20.69	-16849.53 ± 96.53	-18890.82 ± 93.77	-3372.78 ± 80.45	-22263.60 ± 46.55
	<i>Compound 5</i>	-5.06 ± 1.39	-21.99 ± 3.36	-27.05 ± 3.34	-44.43 ± 4.63	-71.48 ± 4.32
	<i>Complex</i>	-34.06 ± 6.27	-35.87 ± 14.03	-69.93 ± 15.25	48.66 ± 12.89	-21.27 ± 5.21

The approximated binding free energy between SFG and the MTase is -34.99 kcal.mol⁻¹, while that of Compound 5 and the MTase is -21.27 kcal.mol⁻¹. This substantial difference in binding energy (~13 kcal.mol⁻¹) between the individual inhibitors and the enzyme corresponds with experimental evidence that SFG binding to the MTase is potent at a lower IC₅₀ than that of Compound 5 [21]. The

estimated van der Waals contributions (ΔE_{vdW}) and electrostatic contributions (ΔE_{elec}) towards total binding free energy in the SFG-MTase system ($-41.73 \text{ kcal.mol}^{-1}$ and $-60.32 \text{ kcal.mol}^{-1}$, respectively) are higher than that of the Compound 5-MTase system ($-34.06 \text{ kcal mol}^{-1}$ and $-35.87 \text{ kcal mol}^{-1}$, respectively). The estimated solvation contribution (ΔG_{solv}) toward the binding free energy in the SFG-MTase system ($67.05 \text{ kcal mol}^{-1}$) is slightly higher than that of the Compound 5-MTase system ($48.66 \text{ kcal mol}^{-1}$). In Table 1, the energy components presented indicate that the most favorable contributions for binding of inhibitors, SFG and Compound 5, derived from ΔE_{vdW} and ΔE_{elec} .

3.2.3 Decomposition Analysis of Binding Site Interaction Energy.

The binding free energy was decomposed further into contributions from specific amino acid residues of the MTase. We present via the graphs in Figures 9 and 10 the contrasting protein–ligand interaction continua between the SFG-bound MTase and the Compound 5-bound MTase, respectively.

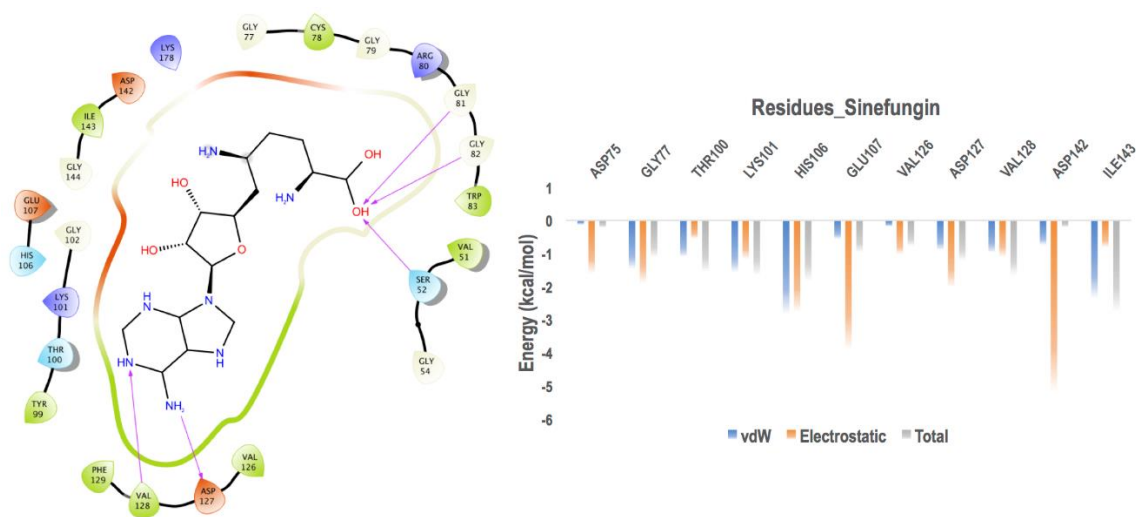


Figure 9: MTase residues that interact with SFG (left) and energy contributions of the highest interacting residues at the SAM-binding site (right).

The per-residue energy decomposition analysis that we've presented in Figure 9 show that the highly contributing binding site amino acid residues toward the energy of the SFG-bound complex were His106 (-2.806 kcal.mol⁻¹ [vdW]; -2.747 kcal.mol⁻¹ [elec]), Glu107 (-3.857 kcal.mol⁻¹ [elec]), Asp142 (-5.139 kcal.mol⁻¹ [elec]) and Ile143 (-2.321 kcal.mol⁻¹ [vdW]). Whereas, energy contributions of other binding site residues that were less include Asp75 (-1,586 kcal.mol⁻¹ [elec]), Gly77 (-1.452 kcal.mol⁻¹ [vdW]; -1.886 kcal.mol⁻¹ [elec]), Thr100 (-1.082 kcal.mol⁻¹ [vdW]; -0.553 kcal.mol⁻¹ [elec]), Lys101 (-1.563 kcal.mol⁻¹ [vdW]; -1.15 kcal.mol⁻¹ [elec]), Val126 (-1.032 kcal.mol⁻¹ [elec]), Asp127 (-0.883 kcal.mol⁻¹ [vdW]; -1.99 kcal.mol⁻¹ [elec]) and Val128 (-0.959 kcal.mol⁻¹ [vdW]; -1.09 kcal.mol⁻¹ [elec]). From Figure 9, it can be observed that the electrostatic energy contribution from residues 106, 107 and 142, and the van der Waals energy from residues 77, 106 and 143 in the SFG-MTase complex are most likely responsible for the high interaction energy in the system ($\Delta G_{bind} = -34.99$ kcal.mol⁻¹).

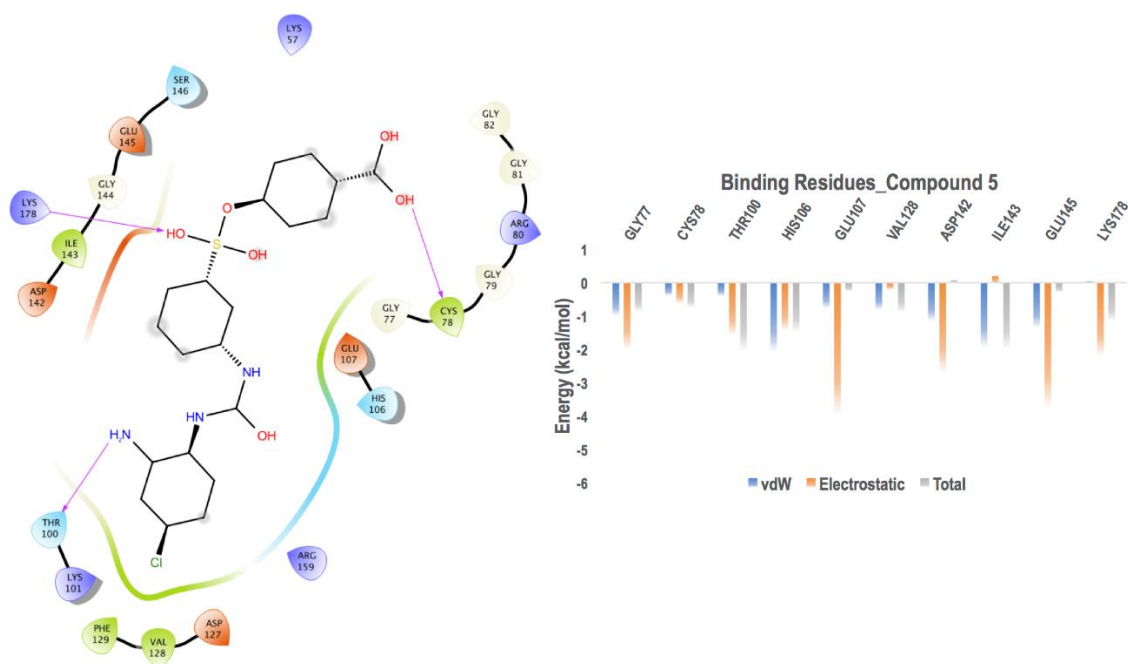


Figure 10: MTase residues that interact with Compound 5 (left) and energy contributions of the highest interacting residues at the SAM-binding site (right).

High-energy contribution from the Compound 5-bound complex stem from interacting residues Gly77 (-1.977 kcal.mol⁻¹ [elec]), His106 (-2.043 kcal.mol⁻¹ [vdW]), Glu107 (-3.94 kcal.mol⁻¹ [elec]), Asp142 (-2.67 kcal.mol⁻¹ [elec]), Ile143 (-1.922 kcal.mol⁻¹ [vdW]), Glu145 (-3.746 kcal.mol⁻¹ [elec]) and Lys178 (-2.19 kcal.mol⁻¹ [elec]). Binding site residues with slightly lower energy contribution to the system were Cys78 (-0.391 kcal.mol⁻¹ [vdW]; -0.602 kcal.mol⁻¹ [elec]), Thr100 (-1.541 kcal.mol⁻¹ [elec]) and Val128 (-0.81 kcal.mol⁻¹ [vdW]). From Figure 10, it can be concluded that the electrostatic energy contribution from residues 107, 142 and 145, and the van der Waals energy from residues 106 and 143 in the Compound 5-MTase complex may be accountable for the high interaction energy in the system ($\Delta G_{bind} = -21.27$).

The large difference in binding affinity between the SFG-bound and Compound 5-bound complexes (~13 kcal.mol⁻¹) may be owing to the increase in electrostatic binding energy of Asp142 of the MTase to SFG, as well as van der Waals and electrostatic energies of His106, as compared to that of Compound 5.

3.3 Fingerprints for the Design of New Chemical Entities (NCEs)

Looking at the binding implications of SFG to the ZIKV NS5 MTase, potential use of SFG could be a promising starting point as a prototype candidate for ZIKV treatment. We therefore created a map depicting the key chemical, structural and pharmacophoric fingerprints of SFG that will assist medicinal chemists and researchers in the identification and design of future new chemical entities for potential ZIKV inhibitors. The pharmacophoric elements that associate with highly contributing residues of the MTase were chosen to build our ensemble as we have illustrated in Figure 11.

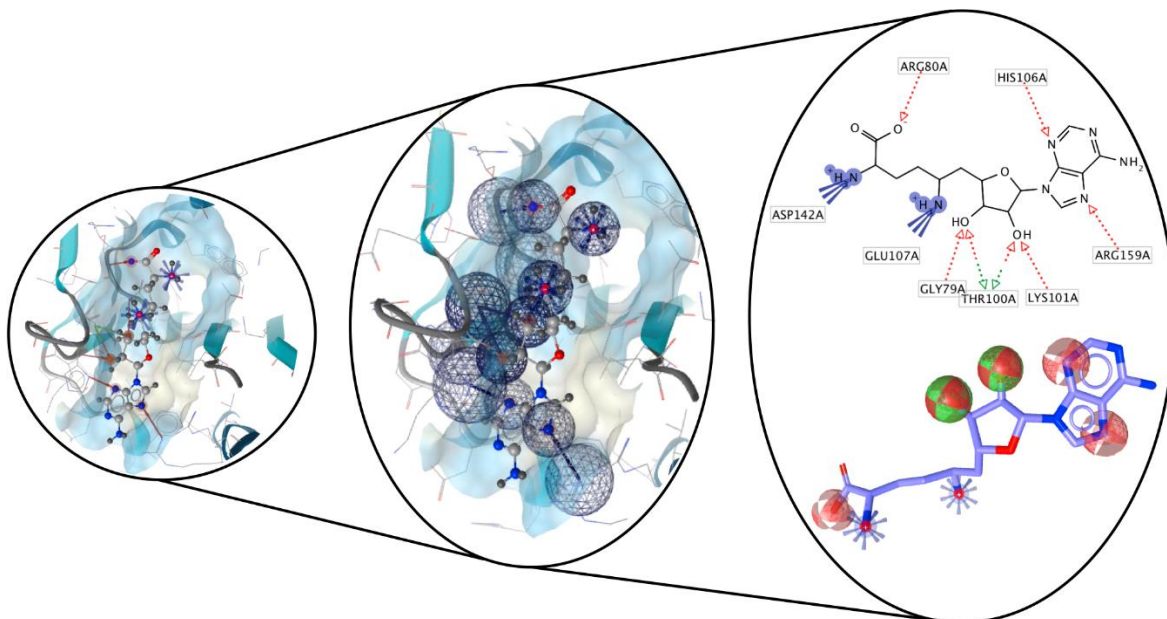


Figure 11: Schematic representation of the key chemical, structural and pharmacophoric fingerprints of SFG.

As we have presented in Figure 11, it can be noticed that the N6 and N7 atoms are crucial to interact with the target by creating positive ionization with Glu107 and Asp142 of the ZIKV MTase, respectively. Retention of N6 and N7 will contribute positive ionizations responsible for ligand-enzyme interactions. Furthermore, the N2, N5, O2, O3 and O5 atoms are essential in the formation of strong hydrogen bonds with Arg159, His106, Gly79, Thr100, Lys101 and Arg80 respectively, which are mandatory for enzyme stability. Preservation of the N2, N5, O2, O3, and O5 atoms will induce stability and strong binding of NCEs to the ZIKV MTase.

4 Conclusion

The ZIKV is a "public health emergency of international concern" and therefore a serious global threat. Apart from ZIKV, Compound 5 and SFG have also shown inhibitory effects in other *flaviviruses*, including DENV, WNV, YFV and JEV. The molecular dynamic analyses described this study reveal the conformational evolutions, i.e. variations in the ZIKV NS5 MTase after binding of

these inhibitors at a molecular level. Molecular dynamic simulations of 200 ns demonstrate radical movements within the MTase, particularly of the loops surrounding the SAM-binding pocket and RNA-binding site. The dynamic loop fluctuations in motion were uncovered in the RMSD and RMSF analyses and substantiated by examining the 3-dimensional molecular landscape of the loops at specific time intervals throughout the simulation.

Upon binding to the MTase, both SFG and Compound 5 have shown to stabilize the rather erratic apo system, although, it was noticed that SFG renders the MTase more stable and more compact than Compound 5. The SFG-bound system also reached convergence while the Compound 5-bound system did not. The binding affinity and binding site interactions (bond and non-bond interactions) between SFG and the SAM-binding pocket of the MTase were stronger than those of Compound 5. Binding energy calculations identified His106, Glu107, Asp127, Asp142 and Ile143 as key players in the binding of SFG to the MTase; and Gly77, Thr100, His106, Glu107, Asp142, Glu145 and Lys178 in the binding of Compound 5 to the MTase.

Binding of SFG to the SAM-binding pocket caused the loop surrounding the pocket (residues 100-110) to shift so that SFG is held tighter in a more compact conformation. SFG-binding also resulted in the loop surrounding the RNA-binding site (residues 30-60) to cover the binding site, to prevent RNA from binding and replication from occurring. Strong and stable binding of SFG would also prevent SAM from binding and activating the MTase, avoiding methylation of RNA and the mRNA cap.

To explore the use of SFG as a potential starting point as a prototype candidate for ZIKV treatment, we created a pharmacophore of SFG that will assist medicinal chemists and researchers in the identification and design of future new chemical entities for potential ZIKV inhibitors.

The information interpreted in this study will improve the understanding of ZIKV and will be beneficial in driving the development of anti-Zika virus drugs. Further experimentation is required to elucidate the roles of SFG and Compound 5 in ZIKV treatment.

Conflict of Interest

Authors declare no potential financial and other conflict of interests

Acknowledgements

This work was financially supported by the National Research Foundation and the Centre for High Performance Computing (CHPC, <http://www.chpc.ac.za>) for computational resources.

References

- [1] WHO, The history of Zika virus **2016**.
- [2] S.-I. Yun, Y.-M. Lee, *J. Microbiol.* **2017**, *55*, 204.
- [3] G. Calvet, R. S. Aguiar, A. S. O. Melo, S. A. Sampaio, I. de Filippis, A. Fabri, et al., *Lancet Infect. Dis.* **2016**, *16*, 653.
- [4] H. El Costa, J. Gouilly, J.-M. Mansuy, Q. Chen, C. Levy, G. Cartron, et al., *Sci. Rep.* **2016**, *6*, 35296.

- [5] H. Retallack, E. Di Lullo, C. Arias, K. A. Knopp, M. T. Laurie, C. Sandoval-Espinosa, et al., *Proc. Natl. Acad. Sci.* **2016**, *113*, 14408.
- [6] J. J. Miner, M. S. Diamond, *Cell Host Microbe* **2017**, *21*, 134.
- [7] A. Sharma, S. K. Lal, *Front. Microbiol.* **2017**, *8*, 110.
- [8] R. K. Singh, K. Dhama, Y. S. Malik, M. A. Ramakrishnan, K. Karthik, R. Tiwari, et al., *Vet. Q.* **2016**, *36*, 150.
- [9] H. Lazear, M. Diamond, *J. Virol.* **2016**, *90*, 4864.
- [10] A. S. Fauci, D. M. Morens, *N. Engl. J. Med.* **2010**, *363*, 1.
- [11] S. E. Reznik, J. C. R. Ashby, *Int. J. Infect. Dis.* **2017**, *55*, 29.
- [12] E. F. Pettersen, T. D. Goddard, C. C. Huang, G. S. Couch, D. M. Greenblatt, E. C. Meng, et al., *J. Comput. Chem.* **2004**, *25*, 1605.
- [13] N. Devnarain, P. Ramharack, M. E. Soliman, *RSC Adv.* **2017**, *7*, 47416.
- [14] B. Coutard, E. Decroly, C. Li, A. Sharff, J. Lescar, G. Bricogne, et al., *Antiviral Res.* **2014**, *106*, 61.
- [15] P. Ramharack, M. E. S. Soliman, *R. Soc. Chem.* **2016**, *6*, 68719.
- [16] W. Duan, H. Song, H. Wang, Y. Chai, C. Su, J. Qi, et al., *EMBO J.* **2017**, *36*, 919.
- [17] H. Dong, L. Liu, G. Zou, Y. Zhao, Z. Li, S. P. Lim, et al., *J. Biol. Chem.* **2010**, *285*, 32586.
- [18] S. P. Lim, Q. Y. Wang, C. G. Noble, Y. L. Chen, H. Dong, B. Zou, et al., *Antiviral Res.* **2013**, *100*, 500.
- [19] P. Stephen, M. Baz, G. Boivin, S. X. Lin, *J. Am. Chem. Soc.* **2016**, *138*, 16212.
- [20] S. C. Weaver, F. Costa, M. A. Garcia-Blanco, A. I. Ko, G. S. Ribeiro, G. Saade, et al., *Antiviral Res.* **2016**, *130*, 69.
- [21] B. Coutard, K. Barral, J. Lichière, B. Selisko, B. Martin, W. Aouadi, et al., *J. Virol.* **2017**, *91*, e02202.
- [22] F. Benmansour, I. Trist, B. Coutard, E. Decroly, G. Querat, A. Brancale, et al., *Eur. J. Med.*

Chem. **2017**, *125*, 865.

- [23] S. P. Lim, L. S. Sonntag, C. Noble, S. H. Nilar, R. H. Ng, G. Zou, et al., *J. Biol. Chem.* **2011**, *286*, 6233.
- [24] R. L. Hamill, M. M. Hoehn, *J. Antibiot. (Tokyo)*. **1973**, *XXVI*, 463.
- [25] K. Hercik, J. Brynda, R. Nencka, E. Boura, *Arch. Virol.* **2017**, *162*, 2091.
- [26] M. D. Hanwell, D. E. Curtis, D. C. Lonie, T. Vandermeersch, E. Zurek, G. R. Hutchison, *J. Cheminform.* **2012**, *4*, 17.
- [27] Z. Yang, K. Lasker, D. Schneidman-Duhovny, B. Webb, C. C. Huang, E. F. Pettersen, et al., *J. Struct. Biol.* **2012**, *179*, 269.
- [28] O. Trott, A. J. Olson, *J. Comput. Chem.* **2010**, *31*, 445.
- [29] H. Alonso, A. A. Bliznyuk, J. E. Gready, *Med. Res. Rev.* **2006**, *26*, 531.
- [30] X.-Y. Meng, H.-X. Zhang, M. Mezei, M. Cui, *Curr. Comput. Drug Des.* **2011**, *7*, 146.
- [31] J. de Ruyck, G. Brysbaert, R. Blossey, M. F. Lensink, *Adv. Appl. Bioinforma. Chem.* **2016**, *9*, 1.
- [32] G. Raabe, In *Molecular Modeling and Simulation*, Springer, Singapore, 2017, pp. 83–113.
- [33] A. Ganesan, M. L. Coote, K. Barakat, *Drug Discov. Today* **2017**, *22*, 249.
- [34] R. Salomon-Ferrer, A. W. Götz, D. Poole, S. Le Grand, R. C. Walker, *J. Chem. Theory Comput.* **2013**, *9*, 3878.
- [35] J. A. Maier, C. Martinez, K. Kasavajhala, L. Wickstrom, K. Hauser, C. Simmerling, *Journal Chem. Theory Comput.* **2015**, *11*, 3696.
- [36] J. Wang, W. Wang, P. a Kollman, D. a Case, *J. Chem. Inf. Comput. Sci.* **2001**, *222*, U403.
- [37] K. G. Sprenger, V. W. Jaeger, J. Pfaendtner, *J. Phys. Chem. B* **2015**, *119*, 5882.
- [38] R. J. Woods, R. Chappelle, *J. Mol. Struct. THEOCHEM* **2000**, *527*, 149.
- [39] S. Genheden, U. Ryde, *Expert Opin. Drug Discov.* **2015**, *10*, 449.

- [40] X. Zhang, H. Pérez-Sánchez, F. C. Lightstone, Springer, Cham, 2015, pp. 584–593.
- [41] K. Kasahara, I. Fukuda, H. Nakamura, *PLoS One* **2014**, *9*, e112419.
- [42] A. Munir, S. Azam, A. Mehmood, *Drug Des. Open Access* **2016**, *5*, 1.
- [43] G. Wolber, T. Langer, *J. Chem. Inf. Model.* **2004**, *45*, 160.
- [44] K. E. Machaba, F. N. Cele, N. N. Mhlongo, M. E. S. Soliman, *Cell Biochem. Biophys.* **2016**, *74*, 473.
- [45] A. Daina, O. Michielin, V. Zoete, *Sci. Rep.* **2017**, *7*, 42717.

CHAPTER 6

Molecular Mechanism of Resveratrol Inhibition of Zika Virus NS3 Helicase - Behind the Scenes

Molecular Mechanism of Resveratrol Inhibition of Zika Virus

NS3 Helicase - Behind the Scenes

Running head:

Resveratrol Inhibition of Zika Virus Helicase

Nikita Devnarain¹ and Mahmoud E. S. Soliman^{1*}

¹Molecular Bio-computation and Drug Design Laboratory, School of Health Sciences,
University of KwaZulu-Natal, Westville, Durban 4001, South Africa

*Mahmoud E. S. Soliman; Email: soliman@ukzn.ac.za; Tel: 0312607413

Summary

Aim: Zika virus (ZIKV) still poses a health risk to women and their babies without FDA-approved vaccines or treatments. Experimentation has proved resveratrol inhibition of ZIKV NS3 helicase without specifying the molecular events during inhibition.

Methods: Herein, we leaped forward to study the molecular dynamics of the bound and unbound enzyme, identifying precise binding residues and interactions, and the enzyme's adaptation to support binding, since loop dynamics affect viral RNA replication.

Results: Resveratrol stabilizes the P-loop and causes the RNA-binding loop to block the RNA-binding pocket for 200ns, which is concurrent with experimental evidence that resveratrol binding significantly reduces ATP hydrolysis activity.

Conclusion: This study illuminates the structural dynamics of ZIKV helicase and druglikeness of resveratrol, which will advance anti- ZIKV drug development.

Keywords (in alphabetical order)

Antiviral therapy; Flavivirus; Molecular Dynamics; NS3 Helicase; Resveratrol; Zika virus

1. Introduction

The Zika virus (ZIKV) is infecting country to country around the globe [1]. With devastating consequences on pregnant women, mothers and their families, the ZIKV remains an unresolved scientific challenge [2]. The global expansion of ZIKV may be due to an increased frequency of travelling that occurs on an international scale, the susceptibility of remote populations, as well as the rise in the vector range due to global warming [3–5].

The ZIKV is composed of multiple enzymes, some of which have been proposed as targets for therapy [6]. The NS3 protein encodes one of the most important viral enzymes and is crucial for polyprotein processing and replication of *flaviviruses* [7]. The NS3 is comprised of an N-terminal protease and a C-terminal RNA helicase domain [8]. The helicase is central to the life cycle and survival of ZIKV [3,9]. Simulation of the helicase by RNA triggers underlying nucleoside triphosphatase activity, which supplies energy for unwinding of intermediates of viral replication [10]. For these reasons, the ZIKV NS3 helicase represents an ideal target for therapy.

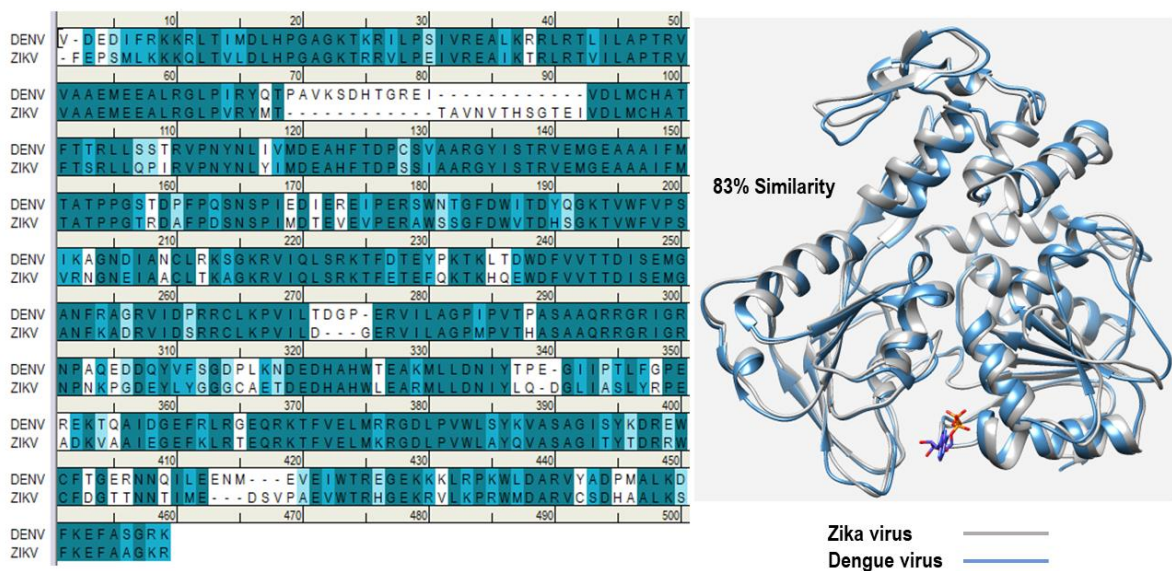


Figure 17: Superimposition of the Zika virus and Dengue virus NS3 helicases as well as their corresponding overlapping sequences showing the similarities and differences in their amino acid residues.

The ZIKV resembles Dengue virus (DENV) (Figure 1), therefore, inhibitors of DENV helicase may exhibit potency in ZIKV helicase inhibition [11]. Pan *et al.*, 2017, have shown that the ATPase inhibitor, resveratrol, substantially reduces NS3 helicase ATP-hydrolysis activity in DENV [12].

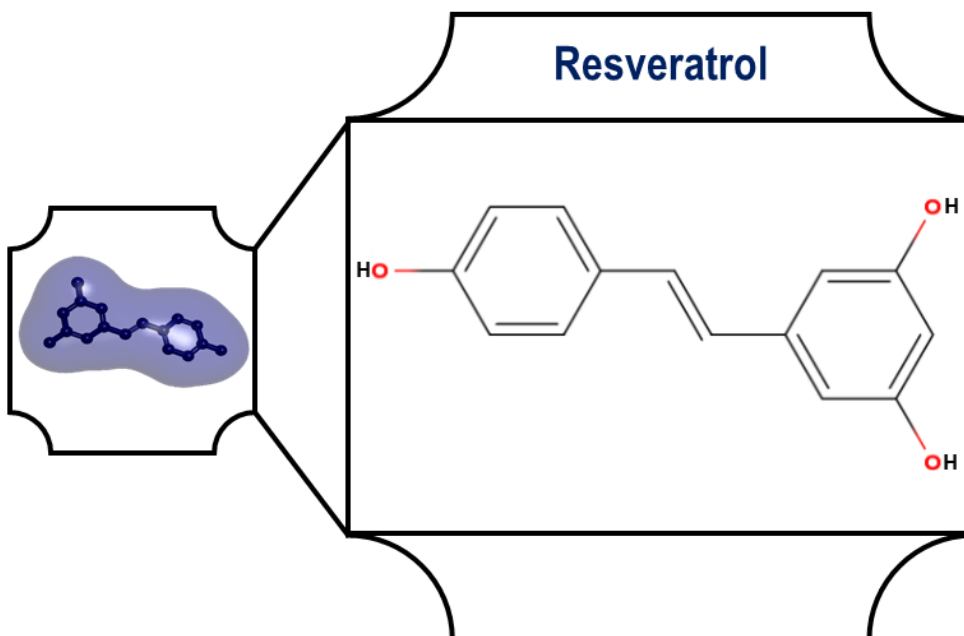


Figure 18: Chemical structure of resveratrol.

Resveratrol, or 3,5,4'-trihydroxy-trans-stilbene, is a natural polyphenol present in red wine, nuts, berries and traditional Asian medicines (Figure 2) [13]. The antioxidant potential of resveratrol is brought about via inhibition of reactive oxygen species, which involves scavenging free radicals such as superoxide anion (O_2^-), hydroxyl radical (OH^\cdot) and lipid hydroperoxyl radicals, as well as the inhibition of glutathione depletion [14]. Resveratrol was reported to have inhibitory effects on gene expression, nucleic acid synthesis, viral replication and protein synthesis for several viruses including hepatitis C virus, influenza virus, human immunodeficiency virus, herpes simplex virus and others [14–17]. The antioxidant and anti-inflammatory effects of resveratrol also benefit the cardiovascular system and function in neuroprotection, as well as treatment of diabetes mellitus [18–20].

Additionally, resveratrol possesses several anticancer properties, which are critical in cancer prevention and treatment [21].

Experimental evidence has shown the ability of resveratrol to significantly decrease ATP hydrolysis activity of the ZIKV helicase [15], although, the molecular structural dynamics within the unbound ZIKV helicase (apo) and the ZIKV helicase bound to resveratrol have not been elucidated. We determine the affinity of resveratrol to the helicase, along with the binding mode and stability of the unbound and bound complexes. The loops surrounding the RNA binding site and the ATP-binding site (P-loop) were focused on, as flexibility of these loops play major roles in viral RNA replication. To our understanding, this is the primary study applying incorporated computational tools to analyze the way resveratrol binding influences the conformation of the ZIKV NS3 helicase. We postulate that this study will enhance the understanding of the structural dynamics of the inhibitor and the ZIKV NS3 helicase and will aid in the search for anti-ZIKV treatment.

2. Zika Virus NS3 Helicase

The ZIKV NS3 protein constitutes 617 amino acid residues, which make up the protease (residues 1-167) and helicase (residues 168-617) enzymes. Processing of the polyprotein as well as viral replication are dependent on the activities of both these enzymes [7]. The serine protease is required for viral maturation via polyprotein processing, while the helicase is essential for RNA synthesis and genome replication of the virus [22].

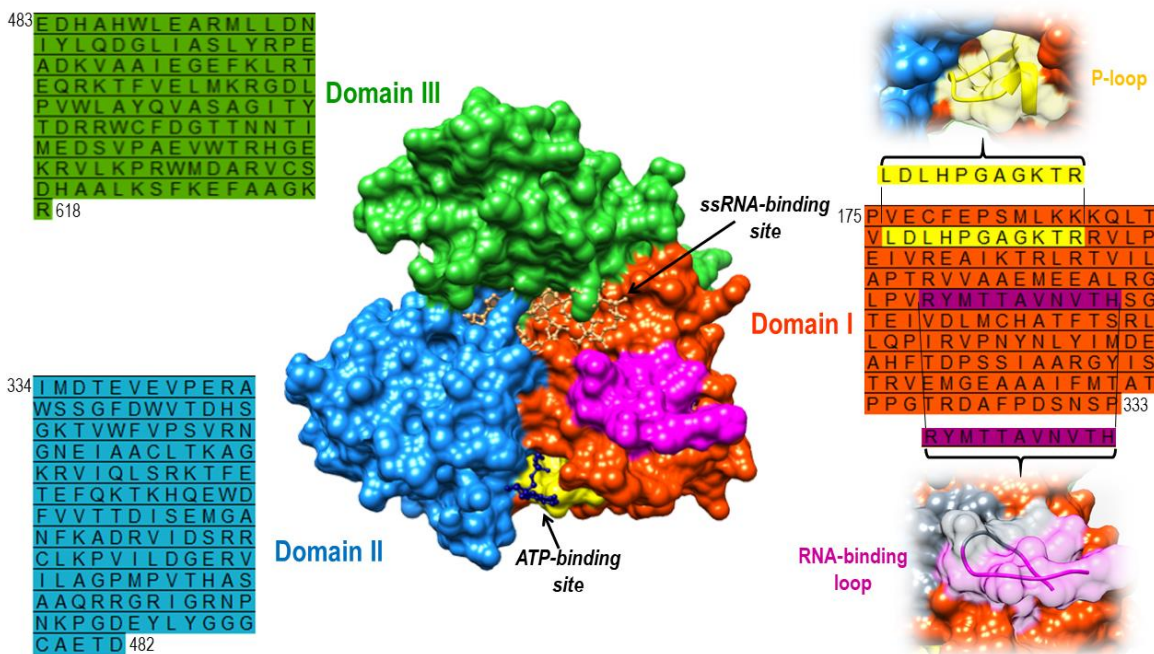


Figure 19: Protein sequences of the different domains of Zika virus NS3 helicase, as well as the major binding sites and loops. ATP: adenosine triphosphate; ssRNA: single-stranded RNA.

The serine protease can be described as a folded globular domain comprising of two β -barrels [23]. The helicase constitutes three domains that resemble each other in size (Figure 3). Domain 1 (residues 182–327) and domain 2 (residues 328–480) are made up of tandem α/β RecA-like folds, which are present in helicases of superfamily 1 and 2. Domain 1 comprises motifs I (Walker A or P loop), Ia, II (Walker B) and III, which line a cleft between motifs IV, IVa, V and VI of domain 2. Motifs I, II and VI are involved in ATP binding and/or hydrolysis, and motifs Ia, IV and V are associated with interdomain communication and RNA binding. The ZIKV helicase, as with the DENV4 helicase, binds ATP at the lower end of the cleft at the interface of domains 1 and 2, while the pocket dividing domains 1 and 2 from domain 3 house the RNA. Domains 2 and 3 interact via a β -hairpin extension of domain 2, which functions as a wedge that facilitates unwinding of double-stranded RNA. Structures

within domain 3 primarily consist of α -helices. Domain 3 interacts with RNA as well as the NS5 RNA-dependent RNA polymerase in other *flaviviruses* [10].

To date, several strains of ZIKV have been isolated. Due to interest in the helicases of different strains, we examined the similarities/differences in the helicase sequences. Multiple sequence analysis showed that the helicases of the French Polynesian (H/PF/2013), African (MR766) and Brazilian (BRA/2016) strains were almost identical, with very few differences in amino acid residues (Figure 4). Certain amino acid residues in the African strain are different from the other two strains. The distinguishing amino acid residues are at positions 41, 226, 233, 298, 309, 409 and 410, none of which are in the ATPase pocket. We can therefore deduce that the manner in which resveratrol binds to this helicase will be comparable to helicases of other strains.

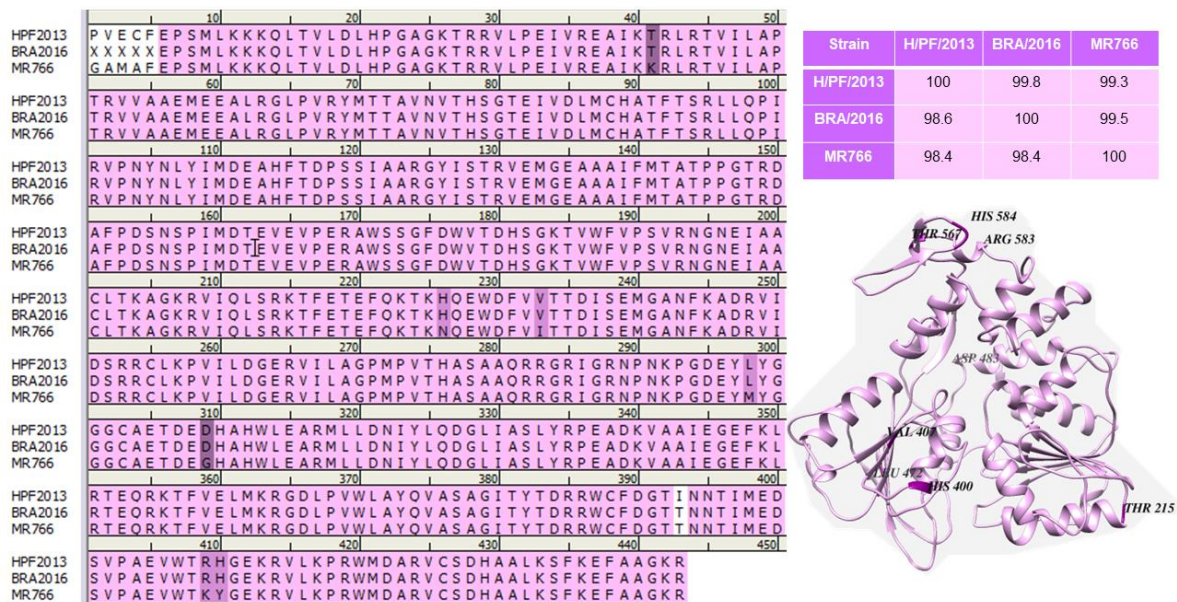


Figure 20: Multiple sequence alignment of three strains of helicase sequences (strains: H/PF/2013, BRA/2016 and MR766).

3. Computational Methods

3.1 Ligand and Receptor Preparation

The crystal structure of the ZIKV NS3 helicase was obtained from RCSB Protein DataBank (PDB: 5JMT) [24,25]. The structure of resveratrol was obtained from PubChem [26] and prepared using Molegro Molecular Viewer software (Molegro-a CLC bio company, Aarhus, Denmark) and UCSF Chimera software package [27]. An apo system (NS3 helicase) and a resveratrol-bound system were subjected to 200 ns molecular dynamic simulations.

3.2 Molecular Docking

Optimized conformations and binding affinities of resveratrol within the ATP-binding pocket of the ZIKV NS3 helicase was achieved through molecular docking. Resveratrol was docked into the ATP-binding pocket (competitive inhibitor of ATP) of the NS3 helicase (grid box of spacing of 0.375 Å and x, y, z dimensions of 32 x 26 x 30) via the AutoDock vina plugin of UCSF Chimera software [27–29]. Ten docked poses of the ligand in the binding pocket of the enzyme were generated in pdbqt format by AutoDock Vina and the most favorable geometric pose with the most negative binding energy (kcal.mol^{-1}) was saved from the ViewDock feature. The best complexes were subjected to molecular dynamic simulations. More detailed information regarding molecular docking can be found in the referenced articles [30–32]. To verify that resveratrol was docked into the correct pocket, Figure S4 demonstrates the superimposition of ATP bound to the helicase (PDB: 5GJC) and the docked complex of resveratrol to the helicase.

3.3 Molecular Dynamic Simulations

Molecular dynamic simulations were carried out using AMBER PMEMD dynamics engine with GPU acceleration [33,34]. The helicase was parameterized using the AMBER force field, FF14SB [35,36]. The inhibitor was hydrogenated and charged with Gasteiger charges, while the helicase protein was dehydrogenated preceding the simulation. Atomic partial charges were created for resveratrol using antechamber which applies the general AMBER force field (GAFF) and restrained electrostatic potential (RESP) methods [35,37,38]. The AMBER 14 LEAP module was used to combine, neutralize and solvate all systems via addition of hydrogen atoms, sodium and chloride ions, followed by suspension into an orthorhombic box of TIP3P water molecules to ensure all atoms were within 10 Å of the box edges. The amino acid residues of the helicase were renumbered from 1. The systems were initially minimized (2500 steps) using a restraint potential of 10 kcal.mol⁻¹ Å⁻² applied to the solutes, for 1000 steps of steepest descent followed by 1000 steps of conjugate gradient minimization. Thereafter, the systems were further fully minimized (200 steps) via unrestrained conjugate gradient algorithm.

A constant-temperature, constant-volume ensemble simulation was carried out for 50 ps from 0 K to 300 K, to preserve a fixed volume and number of atoms in each system. A harmonic restraint of 10 kcal.mol⁻¹ Å⁻² and Langevin thermostat collision frequency of 1.0 ps⁻¹ were applied to the solutes. All systems were then subjected to equilibration (500 ps) with a constant operating temperature (300 K) and pressure (1 bar) using the Berendsen barostat and number of atoms resembling an isobaric-isothermal ensemble. The shake algorithm was

applied to restrain hydrogen bonds during the simulations, which were conducted for 200 ns per system using an SPFP precision model.

3.4 Per-Residue Decomposition Analysis & Binding Free Energy Computation

To establish the binding free energy (ΔG_{bind}) of resveratrol to the ZIKV NS3 helicase enzyme, we employed molecular mechanics integrated with the Poisson-Boltzmann or generalized Born and surface area continuum solvation (MM/PBSA and MM/GBSA) approach [39,40]. These methods have been elaborated in the referred papers [41,42].

The molecular dynamic simulation yielded a trajectory depicted by 50,000 snapshots, which were averaged to generate ΔG_{bind} . The binding strengths between resveratrol and the helicase may be defined as:

$$\begin{aligned}
 (1) \quad & \Delta G_{\text{bind}} = G_{\text{complex}} - G_{\text{receptor}} - G_{\text{ligand}} \\
 (2) \quad & \Delta G_{\text{bind}} = E_{\text{gas}} + G_{\text{sol}} - TS \\
 (3) \quad & E_{\text{gas}} = E_{\text{int}} + E_{\text{vdW}} + E_{\text{ele}} \\
 (4) \quad & G_{\text{sol}} = G_{\text{GB}} + G_{\text{SA}} \\
 (5) \quad & G_{\text{SA}} = \gamma \text{SASA}
 \end{aligned}$$

where:

E_{ele}	Electrostatic potential energy from Coulomb forces
E_{gas}	Gas-phase energy (based on FF14SB force field terms)
E_{int}	Internal energy
E_{vdW}	van der Waals energy
G_{sol}	Solvation free energy
G_{GB}	Polar solvation energy
G_{SA}	non-polar solvation energy
S	Total entropy of solute
SASA	Solvent accessible surface area (water probe radius of 1.4 Å)
T	Total entropy of temperature

A per-residue free energy atomistic decomposition was adopted to estimate the contribution of each residue to the total ΔG_{bind} at the binding site, for significant residues of the helicase using the AMBER14 MM/GBSA method. Further analyses were carried out on the resveratrol-bound complex.

3.5 ADME Assessment of Resveratrol

Using the absorption, distribution, metabolism and excretion (ADME) online prediction tool, SWISS ADME, we assessed the druglikeness of resveratrol. The SWISS ADME website allows the computation of physicochemical descriptors and provides a prediction of druglike nature, pharmacokinetic properties, medicinal chemistry friendliness and ADME parameters small molecules to support drug discovery [43].

4. Results

4.1 Molecular Dynamic Simulations & Systems Stability

The trajectories of 200 ns molecular dynamic simulations of the apo and resveratrol-bound systems were monitored and analyzed post-dynamically to verify stability of the systems.

4.1.1 Atomic Distribution of α -carbons of NS3 Helicase

The deviation of α -carbons within the NS3 helicase during simulation of the systems were established by calculating the root-mean-square deviation (RMSD). In Figure 5, we show that resveratrol brought about different atomic changes in the helicase during the simulation,

when compared to the apo system. Both systems remained within a 1.5 Å range throughout the simulation.

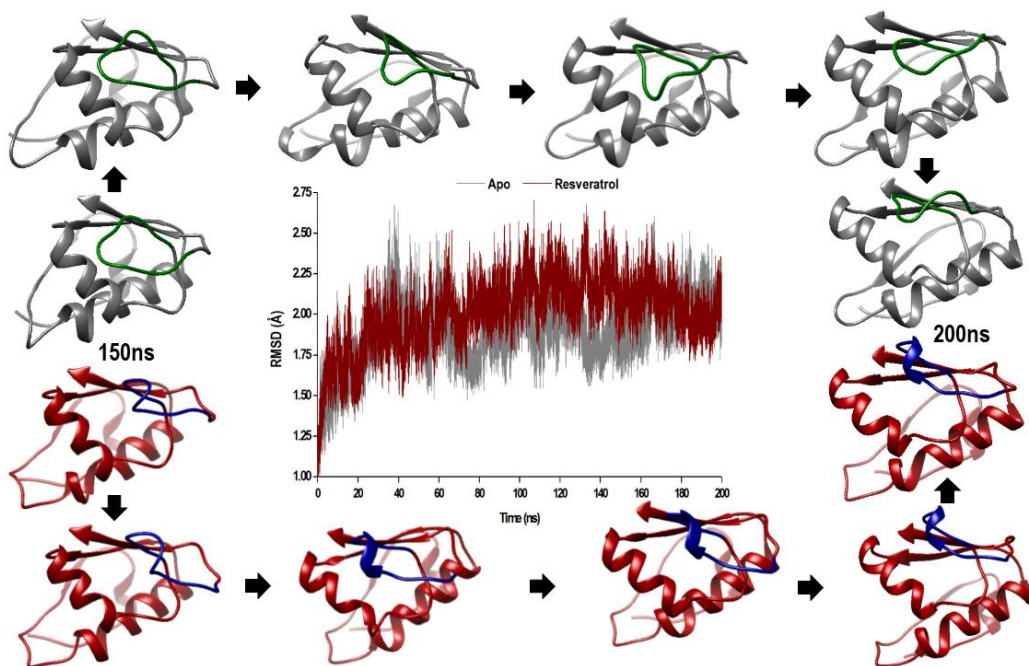


Figure 21: Resveratrol binding to ZIKV NS3 helicase stabilizes the enzyme. Snapshots at 10 ns intervals from 150-200 ns show the spontaneous behaviour of the RNA-binding loop (green) in the apo enzyme (grey), while the same loop (blue) in the bound enzyme (red) becomes stable via formation of a 3_{10} -helix.

The RMSD pattern of the apo system indicates major fluctuations of the system between 34-40 ns and 164-167 ns and convergence in the latter part of the simulation (after 175 ns). The fluctuations of the resveratrol-helicase complex dropped between 180-200 ns, where the helicase became more compact when compared to the apo helicase (Figure S1). The P-loop in the apo also undergoes constant structural variations (deviation=1.783Å), whereas that of the bound enzyme is stable (deviation=0.637Å). Resveratrol also stabilized the helicase during the 34-40 ns and 164-167 ns period when the apo fluctuated. It is noticed in Figure 5 that as the end of the simulation approached, the RNA binding loop moved closer toward the

RNA binding pocket. This may have impeding effects on the entry and binding of RNA in that pocket.

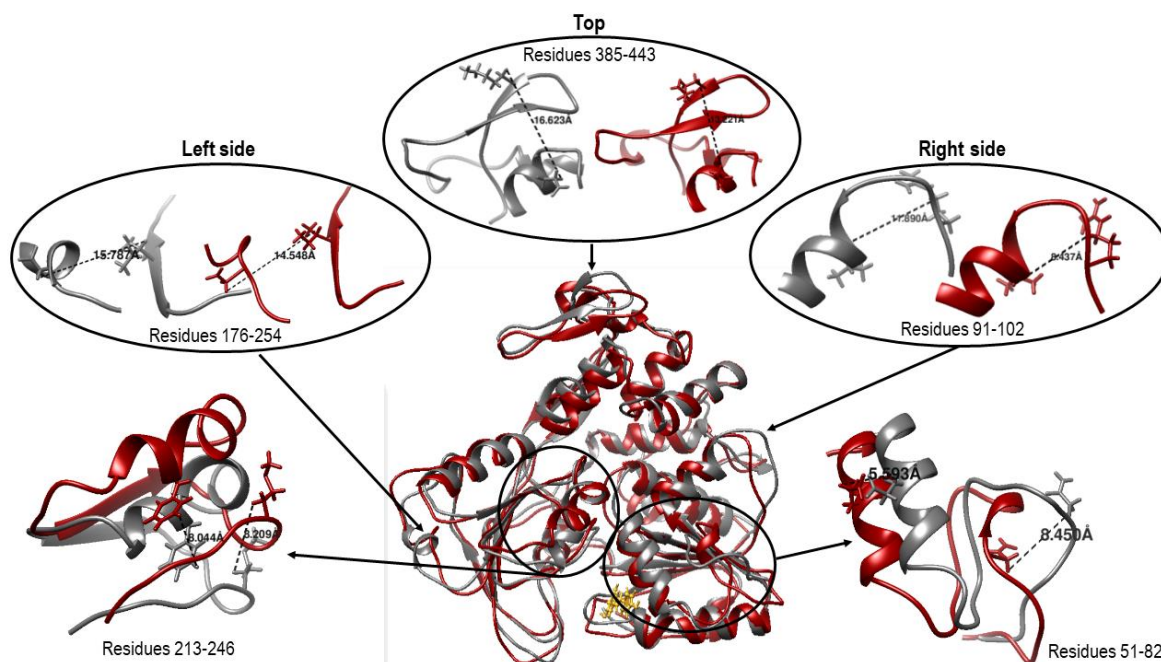


Figure 22: Resveratrol binding to the NS3 helicase (red) induces compactness of the enzyme, as compared to the apo (grey).

Superimposition of the bound (red) and unbound (grey) helicase at 200 ns (Figure 6) demonstrates the impact of resveratrol binding to the ZIKV NS3 helicase. The overall configuration of the helicase is more compact when bound, as the outer loops and coils move inward, suggesting a looser apo conformation. As emphasized in Figure 6, distances between loops on the top, left and right regions (Domain III, II and I, respectively) of the enzyme decreased in the bound complex when compared to the apo. The RNA binding loop and extended coil surrounding the inhibitor (enlarged in bottom right) move inward and the outer loop in Domain II (enlarged in bottom left) move upward conforming the enzyme to a more compact shape.

4.2 Intra- and Intermolecular Interactions in ZIKV NS3 Helicase

4.2.1 Fluctuating Residues within the NS3 Helicase

To provide a better understanding of the residues responsible for the fluctuating energy patterns in Figure 5, we calculated the root-mean-square fluctuation (RMSF) of each residue of both systems.

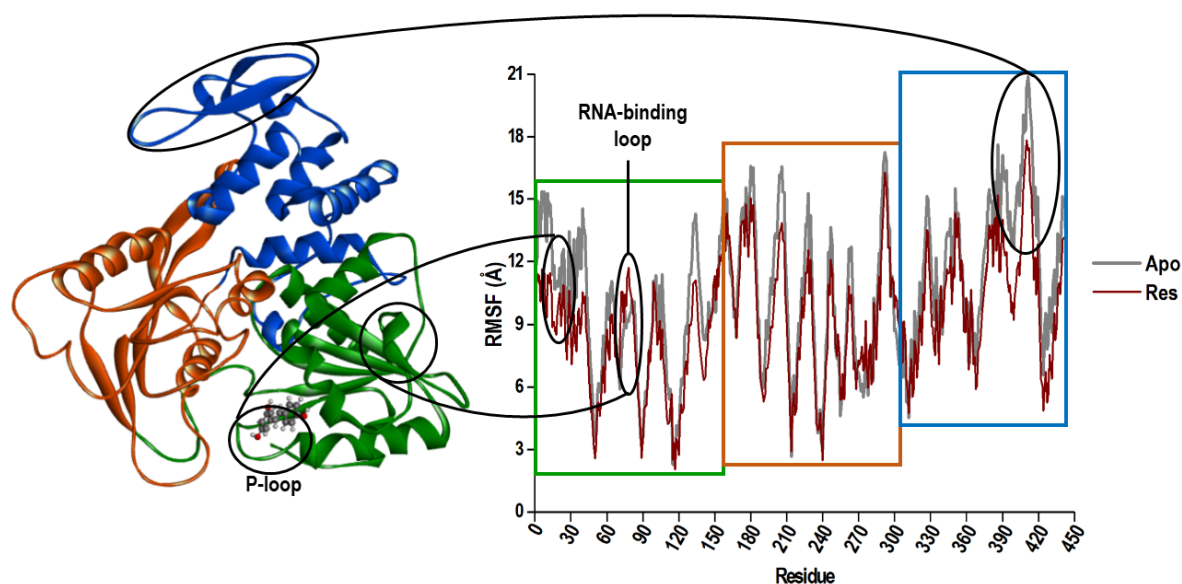


Figure 23: Residues of the apo helicase (grey) fluctuate more than residues of the resveratrol-bound helicase (red).

The pattern in the fluctuation of residues in the apo system bear resemblance to the resveratrol-bound complex, however, residues 1-43, 129-137, 201-208, 389-414 in the apo fluctuate more than the bound complex. In Figure 7, we demonstrate that Domain I of the helicase (green) fluctuates more than Domains II and III. Binding of resveratrol to the helicase decreases movements of the P-loop and causes and increases in movements of the RNA-binding loop. Considering both systems, residues of the apo system are more energetic

and therefore, the apo system is a lot more flexible than the resveratrol-bound system, suggesting that the inhibitor reduces the energies of the residues within the helicase.

4.2.2 Binding Free Energy Calculations and Binding Site Interaction Decomposition Analysis

The intensity of interactions between a ligand and receptor may be quantified by the binding free energy obtained from molecular mechanics with Poisson-Boltzmann surface area (MM/PBSA) calculations. Mean calculations of internal energy changes of the resveratrol-helicase system, and resveratrol and the helicase alone, totaled over the 200 ns simulation are presented in Table 1.

Table 3: A representation of the binding free energy contributions to the Resveratrol-bound system.

	Energy Components (kcal.mol ⁻¹)				
	ΔE_{vdW}	ΔE_{elec}	ΔG_{gas}	ΔG_{solv}	ΔG_{bind}
<i>Helicase</i>	-3555.87 ± 29.16	-29681.50 ± 134.2	-33237.37 ± 133.18	-4769.99 ± 104.63	-38007.37 ± 63.52
<i>Resveratrol</i>	-0.25 ± 0.66	65.32 ± 0.86	65.07 ± 1.08	-18.85 ± 0.3	46.22 ± 1.21
<i>Complex</i>	-26.86 ± 2.53	-36.54 ± 4.69	-63.4 ± 4.64	33.05 ± 3.23	-30.35 ± 2.86

ΔE_{elec} , electrostatic energy; ΔE_{vdW} , van der Waals forces; ΔG_{bind} , binding free energy; ΔG_{gas} , free energy in gas phase; ΔG_{solv} , solvation energy

The estimated binding free energy between resveratrol and the helicase is -30.35 kcal.mol⁻¹. This strong binding is concurrent with experimental evidence that resveratrol binding to the helicase significantly reduces ATP hydrolysis activity and is potent at an IC₅₀ of 94.25 ± 5.02 μM [15]. The

energies shown in Table 1 suggest that the most favorable conditions for resveratrol binding are derived from ΔG_{gas} and ΔE_{elec} .

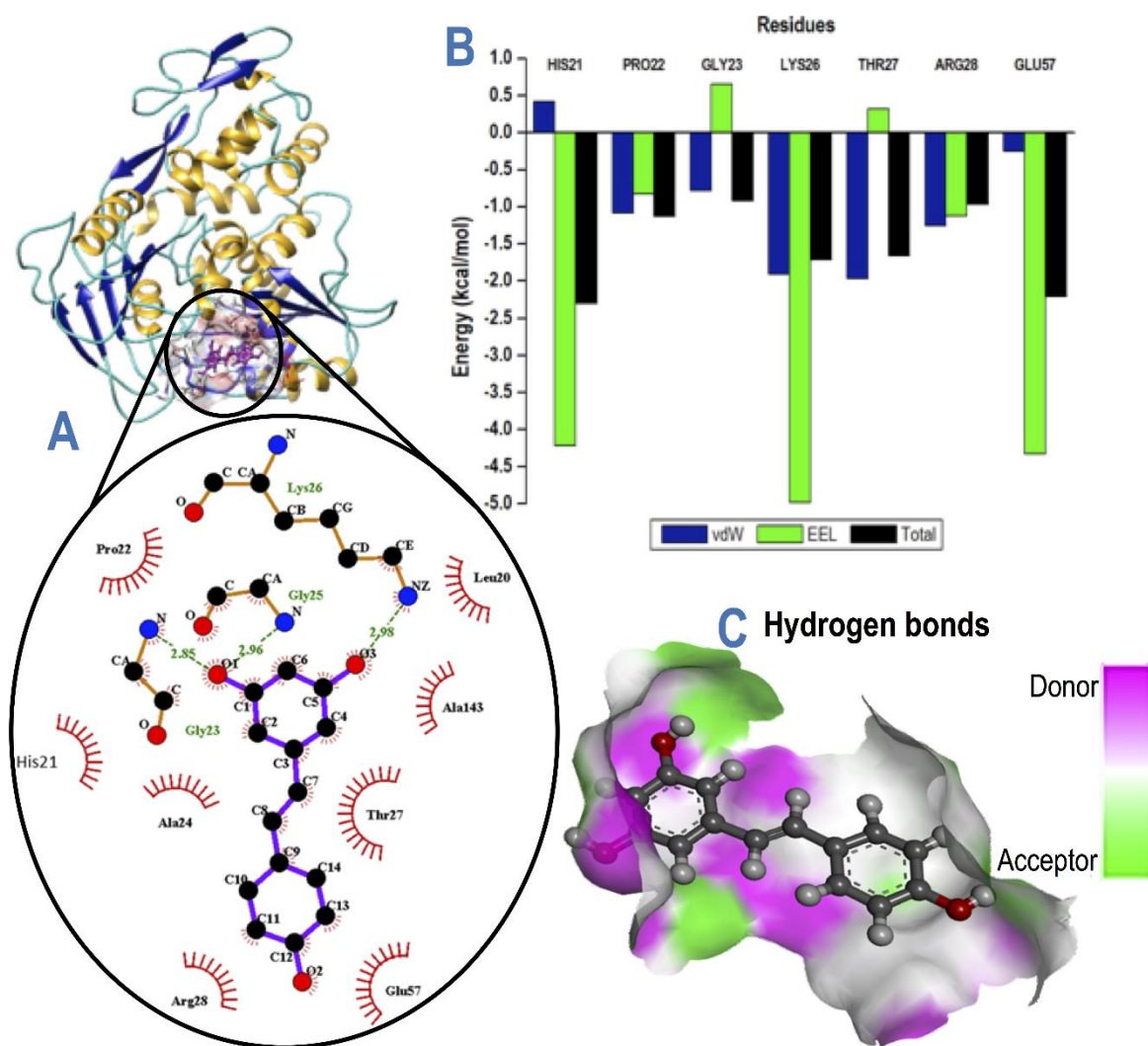


Figure 24: Exploration of the interactions that exist between resveratrol and residues of the ZIKV NS3 helicase. A. Resveratrol within binding pocket of helicase zooming into the hydrophobic interactions and hydrogen bonds between ligand binding residues and resveratrol. B. Per-residue decomposition analysis of ligand binding residues. C. Hydrogen bonding in ligand binding pocket. EEL: electrostatic energy; vdW: van der Waals.

The analysis was expanded into per-residue energy decomposition of resveratrol-binding residues of the helicase. In Figure 8, we show the resveratrol-helicase interaction spectrum. The ligand interaction diagram in Figure 8A clearly illustrates hydrophobic interactions between resveratrol and the helicase, particularly residues Leu20, His21, Pro22, Ala24, Thr27, Arg28, Glu57 and Ala143. Hydrogen bonding is also clearly apparent between Gly23 and Gly25 with the O₁ atom of resveratrol, and between Lys26 and the O₃ atom of resveratrol. The graph in Figure S3 and the hydrogen bond surface surrounding resveratrol in Figure 8C coincide with these results. The results from the graph in Figure 8B is concurrent with the findings in Table 1 that the electrostatic energy contributes more toward total binding free energy than van der Waals forces. Residues His21, Lys26 and Gly57 contributed mostly toward the electrostatic energy that was responsible for binding, and Lys26 and Thr27 contributed more toward van der Waals forces than other binding site residues.

4.3 Resveratrol ADME assessment

Using the online tool, SwissADME, the druglikeness of resveratrol was elucidated (Table 2). Resveratrol is likely to permeate lipophilic membranes, as well as the blood brain barrier (BBB). Clarification of the concept of LogP may be found in Devnarain *et al* (2017) [44]. Resveratrol is water soluble, which is favorable for oral bioavailability. Lipinski's rule of five is used to evaluate druglikeness of a chemical compound [45]. Resveratrol does not violate any of Lipinski's rules, and also adheres to other filters that define druglikeness, including Ghose, Veber, Egan and Muegge. The BOILED-egg diagram of resveratrol generated by SwissADME is represented by Figure S2. The physicochemical and pharmacokinetic properties of resveratrol are favorable for drug discovery

Table 4: Druglikeness of Resveratrol

Formula	C ₁₄ H ₁₂ O ₃
Molecular weight	228.24 g.mol ⁻¹
Lipophilicity (LogP)	1.71
Water solubility (Log S)	Soluble
GI absorption	High
BBB permeant	Yes
Lipinski's Rules	Yes
Ghose, Veber, Egan, Muegge	Yes

5. Discussion

The effects of resveratrol have been studied previously for its inhibition of nucleic acid synthesis, gene expression, viral replication and protein synthesis in several viruses. Experimental studies have shown that resveratrol inhibits ZIKV *in vitro*, however, the binding mechanism and binding interactions of resveratrol to the ZIKV NS3 helicase were not elucidated. The 200 ns molecular dynamic simulations of the apo helicase and resveratrol-bound helicase have allowed us to understand the shifts that occur in the enzyme upon binding and the affinity of the helicase for resveratrol.

A “loose” and expanded structure of the helicase is necessary to accommodate RNA in its binding pocket for viral RNA replication. Resveratrol binding renders the helicase more compact than when unbound, limiting the space within the RNA-binding pocket. The P-loop

regulates ATP binding and hydrolysis during ZIKV replication. Resveratrol stabilized the P-loop when compared to the apo and resulted in major shifts and conformational changes in the RNA-binding loop. Since resveratrol binding to the helicase decreases ATP hydrolysis, we speculate that resveratrol binding may also hinder RNA binding and replication due to movements of the RNA-binding loop in front of the entrance of the RNA-binding pocket, however, further experimentation is required to substantiate this theory. Strong binding interactions, including hydrophobic and hydrogen bonding, between resveratrol and residues of the helicase also reduce fluctuations of the enzyme domains, thus explaining the high potency of resveratrol inhibition on the ZIKV NS3 helicase. Conformational ensembles generated from the molecular dynamic simulations in this study match with the experimental data.

6 Conclusion

To our understanding, this is the first study to have presented data describing the events that occur at a molecular level when resveratrol binds to the ZIKV NS3 helicase enzyme. Since resveratrol is a competitive-inhibitor of ATP and stably binds to the ATPase pocket in the helicase, we can speculate that inhibition of ZIKV by resveratrol at an organism level may render the enzyme “powerless” and may even lead to resveratrol being a potent inhibitor of multiple viruses including other *flaviviruses* such as DENV, WNV and JEV. Resveratrol is also a natural antioxidant, therefore, its use as a multipurpose antiviral implies safety, easy availability and accessibility, and cost effectiveness, particularly in rural communities.

This material refines the knowledge surrounding resveratrol inhibition of the ZIKV NS3 helicase and will aid the search for anti-ZIKV drugs. Additional investigations are vital to substantiate the role of resveratrol in the treatment of ZIKV. Further analysis will also include the interactions between resveratrol and other members of the *Flavivirus* genus of viruses.

Summary Points

- The Zika virus (ZIKV) continues to affect pregnant women and their infants without FDA-approved vaccines or treatments.
- There is still very much to learn about ZIKV before we can effectively treat it.
- Understanding the molecular dynamics behind potential organism level inhibition could help prevent future resistance of ZIKV to drugs.
- Hence, we studied the molecular dynamics of the unbound and resveratrol-bound helicase for 200ns.
- Molecular dynamic simulations and post-dynamic analyses allowed us to pinpoint the precise residues and interactions that are key in the binding of resveratrol to the helicase.
- The movements of loops surrounding RNA and inhibitor binding sites also regulate binding and replication, therefore, we analyzed the shifts in loops surrounding the ATPase pocket and RNA binding site.
- The druglikeness of resveratrol was also established using computational tools, which led to the conclusion that resveratrol follows all of Lipinski's rules and can pass the blood-brain barrier, making it suitable for the treatment of ZIKV.

- This material demonstrates the structural dynamics of the ZIKV NS3 helicase upon resveratrol binding, which will advance anti- ZIKV drug development.

Conflict of Interest

Authors declare no potential financial and other conflict of interests.

Financial & Competing Interests Disclosure

This work was financially supported by the German Academic Exchange Service (DAAD) and the National Research Foundation (NRF). Computational support was provided by the Centre for High Performance Computing (CHPC, <http://www.chpc.ac.za>). The authors have no other relevant affiliations or financial involvement with any organization or entity with a financial interest in or financial conflict with the subject matter or materials discussed in the manuscript apart from those disclosed. No writing assistance was utilized in the production of this manuscript

References

Papers of interest are identified as: * of interest; ** of considerable interest

1. Ghosh D. Zika virus – a global emergency. *Curr. Sci.* 114(4), 725 (2018).
2. Dhama K, Karthik K, Tiwari R, *et al.* Zika Virus / Zika Fever : A Comprehensive Update. *J. Exp. Biol. Agric. Sci.* 6(1), 1–31 (2018).

3. Nandy A, Basak SC. The Epidemic that Shook the World — The Zika Virus Rampage. *Explor. Res. Hypothesis Med.* 2(3), 43–56 (2017).
4. Kindhauser MK, Allen T, Frank V, Santhana RS, Dye C. Zika: the origin and spread of a mosquito-borne virus. *Bull. World Health Organ.* 94(9), 675–686 (2016).
5. Ryan SJ, Carlson CJ, Mordecai EA, Johnson LR. Climate change drives uncertain global shifts in potential distribution and seasonal risk of Aedes-transmitted viruses. *bioRxiv.* , 172221 (2017).
6. Jain R, Coloma J, García-Sastre A, Aggarwal AK. Structure of the NS3 helicase from Zika virus. *Nat. Struct. Mol. Biol.* [Internet]. 23(8), 752–754 (2016). Available from: <http://dx.doi.org/10.1038/nsmb.3258>.
7. Mishra PM, Uversky VN, Giri R. Molecular Recognition Features in Zika Virus Proteome. *J. Mol. Biol.* [Internet]. 430(16), 2372–2388 (2017). Available from: <https://doi.org/10.1016/j.jmb.2017.10.018>.
8. Wang A, Thurmond S, Islas L, Hui K, Hai R. Zika virus genome biology and molecular pathogenesis. *Emerg. Microbes Infect.* [Internet]. 6(3), e13 (2017). Available from: <http://www.nature.com/doi/10.1038/emi.2016.141>.
9. Tian H, Ji X, Yang X, *et al.* The crystal structure of Zika virus helicase: basis for antiviral drug design. *Protein Cell.* 7(6), 450–454 (2016).
10. Tian H, Ji X, Yang X, *et al.* Structural basis of Zika virus helicase in recognizing its substrates. *Protein Cell.* 7(8), 562–570 (2016).
11. Devnarain N, Soliman MES. A Panoptic Uncovering of the Dynamical Evolution of the Zika Virus NS5 Methyltransferase Binding Site Loops- Zeroing in on the Molecular Landscape. *Chem. Biol. Drug Des.* [Internet]. , 1–13 (2018). Available from: <http://www.ncbi.nlm.nih.gov/pubmed/29923677%0Ahttp://doi.wiley.com/10.1111/cbdd.13353>.
12. Pan A, Saw WG, Manimekalai MSS, *et al.* Structural features of NS3 of Dengue virus serotypes 2 and 4 in solution and insight into RNA binding and the inhibitory role of quercetin. *Acta Crystallogr. Sect. D Struct. Biol.* 73(5), 402–419 (2017).
13. Lee JH, Wendorff TJ, Berger JM. Resveratrol: A novel type of topoisomerase II inhibitor. *J. Biol. Chem.* 292(51), 21011–21022 (2017).
14. Abba Y, Hassim H, Hamzah H, Noordin MM. Antiviral Activity of Resveratrol against

Human and Animal Viruses. *Adv. Virol.* 2015, 1–7 (2015).

15. Saw WG, Pan A, Subramanian Manimekalai MS, Grüber G. Structural features of Zika virus non-structural proteins 3 and -5 and its individual domains in solution as well as insights into NS3 inhibition. *Antiviral Res.* [Internet]. 141(1), 73–90 (2017). Available from: <https://www.sciencedirect.com/science/article/pii/S0166354216306799>.
16. Fatima K, Mathew S, Suhail M, *et al.* Docking studies of Pakistani HCV NS3 helicase: A possible antiviral drug target. *PLoS One.* 9(9), 1–12 (2014).
17. Campagna M, Rivas C. Antiviral activity of resveratrol. *Biochem. Soc. Trans.* [Internet]. 38(1), 50–53 (2010). Available from: <http://www.ncbi.nlm.nih.gov/pubmed/20074034> <http://biochemsoctrans.org/lookup/doi/10.1042/BST0380050>.
18. Hausenblas HA, Schoulda JA, Smoliga JM. Resveratrol treatment as an adjunct to pharmacological management in type 2 diabetes mellitus-systematic review and meta-analysis. *Mol. Nutr. Food Res.* 59(1), 147–159 (2015).
19. Xia N, Daiber A, Förstermann U, Li H. Antioxidant effects of resveratrol in the cardiovascular system. *Br. J. Pharmacol.* 174(12), 1633–1646 (2017).
20. Bastianetto S, Ménard C, Quirion R. Neuroprotective action of resveratrol. *Biochim. Biophys. Acta - Mol. Basis Dis.* [Internet]. 1852(6), 1195–1201 (2015). Available from: <http://dx.doi.org/10.1016/j.bbadis.2014.09.011>.
21. Borriello A. Resveratrol in Cancer Prevention and Treatment: focusing on Molecular Targets and Mechanism of Action. *Proceedings* [Internet]. 1(10), 976 (2017). Available from: <http://www.mdpi.com/2504-3900/1/10/976>.
22. Luo D, Vasudevan SG, Lescar J. The flavivirus NS2B-NS3 protease-helicase as a target for antiviral drug development. *Antiviral Res.* 118(1), 148–158 (2015).
23. Lei J, Hansen G, Nitsche C, Klein CD, Zhang L, Hilgenfeld R. Crystal structure of Zika virus NS2B-NS3 protease in complex with a boronate inhibitor. *Science.* 353(6298), 503–505 (2016).
24. Rose PW, Prlić A, Altunkaya A, *et al.* The RCSB protein data bank: integrative view of protein, gene and 3D structural information. *Nucleic Acids Res.* [Internet]. 45(D1), D271–D281 (2016). Available from: <https://academic.oup.com/nar/article-lookup/doi/10.1093/nar/gkw1000>.

25. Tian H, Ji X, Yang X, *et al.* The crystal structure of Zika virus helicase: basis for antiviral drug design. *Protein Cell.* 7(6), 450–454 (2016).
26. Kim S, Thiessen PA, Bolton E., *et al.* PubChem Substance and Compound databases. *Nucleic Acids Res.* 44(D1), D1202-13 (2016).
27. Yang Z, Lasker K, Schneidman-Duhovny D, *et al.* UCSF Chimera, MODELLER, and IMP: an Integrated Modeling System. *J. Struct. Biol.* [Internet]. 179(3), 269–278 (2012). Available from: <https://www.ncbi.nlm.nih.gov/pmc/articles/PMC3410985/pdf/nihms-371777.pdf>.
28. de Ruyck J, Brysbaert G, Blossey R, Lensink MF. Molecular docking as a popular tool in drug design, an in silico travel. *Adv. Appl. Bioinforma. Chem.* 9(1), 1–11 (2016).
29. Trott O, Olson AJ. AutoDock Vina: improving the speed and accuracy of docking with a new scoring function, efficient optimization and multithreading. *J. Comput. Chem.* 31(1), 445–461 (2010).
30. Alonso H, Bliznyuk AA, Gready JE. Combining Docking and Molecular Dynamic Simulations in Drug Design. *Med. Res. Rev.* [Internet]. 26(5), 531–568 (2006). Available from: http://www.cmbi.ru.nl/edu/bioinf4/articles/pdf/mdy_md_docking_alonso.pdf.
31. Munir A, Azam S, Mehmood A. Structure-Based Pharmacophore Modeling, Virtual Screening and Molecular docking for the Treatment of ESR1 Mutations in Breast Cancer. *Drug Des. Open Access* [Internet]. 5(137), 2169-0138 (2016). Available from: <https://www.omicsgroup.org/journals/structurebased-pharmacophore-modeling-virtual-screening-andmolecular-docking-for-the-treatment-of-esr1-mutations-in-breast-cancer-2169-0138-1000137.php?aid=82519>.
32. Meng X-Y, Zhang H-X, Mezei M, Cui M. Molecular Docking: A powerful approach for structure-based drug discovery. *Curr. Comput. Drug Des.* 7(2), 146–157 (2011).
33. Case DA, Cheatham TE, Darden T, *et al.* The Amber biomolecular simulation programs. *J. Comput. Chem.* 26(16), 1668–1688 (2005).
34. Salomon-Ferrer R, Götz AW, Poole D, Le Grand S, Walker RC. Routine Microsecond Molecular Dynamics Simulations with AMBER on GPUs. 2. Explicit Solvent Particle Mesh Ewald. *J. Chem. Theory Comput.* [Internet]. 9(9), 3878–3888 (2013). Available from: <http://pubs.acs.org/doi/abs/10.1021/ct400314y>.
35. Sprenger KG, Jaeger VW, Pfaendtner J. The general AMBER force field (GAFF) can accurately predict thermodynamic and transport properties of many ionic liquids. *J. Phys. Chem. B.* 119(18), 5882–5895 (2015).

36. Miner JJ, Cao B, Govero J, *et al.* Zika Virus Infection during Pregnancy in Mice Causes Placental Damage and Fetal Demise. *Cell*. 165(5), 1081–1091 (2016).
37. Wang J, Wang W, Kollman P a, Case D a. Antechamber, An Accessory Software Package For Molecular Mechanical Calculations. *J. Chem. Inf. Comput. Sci.* 222(2), U403 (2001).
38. Woods RJ, Chappelle R. Restrained electrostatic potential atomic partial charges for condensed-phase simulations of carbohydrates. *J. Mol. Struct. THEOCHEM* [Internet]. 527(1), 149–156 (2000). Available from: <https://www.ncbi.nlm.nih.gov/pmc/articles/PMC4191892/pdf/nihms-632958.pdf>.
39. Genheden S, Ryde U. The MM/PBSA and MM/GBSA methods to estimate ligand-binding affinities. *Expert Opin. Drug Discov.* [Internet]. 10(5), 449–461 (2015). Available from: <http://www.tandfonline.com/doi/full/10.1517/17460441.2015.1032936>.
40. Vanommeslaeghe K, Guvench O, Mackerell AD. Molecular Mechanics. *Curr Pharm Des.* 20(20), 3281–3292 (2014).
41. Wang H, Guo C, Chen BZ, Ji M. Computational study on the drug resistance mechanism of HCV NS5B RNA-dependent RNA polymerase mutants V494I, V494A, M426A, and M423T to Filibuvir. *Antiviral Res.* [Internet]. 113(1), 79–92 (2015). Available from: <http://dx.doi.org/10.1016/j.antiviral.2014.11.005>.
42. Cele FN, Ramesh M, Soliman MES. Per-residue energy decomposition pharmacophore model to enhance virtual screening in drug discovery: A study for identification of reverse transcriptase inhibitors as potential anti-HIV agents. *Drug Des. Devel. Ther.* 10, 1365–1377 (2016).
43. Daina A, Michielin O, Zoete V. SwissADME : a free web tool to evaluate pharmacokinetics , drug-likeness and medicinal chemistry friendliness of small molecules. *Sci. Rep.* [Internet]. 7, 42717 (2017). Available from: <http://dx.doi.org/10.1038/srep42717>.
44. Devnarain N, Ramharack P, Soliman ME. Brain grants permission of access to Zika virus but denies entry to drugs: a molecular modeling perspective to infiltrate the boundary. *RSC Adv.* [Internet]. 7(75), 47416–47424 (2017). Available from: <http://xlink.rsc.org/?DOI=C7RA05918C>.
45. Lipinski CA. Lead- and drug-like compounds: The rule-of-five revolution. *Drug Discov. Today Technol.* 1(4), 337–341 (2004).

CHAPTER 7: SYNTHESIS

1 Conclusion

The rampant ZIKV and its devastating clinical outcomes led to a rapid research response since the 2015 ZIKV epidemic in Brazil (Campos, Bandeira and Sardi, 2015), which have begun explaining why ZIKV shifted from being inconspicuous to notorious. It has become critical that a cure for ZIKV is discovered. Major breakthroughs have been made in the scientific community surrounding the design of potential anti-ZIKV small molecule inhibitors and vaccines, although, none have passed clinical trials (da Silva, Martins and Jardim, 2018).

In this study, a major challenge of anti-ZIKV drug design - the ability of a drug to cross the BBB – is addressed by providing a route map of strategic approaches to design drugs with improved BBB permeability and to transport drugs that are BBB-impermeable. Moreover, an assessment of the bioavailability of screened drugs as potential ZIKV inhibitors is presented.

This study also improves the knowledge base surrounding the structural and functional features of pharmacological targets of ZIKV, in this case being the NS3 helicase and NS5 MTase enzymes, to enable the design and discovery of effective ZIKV inhibitors. The binding mechanisms of two potential ZIKV MTase inhibitors – Sinefungin and compound 5- were elucidated using molecular dynamics, which revealed that Sinefungin is a more stable inhibitor of the MTase than compound. This is also in agreement with experimental findings (Coutard *et al.*, 2017). The molecular mechanism of inhibition by resveratrol, an antioxidant, on the NS3 helicase describes the modification of the enzyme to accommodate inhibitor binding, particularly since ZIKV RNA replication is influenced by loop movements. The druglike nature of resveratrol was established and based on its chemical features, it has the ability to pass the BBB. Additionally, this study provided specific amino acid residues of the NS3 helicase and NS5 MTase enzymes that highly contribute to inhibitor-binding, as well as precise moieties of potential ZIKV inhibitors that are of significance, to assist in the discovery of more potent ZIKV inhibitors.

In conclusion, the outcomes presented in this study are of scientific merit and should serve as a cornerstone for anti-ZIKV drug design and discovery through molecular modeling and CADD.

2 Future Perspectives

The potential ZIKV inhibitors referred to in this study have demonstrated favorable protein-ligand binding energies and interactions, thus hold potential as lead compounds. Although, these *in silico* studies must be further validated through biological testing.

The substantial research response after the ZIKV outbreak triggered the discovery of a flood of potential small molecule inhibitors and vaccines, which are now in clinical trials. However, the effects of these potential vaccines and inhibitors on humans, particularly on pregnant women and their infants, are yet to be established. Since neuronal cells are predominantly affected by ZIKV, more validations are required to learn the effects of vaccines and inhibitors on neurons to eliminate the risk of any further damage to the brain. Moreover, further research must be put into the design of drugs that can pass the BBB to allow it to act on neuronal cells. This study described approaches that may be used to ensure anti-ZIKV drugs can pass the BBB, however, experiments must be designed and carried out to analyze its efficacy.

The outcomes of this study and future studies of effective ZIKV inhibitors may be applicable to other viruses that result in future unforeseen clinical conditions.

3 References

Campos, G. S., Bandeira, A. C. and Sardi, S. I. (2015) 'Zika Virus Outbreak, Bahia Brazil', *Emerging Infectious Diseases*, 21(10), pp. 1885–1886. doi: 10.32301/eid2110.150847.

Coutard, B. *et al.* (2017) 'Zika Virus Methyltransferase: Structure and Functions for Drug Design Perspectives', *Journal of Virology*, 91(5), pp. e02202-16. doi: 10.1128/JVI.02202-16.

da Silva, S., Martins, D. O. S. and Jardim, A. C. G. (2018) 'A Review of the Ongoing Research on Zika Virus Treatment.', *Viruses*. Multidisciplinary Digital Publishing Institute (MDPI), 10(255), pp. 1–18. doi: 10.3390/v10050255.

APPENDICES

Biomedical Research Ethics Committee (BREC) exemption letter



RESEARCH OFFICE
BIOMEDICAL RESEARCH ETHICS ADMINISTRATION
Westville Campus
Govan Mbeki Building
Private Bag X 54001
Durban
4000
KwaZulu-Natal, SOUTH AFRICA
Tel: 27 31 2604769 - Fax: 27 31 260-4609
Email: bbrc@ukzn.ac.za

Website: <http://research.ukzn.ac.za/Research-Ethics/Biomedical-Research-Ethics.aspx>

14 September 2018

Ms N Devnarain (211531113)
School of Health Sciences
College of Health Sciences
soliman@ukzn.ac.za

Dear Ms Devnarain

Protocol: A bio-computational perspective of pharmacological targets of the Zika virus: a molecular conception of the structural dynamics of the Zika virus enzyme.
Degree: PhD
BREC Ref No: EXM520/18

I refer to your application to BREC received on 20 August 2018 and wish to advise you that exemption of ethics review has been granted for this study.

This exemption will be noted at the next Biomedical Research Ethics Committee meeting to be held on 09 October 2018.

Yours sincerely



Prof N Rambiritch
Chair: Biomedical Research Ethics Committee



Cite this: *RSC Adv.*, 2017, 7, 47416

Brain grants permission of access to Zika virus but denies entry to drugs: a molecular modeling perspective to infiltrate the boundary†

Nikita Devnarain, Pritika Ramharack and Mahmoud E. Soliman *

The magnetism of the Zika virus to neuronal cells proves to be one of the major concerns in the development of effective inhibitors. Although the blood–brain barrier limits the entry of most drugs, tailored small molecule inhibitors and drug delivery systems are currently being designed to overcome this obstacle. We have identified the core challenge to be addressed – blood–brain barrier permeability – and provided insight into strategies that can be used to improve drug delivery to the brain. We have compiled drugs that have previously been proposed as potential Zika virus inhibitors and classified chemical features of those drugs, which influence blood–brain barrier permeability. Thereafter, we created a route map to design drugs with improved blood–brain barrier permeability. An alternative approach using drug delivery systems to transport membrane-impermeable Zika virus inhibitors to the brain is also proposed, along with descriptions of known drug carriers. This review provides information for further research toward inhibitors of Zika virus.

Received 26th May 2017
 Accepted 19th September 2017

DOI: 10.1039/c7ra05918c

rsc.li/rsc-advances

The tale of Zika virus

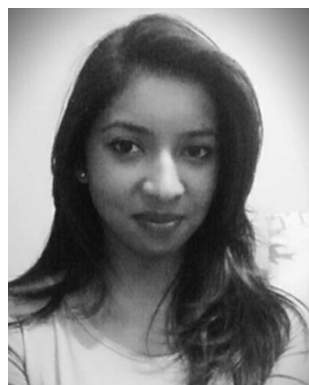
The Zika virus (ZIKV), a mosquito-borne virus, belongs to the Flaviviridae family and has similar characteristics to other flaviviruses such as Dengue virus, West Nile virus and Japanese Encephalitis virus.¹ The rapid disseminating potential and repercussion in humans are attributed to the various modes of

transmission, primarily through the bite of an infected *Aedes aegypti* mosquito.² The ZIKV is also transmitted through sexual intercourse,³ blood transfusions⁴ and from a mother to child perinatally.⁵

The ZIKV was originally isolated in Uganda in the Zika forest in 1947.⁶ For nearly 7 decades thenceforth, sporadic infections caused by ZIKV were reported in several countries worldwide. These include more equatorial countries of Africa such as Tanzania, Egypt, Kenya, Nigeria, Central African Republic, and Gabon; some Asian countries including Pakistan, India, Malaysia, Thailand, the Philippines and Indonesia; and many islands in the Pacific Ocean.^{7–10} The most devastating and

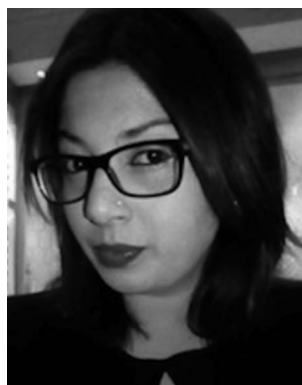
Molecular Bio-computation and Drug Design Laboratory, School of Health Sciences, University of KwaZulu-Natal, Westville Campus, Durban 4001, South Africa. E-mail: soliman@ukzn.ac.za; Fax: +27 31 260 7872; Tel: +27 31 260 8048

† Electronic supplementary information (ESI) available. See DOI: 10.1039/c7ra05918c



Nikita Devnarain obtained her BSc Biomedical Science degree in 2013 and graduated with her Honours and Masters in Medical Biochemistry and Chemical Pathology at UKZN by the end of 2016. She is now a Ph.D. student in Prof Mahmoud E. S. Soliman's Molecular Bio-computation and Drug Design Laboratory at the Department of Pharmaceutical Sciences. Her current research directions

include in silico design and exploration of inhibitors against the Zika virus.



Pritika Ramharack currently holds a postdoctoral position at the Molecular Bio-computation and Drug Design Laboratory, Department of Pharmaceutical Sciences, University of Kwa-Zulu Natal, South Africa. Her current research concentrates on the Design of Inhibitors against numerous infectious diseases including HIV and Tuberculosis.



highly publicized outbreak that captured the world's attention occurred in Brazil in 2015, which triggered global panic as it rapidly spread across America.¹¹ In 2016, the ZIKV broadened its geographic spectrum to North American Florida and Texas where the infection was locally transmitted.¹⁰

There has been prior ambiguity regarding the diagnosis of ZIKV, as its infection manifests similarly to common colds and other *flavivirus* infections.¹² These symptoms include fever, headaches, conjunctivitis, joint pain, muscle pain and skin rash.^{13,14} The speculation of ZIKV infection depends on its manifestation and history of mosquito bites.¹² The ZIKV is detectable in bodily fluids such as saliva,¹⁵ semen,^{16,17} urine¹⁸ and amniotic fluid,¹⁹ which can be verified in the laboratory.²⁰ The various modes of transmission of ZIKV make the human body highly susceptible to infection. When ZIKV enters the body through an infected female mosquito bite, the infection manifests as a rash in the vicinity of the bite.⁹ This occurs due to the release of virions into dermal and epidermal layers of the skin, where ZIKV is introduced to the bloodstream and advances to the lymph nodes to replicate and cause viremia.²¹

The ZIKV is an enveloped icosahedral virus that is made up of a single-stranded, positive-sense genome. The enveloped virion comprises of an 11 kilobase genome consisting of 10 794 nucleotides encoding 3419 amino acids.²² The open reading frame (ORF) of the 5' and 3' untranslated region (UTR) encodes a polyprotein that is cleaved into three structural proteins, being the capsid (C), precursor membrane (prM), and envelope (E).²³ Seven non-structural (NS) proteins are also found in this assembly, namely, NS1, NS2a, NS2b, NS3, NS4a, NS4b, and NS5 (largest viral protein).²⁴ The genomic protein organization is 5'-C-prM-E-NS1-NS2a-NS2b-NS3-NS4a-NS4b-NS5-3'²⁵ and contains

an m⁷gpppAmpN₂ at the 5' end and lacks a poly-A tail at the 3' end.²⁶ A highly conserved 90–120-nucleotide strand is situated close to the 3' end that develops into a hairpin loop and is vital for replication.^{26,27} Of the non-structural proteins, NS1, NS3 and NS5 are highly conserved whereas the NS2a, NS2b, NS4a and NS4b are small and hydrophobic.²⁴ Of critical importance is the proteolytic cleavage of prM to produce the pr and M protein by furin-like protease located in the *trans*-Golgi network during the egress of the particles as this promotes maturation of virions.²⁸

The ramifications of ZIKV infections have heavily impacted thousands worldwide, particularly in newborns, since ZIKV-infected pregnant women have given birth to babies with congenital brain abnormalities, predominantly microcephaly and intracranial calcification.¹³ The ZIKV infection has also been shown to elicit Guillain-Barré Syndrome, which ultimately advances to paralysis and death.²⁹

Studies have shown tropism of the ZIKV for cells of the nervous system, whereby entry into neuronal and endothelial cells occur *via* AXL receptors situated on the cell surface.^{30–32} The ZIKV has also affected retinal cells that line the blood-retinal barrier (*i.e.* retinal pigment epithelium and retinal endothelium) in mice, which also express AXL receptors. This presents as conjunctivitis.³³

Blood–brain barrier permeability as a core challenge in ZIKV therapy

Treating the symptoms of ZIKV will not yield permanent results; hence nipping the cause at the bud may be the best route to a solution. The blood–brain barrier (BBB) and placental barrier are surrounded by lipophilic membranes and junctions, through which only certain compounds can permeate.³⁴ It has been shown that the placenta is permissive to most drugs as it serves to allow for the exchange of nutrients for its biological purpose.³⁵ The ZIKV can penetrate these membranes, which is evident by its downstream pathogenic effects in fetal nervous systems.^{13,26,29,30}

The specific characteristics of a compound govern the method by which it is transported across the BBB, or whether or not it is transported at all. Compounds that have surface hydrogen bonds (hydrophilic compounds) are only permissive through tight junctions of the BBB, which ultimately serve to prevent the passage of molecules between cells of the endothelium. These hydrophilic compounds are impermeable through the lipophilic endothelium and require lipid-mediated transport in order to permeate transcellularly. Large molecules, such as insulin and transferrin, require receptors, whereas small molecules require carrier-mediated transport to move across the barrier. There is also active efflux transport for endogenous BBB transporters (Fig. 1 – BBB).^{34,36–38}

Bioavailability features of screened drugs as prospective ZIKV inhibitors

There are FDA-approved drugs that have been proposed as anti-ZIKV drugs based on their diverse antiviral/antimicrobial/antibacterial activities in diseases other than ZIKV,³⁹ however,



Prof. Mahmoud Soliman (B. Pharm., M. Pharm., MPhil/PhD) is the Dean and Head of School of Health Sciences, UKZN, Westville Campus, and the Head and principal investigator of Molecular Bio-computation and Drug Design Laboratory. Soliman has joined the School in 2012 after completing his postgraduate degrees (MPhil/PhD – Oct. 2009) at the University of Bath, United Kingdom in field of Molecular

Modeling, computational chemistry and drug design, under supervision of Prof. Ian Williams. Prof. Soliman is Editor of Journal of Cell Biochemistry and Biophysics (Springer), Editor-in-Chief of the journal of Organic and Biomolecular Simulations (JOBS), editor of Journal of Pharmaceutical Chemistry, Journal of Drug Design and Research and International Journal of Molecular Biology and Medicine. Soliman is also academic visitor at the University of Bath, UK, collaborating with Prof. Ian Williams' lab. Prof. Soliman is a C-rated NRF researcher. Soliman's research mainly focuses on studying of biomolecular systems and drug–protein interactions at molecular level.



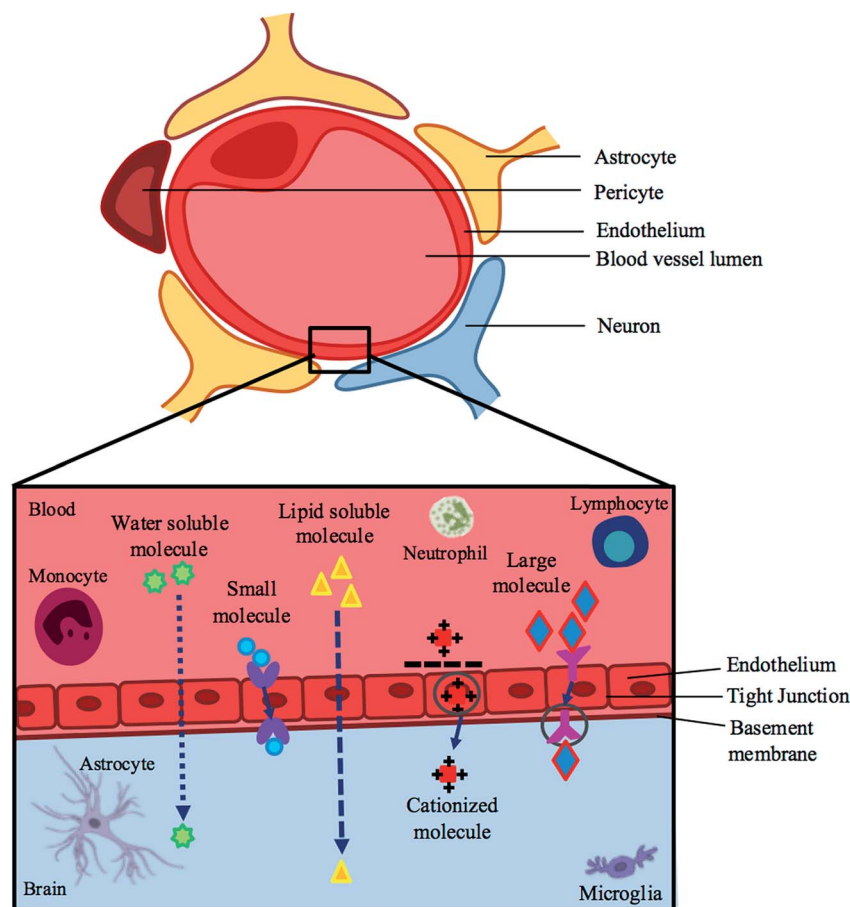


Fig. 1 A schematic representation of the blood–brain barrier and pathways across this barrier.

the ability of those drugs to pass the BBB, their properties as hydrophilic/lipophilic compounds, and their ability to be absorbed by the gastrointestinal tract (GIT) have not yet been clearly elucidated. To this effect, we have taken a step further and utilized a chemical data base, PubChem, along with ADME prediction tools, Swiss ADME⁴⁰ to predict specific characteristics of these candidate anti-ZIKV drugs and to verify whether or not the proposed compounds by Barrows *et al.* (2016) could be potential anti-ZIKV drugs with BBB-permeable profiles. SWISS ADME is a “website allows you to compute physicochemical descriptors as well as to predict ADME parameters, pharmacokinetic properties, druglike nature and medicinal chemistry friendliness of one or multiple small molecules to support drug discovery”.⁴⁰ The proposed compounds are listed in Table 1.

The partition coefficient ($\log P$) measures how hydrophilic or hydrophobic a molecule is. The desired $\log P$ value of a molecule likely to permeate lipophilic membranes should lie between 0–5.⁴¹ The ability of a drug to pass through the BBB is influenced by their unique but varying properties.³⁶ In Table 1, ~80% of the drugs described have the ability to pass through lipophilic membranes, however, less than 20% of those drugs can penetrate the BBB.⁴⁰ Efficient GIT absorption of orally administered drugs is required for entry into the bloodstream and sufficient drug delivery,⁴² although, just half the drugs mentioned are highly absorbed *via* the GIT. The results of this

table suggest that the ability of a compound to pass through the BBB depends on factors additional to lipophilicity. From this exercise we highlight 5 compounds that are predicted to pass the BBB and the hydrophobic spots of each compound are shadowed in yellow in Fig. 2.

Hydrophobic groups of compounds are required for hydrophobic interactions with target molecules. Hydrophobic interactions are comparably stronger than some weak intermolecular forces, such as hydrogen bonds or van der Waals interactions, and ensure protein–ligand complexes remain stable and biologically active.⁴³ As depicted in Fig. 2, all five compounds from Table 1 that have the ability to pass the BBB bear hydrophobic groups and therefore, possess the potential to form hydrophobic interactions with target molecules. Although, fingomolid and sertraline have more hydrophobic spots than the other compounds in Fig. 2, and therefore, are more likely to form stronger hydrophobic interactions.

Systematic approach to tackle the challenge

To overcome the hurdle faced by most drug therapies, we are presenting two main strategies that could potentially assist with the design and bioavailability of compounds with an improved BBB permeability profile. Furthermore, we include an approach



Table 1 Predicted bioavailability features of prospective anti-ZIKV inhibitors

Drug name	Lipid solubility (log <i>P</i>)	BBB permeation	GIT absorption
Auranofin	0.00	No	High
Azathioprine	0.72	No	Low
Bortezomib	0.00	No	High
Clofazimine	4.72	No	Low
Cyclosporine A	6.16	No	Low
Dactinomycin	5.33	No	Low
Daptomycin	0.79	No	Low
Deferasirox	2.48	No	High
Digoxin	4.69	No	Low
Fingolimod	3.76	Yes	High
Gemcitabine HCl	0.00	No	High
Ivermectin	6.31	No	Low
Mebendazole	1.27	No	High
Mefloquine HCl	0.00	No	Low
Mercaptopurine hydrate	0.47	No	High
Methoxsalen	2.22	Yes	High
Micafungin	-0.72	No	Low
Mycophenolate mofetil	3.67	No	High
Mycophenolic acid	2.38	No	High
NITD008	1.30	No	Low
Palonosetron HCl	0.00	Yes	High
Pyrimethamine	2.15	Yes	High
Sertraline	3.40	Yes	High
Sofosbuvir	3.05	No	Low
Sorafenib tosylate	3.84	No	Low
Thioguanine	0.14	No	High

that relies on the pre-existing BBB-impermeable drugs conjugated to drug delivery systems. These strategies are: (1) improve the inhibitor and (2) carry the cargo.

Improve the inhibitor

In this approach, *in silico* tools may be used to model and optimize potential compounds (Fig. 3), followed by compound

synthesis and biological testing. Phase 1 includes targeted selection of potential anti-ZIKV compounds. This incorporates screening for potential compounds with specific physicochemical properties and antiviral activities using chemical databases, and the use of absorption, distribution, metabolism, excretion (ADME) prediction tools such as Swiss ADME, in order to filter out compounds that encompass the ability to pass the BBB. The ability of a compound to pass through the BBB is governed by a function of lipophilicity, the molecular characteristics of charged and hydrophobic residues of the compound as well as molecular weight.³⁷ The main lipophilic properties that must be considered include the Hansch constant (π), hydrophobic fragmental constant (f), log *P*, capacity factor values from RP-HPLC (log *k*_w), calculated log *P* values (CLOGP) and molecular lipophilic potential (MLP).⁴⁴ With regard to the charge of the compound, only uncharged molecules can diffuse across the membrane to become reprotonated once it leaves the membrane and enters the brain fluid.³⁷ As the size of a compound gets larger, its ability to permeate the BBB decreases.⁴⁵

Phase 2 involves the prediction of lipid permeability of the potential anti-ZIKV compounds using molecular dynamic simulations and 3D-modelled lipid bilayer simulations. Due to the surrounding lipid membrane in the BBB, it is necessary to assess compound interactions with the target enzyme within lipid membrane.⁴⁶

Phase 3 involves the estimation of binding affinities between potential compounds, which pass through the BBB, and viral enzymes. This may be achieved *via* binding free energy calculations or molecular docking of the compound of interest into the active site of the target enzyme.⁴⁷

Following the design process, the compounds must be synthesized for further testing. Synthesis of the compound involves construction of the carbon framework and the addition/deletion/transformation of functional groups for functionality of compound. Validation of synthesis is carried out by ligand-binding assays which involves placing the target

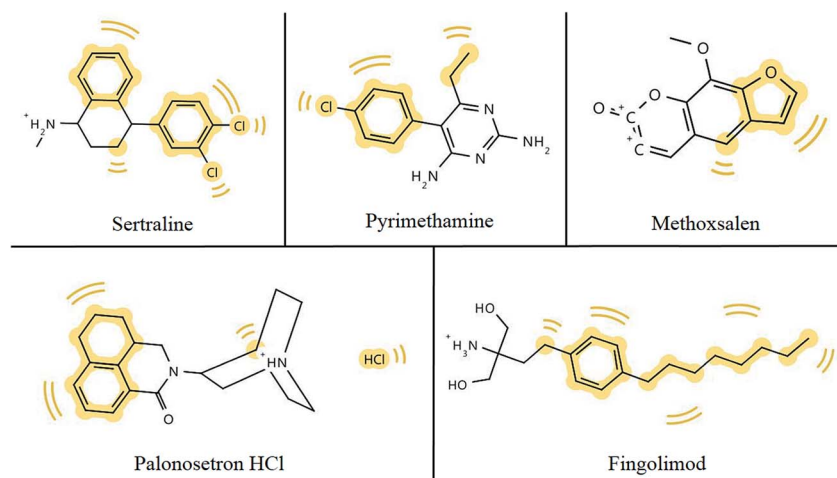


Fig. 2 Hydrophobic footprints (highlighted in yellow) in chemical structures of potential anti-ZIKV compounds which have the ability to permeate the BBB.



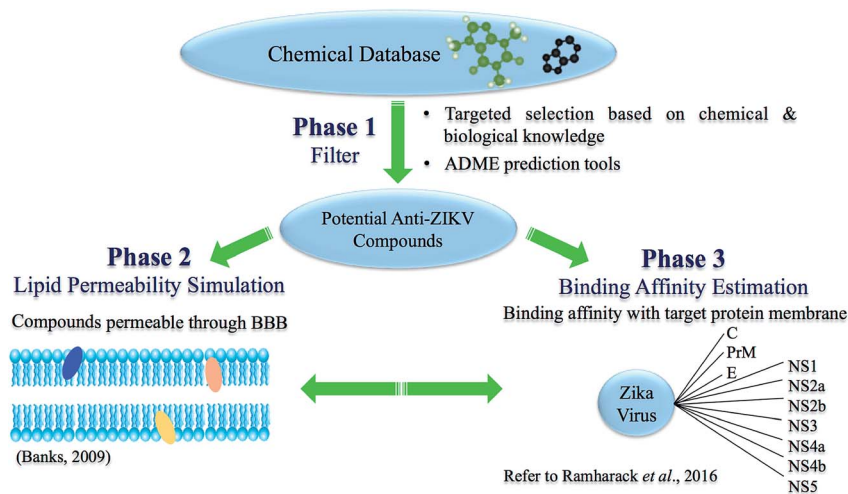


Fig. 3 Phases involved in the suggested approach to improve the BBB-permeability profile of the inhibitor.

enzyme and compound of interest into a solvent (*e.g.* water) to allow the compound to interact with the active site residues of the enzyme.⁴⁸ Binding studies provide reliable assessments of binding affinities, errors and binding mode.⁴⁸ Further studies including biological testing will investigate toxicity and efficacy of the compound, including *in vitro* studies (cellular level), *in vivo* studies (organism level) and ultimately clinical trials. Microscale thermophoresis (MST) may also be used in order to analyze the interaction between the inhibitors and receptors, experimentally, which is established on the controlled movement of particles along a temperature gradient.⁴⁹

Carry the cargo

An alternate to creating new BBB-permeable drugs will involve the utilization of drug carriers that have already been successful in delivering drugs to the brain. This approach eliminates the additional time and expense required to design and formulate new drugs and drug delivery systems. A drug carrier could be used to transport a BBB-impermeable drug to the brain and allow for the drug to carry out its function against ZIKV.

There are existing drugs that have been proven to inhibit ZIKV replication in isolated ZIKV infected cells, such as NITD008 (ref. 50) and sofosbuvir,⁵¹ however the drugs cannot pass the BBB to counteract the virus (Table 1). With half the battle won due to their ability to inhibit ZIKV, ultimate triumph over ZIKV would entail overcoming impermeability, which requires the potential ZIKV inhibitors to be transported across the BBB.

Previously utilized membrane-permeable drug delivery approaches have been successful in transporting membrane-impermeable drugs across the BBB for other infections and diseases, such as Parkinson's disease and Alzheimer's disease.^{52–55} Some known drug delivery systems used in various disease cases include polymers and polymeric nanoparticles such as micro/nanospheres, micro/nanocapsules, dendrimers, liposomes, hydrogels, gold nanoparticles, micelles; others include lipoproteins and aptamers (Table 2).^{54,56}

The inhibitor-carrier approach will involve techniques similar to the previous suggested approach. The first step would be to create an inhibitor-carrier complex by binding the known ZIKV inhibitor to the carrier. The complex must then be simulated to analyze the trajectory of the complex as well as the potential energy of the entire complex through a lipid bilayer. Once there is computational evidence to show that the inhibitor can theoretically bind to the carrier and move through a lipid membrane, the inhibitor-carrier complex must be synthesized to test it biologically (*e.g.* *in vivo* testing), which will be used to confirm drug delivery through the BBB to the brain. Examples of computationally docking a compound-polymer complex are provided in the ESI.†

Technical guidance

A number of tools are available which can be utilized to screen for compounds on chemical databases based on a set of criteria. Structure-based virtual screening will allow searching through combinatorial chemistry libraries for compounds that may be potential inhibitors of a target protein and will rapidly dock them into the 3D target's active pocket.^{47,78} Screening for potential compounds can be carried out on ZINC Database⁷⁹ or ZincPharmer.⁸⁰ Several molecules may have the potential to bind to the active site of the protein; therefore, the free binding energy of every pose is calculated. Binding affinity estimations may be carried out using molecular docking approaches and free binding energy calculations. This will generate a scoring function to rank the ligands that best suit the target protein.⁴⁷ Computational software that can be used to calculate binding affinities include UCSF Chimera⁸¹ and AutoDock Vina.⁸² Protein-ligand complexes of lowest free binding energy may be used as inhibitor candidates, which may subsequently be validated *via* molecular dynamic simulations, as binding affinity predictions may not be one hundred percent accurate.^{78,83–86}

Molecular dynamic simulations calculate the potential energy of a system and analyze free binding energies and binding modes between compounds and enzymes.⁸⁷ Force



Table 2 Pre-existing drug delivery systems and their principle roles in disease and virus therapies

Drug delivery system	Description	Disease/viral target	References
Dendrimer	<ul style="list-style-type: none"> • Hyperbranched, monodispersed, water soluble (1–100 nm) macromolecule • Encapsulated drug in its interior or adsorbs drug on and conjugates to its surface groups • Releases free 5-fluorouracil upon hydrolysis • Intracellular delivery of poorly soluble drugs • Carriers in gene therapy 	<ul style="list-style-type: none"> • Inhibitors of haemagglutinin of human erythrocytes by Influenza virus • Amino groups of dendrimer react with nucleic acid phosphate groups to form transfection complexes 	56 and 57
Microsphere & nanocapsule	<ul style="list-style-type: none"> • Microsphere – drug is dispersed within polymer throughout particle • Nanocapsule-cavity contains drug surrounded by polymer membrane • Drug release through diffusion through polymer or degradation of polymer 	<ul style="list-style-type: none"> • Entraps luteinizing hormone-releasing hormone in prostate cancer 	57 and 58
Liposomes	<ul style="list-style-type: none"> • Amphiphilic vesicular structures made up of cholesterol & phospholipids • Core suited for hydrophilic drug delivery • Phospholipid membrane encapsulate hydrophobic drugs 	<ul style="list-style-type: none"> • Facultative intracellular bacteria-mediated infections • Parasites (<i>e.g.</i> Leishmania) • Viruses • Systemic fungal diseases in cancer • Melanomas 	56, 59 and 60
Micelles	<ul style="list-style-type: none"> • Core comprised of hydrophobic polymers • Shell comprised of hydrophilic polymers • Suitable for drugs with poor solubility • Nanosize; <i>in vivo</i> endurance; remains stable in plasma • Delivery of drugs & small interfering RNA 	<ul style="list-style-type: none"> • Targets tumour sites in cancer by active/passive mechanisms 	56, 61 and 62
Hydrogel	<ul style="list-style-type: none"> • Network of natural/synthetic hydrophilic polymers that are cross-linked • Highly absorbent, biodegradable, high porosity, biocompatible • Swell rapidly in aqueous solution • Used in oral & topical drug delivery 	<ul style="list-style-type: none"> • Local & systemic diseases • Oral delivery of insulin in diabetes; salmon calcitonin for postmenopausal osteoporosis; growth hormone for decelerated/stunted growth-associated diseases 	56, 63 and 64
Gold/silver nanoparticle	<ul style="list-style-type: none"> • Low toxicity; high specificity & selectivity • Easily controlled & modifiable • High ratio of surface area:amount • Conjugation of proteins on colloidal gold nanoparticles occurs <i>via</i> electrostatic interactions between citrate (–) on surfaces of gold nanoparticles & groups (+) on proteins • Effortless cellular penetration 	<ul style="list-style-type: none"> • Selective damage of tumour cells • Certain infectious & dermal diseases • H1N1, H3N2, H5N1 Influenza A virus • Herpes simplex virus • Human immunodeficiency virus • Hepatitis B virus • Metapneumovirus • Respiratory syncytial virus 	65–68
Lipid nanoparticle	<ul style="list-style-type: none"> • 10–1000 nm • Carriers with dispersed melted lipid in surfactant • Colloidal system with hydrophobic core that encloses drug & surface coated with hydrophilic polymers 	<ul style="list-style-type: none"> • Humoral immunity against Ebola infection • Silencing of hepatitis C virus replication • Gene therapy 	56 and 69–72
Aptamer	<ul style="list-style-type: none"> • Short, single-stranded (ss) DNA or RNA that have definitive 2° & 3° structures that strongly bind to specific target proteins • Low immunogenicity & toxicity • Variety of targets & modifiable chemical structure 	<ul style="list-style-type: none"> • α-Thrombin in thrombosis • PTK7 and nucleoin in cancer • IGHM in lymphoma • VEGF in age-related macular degeneration • A1 domain of vWF in thrombotic microangiopathies & carotid artery disease • Neutralizes r5 strains of HIV-1 • Blocks gp120-CCR5 interaction 	73–77

fields are used to calculate potential energies of particles and electrostatic forces that occur between atoms in a system.⁸⁸ Some force fields that can be used for molecular dynamic simulations include NAMD,⁸⁹ Gromacs,⁹⁰ Amber⁹¹ and Charm.⁹² Complexes can also be simulated through lipid bilayer, in cases where potential compounds need to enter

certain target tissues, which are surrounded by lipophilic membranes. This can give a prediction as to whether or not the potential compound will be able to pass through the lipid membrane or not. Softwares that can be used to generate a 3D lipid bilayer model include CHARRM-GUI and Visual Molecular Dynamics (MEMBPLUGIN).^{46,93} A brief background and the



Table 3 Various molecular modeling approaches in drug discovery

	Description/application	Reference
Molecular mechanics (MM) calculations	Molecular systems are modeled using MM, which employs force fields to calculate a system's potential energy. MM may be used to analyze molecular systems of various sizes and complexity, and is the preferred approach for the simulation of proteins	25, 94 and 95
Quantum mechanics (QM/MM) calculations	The hybrid QM/MM method is a molecular dynamic simulation approach that integrates the accuracy of QM and speed of MM, to allow for chemical processes within proteins and solutions to be studied. QM/MM provides enhanced mechanistic aspects and binding energies of the interaction between a ligand and receptor	66, 94 and 96
Virtual screening	Virtual screening involves screening through databases for compounds with similar features. There are two types of approaches involved in virtual screening: (1) ligand or pharmacophore-based virtual screening which requires knowledge of an active ligand, and (2) structure-based virtual screening which relies on a known 3D structure of the protein	79, 83, 84, 86 and 97
Molecular docking	Molecular docking is utilized for: (1) studying potential ligand conformations within a protein's binding site and (2) approximation of the force of ligand–protein interactions. During docking, Cartesian coordinates of a separate ligand and receptor are utilized to anticipate the conformation of the ligand that fits into the binding site of the protein the best, producing a ligand–protein complex. Molecular docking uses a scoring function, which ranks each docking “pose” according to its binding energy	47, 78, 87 and 97
Molecular dynamics	Influential tool for analyzing energetics, mechanisms and dynamics of proteins and ligand–protein complexes. Molecular dynamics provide a perspective of the interaction between a ligand and protein at a molecular level, presenting an improved understanding of the experimental conclusions. These are effective in the identification of specific biological properties, e.g., binding mode, per-residue protonation state, and protein flexibility	87–89, 92, 97 and 98

applications of the methods that have been mentioned above are shown in Table 3.

A full expansion of the methods explained in Table 3 may be found in Honarparvar *et al.*, 2014.⁹⁷

Conclusion

The various challenges associated with ZIKV treatment has led to the ongoing search for a cure – one of the major problems being drug delivery across the BBB. The approaches described in this review serve to provide information that can be used for further research into the design of drugs with improved BBB-permeability profile that may have a greater ability to inhibit ZIKV. Though experimental validation is necessary, this is not the scope of the current study. Instead, this study serves as a cornerstone that will open doors to further experimental and molecular validation regarding ZIKV therapy.

Conflicts of interest

Authors declare no potential conflicts of interest.

Acknowledgements

The authors acknowledge the College of Health Sciences, UKZN, and the National Research Foundation (NRF) of South Africa.

References

- I. Briguglio, S. Piras, P. Corona and A. Carta, *Int. J. Med. Chem.*, 2011, **2011**, 1–22.
- R. K. Singh, K. Dhama, Y. S. Malik, M. A. Ramakrishnan, K. Karthik, R. Tiwari, S. Saurabh, S. Sachan and S. K. Joshi, *Vet. Q.*, 2016, **36**, 150–175.
- D. Musso, C. Roche, E. Robin, T. Nhan, A. Teissier and V. M. Cao-Lormeau, *Emerging Infect. Dis.*, 2015, **21**, 359–361.
- D. Musso, T. Nhan, E. Robin, C. Roche, D. Bierlaire, K. Zisou, A. Shan Yan, V. M. Cao-Lormeau and J. Broult, *Eurosurveillance*, 2014, **19**, 14–16.
- M. Besnard, S. Lastère, A. Teissier, V. M. Cao-Lormeau and D. Musso, *Eurosurveillance*, 2014, **19**, 8–11.
- G. W. A. Dick, S. F. Kitchen and A. J. Haddow, *Trans. R. Soc. Trop. Med. Hyg.*, 1952, **55**, 509–520.
- M. R. Duffy, C. Tai-Ho, T. Hancock, A. M. Powers, J. L. Kool, R. S. Lanciotti, M. Pretrick, C. Dubray, L. Guillaumot, A. Griggs, M. Bel, A. J. Lambert, J. Laven, O. Kosoy, A. Panella, B. J. Biggerstaff, M. Fischer and E. B. Hayes, *N. Engl. J. Med.*, 2009, **360**, 2536–2543.
- D. Musso, E. J. Nilles and V. M. Cao-Lormeau, *Clin. Microbiol. Infect.*, 2014, **20**, O595–O596.
- V. Sikka, V. K. Chattu, R. K. Popli, T. J. Galwankar, C. Sagar, D. Kelkar, S. G. Sawicki, S. P. Stawicki and T. J. Papadimos, *J. Global Infect. Dis.*, 2016, **8**, 3–15.
- S.-I. Yun and Y.-M. Lee, *J. Microbiol.*, 2017, **55**, 204–219.
- G. S. Campos, A. C. Bandeira and S. I. Sardi, *Emerging Infect. Dis.*, 2015, **21**, 1885–1886.
- D. Musso and D. J. Gubler, *Nature*, 2016, **11**, 10–20.
- F. Krauer, M. Riesen, L. Reveiz, O. T. Oladapo, R. Martínez-Vega, T. V. Porgo, A. Haefliger, N. J. Broutet and N. Low, *PLoS Med.*, 2017, **14**, 1–27.
- P. Ramharack and M. E. S. Soliman, *RSC Adv.*, 2016, **6**, 68719–68731.



- 15 D. Musso, C. Roche, T. X. Nhan, E. Robin, A. Teissier and V. M. Cao-Lormeau, *J. Clin. Virol.*, 2015, **68**, 53–55.
- 16 J. M. Mansuy, M. Dutertre, C. Mengelle, C. Fourcade, B. Marchou, P. Delobel, J. Izopet and G. Martin-Blondel, *Lancet Infect. Dis.*, 2016, **16**, 405.
- 17 J. M. Turmel, P. Abgueguen, B. Hubert, Y. M. Vandamme, M. Maquart, H. Le Guillou-Guillemette and I. Leparcoffart, *Lancet*, 2016, **387**, 2501.
- 18 A. C. Gourinat, O. O'Connor, E. Calvez, C. Goarant and M. Dupont-Rouzeyrol, *Emerging Infect. Dis.*, 2015, **21**, 84–86.
- 19 G. Calvet, R. S. Aguiar, A. S. O. Melo, S. A. Sampaio, I. de Filippis, A. Fabri, E. S. M. Araujo, P. C. de Sequeira, M. C. L. de Mendonça, L. de Oliveira, D. A. Tschoeke, C. G. Schrago, F. L. Thompson, P. Brasil, F. B. dos Santos, R. M. R. Nogueira, A. Tanuri and A. M. B. de Filippis, *Lancet Infect. Dis.*, 2016, **16**, 653–660.
- 20 O. Faye, O. Faye, A. Dupressoir, M. Weidmann, M. Ndiaye and A. Alpha Sall, *J. Clin. Virol.*, 2008, **43**, 96–101.
- 21 R. Hamel, O. Dejarnac, S. Wichit, P. Ekcharyawat, A. Neyret, N. Luplertlop, M. Perera-Lecoin, P. Surasombattana, L. Talignani, F. Thomas, V. M. Cao-Lormeau, V. Choumet, L. Briant, P. Despres, A. Amara, H. Yssel and D. Misse, *J. Virol.*, 2015, **89**, 8880–8896.
- 22 O. Faye, C. C. M. Freire, A. Iamarino, O. Faye, J. Velasco, C. De Oliveira, M. Diallo, P. M. A. Zanotto and A. A. Sall, *PLoS Neglected Trop. Dis.*, 2014, **8**, 1–10.
- 23 H. Tian, X. Ji, X. Yang, W. Xie, K. Yang, C. Chen, C. Wu, H. Chi, Z. Mu, Z. Wang and H. Yang, *Protein Cell*, 2016, **7**, 450–454.
- 24 H. Tian, X. Ji, X. Yang, Z. Zhang, Z. Lu, K. Yang, C. Chen, Q. Zhao, H. Chi, Z. Mu, W. Xie, Z. Wang, H. Lou, H. Yang and Z. Rao, *Protein Cell*, 2016, **7**, 562–570.
- 25 B. Ganguly and E. Ganguly, *bioRxiv*, 2016, p. 54486.
- 26 M. K. White, H. S. Wollebo, J. David Beckham, K. L. Tyler and K. Khalili, *Ann. Neurol.*, 2016, **80**, 479–489.
- 27 N. J. da Fonseca Jr, *et al.*, *Biochem. Biophys. Res. Commun.*, 2017, DOI: 10.1016/j.bbrc.2017.01.041.
- 28 G. Li, M. Poulsen, C. Fenyvuesvolgyi, Y. Yashiroda, M. Yoshida and J. M. Simard, *Proc. Natl. Acad. Sci. U. S. A.*, 2016, **114**, 201619735.
- 29 P. Brasil, P. C. Sequeira, A. D. Freitas, H. E. Zogbi, G. A. Calvet, R. V. de Souza, A. M. Siqueira, M. C. de Mendonca, R. M. Nogueira, A. M. de Filippis and T. Solomon, *Lancet*, 2016, **387**, 1482.
- 30 J. J. Miner and M. S. Diamond, *Cell Stem Cell*, 2016, **18**, 559–560.
- 31 T. J. Nowakowski, A. A. Pollen, E. Di Lullo, C. Sandoval-Espinosa, M. Bershteyn and A. R. Kriegstein, *Cell Stem Cell*, 2016, **18**, 591–596.
- 32 H. Retallack, E. Di Lullo, C. Arias, K. A. Knopp, M. T. Laurie, C. Sandoval-Espinosa, W. R. M. Leon, R. Krencik, E. M. Ullian, J. Spatazza, A. A. Pollen, C. Mandel-Brehm, T. J. Nowakowski, A. R. Kriegstein, J. L. Derisi, N. Sestan and P.-Y. Shi, *Proc. Natl. Acad. Sci. U. S. A.*, 2016, **113**, 14408–14413.
- 33 P. K. Singh, J.-M. Guest, M. Kanwar, J. Boss, N. Gao, M. S. Juzych, G. W. Abrams, F.-S. Yu and A. Kumar, *JCI Insight*, 2017, **2**(4), DOI: 10.1172/jci.insight.92340.
- 34 N. R. Saunders, M. D. Habgood, K. Møllgård and K. M. Dziegielewska, *F1000Research*, 2016, **5**, 1–15.
- 35 M. R. Syme, J. W. Paxton and J. a. Keelan, *Clin. Pharmacokinet.*, 2004, **43**, 487–514.
- 36 W. A. Banks, *BMC Neurol.*, 2009, **9**, S3.
- 37 A. Seelig, R. Gottschlich and R. M. Devant, *Proc. Natl. Acad. Sci. U. S. A.*, 2016, **91**, 68–72.
- 38 J. M. Tarbell and M. Y. Pahakis, *J. Intern. Med.*, 2006, **259**, 339–350.
- 39 N. J. Barrows, R. K. Campos, S. T. Powell, K. R. Prasanth, G. Schott-Lerner, R. Soto-Acosta, G. Galarza-Muñoz, E. L. McGrath, R. Urrabaz-Garza, J. Gao, P. Wu, R. Menon, G. Saade, I. Fernandez-Salas, S. L. Rossi, N. Vasilakis, A. Routh, S. S. Bradrick and M. A. Garcia-Blanco, *Cell Host Microbe*, 2016, **20**, 259–270.
- 40 A. Daina, O. Michielin and V. Zoete, *Sci. Rep.*, 2017, **7**, 1–13.
- 41 A. Daina, O. Michielin and V. Zoete, *J. Chem. Inf. Model.*, 2014, **54**, 3284–3301.
- 42 Y. N. Gavhane and A. V. Yadav, *Saudi Pharm. J.*, 2012, **20**, 331–344.
- 43 P. Atkins and J. De Paula, *Physical chemistry for the life sciences*, 2011.
- 44 P. P. Kore, M. M. Mutha, R. V. Antre, R. J. Oswal and S. S. Kshirsagar, *J. Med. Chem.*, 2012, **2**, 139–148.
- 45 J. A. Arnott and S. L. Planey, *Expert Opin. Drug Discovery*, 2012, **7**, 863–875.
- 46 R. Guixà-González, I. Rodríguez-Espigares, J. M. Ramírez-Angueta, P. Carrió-Gaspar, H. Martínez-Seara, T. Giorgino and J. Selent, *Bioinformatics*, 2014, **30**, 1478–1480.
- 47 X.-Y. Meng, H.-X. Zhang, M. Mezei and M. Cui, *Curr. Comput.-Aided Drug Des.*, 2011, **7**, 146–157.
- 48 E. C. Hulme and M. A. Trevethick, *Br. J. Pharmacol.*, 2010, **161**, 1219–1237.
- 49 T. H. Scheuermann, S. B. Padrick, K. H. Gardner and C. A. Brautigam, *Anal. Biochem.*, 2016, **496**, 79–93.
- 50 Y. Q. Deng, N. N. Zhang, C. F. Li, M. Tian, J. N. Hao, X. P. Xie, P. Y. Shi and C. F. Qin, *Open Forum Infect. Dis.*, 2016, **3**, 6–9.
- 51 S. E. Reznik and C. R. Ashby, *Int. J. Infect. Dis.*, 2017, **55**, 29–30.
- 52 C. Roney, P. Kulkarni, V. Arora, P. Antich, F. Bonte, A. Wu, N. N. Mallikarjuana, S. Manohar, H.-F. Liang, A. R. Kulkarni, H.-W. Sung, M. Sairam and T. M. Aminabhavi, *J. Controlled Release*, 2005, **108**, 193–214.
- 53 C. Spuch and C. Navarro, *J. Drug Delivery*, 2011, **2011**, 1–12.
- 54 M. S. Gunay, A. Y. Ozer and S. Chalon, *Curr. Neuropharmacol.*, 2016, **14**, 376–391.
- 55 E. Blanco, H. Shen and M. Ferrari, *Nat. Biotechnol.*, 2015, **33**, 941–951.
- 56 A. Srivastava, T. Yadav, S. Sharma, A. Nayak, A. Kumari and N. Mishra, *J. Biosci. Med.*, 2016, **4**, 69–84.
- 57 W. B. Liechty, D. R. Kryscio, B. V. Slaughter and N. A. Peppas, *Annu. Rev. Chem. Biomol. Eng.*, 2010, **1**, 149–173.
- 58 Z. Abouelfadel and D. Crawford, *Ther. Clin. Risk Manage.*, 2008, **4**, 513–526.
- 59 A. Coune, *Infection*, 1988, **16**, 141–147.
- 60 M. A. Tran, R. J. Watts and G. P. Robertson, *Pigm. Cell Melanoma Res.*, 2009, **22**, 388–399.



- 61 U. Kedar, P. Phutane, S. Shidhaye and V. Kadam, *Nanomedicine*, 2010, **6**, 714–729.
- 62 X.-B. Xiong, H. Uludağ and A. Lavasanifar, *Biomaterials*, 2010, **31**, 5886–5893.
- 63 D. Bhowmik, H. Gopinath, B. Pragati Kumar, S. Duraivel and K. P. Sampath Kumar, *Pharma Innovation*, 2012, **1**, 12–31.
- 64 L. A. Sharpe, A. M. Daily, S. D. Horava and N. A. Peppas, *Expert Opin. Drug Delivery*, 2014, **11**, 901–915.
- 65 X. Yu, I. Trase, M. Ren, K. Duval, X. Guo and Z. Chen, *J. Nanomater.*, 2016, DOI: 10.1155/2016/1087250.Design.
- 66 H. Daraee, A. Eatemadi, E. Abbasi, S. Fekri Aval, M. Kouhi and A. Akbarzadeh, *Artif. Cells, Nanomed., Biotechnol.*, 2014, **1401**, 1–13.
- 67 W. Tao, B. L. Hurst, A. K. Shakya, M. J. Uddin, R. S. J. Ingrole, M. Hernandez-Sanabria, R. P. Arya, L. Bimler, S. Paust, E. B. Tarbet and H. S. Gill, *Antiviral Res.*, 2017, **141**, 62–72.
- 68 M. Rai, S. D. Deshmukh, A. P. Ingle, I. R. Gupta, M. Galdiero and S. Galdiero, *Crit. Rev. Microbiol.*, 2014, **42**, 46–56.
- 69 S. Mukherjee, S. Ray and R. S. Thakur, *Indian J. Pharm. Sci.*, 2009, **71**, 349–358.
- 70 J. D. Bazzill, C. L. Cooper, Y. Fan, S. Bavari and J. J. Moon, *J. Immunol.*, 2016, **196**(1 Suppl.), 76.
- 71 J. Torrecilla, A. del Pozo-Rodríguez, M. ñngeles Solinís, P. S. Apaolaza, B. Berzal-Herranz, C. Romero-López, A. Berzal-Herranz and A. Rodríguez-Gascón, *Colloids Surf., B*, 2016, **146**, 808–817.
- 72 A. del Pozo-Rodríguez, M. Á. Solinís and A. Rodríguez-Gascón, *Eur. J. Pharm. Biopharm.*, 2016, **109**, 184–193.
- 73 A. K. Dey, M. Khati, M. Tang, R. Wyatt, S. M. Lea and W. James, *J. Virol.*, 2005, **79**, 13806–13810.
- 74 F. Jiang, B. Liu, J. Lu, F. Li, D. Li, C. Liang, L. Dang, J. Liu, B. He, S. A. Badshah, C. Lu, X. He, B. Guo, X. B. Zhang, W. Tan, A. Lu and G. Zhang, *Int. J. Mol. Sci.*, 2015, **16**, 23784–23822.
- 75 S. D. Jayasena, *Clin. Chem.*, 1999, **45**, 1628–1650.
- 76 P. Ray and R. R. White, *Pharmaceuticals*, 2010, **3**, 1761–1778.
- 77 M. Blind and M. Blank, *Mol. Ther.–Nucleic Acids*, 2015, **4**, e223.
- 78 E. Lionta, G. Spyrou, D. K. Vassilatis and Z. Cournia, *Curr. Top. Med. Chem.*, 2014, **14**, 1923–1938.
- 79 J. J. Irwin and B. K. Shoichet, *J. Chem. Inf. Model.*, 2005, **45**, 177–182.
- 80 D. R. Koes and C. J. Camacho, *Nucleic Acids Res.*, 2012, **40**, 409–414.
- 81 E. F. Pettersen, T. D. Goddard, C. C. Huang, G. S. Couch, D. M. Greenblatt, E. C. Meng and T. E. Ferrin, *J. Comput. Chem.*, 2004, **25**, 1605–1612.
- 82 O. Trott and A. J. Olson, *J. Comput. Chem.*, 2010, **31**, 445–461.
- 83 N. Mhlongo and M. E. Soliman, *Lett. Drug Des. Discovery*, 2016, **13**, 1033–1046.
- 84 F. N. Cele, R. Muthusamy and M. E. Soliman, *Drug Des., Dev. Ther.*, 2016, **10**, 1365–1377.
- 85 A. Skelton, Y. Maharaj and M. E. Soliman, *Cell. Mol. Bioeng.*, 2014, **7**, 45–57.
- 86 E. O. Pyzer-Knapp, C. Suh, R. Gómez-Bombarelli, J. Aguilera-Iparraguirre and A. Aspuru-Guzik, *Annu. Rev. Mater. Res.*, 2015, **45**, 195–216.
- 87 H. Alonso, A. A. Bliznyuk and J. E. Gready, *Med. Res. Rev.*, 2006, **26**, 531–568.
- 88 M. A. González, *Collection SFN*, 2011, **12**, 169–200.
- 89 M. Nelson, W. Humphrey, A. Gursoy, A. Dalke, L. Kal, R. D. Skeel and K. Schulten, *Int. J. High Perform. Comput. Appl.*, 1996, **251–268**, 251–268.
- 90 B. Hess, C. Kutzner, D. Van Der Spoel and E. Lindahl, *J. Chem. Theory Comput.*, 2008, **4**, 435–447.
- 91 D. A. Case, T. E. Cheatham, T. Darden, H. Gohlke, R. Luo, K. M. Merz, A. Onufriev, C. Simmerling, B. Wang and R. J. Woods, *J. Comput. Chem.*, 2005, **26**, 1668–1688.
- 92 B. R. Brooks, R. E. Bruccoleri, B. D. Olafson, D. J. States, S. Swaminathan and M. Karplus, *J. Comput. Chem.*, 1983, **4**, 187–217.
- 93 Y. Qi, X. Cheng, J. Lee, J. V. Vermaas, T. V. Pogorelov, E. Tajkhorshid, S. Park, J. B. Klauda and W. Im, *Biophys. J.*, 2015, **109**, 2012–2022.
- 94 A. W. Duster, C.-H. Wang, C. M. Garza, D. E. Miller and H. Lin, *WIREs Computational Molecular Science*, 2017, DOI: 10.1002/wcms.1310.
- 95 K. Vanommeslaeghe, O. Guvench and A. D. Mackerell, *Curr. Pharm. Des.*, 2014, **20**, 3281–3292.
- 96 S. B. Vepuri, H. C. Devarajgowda and M. E. Soliman, *J. Mol. Struct.*, 2016, **1105**, 194–204.
- 97 B. Honarparvar, T. Govender, G. E. M. Maguire, M. E. S. Soliman and H. G. Kruger, *Chem. Rev.*, 2013, **114**(1), 493–537.
- 98 A. Ganesan, M. L. Coote and K. Barakat, *Drug Discovery Today*, 2017, **22**, 249–269.



A panoptic uncovering of the dynamical evolution of the Zika Virus NS5 methyltransferase binding site loops—zeroing in on the molecular landscape

Nikita Devnarain | Mahmoud E. S. Soliman 

Molecular Bio-computation and Drug Design Laboratory, School of Health Sciences, University of KwaZulu-Natal, Durban, South Africa

Correspondence

Mahmoud E. S. Soliman, Molecular Bio-computation and Drug Design Laboratory, School of Health Sciences, University of KwaZulu-Natal, Westville, Durban 4001, South Africa.
Email: soliman@ukzn.ac.za

Funding information

DAAD-NRF JOINT IN-COUNTRY DOCTORAL SCHOLARSHIP PROGRAMME, Grant/Award Number: DAAD170602236415

The global threat of the Zika virus to humanity is real. Innovative and potent anti-Zika virus drugs are still at large, due to the lack of anti-Zika virus drugs that have passed phase 1 trials. Experimental research has revealed novel inhibitors of Zika virus NS5 methyltransferase enzyme. This study has taken a step further to provide insight into the molecular dynamics of Zika virus and inhibitor binding, which have not been established experimentally. Movements of the methyltransferase binding site loops have a large role to play in the methylation of the viral mRNA cap, which is essential for Zika virus replication. Here, we pinpoint the binding interactions between each potential inhibitor and the methyltransferase, residues that are responsible for binding, as well as which inhibitor-bound complex renders the methyltransferase more stable. We also highlight the conformational changes that occur within the methyltransferase to accommodate binding of inhibitors and consequences of those changes upon the RNA- and cap-binding sites in the methyltransferase. This research will improve the understanding of the Zika virus NS5 methyltransferase enzyme, and will be beneficial in driving the development of anti-Zika virus drugs.

KEYWORDS

methyltransferase, molecular dynamics, NS5, Zika virus inhibitors

1 | INTRODUCTION

In the beginning of 2016, the World Health Organization declared the escalating Zika virus (ZIKV) a public health crisis due to its association with neonatal microcephaly and Guillain-Barré syndrome.^[1] ZIKV, the rapidly disseminating pathogen, which belongs to the *flavivirus* genus of the *Flaviviridae* family, is related to other *flaviviruses*, including West Nile virus (WNV), Yellow fever virus (YFV), Japanese encephalitis virus (JEV), and Dengue virus (DENV).^[2] ZIKV has revealed a tropism for a broad range of tissues including sensory organs and organs of the gastrointestinal tract, respiratory system, and reproductive system.^[3–6]

The preeminent mode of transmission of ZIKV is through the bite of a previously infected *Aedes aegypti* mosquito,

which acts as a viral vector. ZIKV may also be distributed via sexual intercourse, blood transfusion, maternal transmission, and physical contact.^[7] Control measures have been put in place to curb the spread of the virus, however, ultimate success is yet to be attained.^[8] Vaccine development is still several years away since vaccine candidates are still in preclinical trials.^[9] Additionally, due to the erratic and spontaneous temperament of *flavivirus* outbreaks, vaccine development against *flaviviruses* is restricted.^[10]

As a result of the extensive period involved in establishing a ZIKV vaccine, there are current endeavors toward developing antiviral therapeutics.^[11] To date, *flavivirus* infections prevail with no approved antiviral treatment. Present-day treatment of ZIKV is based on the symptoms of infection.^[12] There is also the question of whether or not novel inhibitors

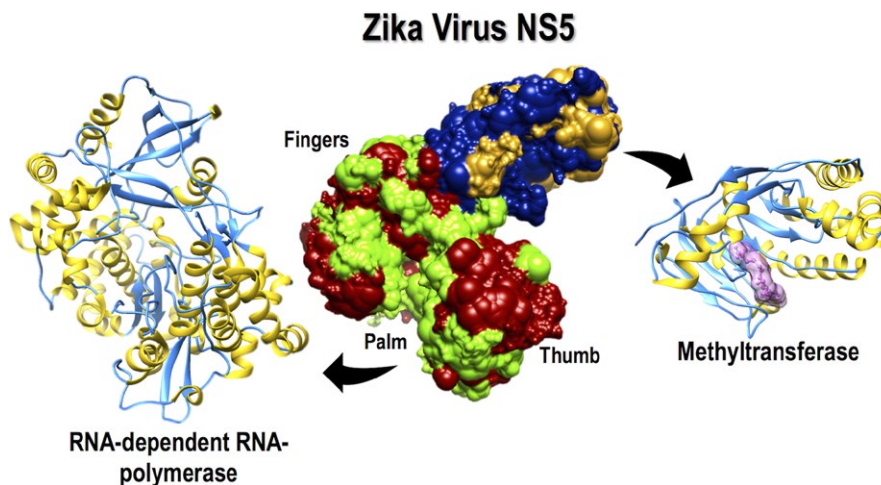


FIGURE 1 A schematic representation of the Zika virus NS5 enzyme. The structural protein of zika virus NS5 is divided into its two major subunits, the methyltransferase (bound to its natural substrate) and the RNA-dependent RNA-polymerase [Colour figure can be viewed at wileyonlinelibrary.com]

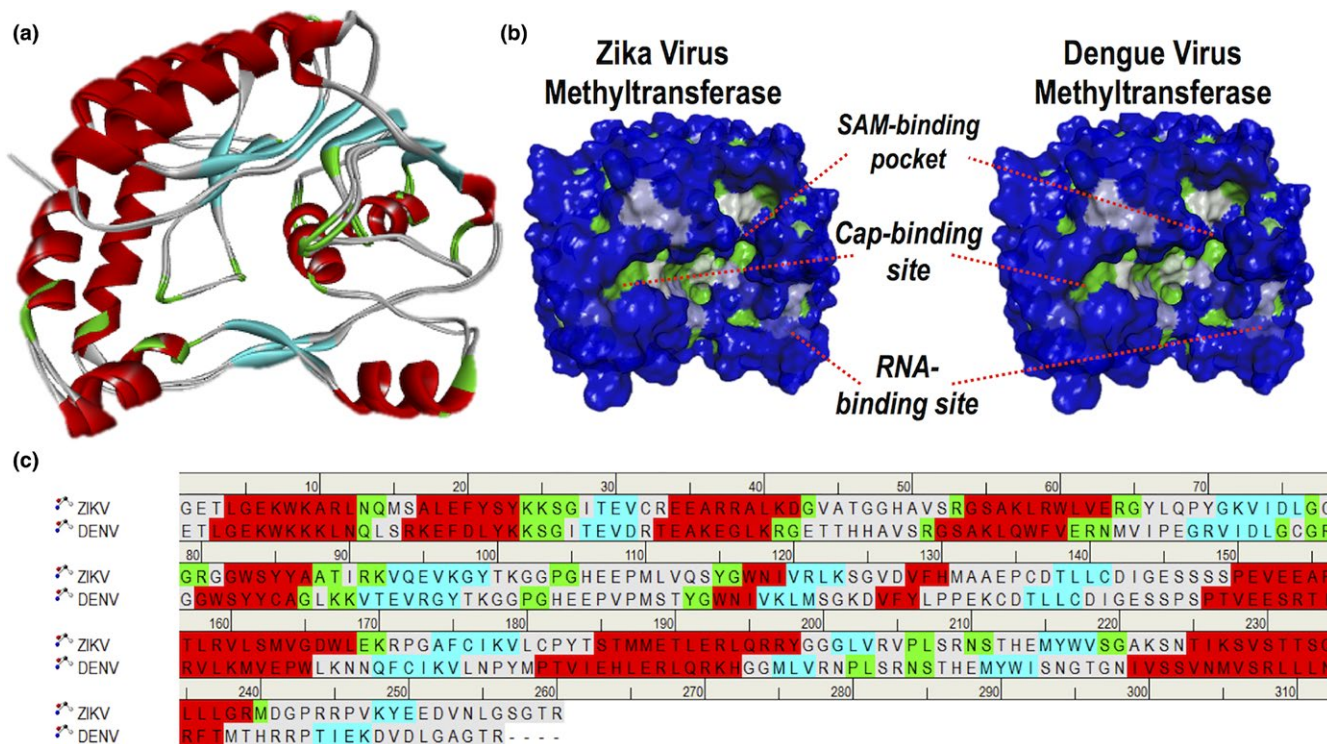


FIGURE 2 (a) Superimposed crystal structures of DENV and ZIKV NS5 MTases showing similarities and differences in coils, β -sheets and α -helices. (b) Structures of ZIKV and DENV MTases illustrating similar binding pockets and solvent accessible surface areas. (c) Sequence similarities and differences between ZIKV and DENV [Colour figure can be viewed at wileyonlinelibrary.com]

will pass the blood-brain barrier.^[13] Generally, research is turned toward drugs that inhibit enzymes involved in critical steps in the life cycle of the virus.^[14–16] There has been a compelling amount of research in the last 10 years, which had been directed toward the establishment of inhibitors of targeted enzymes of other *flaviviruses* including DENV, WNV, and YFV.^[17,18]

There may be no elixir for treating ZIKV, but recognizing the targets that provide optimal therapy will aid science in establishing the most effective therapeutics. The *flavivirus* NS5 methyltransferase (MTase) enzyme is an attractive target for the development of inhibitors due to its fundamental roles in viral replication via formation of the viral mRNA cap as well as modulation of immune response.^[16] We illustrate in

Figure 1, the ZIKV NS5 MTase responsible for methylation of the viral mRNA cap, as well as the RNA-dependent RNA-polymerase (RdRp) responsible for viral RNA replication.^[17] Together, these subunits work in harmony to ensure viral replication.^[19]

By virtue of the resemblance between *flaviviruses*, particularly between DENV and ZIKV, as we have presented in Figure 2, a great deal of the information regarding the drug discovery of DENV may possibly be enforced toward the establishment of ZIKV inhibitors.^[7,20] Inhibitors that have been shown to suppress the MTase of DENV have also been potent in the inhibition of ZIKV MTase.^[14,21,22]

A profoundly essential molecule for both DENV and ZIKV replication, particularly regarding the MTase component, includes S-adenosyl-L-methionine (SAM).^[21] Being the natural substrate of the MTase, SAM serves as a methyl donor and allows for methylation of the mRNA cap, which is imperative for viral replication.^[23] We demonstrate in Figure 3, that an absence of SAM-binding, as a result of displacement by an alternative compound, causes avoidance of viral replication since methylation of RNA does not occur.

The adenosine derivative, sinefungin (SFG), was initially isolated as an antifungal antibiotic from *Streptomyces griseolus*, and accomplishes its inhibition by competitively binding to the SAM-binding pocket in the MTase.^[24] Previously, SFG demonstrated inhibitory effects on MTases of DENV,

WNV, and YFV,^[17] and thus presented as a potential inhibitor of ZIKV.^[25] Experimental evidence shows that even low concentrations of SFG inhibit ZIKV MTase and terminates internal methylation *in vitro*.^[21] Coutard et al. in 2017 also demonstrated ZIKV suppression by another DENV inhibitor, Compound 5, which inhibits ZIKV MTase activity and is more potent against ZIKV MTase compared to MTases of DENV and WNV.^[14,21,22] In Figure 4, we illustrate the structures of SFG and Compound 5.

Based on preliminary viral inhibition and structural novelty, we considered further exploring the structural dynamics that take place at a molecular level within the independent ZIKV MTase (Apo), as well as ZIKV MTase bound to SFG and Compound 5, distinctly. We also compare the binding affinity, binding mode and stability of the bound complex of SFG to that of Compound 5. Two major loops in the MTase were focused on more than the rest, as one of the loops surrounds the SAM-binding pocket and the other surround the RNA-binding site. To our knowledge, this is the first study that utilizes integrated computational methods to analyze how binding of inhibitors, SFG and Compound 5, impact the conformational changes that occur within the ZIKV NS5 MTase. Furthermore, we speculate that this study will improve the understanding of the structural information of the inhibitors and the ZIKV NS5 MTase, and will be valuable in anti-ZIKV drug design.

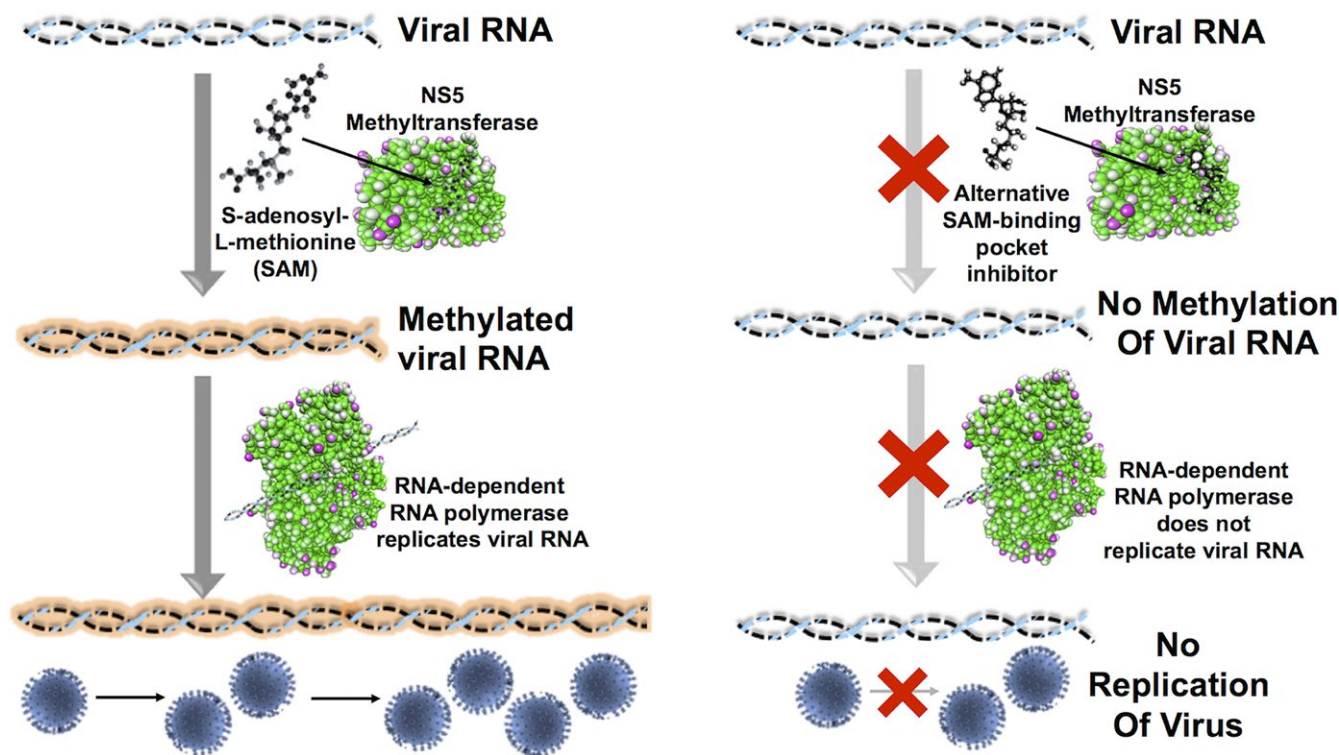
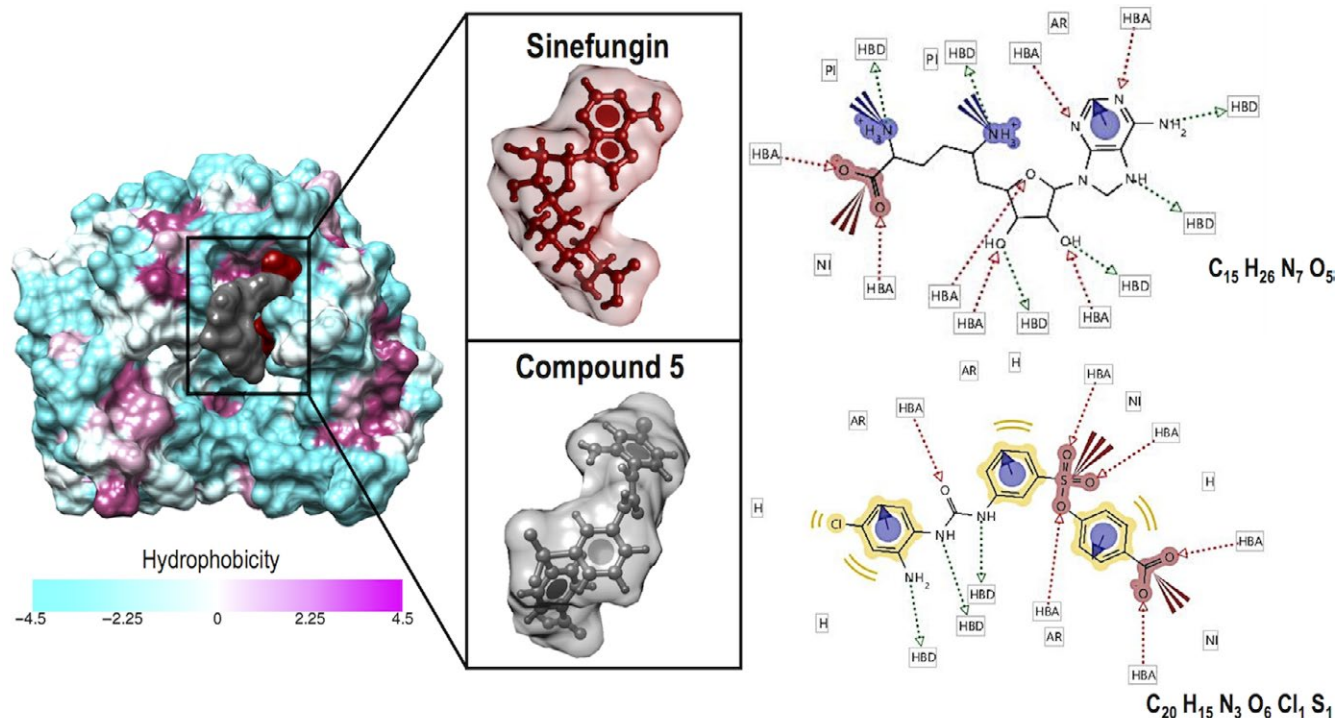


FIGURE 3 Implications of lack of SAM binding to MTase. Illustration of SAM-binding to the MTase as a prerequisite for viral RNA methylation and viral replication (left), and the consequence of an alternative molecule binding in the SAM-binding pocket and inhibiting viral RNA methylation and replication (right) [Colour figure can be viewed at wileyonlinelibrary.com]



HBD: Hydrogen Bond Donor; HBA: Hydrogen Bond Acceptor; AR: Aromatic ring; Ni: Negative Ionizable; Pi: Positive Ionizable

FIGURE 4 Potential ZIKV inhibitors. Chemical structure of SFG and Compound **5** (left), as well as the chemical formula and functional groups of SFG (top right) and Compound **5** (bottom right) [Colour figure can be viewed at wileyonlinelibrary.com]

2 | COMPUTATIONAL METHODS

2.1 | System preparation

The crystal structure of the NS5 MTase of ZIKV in complex with SFG was accessed from RCSB Protein Data Bank (PDB code: 5MRK).^[25] The protein (MTase) and ligands (SFG and Compound **5**) were prepared using Molegro Molecular Viewer software (Molegro-a CLC bio company, Aarhus, Denmark) and UCSF Chimera software package.^[12] The crystal structure of the MTase protein consists of chains A and B, however, in order to save computational time and expense, the distinct ligands conjugated to the singular chain A was utilized. Compound **5** was modeled using Avodagro.^[26] Three systems including the Apo MTase, SFG-bound MTase and Compound **5**-bound MTase were subjected to a 200 ns molecular dynamic simulation (described in Section 2.3).

2.2 | Molecular docking

Molecular docking was used to predict optimized conformations and binding affinities of SFG and Compound **5** within the SAM-binding pocket of ZIKV NS5 MTase.^[27] Docking software that was used in this study includes UCSF Chimera^[12,27] and AutoDock Vina.^[28] SFG and Compound **5** were docked into the SAM-binding pocket of the NS5 MTase (grid box spacing of 0.375 Å and x , y , z dimensions

of $28 \times 32 \times 34$). The complex with the most negative binding energy (kcal/mol) was subjected to molecular dynamic simulations. A greater expansion of molecular docking can be found in the referenced articles.^[29–31]

2.3 | Molecular dynamic simulation

Molecular dynamic simulations were implemented using AMBER PMEMD dynamics engine with GPU acceleration and the protein was parameterized with the AMBER force field, FF14SB.^[32–35] Hydrogen atoms were removed from the MTase protein, while SFG and Compound **5** were hydrogenated and charged with Gasteiger charges preceding the simulation. Antechamber created atomic partial charges for SFG and Compound **5** using the general AMBER force field (GAFF) and restrained electrostatic potential (RESP) methods.^[36–38] The LEAP module implemented in AMBER 14 was used to combine, neutralize, and solvate the systems by adding hydrogen atoms, chloride and sodium ions and suspending them in an orthorhombic box of TIP3P water molecules such that all atoms were within 10 Å of the box edges. The amino acid residues of the protein were renumbered due to missing residues in the initial crystal structure; therefore, all residue numbers reported from these findings are in fact four residues less than stated. An initial energy minimization of 2,500 steps was performed with a restraint potential of $10 \text{ kcal mol}^{-1} \text{ \AA}^{-2}$ applied to the solutes, for 1,000 steps

of steepest descent followed by 1,000 steps of conjugate gradient minimization. An additional unrestrained full minimization of 200 steps was performed by conjugate gradient algorithm.

A canonical ensemble (NVT) simulation was carried out for 50 ps from 0 to 300 K, so that a fixed volume and number of atoms in each system was maintained. The systems' solutes were enforced with Langevin thermostat collision frequency of 1.0 ps^{-1} and a potential harmonic restraint of $10 \text{ kcal mol}^{-1} \text{ \AA}^{-2}$. Thereafter, each system was equilibrated for 500 ps with a constant operating temperature of 300 K, as well as a constant pressure of 1 bar using the Berendsen barostat and number of atoms resembling an isobaric-isothermal ensemble. The overall simulation was conducted for 200 ns, where each simulation incorporated the shake algorithm to restrain hydrogen bonds. An SPFP precision model was utilized.

2.4 | Postdynamic analysis

2.4.1 | Computation of thermodynamic binding free energy and per-residue decomposition analysis

A well-known method utilized to determine the binding free energy (ΔG_{bind}) of small ligands to biological macromolecules includes molecular mechanics incorporated with the Poisson-Boltzmann or generalized Born and surface area continuum solvation (MM/PBSA and MM/GBSA) approach.^[39] These methods are generally established on molecular dynamics simulations of the protein-ligand complex and are thus transitional in precision between empirical scoring and strict enzymatic perturbation methods.^[40]

ΔG_{bind} was averaged over 50,000 snapshots derived from the 200 ns trajectory. The binding strength estimated using this method for the MTase, SFG- and Compound **5**-complexes could be represented as:

$$\Delta G_{\text{bind}} = G_{\text{complex}} - G_{\text{receptor}} - G_{\text{ligand}} \quad (1)$$

$$\Delta G_{\text{bind}} = E_{\text{gas}} + G_{\text{sol}} - TS \quad (2)$$

$$E_{\text{gas}} = E_{\text{int}} + E_{\text{vdW}} + E_{\text{ele}} \quad (3)$$

$$G_{\text{sol}} = G_{\text{GB}} + G_{\text{SA}} \quad (4)$$

$$G_{\text{SA}} = \gamma \text{SASA} \quad (5)$$

where E_{ele} , Electrostatic potential energy from Coulomb forces; E_{gas} , Gas-phase energy (based on FF14SB force field terms); E_{int} , Internal energy; E_{vdW} , van der Waals energy; G_{sol} , Solvation free energy; G_{GB} , Polar solvation energy; G_{SA} , non-polar solvation energy; S, Total entropy of solute; SASA, Solvent accessible surface area (water probe radius of 1.4 \AA). T, Total entropy of temperature.

To determine the per-residue contribution of SFG and Compound **5** to the total ΔG_{bind} at the SAM-binding site, atomic level per-residue free energy decomposition was implemented for significant residues of each ligand using the AMBER14 MM/GBSA approach. The SFG- and Compound **5**-bound complexes were subjected to further analysis.

2.4.2 | Dynamic cross-correlation

Dynamic Cross-Correlation (DCC) is a well-known approach that may be utilized in the interpretation of molecular dynamic simulation-derived trajectories, by quantifying the correlation coefficients of motions between atoms.^[41] The analysis of fluctuations between residues within the Apo MTase, SFG-bound MTase and Compound **5**-bound MTase were calculated using the CPPTRAJ module in the AMBER 14 suite. The equation that defines DCC is provided below:

$$C_{ij} = \frac{\langle \Delta r_i \Delta r_j \rangle}{\left(\langle \Delta r_i^2 \rangle \langle \Delta r_j^2 \rangle \right)^{1/2}}$$

where C_{ij} , Cross-correlation coefficient (-1 [fully correlated] to $+1$ [anti-correlated]); i , i th residue; j , j th residue; Δr_i , displacement vectors correspond to i th; Δr_j , displacement vectors correspond to j th.

The DCC matrix produced from each simulated system was constructed using Origin software.

2.5 | Pharmacophore model generation and structure-based screening

The creation and analysis of a pharmacophore model is established as a vital part of drug design, as it is a beneficial tool for detection and development of new chemical entities (NCEs).^[42] LigandScout^[43] tool was used to generate a pharmacophore model from the simulation of SFG.

3 | RESULTS AND DISCUSSION

3.1 | Molecular dynamic simulations and systems stability

Trajectories of the Apo MTase system, as well as the SFG- and Compound **5**-bound MTase systems were monitored during a 200-ns simulation to confirm the systems' stability, together with the precision of ensuing postdynamic analyses.

3.1.1 | Deviation of α -carbons within NS5 MTase

The stability of the 200-ns molecular dynamic simulations of the Apo MTase versus SFG-bound MTase versus Compound **5**-bound MTase systems were explored by calculating the

RMSD. In Figure 5, we demonstrate that during the simulation, the two inhibitor-bound complexes showed various RMSD patterns.

The Compound 5-bound complex had reached convergence after 20 ns; however, the system began to fluctuate after 143 ns, although remaining within a 2.0 Å range until the end of the simulation. The SFG-MTase complex reached convergence after 169 ns, with fluctuations less than 1.5 Å. Indeed, both bound systems demonstrate stability; however,

binding of SFG to the NS5 MTase renders the enzyme more stable than that of Compound 5, as convergence was maintained upon SFG-binding.

It was also noticed that binding of SFG to the MTase not only causes the SAM-binding site to become closed by the surround binding site loop (residues 100–110), but the MTase also conforms to close the RNA-binding site as the surrounding loop (residues 30–60) moves to prevent RNA from binding. Should RNA not bind to the MTase, replication off viral

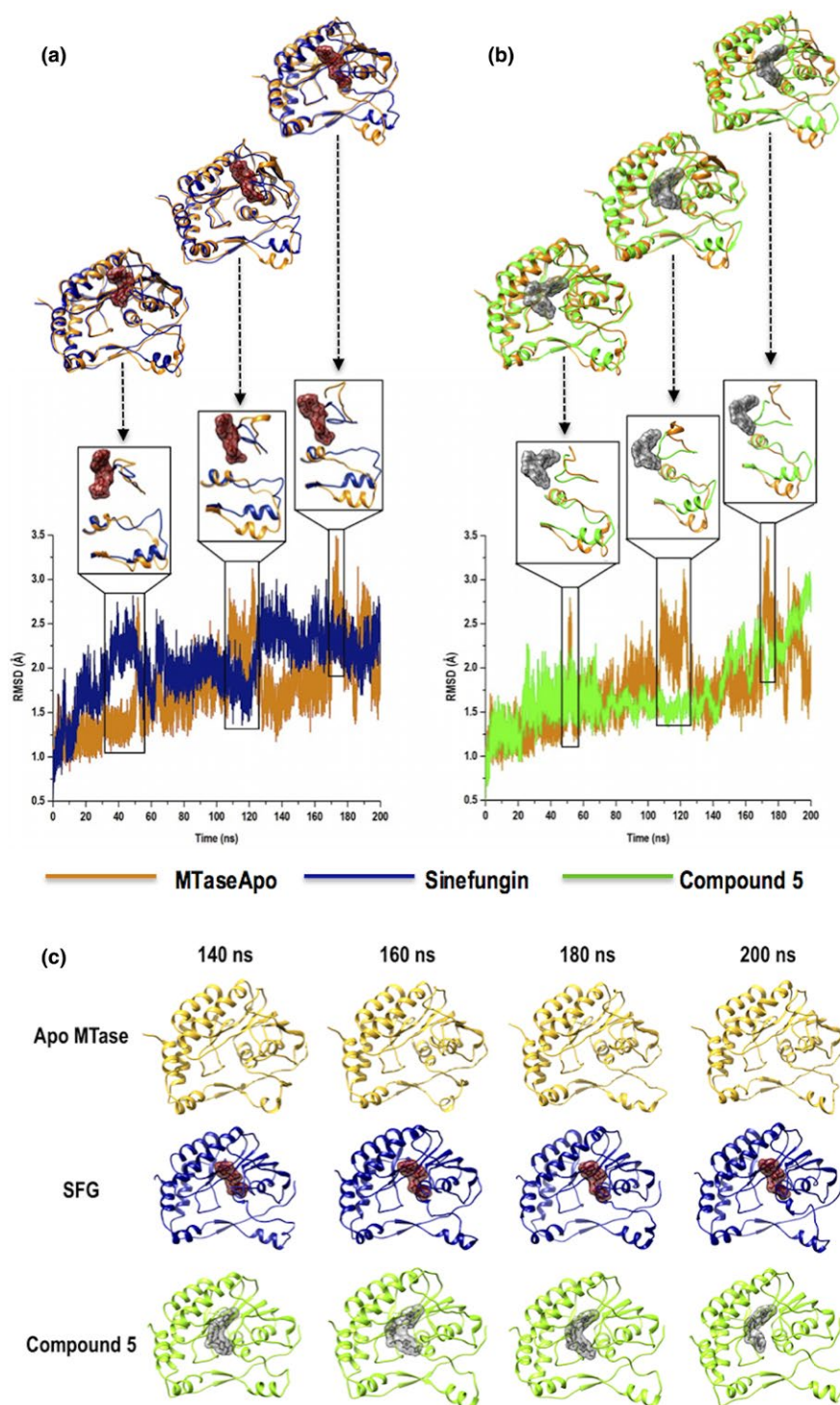


FIGURE 5 Fluctuations in rigidity of SFG-bound and Compound 5-bound complexes compared to apo are shown in (a) and (b), respectively, with emphasis on loop movements during the 52, 122, and 173 ns periods of the simulation. (c) SFG reached convergence and was less flexible toward the latter period of the simulation, as compared to that of the apo and Compound 5-bound systems [Colour figure can be viewed at wileyonlinelibrary.com]

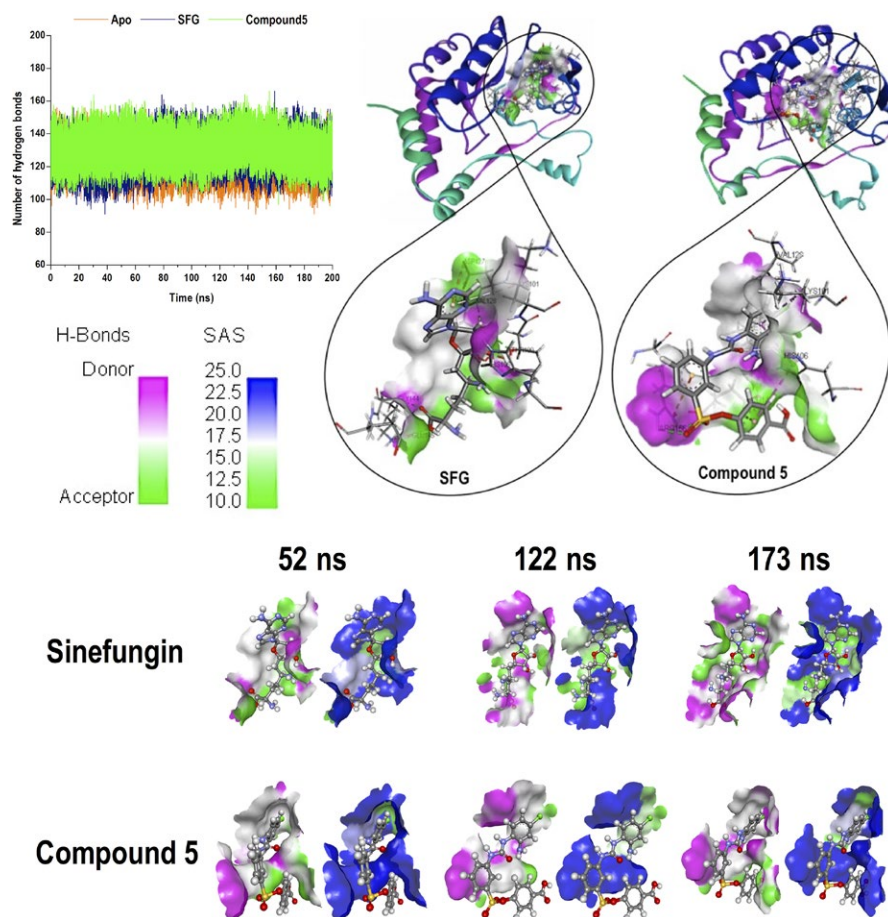


FIGURE 6 (Top left) Graph depicts hydrogen-bonding analysis of the apo and bound systems. (Top right) Bond and non-bond interactions that exist between each inhibitor and their binding site residues, as well as the interacting areas of the ligand which are hydrogen donors and acceptors. (Bottom) Surface areas of each inhibitor in the MTase pocket describing the hydrogen bonding capacity of each ligand during parts of the simulation that correspond to fluctuations in energy, along with the solvent accessible surface areas of the MTase at those points which correspond to ligand movement in the SAM-binding pocket [Colour figure can be viewed at wileyonlinelibrary.com]

RNA by the RdRp will most likely not occur, preventing viral replication from occurring.

The fluctuation in rigidity in the Apo MTase (greater than 2 Å) prevented the system from reaching convergence, even toward the latter period of the simulation, indicating instability of the Apo MTase. These major rigorous fluctuations, as well as the fact that the bound systems had reached convergence while the unbound system had not, suggest that the MTase only stabilized upon binding of inhibitors, SFG and Compound 5.

3.1.2 | Atomic distribution of NS5 MTase backbone

The radius of gyration (RoG) is an indicator of a structure's stability during a molecular dynamic simulation, as is associated with the compactness of secondary protein structures into 3D structures.^[44] To assess the conformations of the Apo MTase, SFG- and Compound 5-bound MTase complexes, RoG was analyzed and plotted (Supporting Information Figure S1).

It was noticed that in the RMSD plot (Figure 6), at 52, 122 and 173 ns the Apo MTase fluctuated significantly, while binding of both inhibitors, SFG and Compound 5, had stabilized the enzyme at those points in the simulation.

Correspondingly, the RoG plots showed similar trends at 52, 122 and 173 ns, as both inhibitors caused the MTase to become more compact to accommodate binding. The Apo MTase had a greater atomic distribution than the inhibitor-bound complexes and is therefore, more flexible and less compact than when bound.

3.2 | Intra- and intermolecular interactions in ZIKV NS5 MTase

3.2.1 | Intermolecular hydrogen bond patterns

Hydrogen bonding between amino acid residues is subject to the spatial arrangement of the associated atoms, and is a major driving force in structural changes that occur within proteins. To further analyze the forces that drive the conformational changes within the enzyme, we evaluated the hydrogen bonding pattern of the apo, SFG-bound and Compound 5-bound MTase systems throughout the simulation.

We present in Figure 6 very similar hydrogen bonding patterns between the SFG-bound and Compound 5-bound MTase complexes. The SFG-bound MTase exhibited a slightly lesser number of hydrogen bonds than the Compound 5-bound

MTase, during 25–75 and 130–155 ns, which correspond with the flexibility of the protein during that period of the simulation. Nonetheless, toward the latter period of the simulation, i.e. between 170 and 200 ns, the number of hydrogen bonds was approximately consistent in both inhibitor-bound MTase complexes. Although, the apo MTase displayed a reduced number of hydrogen bonds than both inhibitor-bound complexes, indicating that the apo system was less stable than bound systems.

3.2.2 | Residual variations within the NS5 MTase

To determine the flexibility of amino acid residues in the Apo and bound systems, root of mean square fluctuation (RMSF) of the residue α -carbons were calculated. In Figures 7 and 8, we illustrate that the MTase is more flexible when unbound, as compared to SFG- and Compound 5-bound enzymes,

respectively. Binding of SFG and Compound 5 lower the systems' energy fluctuations making them more stable.

Most binding site residues displayed resemblance in energy patterns in both inhibitor-bound and unbound conformations (binding site residues of SFG: Ser52, Gly54, Ser55, Asp75, Gly77, Cys78, Gly79, Gly82, Trp83, Tyr99, Thr100, Lys101, Gly102, His106, Glu107, Val126, Asp127, Val128, Phe129, Asp142, Ile143, and Lys178; binding site residues of Compound 5: Lys57, Gly77, Cys78, Gly79, Arg80, Gly81, Gly82, Thr100, Lys101, His106, Glu107, Asp127, Val128, Phe129, Asp142, Ile143, Gly144, Glu145, Ser146, Arg159, and Lys178), while others fluctuated significantly. Those binding site residues that altered in motion greatly throughout the simulation include 106 and 107 upon SFG binding, as well as 100, 101, 102, 127, 128, and 129 upon Compound 5 binding. An intriguing observation is that although the residues that form a loop at the binding site (residues 100–107) altered in conformation majorly throughout

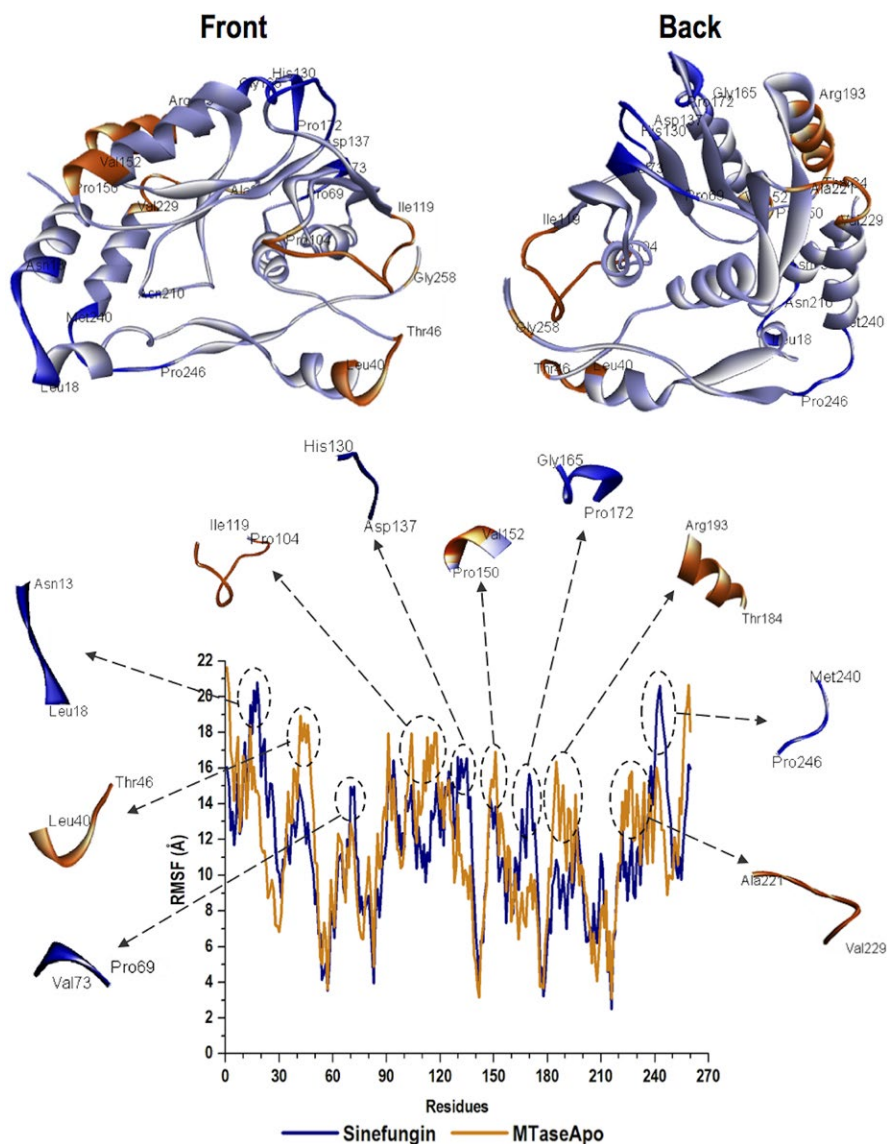


FIGURE 7 The average energy interpretation of each residue throughout the simulation of the apo MTase versus SFG-bound MTase. Highly fluctuating residues in the system are also illustrated in the crystal structure of the MTase and correlated with the peaks in the graph [Colour figure can be viewed at wileyonlinelibrary.com]

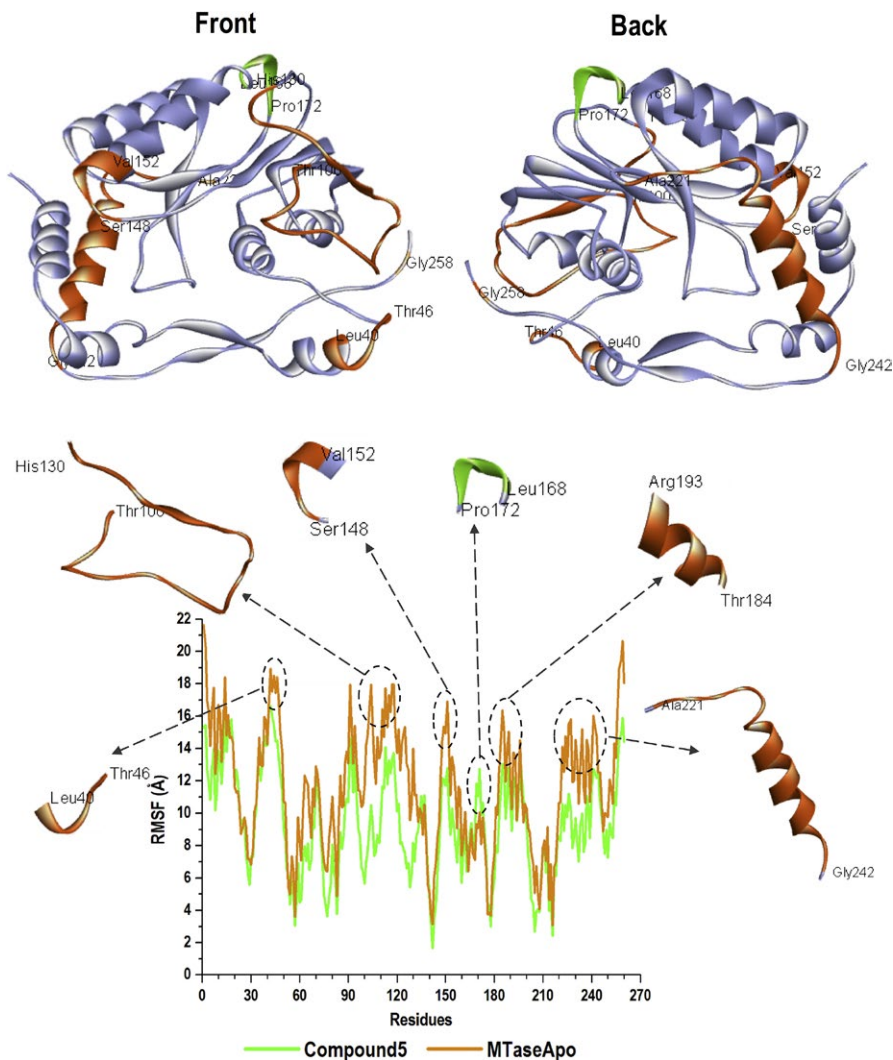


FIGURE 8 The average energy interpretation of each residue throughout the simulation of the apo MTase versus Compound **5**-bound MTase. Highly fluctuating residues in the system are also illustrated in the crystal structure of the MTase and correlated with the peaks in the graph [Colour figure can be viewed at wileyonlinelibrary.com]

the simulation, the residues that form a loop beneath the SAM-binding site (residues 34–53) fluctuated more. This finding was observed in the SFG-MTase complex (Figure 7), but quite the opposite in the Compound **5**-MTase complex (Figure 8), where more fluctuation occurred at the binding site loop rather than the loop below the binding site. Binding of inhibitors rendered the MTase more stable as the flexibility of those residues decreased and the enzyme became more compact to accommodate inhibitor binding. The presence of these inhibitors in the SAM-binding site strongly affected the global dynamics of most loops and helices in the MTase enzyme.

These results are concurrent to those of DCC, which was utilized in the analysis of fluctuations of atoms within the NS5 MTase backbone, as well as domain motions, focusing specifically on the α -carbons. Variations of colors represent residue distance analysis plots, where red to yellow areas signify positive/strong-correlated movements between α -carbons of residues and blue to black areas signify negative/anti-correlated movements. In Supporting Information Figure S2, it can be noticed that the Apo MTase fluctuates

more than when bound. It is evident that highly fluctuating residues that are shown in RMSF graphs are parallel to the anti-correlative residual movements in the DCC plots of each system. Likewise, residues that follow similar trends in movement throughout the simulation show strong correlation patterns.

3.2.3 | Binding free energy calculations

Average measures of the all factors of molecular mechanics computed over the 200-ns molecular dynamic simulation of the SFG-MTase and the Compound **5**-MTase systems are tabulated in Table 1.

The approximated binding free energy between SFG and the MTase is -34.99 kcal/mol, while that of Compound **5** and the MTase is -21.27 kcal/mol. This substantial difference in binding energy (~ 13 kcal/mol) between the individual inhibitors and the enzyme corresponds with experimental evidence that SFG binding to the MTase is potent at a lower IC_{50} than that of Compound **5**.^[21] The estimated van der Waals contributions (ΔE_{vdW}) and electrostatic contributions

TABLE 1 An outline of the MM/PBSA binding free energy contributions to the SFG-MTase system and the Compound 5-MTase system

	Energy components (kcal/mol)				
	ΔE_{vdw}	ΔE_{elec}	ΔG_{gas}	ΔG_{solv}	ΔG_{bind}
SFG-MTase system					
MTase	-2047.42 ± 20.73	-16727.67 ± 113.43	-18775.10 ± 111.10	-3474.49 ± 96.04	-22249.58 ± 52.82
SFG	-4.37 ± 1.59	-93.06 ± 7.97	-97.43 ± 7.75	-42.69 ± 3.32	-140.12 ± 6.51
Complex	-41.73 ± 4.86	-60.32 ± 23.63	-102.04 ± 26.13	67.05 ± 19.46	-34.99 ± 8.02
Compound 5-MTase system					
MTase	-2041.29 ± 20.69	-16849.53 ± 96.53	-18890.82 ± 93.77	-3372.78 ± 80.45	-22263.60 ± 46.55
Compound 5	-5.06 ± 1.39	-21.99 ± 3.36	-27.05 ± 3.34	-44.43 ± 4.63	-71.48 ± 4.32
Complex	-34.06 ± 6.27	-35.87 ± 14.03	-69.93 ± 15.25	48.66 ± 12.89	-21.27 ± 5.21

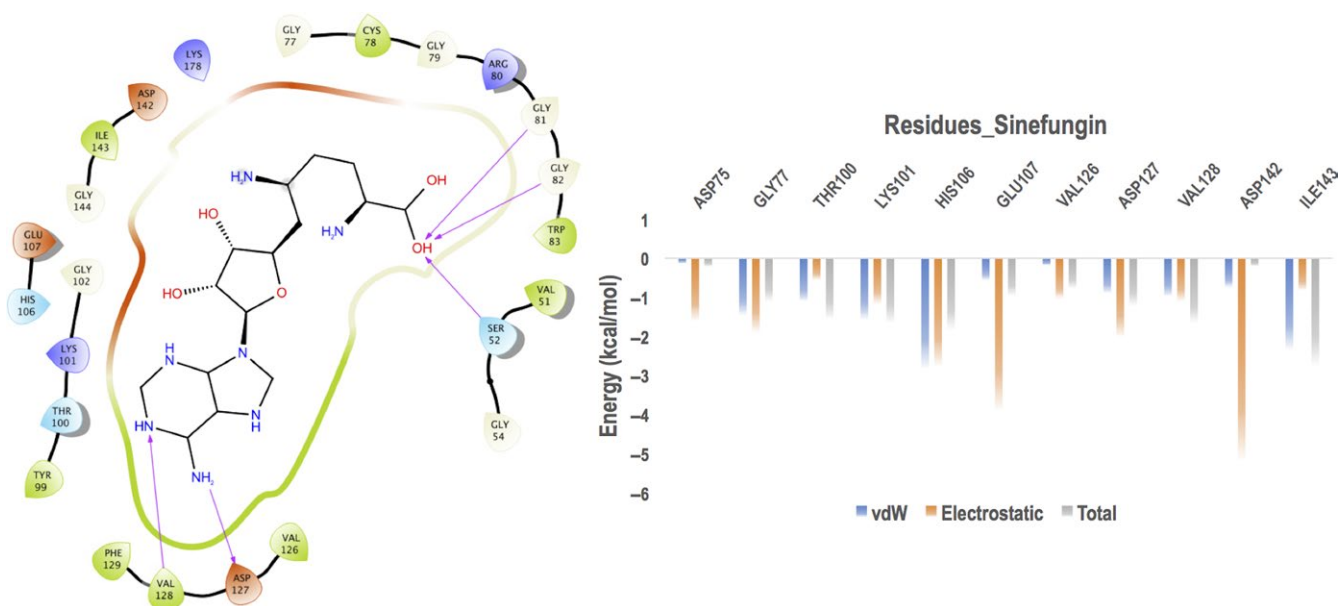
(ΔE_{elec}) towards total binding free energy in the SFG-MTase system (-41.73 and -60.32 kcal/mol, respectively) are higher than that of the Compound 5-MTase system (-34.06 and -35.87 kcal/mol, respectively). The estimated solvation contribution (ΔG_{solv}) toward the binding free energy in the SFG-MTase system (67.05 kcal/mol) is slightly higher than that of the Compound 5-MTase system (48.66 kcal/mol). In Table 1, the energy components presented indicate that the most favorable contributions for binding of inhibitors, SFG and Compound 5, derived from ΔE_{vdw} and ΔE_{elec} .

3.2.4 | Decomposition analysis of binding site interaction energy

The binding free energy was decomposed further into contributions from specific amino acid residues of the MTase. We present via the graphs in Figures 9 and 10 the contrasting

protein-ligand interaction continua between the SFG-bound MTase and the Compound 5-bound MTase, respectively.

The per-residue energy decomposition analysis that we've presented in Figure 9 show that the highly contributing binding site amino acid residues toward the energy of the SFG-bound complex were His106 (-2.806 kcal/mol [vdW]; -2.747 kcal/mol [elec]), Glu107 (-3.857 kcal/mol [elec]), Asp142 (-5.139 kcal/mol [elec]) and Ile143 (-2.321 kcal/mol [vdW]). Whereas, energy contributions of other binding site residues that were less include Asp75 (-1.586 kcal/mol [elec]), Gly77 (-1.452 kcal/mol [vdW]; -1.886 kcal/mol [elec]), Thr100 (-1.082 kcal/mol [vdW]; -0.553 kcal/mol [elec]), Lys101 (-1.563 kcal/mol [vdW]; -1.15 kcal/mol [elec]), Val126 (-1.032 kcal/mol [elec]), Asp127 (-0.883 kcal/mol [vdW]; -1.99 kcal/mol [elec]) and Val128 (-0.959 kcal/mol [vdW]; -1.09 kcal/mol [elec]). From Figure 9, it can be observed that the electrostatic energy contribution from residues

**FIGURE 9** MTase residues that interact with SFG (left) and energy contributions of the highest interacting residues at the SAM-binding site (right) [Colour figure can be viewed at wileyonlinelibrary.com]

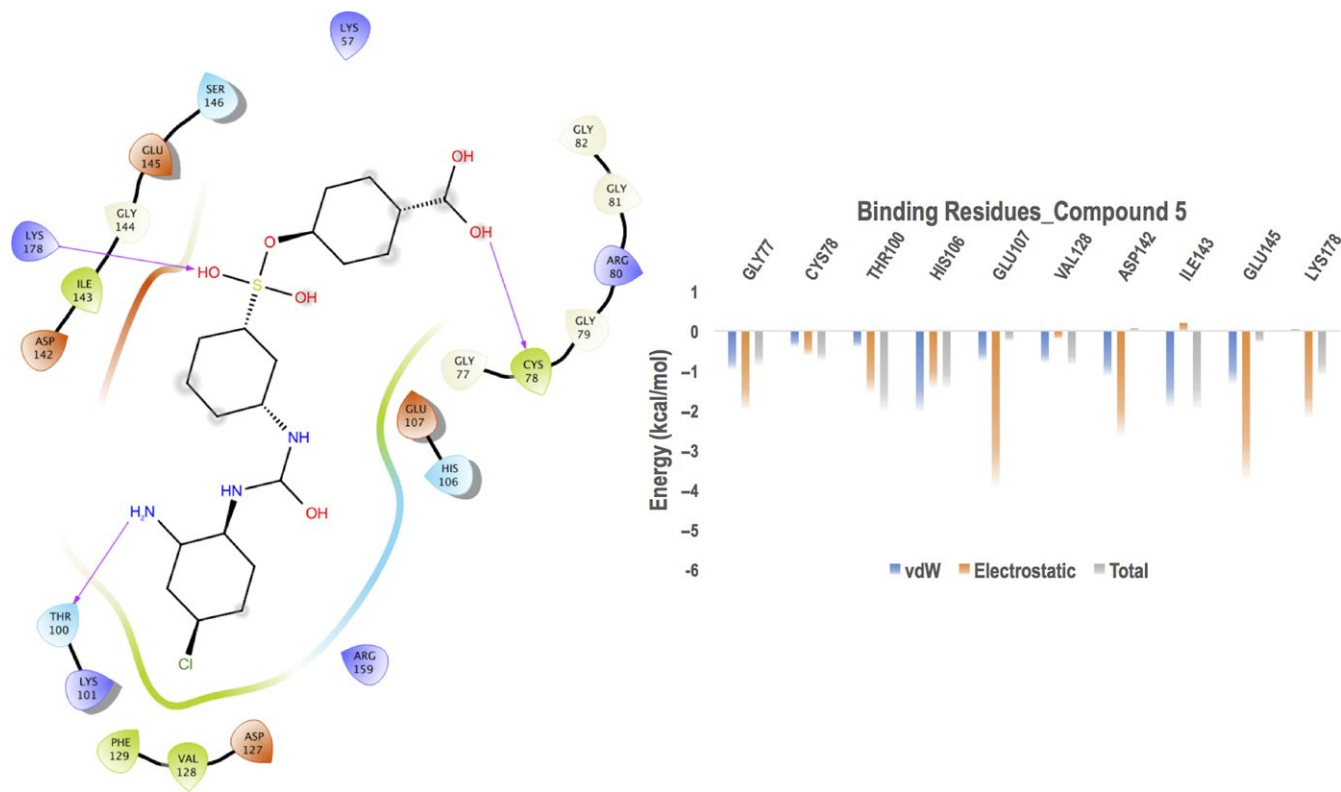


FIGURE 10 MTase residues that interact with Compound 5 (left) and energy contributions of the highest interacting residues at the SAM-binding site (right) [Colour figure can be viewed at wileyonlinelibrary.com]

106, 107, and 142, and the van der Waals energy from residues 77, 106, and 143 in the SFG-MTase complex are most likely responsible for the high interaction energy in the system ($\Delta G_{\text{bind}} = -34.99$ kcal/mol). Binding site interactions of SFG to the MTase in the original 5MRK pdb is shown in Supporting Information Figure S3 for comparison purposes.

High-energy contribution from the Compound 5-bound complex stem from interacting residues Gly77 (-1.977 kcal/mol [elec]), His106 (-2.043 kcal/mol [vdW]), Glu107 (-3.94 kcal/mol [elec]), Asp142 (-2.67 kcal/mol [elec]), Ile143 (-1.922 kcal/mol [vdW]), Glu145 (-3.746 kcal/mol [elec]), and Lys178 (-2.19 kcal/mol [elec]). Binding site residues with slightly lower energy contribution to the system were Cys78 (-0.391 kcal/mol [vdW]; -0.602 kcal/mol [elec]), Thr100 (-1.541 kcal/mol [elec]), and Val128 (-0.81 kcal/mol [vdW]). From Figure 10, it can be concluded that the electrostatic energy contribution from residues 107, 142, and 145, and the van der Waals energy from residues 106 and 143 in the Compound 5-MTase complex may be accountable for the high interaction energy in the system ($\Delta G_{\text{bind}} = -21.27$).

The large difference in binding affinity between the SFG-bound and Compound 5-bound complexes (~ 13 kcal/mol) may be owing to the increase in electrostatic binding energy of Asp142 of the MTase to SFG, as well as van der Waals and electrostatic energies of His106, as compared to that of Compound 5.

3.3 | Fingerprints for the design of new chemical entities (NCEs)

Looking at the binding implications of SFG to the ZIKV NS5 MTase, potential use of SFG could be a promising starting point as a prototype candidate for ZIKV treatment. We therefore created a map depicting the key chemical, structural, and pharmacophoric fingerprints of SFG that will assist medicinal chemists and researchers in the identification and design of future new chemical entities for potential ZIKV inhibitors. The pharmacophoric elements that associate with highly contributing residues of the MTase were chosen to build our ensemble as we have illustrated in Figure 11.

As we have presented in Figure 11, it can be noticed that the N6 and N7 atoms are crucial to interact with the target by creating positive ionization with Glu107 and Asp142 of the ZIKV MTase, respectively. Retention of N6 and N7 will contribute positive ionizations responsible for ligand-enzyme interactions. Furthermore, the N2, N5, O2, O3, and O5 atoms are essential in the formation of strong hydrogen bonds with Arg159, His106, Gly79, Thr100, Lys101, and Arg80, respectively, which are mandatory for enzyme stability. Preservation of the N2, N5, O2, O3, and O5 atoms will induce stability and strong binding of NCEs to the ZIKV MTase.

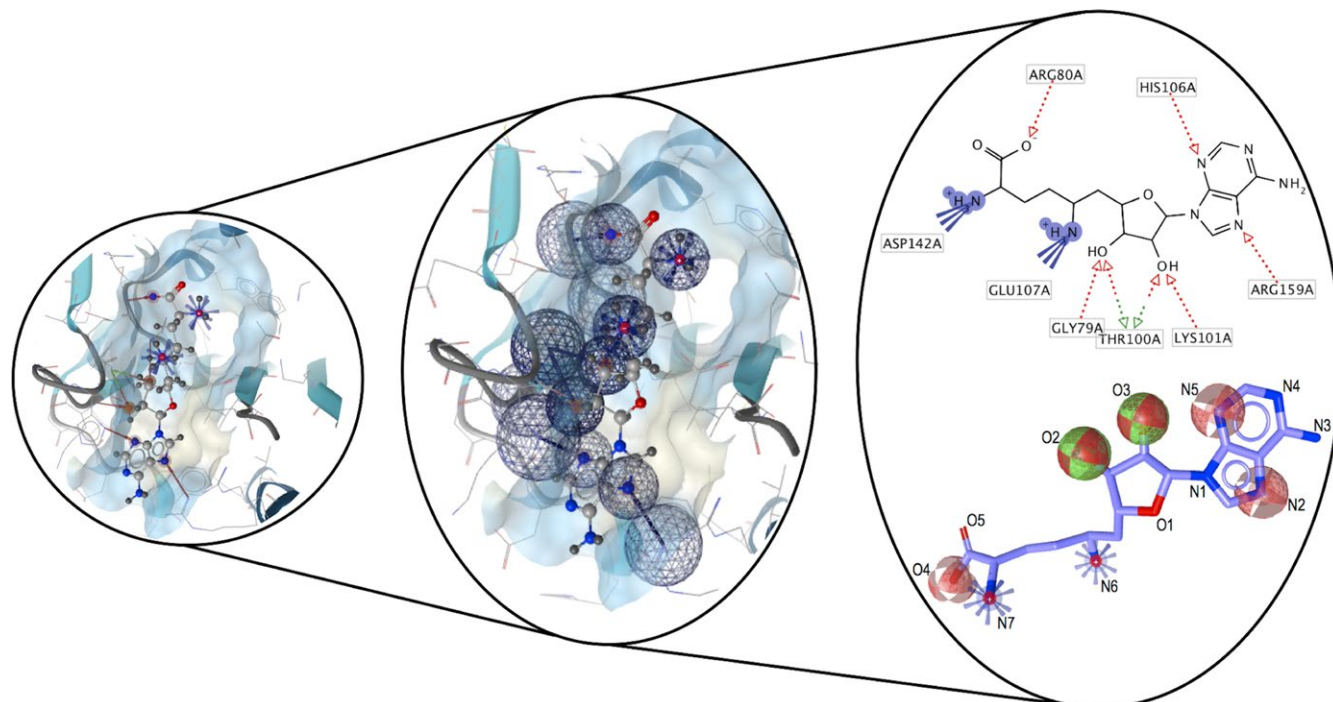


FIGURE 11 Schematic representation of the key chemical, structural and pharmacophoric fingerprints of SFG [Colour figure can be viewed at wileyonlinelibrary.com]

4 | CONCLUSIONS

The ZIKV is a “public health emergency of international concern” and therefore a serious global threat. Apart from ZIKV, Compound **5** and SFG have also shown inhibitory effects in other *flaviviruses*, including DENV, WNV, YFV, and JEV. The molecular dynamic analyses described in this study reveal the conformational evolutions, i.e. variations in the ZIKV NS5 MTase after binding of these inhibitors at a molecular level. Molecular dynamic simulations of 200 ns demonstrate radical movements within the MTase, particularly of the loops surrounding the SAM-binding pocket and RNA-binding site. The dynamic loop fluctuations in motion were uncovered in the RMSD and RMSF analyses and substantiated by examining the three-dimensional molecular landscape of the loops at specific time intervals throughout the simulation.

Upon binding to the MTase, both SFG and Compound **5** have shown to stabilize the rather erratic apo system, although, it was noticed that SFG renders the MTase more stable and more compact than Compound **5**. The SFG-bound system also reached convergence while the Compound **5**-bound system did not. The binding affinity and binding site interactions (bond and non-bond interactions) between SFG and the SAM-binding pocket of the MTase were stronger than those of Compound **5**. Binding energy calculations identified His106, Glu107, Asp127, Asp142, and Ile143 as key players in the binding of SFG to the MTase; and Gly77, Thr100, His106, Glu107, Asp142, Glu145, and Lys178 in the binding of Compound **5** to the MTase.

Binding of SFG to the SAM-binding pocket caused the loop surrounding the pocket (residues 100–110) to shift so that SFG is held tighter in a more compact conformation. SFG-binding also resulted in the loop surrounding the RNA-binding site (residues 30–60) to cover the binding site, to prevent RNA from binding and replication from occurring. Strong and stable binding of SFG would also prevent SAM from binding and activating the MTase, avoiding methylation of RNA and the mRNA cap.

To explore the use of SFG as a potential starting point as a prototype candidate for ZIKV treatment, we created a pharmacophore of SFG that will assist medicinal chemists and researchers in the identification and design of future new chemical entities for potential ZIKV inhibitors.

The information interpreted in this study will improve the understanding of ZIKV and will be beneficial in driving the development of anti-ZIKV drugs. Further experimentation is required to elucidate the roles of SFG and Compound **5** in ZIKV treatment.

ACKNOWLEDGMENTS

This work was financially supported by the National Research Foundation and the Centre for High Performance Computing (CHPC, <http://www.chpc.ac.za>) for computational resources.

CONFLICT OF INTEREST

Authors declare no potential financial and other conflict of interests.

ORCID

Mahmoud E. S. Soliman  <http://orcid.org/0000-0002-8711-7783>

REFERENCES

- [1] WHO, The history of Zika virus **2016**.
- [2] S.-I. Yun, Y.-M. Lee, *J. Microbiol.* **2017**, *55*, 204.
- [3] G. Calvet, R. S. Aguiar, A. S. O. Melo, S. A. Sampaio, I. de Filippis, A. Fabri, E. S. M. Araujo, P. C. de Sequeira, M. C. L. de Mendonça, L. de Oliveira, D. A. Tschoeke, C. G. Schrago, F. L. Thompson, P. Brasil, F. B. Dos Santos, R. M. R. Nogueira, A. Tanuri, A. M. B. de Filippis, *Lancet Infect. Dis.* **2016**, *16*, 653.
- [4] H. El Costa, J. Gouilly, J. M. Mansuy, Q. Chen, C. Levy, G. Cartron, F. Veas, R. Al-Daccak, J. Izopet, N. Jabrane-Ferrat, *Sci. Rep.* **2016**, *6*, 35296.
- [5] H. Retallack, E. Di Lullo, C. Arias, K. A. Knopp, M. T. Laurie, C. Sandoval-Espinosa, W. R. Mancía Leon, R. Krencik, E. M. Ullian, J. Spatazza, A. A. Pollen, C. Mandel-Brehm, T. J. Nowakowski, A. R. Kriegstein, J. L. DeRisi, *Proc. Natl Acad. Sci.* **2016**, *113*, 14408.
- [6] J. J. Miner, M. S. Diamond, *Cell Host Microbe* **2017**, *21*, 134.
- [7] A. Sharma, S. K. Lal, *Front. Microbiol.* **2017**, *8*, 110.
- [8] R. K. Singh, K. Dhama, Y. S. Malik, M. A. Ramakrishnan, K. Karthik, R. Tiwari, S. Saurabh, S. Sachan, S. K. Joshi, *Vet. Q* **2016**, *36*, 150.
- [9] H. Lazear, M. Diamond, *J. Virol.* **2016**, *90*, 4864.
- [10] A. S. Fauci, D. M. Morens, *N. Engl. J. Med.* **2010**, *363*, 1.
- [11] S. E. Reznik, J. C. R. Ashby, *Int. J. Infect. Dis.* **2017**, *55*, 29.
- [12] E. F. Pettersen, T. D. Goddard, C. C. Huang, G. S. Couch, D. M. Greenblatt, E. C. Meng, T. E. Ferrin, *J. Comput. Chem.* **2004**, *25*, 1605.
- [13] N. Devnarain, P. Ramharack, M. E. Soliman, *RSC Adv.* **2017**, *7*, 47416.
- [14] B. Coutard, E. Decroly, C. Li, A. Sharff, J. Lescar, G. Bricogne, K. Barral, *Antiviral Res.* **2014**, *106*, 61.
- [15] P. Ramharack, M. E. S. Soliman, *R. Soc. Chem.* **2016**, *6*, 68719.
- [16] W. Duan, H. Song, H. Wang, Y. Chai, C. Su, J. Qi, Y. Shi, G. F. Gao, *EMBO J.* **2017**, *36*, 919.
- [17] H. Dong, L. Liu, G. Zou, Y. Zhao, Z. Li, S. P. Lim, P. Y. Shi, H. Li, *J. Biol. Chem.* **2010**, *285*, 32586.
- [18] S. P. Lim, Q. Y. Wang, C. G. Noble, Y. L. Chen, H. Dong, B. Zou, F. Yokokawa, S. Nilar, P. Smith, D. Beer, J. Lescar, P. Y. Shi, *Antiviral Res.* **2013**, *100*, 500.
- [19] P. Stephen, M. Baz, G. Boivin, S. X. Lin, *J. Am. Chem. Soc.* **2016**, *138*, 16212.
- [20] S. C. Weaver, F. Costa, M. A. Garcia-Blanco, A. I. Ko, G. S. Ribeiro, G. Saade, P. Y. Shi, N. Vasilakis, *Antiviral Res.* **2016**, *130*, 69.
- [21] B. Coutard, K. Barral, J. Lichière, B. Selisko, B. Martin, W. Aouadi, M. O. Lombardia, F. Debart, J. J. Vasseur, J. C. Guillemot, B. Canard, E. Decroly, *J. Virol.* **2017**, *91*, e02202.
- [22] F. Benmansour, I. Trist, B. Coutard, E. Decroly, G. Querat, A. Brancale, K. Barral, *Eur. J. Med. Chem.* **2017**, *125*, 865.
- [23] S. P. Lim, L. S. Sonntag, C. Noble, S. H. Nilar, R. H. Ng, G. Zou, P. Monaghan, K. Y. Chung, H. Dong, B. Liu, C. Bodenreider, G. Lee, M. Ding, W. L. Chan, G. Wang, Y. L. Jian, A. T. Chao, J. Lescar, Z. Yin, T. R. Vedananda, T. H. Keller, P. Y. Shi, *J. Biol. Chem.* **2011**, *286*, 6233.
- [24] R. L. Hamill, M. M. Hoehn, *J. Antibiot. (Tokyo)* **1973**, *XXVI*, 463.
- [25] K. Hercik, J. Brynda, R. Nencka, E. Boura, *Arch. Virol.* **2017**, *162*, 2091.
- [26] M. D. Hanwell, D. E. Curtis, D. C. Lonie, T. Vandermeersch, E. Zurek, G. R. Hutchison, *J. Cheminform.* **2012**, *4*, 17.
- [27] Z. Yang, K. Lasker, D. Schneidman-Duhovny, B. Webb, C. C. Huang, E. F. Pettersen, T. D. Goddard, E. C. Meng, A. Sali, T. E. Ferrin, *J. Struct. Biol.* **2012**, *179*, 269.
- [28] O. Trott, A. J. Olson, *J. Comput. Chem.* **2010**, *31*, 445.
- [29] H. Alonso, A. A. Bliznyuk, J. E. Gready, *Med. Res. Rev.* **2006**, *26*, 531.
- [30] X.-Y. Meng, H.-X. Zhang, M. Mezei, M. Cui, *Curr. Comput. Drug Des.* **2011**, *7*, 146.
- [31] J. de Ruyck, G. Brysbaert, R. Blossey, M. F. Lensink, *Adv. Appl. Bioinforma. Chem.* **2016**, *9*, 1.
- [32] G. Raabe, In *Molecular Modeling and Simulation*, Springer, Singapore **2017**, pp. 83–113.
- [33] A. Ganesan, M. L. Coote, K. Barakat, *Drug Discov. Today* **2017**, *22*, 249.
- [34] R. Salomon-Ferrer, A. W. Götz, D. Poole, S. Le Grand, R. C. Walker, *J. Chem. Theory Comput.* **2013**, *9*, 3878.
- [35] J. A. Maier, C. Martinez, K. Kasavajhala, L. Wickstrom, K. Hauser, C. Simmerling, *J. Chem. Theory Comput.* **2015**, *11*, 3696.
- [36] J. Wang, W. Wang, P. A. Kollman, D. A. Case, *J. Chem. Inf. Comput. Sci.* **2001**, *222*, U403.
- [37] K. G. Sprenger, V. W. Jaeger, J. Pfaendtner, *J. Phys. Chem. B* **2015**, *119*, 5882.
- [38] R. J. Woods, R. Chappelle, *J. Mol. Struct. Theochem.* **2000**, *527*, 149.
- [39] S. Genheden, U. Ryde, *Expert Opin. Drug Discov.* **2015**, *10*, 449.
- [40] X. Zhang, H. Pérez-Sánchez, F. C. Lightstone, *Molecular Dynamics Simulations of Ligand Recognition upon Binding Antithrombin: A MM/GBSA Approach*, Springer, Cham **2015**, pp. 584–593.
- [41] K. Kasahara, I. Fukuda, H. Nakamura, *PLoS ONE* **2014**, *9*, e112419.
- [42] A. Munir, S. Azam, A. Mehmood, *Drug Des. Open Access* **2016**, *5*, 1.
- [43] G. Wolber, T. Langer, *J. Chem. Inf. Model.* **2004**, *45*, 160.
- [44] K. E. Machaba, F. N. Cele, N. N. Mhlongo, M. E. S. Soliman, *Cell Biochem. Biophys.* **2016**, *74*, 473.

SUPPORTING INFORMATION

Additional supporting information may be found online in the Supporting Information section at the end of the article.

How to cite this article: Devnarain N, Soliman MES.

A panoptic uncovering of the dynamical evolution of the Zika Virus NS5 methyltransferase binding site loops—zeroing in on the molecular landscape. *Chem Biol Drug Des.* 2018;92:1838–1850. <https://doi.org/10.1111/cbdd.13353>

Molecular mechanism of resveratrol inhibition of Zika virus NS3 helicase: behind the scenes

Nikita Devnarain¹ & Mahmoud ES Soliman^{*,1}¹ Molecular Bio-computation & Drug Design Laboratory, School of Health Sciences, University of KwaZulu-Natal, Westville, Durban 4001, South Africa*Author for correspondence: Tel.: +0312607413; soliman@ukzn.ac.za

Aim: Zika virus (ZIKV) still poses a health risk to women and their babies without US FDA-approved vaccines or treatments. Experimentation has proved resveratrol inhibition of ZIKV NS3 helicase without specifying the molecular events during inhibition. **Materials & methods:** Herein, we leaped forward to study the molecular dynamics of the bound and unbound enzyme, identifying precise binding residues and interactions, and the enzyme's adaptation to support binding, since loop dynamics affect viral RNA replication. **Results:** Resveratrol stabilizes the P-loop and causes the RNA-binding loop to block the RNA-binding pocket for 200 ns, which is concurrent with experimental evidence that resveratrol binding significantly reduces ATP hydrolysis activity. **Conclusion:** This study illuminates the structural dynamics of ZIKV helicase and druglikeness of resveratrol, which will advance anti-ZIKV drug development.

First draft submitted: 11 October 2018; Accepted for publication: 21 December 2018; Published online: 18 January 2019

Keywords: antiviral therapy • flavivirus • molecular dynamics • NS3 helicase • resveratrol • Zika virus

The Zika virus (ZIKV) is infecting country to country around the globe [1]. With devastating consequences on pregnant women, mothers and their families, the ZIKV remains an unresolved scientific challenge [2]. The global expansion of ZIKV may be due to an increased frequency of traveling that occurs on an international scale, the susceptibility of remote populations, as well as the rise in the vector range due to global warming [3–5].

The ZIKV is composed of multiple enzymes, some of which have been proposed as targets for therapy [6]. The NS3 protein encodes one of the most important viral enzymes and is crucial for polyprotein processing and replication of *flaviviruses* [7]. The NS3 is comprised of an N-terminal protease and a C-terminal RNA helicase domain [8]. The helicase is central to the life cycle and survival of ZIKV [3,9]. Simulation of the helicase by RNA triggers underlying nucleoside triphosphatase activity, which supplies energy for unwinding of intermediates of viral replication [10]. For these reasons, the ZIKV NS3 helicase represents an ideal target for therapy.

The ZIKV resembles dengue virus (DENV) (Figure 1); therefore, inhibitors of DENV helicase may exhibit potency in ZIKV helicase inhibition [11]. Pan *et al.*, 2017, have shown that the ATPase inhibitor, resveratrol, substantially reduces NS3 helicase ATP hydrolysis activity in DENV [12].

Resveratrol or 3,5,4'-trihydroxy-trans-stilbene is a natural polyphenol present in red wine, nuts, berries and traditional Asian medicines (Figure 2) [13]. The antioxidant potential of resveratrol is brought about via inhibition of reactive oxygen species, which involves scavenging free radicals such as superoxide anion (O_2^-), hydroxyl radical (OH^\cdot) and lipid hydroperoxyl radicals, as well as the inhibition of glutathione depletion [14]. Resveratrol was reported to have inhibitory effects on gene expression, nucleic acid synthesis, viral replication and protein synthesis for several viruses including hepatitis C virus, influenza virus, human immunodeficiency virus, herpes simplex virus and others [14–17]. The antioxidant and anti-inflammatory effects of resveratrol also benefit the cardiovascular system and function in neuroprotection, as well as treatment of diabetes mellitus [18–20]. Additionally, resveratrol possesses several anticancer properties that are critical in cancer prevention and treatment [21].

Experimental evidence has shown the ability of resveratrol to significantly decrease ATP hydrolysis activity of the ZIKV helicase [15], although the molecular structural dynamics within the unbound ZIKV helicase (apo) and

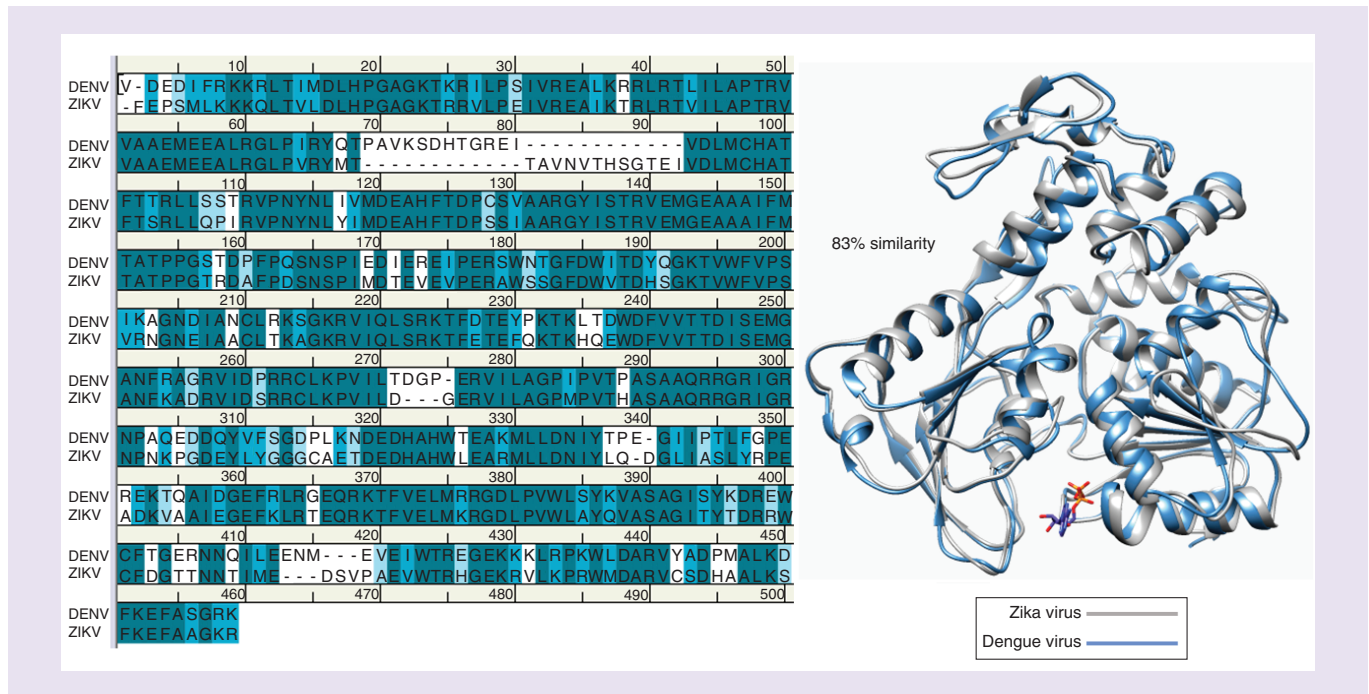


Figure 1. Superimposition of the Zika virus and dengue virus NS3 helicases as well as their corresponding overlapping sequences showing the similarities and differences in their amino acid residues.

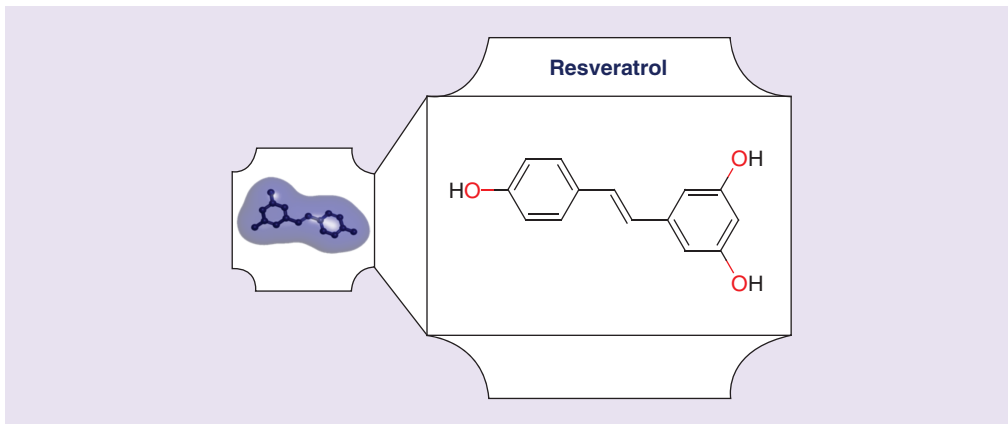


Figure 2. Chemical structure of resveratrol.

the ZIKV helicase bound to resveratrol have not been elucidated. We determine the affinity of resveratrol to the helicase, along with the binding mode and stability of the unbound and bound complexes. The loops surrounding the RNA-binding site and the ATP-binding site (P-loop) were focused on, as flexibility of these loops play major roles in viral RNA replication. To our understanding, this is the primary study applying incorporated computational tools to analyze the way resveratrol binding influences the conformation of the ZIKV NS3 helicase. We postulate that this study will enhance the understanding of the structural dynamics of the inhibitor and the ZIKV NS3 helicase and will aid in the search for anti-ZIKV treatment.

ZIKV NS3 helicase

The ZIKV NS3 protein constitutes 617 amino acid residues, which make up the protease (residues 1–167) and helicase (residues 168–617) enzymes. Processing of the polyprotein as well as viral replication are dependent on the

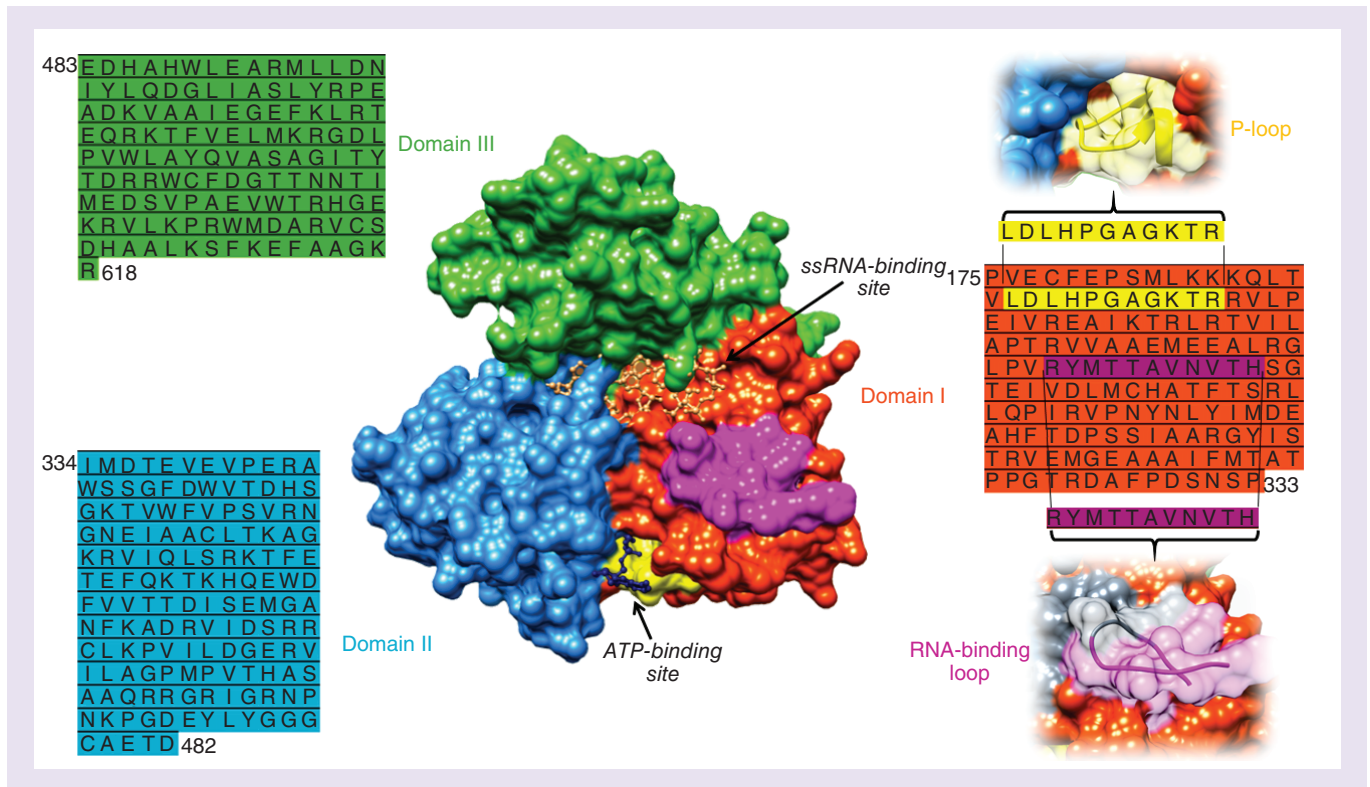


Figure 3. Protein sequences of the different domains of Zika virus NS3 helicase, as well as the major binding sites and loops.

activities of both these enzymes [7]. The serine protease is required for viral maturation via polyprotein processing, while the helicase is essential for RNA synthesis and genome replication of the virus [22].

The serine protease can be described as a folded globular domain comprising of two β -barrels [23]. The helicase constitutes three domains that resemble each other in size (Figure 3). Domain 1 (residues 182–327) and domain 2 (residues 328–480) are made up of tandem α/β RecA-like folds, which are present in helicases of superfamily 1 and 2. Domain 1 comprises motifs I (Walker A or P-loop), Ia, II (Walker B) and III, which line a cleft between motifs IV, IVa, V and VI of domain 2. Motifs I, II and VI are involved in ATP binding and/or hydrolysis, and motifs Ia, IV and V are associated with interdomain communication and RNA binding. The ZIKV helicase, as with the DENV4 helicase, binds ATP at the lower end of the cleft at the interface of domains 1 and 2, while the pocket dividing domains 1 and 2 from domain 3 house the RNA. Domains 2 and 3 interact via a β -hairpin extension of domain 2, which functions as a wedge that facilitates unwinding of double-stranded RNA. Structures within domain 3 primarily consist of α -helices. Domain 3 interacts with RNA as well as the NS5 RNA-dependent RNA polymerase in other *flaviviruses* [10].

To date, several strains of ZIKV have been isolated. Due to interest in the helicases of different strains, we examined the similarities/differences in the sequences of the helicases. Multiple sequence analysis showed that the helicases of the French Polynesian (H/PF/2013), African (MR766) and Brazilian (BRA/2016) strains were almost identical, with very few differences in amino acid residues (Figure 4). Certain amino acid residues in the African strain are different from the other two strains. The distinguishing amino acid residues are at positions 41, 226, 233, 298, 309, 409 and 410, none of which are in the ATPase pocket. We can, therefore, deduce that the manner in which resveratrol binds to this helicase will be comparable with helicases of other strains.

Computational methods

Ligand & receptor preparation

The crystal structure of the ZIKV NS3 helicase was obtained from RCSB Protein DataBank (PDB: 5JMT) [24,25]. The structure of resveratrol was obtained from PubChem [26] and prepared using Molegro Molecular Viewer



Figure 4. Multiple sequence alignment of helicase sequences of strains of H/PF/2013, BRA/2016 and MR766.

software (Molegro-a CLC Bio Company, Aarhus, Denmark) and UCSF Chimera software package [27]. An apo system (NS3 helicase) and a resveratrol-bound system were subjected to 200 ns molecular dynamic simulations.

Molecular docking

Optimized conformations and binding affinities of resveratrol within the ATP-binding pocket of the ZIKV NS3 helicase were achieved through molecular docking. Resveratrol was docked into the ATP-binding pocket (competitive inhibitor of ATP) of the NS3 helicase (grid box of spacing of 0.375 Å and x, y, z dimensions of 32 × 26 × 30) via the AutoDock vina plugin of UCSF Chimera software [27–29]. Ten docked poses of the ligand in the binding pocket of the enzyme were generated in PDBQT format by AutoDock Vina and the most favorable geometric pose with the most negative binding energy (kcal.mol⁻¹) was saved from the ViewDock feature. The best complexes were subjected to molecular dynamic simulations. More detailed information regarding molecular docking can be found in the referenced articles [30–32]. To verify that resveratrol was docked into the correct pocket, Supplementary Figure 4 demonstrates the superimposition of ATP bound to the helicase (PDB: 5GJC) and the docked complex of resveratrol to the helicase.

Molecular dynamic simulations

Molecular dynamic simulations were carried out using AMBER PMEMD dynamics engine with GPU acceleration [33,34]. The helicase was parameterized using the AMBER force field, FF14SB [35,36]. The inhibitor was hydrogenated and charged with Gasteiger charges, while the helicase protein was dehydrogenated preceding the simulation. Atomic partial charges were created for resveratrol using antechamber which applies the general AMBER force field and restrained electrostatic potential methods [35,37,38]. The AMBER 14 LEAP module was used to combine, neutralize and solvate all systems via addition of hydrogen atoms, sodium and chloride ions, followed by suspension into an orthorhombic box of TIP3P water molecules to ensure all atoms were within 10 Å of the box edges. The amino acid residues of the helicase were renumbered from one. The systems were initially minimized (2500 steps) using a restraint potential of 10 kcal.mol⁻¹ Å⁻² applied to the solutes, for 1000 steps of steepest descent

followed by 1000 steps of conjugate gradient minimization. Thereafter, the systems were further fully minimized (200 steps) via unrestrained conjugate gradient algorithm.

A constant-temperature, constant-volume ensemble simulation was carried out for 50 ps from 0 to 300 K, to preserve a fixed volume and number of atoms in each system. A harmonic restraint of $10 \text{ kcal.mol}^{-1} \text{ \AA}^{-2}$ and Langevin thermostat collision frequency of 1.0 ps^{-1} were applied to the solutes. All systems were then subjected to equilibration (500 ps) with a constant operating temperature (300 K) and pressure (1 bar) using the Berendsen barostat and number of atoms resembling an isobaric–isothermal ensemble. The shake algorithm was applied to restrain hydrogen bonds during the simulations, which were conducted for 200 ns per system using a single-precision floating-point (SPFP) precision model.

Per-residue decomposition analysis & binding free energy computation

To establish the binding free energy (ΔG_{bind}) of resveratrol to the ZIKV NS3 helicase enzyme, we employed molecular mechanics integrated with the Poisson–Boltzmann or generalized Born and surface area continuum solvation approach [39,40]. These methods have been elaborated in the referred papers [41,42].

The molecular dynamic simulation yielded a trajectory depicted by 50,000 snapshots, which were averaged to generate ΔG_{bind} . The binding strengths between resveratrol and the helicase may be defined as:

$$\Delta G_{\text{bind}} = G_{\text{complex}} - G_{\text{receptor}} - G_{\text{ligand}} \quad (1)$$

$$\Delta G_{\text{bind}} = E_{\text{gas}} + G_{\text{sol}} - TS \quad (2)$$

$$E_{\text{gas}} = E_{\text{int}} + E_{\text{vdW}} + E_{\text{ele}} \quad (3)$$

$$G_{\text{sol}} = G_{\text{GB}} + G_{\text{SA}} \quad (4)$$

$$G_{\text{SA}} = \gamma \text{SASA} \quad (5)$$

where:

E_{ele}	Electrostatic potential energy from Coulomb forces
E_{gas}	Gas-phase energy (based on FF145B force field terms)
E_{int}	Internal energy
E_{vdW}	van der Waals energy
G_{sol}	Solvation free energy
G_{GB}	Polar solvation energy
G_{SA}	Nonpolar solvation energy
S	Total entropy of solute
SASA	Solvent accessible surface area (water probe radius of 1.4 Å)
T	Total entropy of temperature

A per-residue free energy atomistic decomposition was adopted to estimate the contribution of each residue to the total ΔG_{bind} at the binding site, for significant residues of the helicase using the AMBER14 molecular mechanics integrated with generalized born surface area method. Further analyses were carried out on the resveratrol-bound complex.

Absorption, distribution, metabolism & excretion assessment of resveratrol

Using the absorption, distribution, metabolism and excretion (ADME) online prediction tool, SWISS ADME, we assessed the druglikeness of resveratrol. The SWISS ADME website allows the computation of physicochemical de-

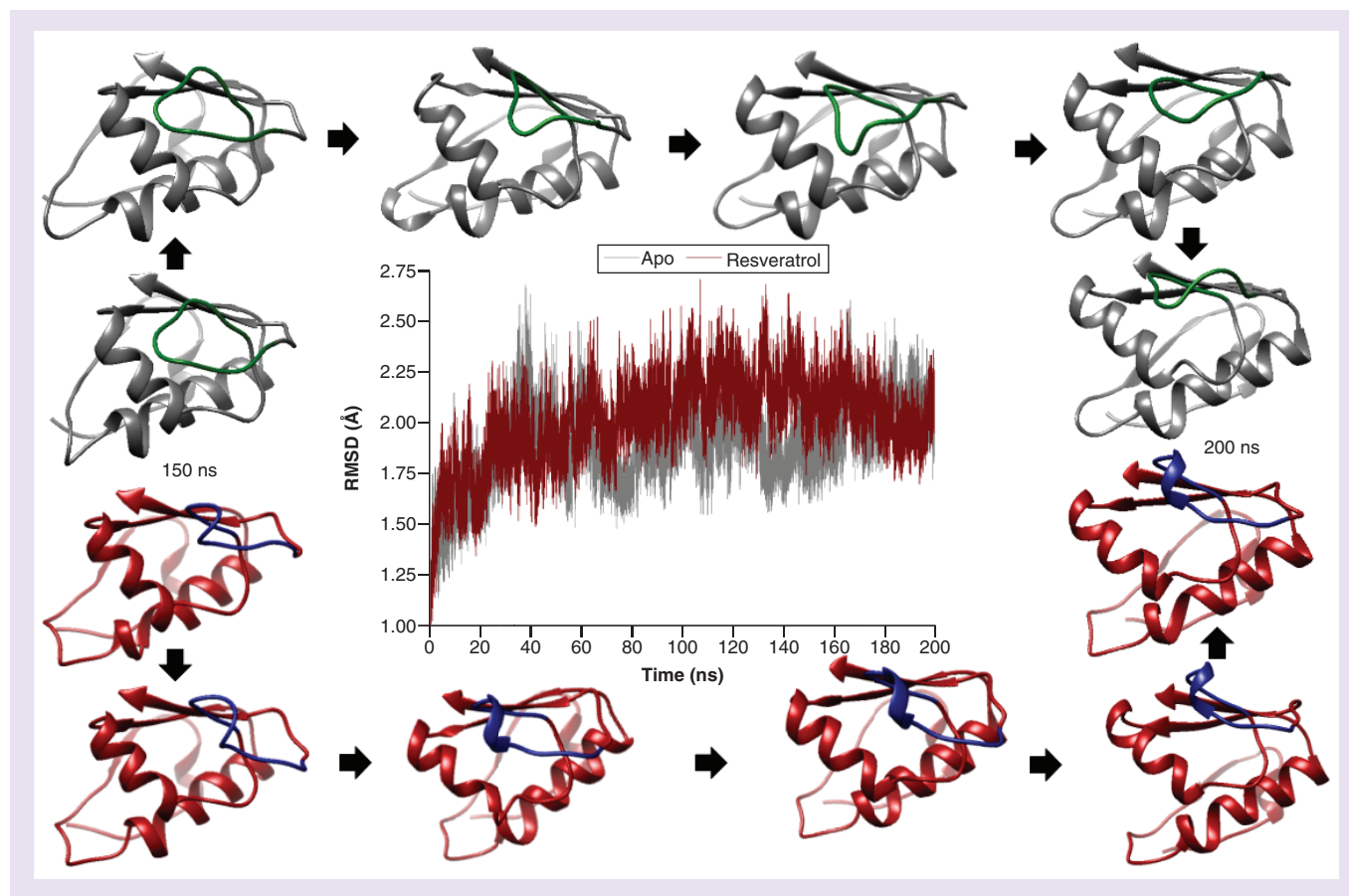


Figure 5. Resveratrol binding to Zika virus NS3 helicase stabilizes the enzyme. Snapshots at 10 ns intervals from 150 to 200 ns show the spontaneous behavior of the RNA-binding loop (green) in the apo enzyme (gray), while the same loop (blue) in the bound enzyme (red) becomes stable via formation of a 3_{10} -helix.

scriptors and provides a prediction of druglike nature, pharmacokinetic properties, medicinal chemistry friendliness and ADME parameters small molecules to support drug discovery [43].

Results

Molecular dynamic simulations & systems stability

The trajectories of 200 ns molecular dynamic simulations of the apo and resveratrol-bound systems were monitored and analyzed postdynamically to verify stability of the systems.

Atomic distribution of α -carbons of NS3 helicase

The deviation of α -carbons within the NS3 helicase during simulation of the systems was established by calculating the root-mean-square deviation. In Figure 5, we show that resveratrol brought about different atomic changes in the helicase during the simulation, when compared with the apo system. Both systems remained within a 1.5 Å range throughout the simulation.

The root-mean-square deviation pattern of the apo system indicates major fluctuations of the system between 34 and 40 ns and 164 and 167 ns, and convergence in the latter part of the simulation (after 175 ns). The fluctuations of the resveratrol-helicase complex dropped between 180 and 200 ns, where the helicase became more compact when compared with the apo helicase (Supplementary Figure 1). The P-loop in the apo also undergoes constant structural variations (deviation = 1.783 Å), whereas that of the bound enzyme is stable (deviation = 0.637 Å). Resveratrol also stabilized the helicase during the 34–40 ns and 164–167 ns period when the apo fluctuated. It is noticed in Figure 5 that as the end of the simulation approached, the RNA-binding loop moved closer toward the RNA-binding pocket. This may have impeding effects on the entry and binding of RNA in that pocket.

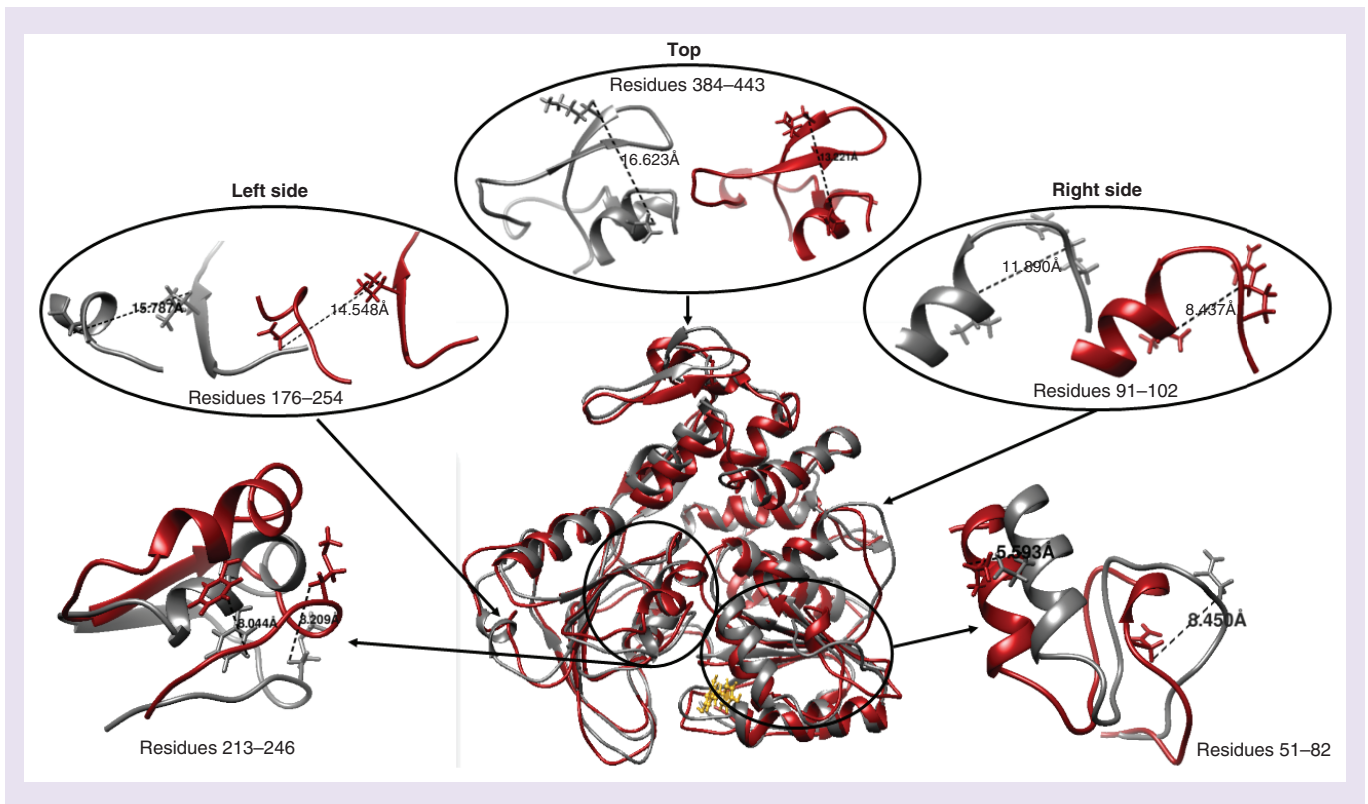


Figure 6. Resveratrol binding to the NS3 helicase (red) induces compactness of the enzyme, as compared with the apo (gray).

Superimposition of the bound (red) and unbound (gray) helicase at 200 ns (Figure 6) demonstrates the impact of resveratrol binding to the ZIKV NS3 helicase. The overall configuration of the helicase is more compact when bound, as the outer loops and coils move inward, suggesting a looser apo conformation. As emphasized in Figure 6, distances between loops on the top, left and right regions (domain III, II and I, respectively) of the enzyme decreased in the bound complex when compared with the apo. The RNA-binding loop and extended coil surrounding the inhibitor (enlarged in bottom right) move inward and the outer loop in domain II (enlarged in bottom left) move upward conforming the enzyme to a more compact shape.

Intra & intermolecular interactions in ZIKV NS3 helicase

Fluctuating residues within the NS3 helicase

To provide a better understanding of the residues responsible for the fluctuating energy patterns in Figure 5, we calculated the root-mean-square fluctuation of each residue of both systems.

The pattern in the fluctuation of residues in the apo system bear resemblance to the resveratrol-bound complex; however, residues 1–43, 129–137, 201–208 and 389–414 in the apo fluctuate more than the bound complex. In Figure 7, we demonstrate that domain I of the helicase (green) fluctuates more than domains II and III. Binding of resveratrol to the helicase decreases movements of the P-loop and causes increase in movements of the RNA-binding loop. Considering both systems, residues of the apo system are more energetic and therefore, the apo system is a lot more flexible than the resveratrol-bound system, suggesting that the inhibitor reduces the energies of the residues within the helicase.

Binding free energy calculations & binding site interaction decomposition analysis

The intensity of interactions between a ligand and receptor may be quantified by the binding free energy obtained from molecular mechanics with Poisson–Boltzmann surface area calculations. Mean calculations of internal energy changes of the resveratrol-helicase system, and resveratrol and the helicase alone, totaled over the 200 ns simulation are presented in Table 1.

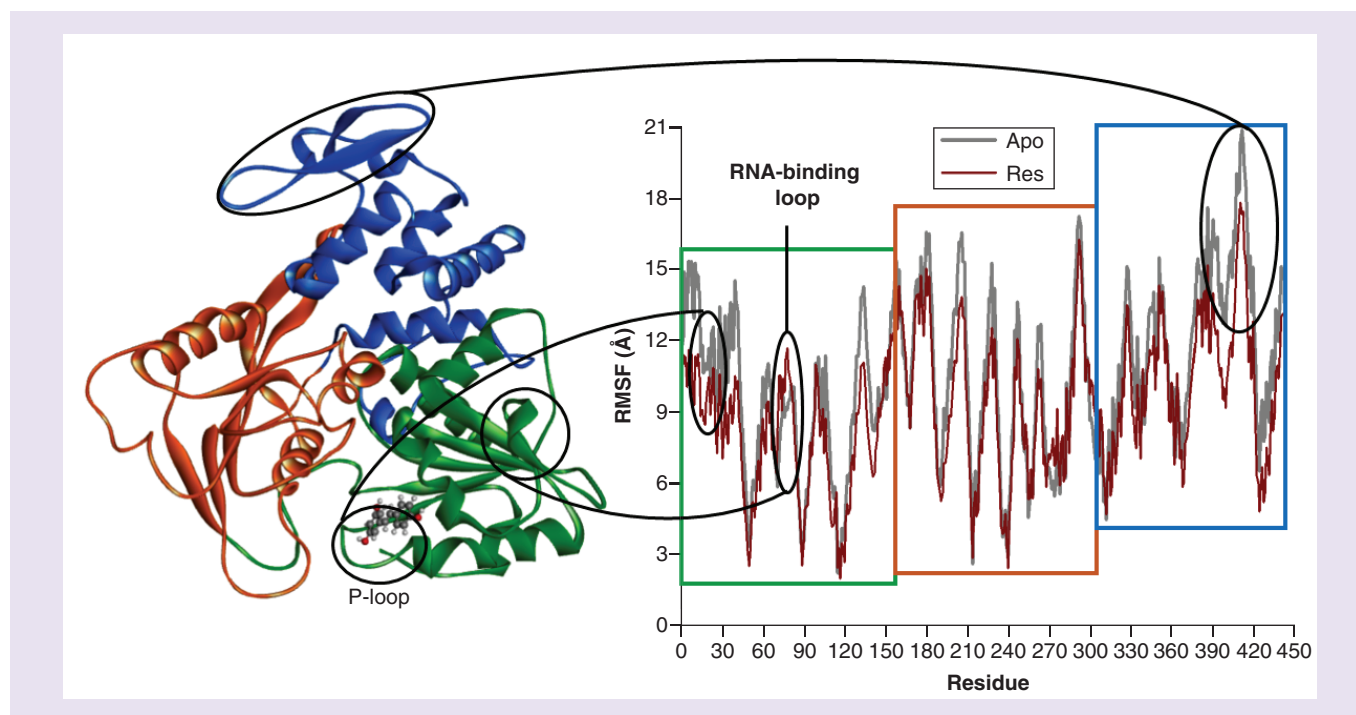


Figure 7. Residues of the apo helicase (gray) fluctuate more than residues of the resveratrol-bound helicase (red).

Table 1. A representation of the binding free energy contributions to the resveratrol-bound system.

	Energy components (kcal.mol ⁻¹)				
	ΔE_{vdW}	ΔE_{elec}	ΔG_{gas}	ΔG_{solv}	ΔG_{bind}
Helicase	-3555.87 ± 29.16	-29681.50 ± 134.2	-33237.37 ± 133.18	-4769.99 ± 104.63	-38007.37 ± 63.52
Resveratrol	-0.25 ± 0.66	65.32 ± 0.86	65.07 ± 1.08	-18.85 ± 0.3	46.22 ± 1.21
Complex	-26.86 ± 2.53	-36.54 ± 4.69	-63.4 ± 4.64	33.05 ± 3.23	-30.35 ± 2.86

ΔG_{bind} : Binding free energy; ΔE_{elec} : Electrostatic energy; ΔG_{gas} : Free energy in gas phase; ΔG_{solv} : Solvation energy; ΔE_{vdW} : van der Waals force.

The estimated binding free energy between resveratrol and the helicase is -30.35 kcal.mol⁻¹. This strong binding is concurrent with experimental evidence that resveratrol binding to the helicase significantly reduces ATP hydrolysis activity and is potent at an IC₅₀ of 94.25 ± 5.02 μM [15]. The energies shown in Table 1 suggest that the most favorable conditions for resveratrol binding are derived from ΔG_{gas} and ΔE_{elec} .

The analysis was expanded into per-residue energy decomposition of resveratrol-binding residues of the helicase. In Figure 8, we show the resveratrol-helicase interaction spectrum. The ligand interaction diagram in Figure 8A clearly illustrates hydrophobic interactions between resveratrol and the helicase, particularly residues Leu20, His21, Pro22, Ala24, Thr27, Arg28, Glu57 and Ala143. Hydrogen bonding is also clearly apparent between Gly23 and Gly25 with the O₁ atom of resveratrol, and between Lys26 and the O₃ atom of resveratrol. The graph in Supplementary Figure 3 and the hydrogen bond surface surrounding resveratrol in Figure 8C coincide with these results. The results from the graph in Figure 8B are concurrent with the findings in Table 1 that the electrostatic energy contributes more toward total binding free energy than van der Waals forces. Residues His21, Lys26 and Gly57 contributed mostly toward the electrostatic energy that was responsible for binding, and Lys26 and Thr27 contributed more toward van der Waals forces than other binding site residues.

Resveratrol ADME assessment

Using the online tool, SwissADME, the druglikeness of resveratrol was elucidated (Table 2). Resveratrol is likely to permeate lipophilic membranes, as well as the blood–brain barrier. Clarification of the concept of LogP may be found in Devnarain *et al.* (2017) [44]. Resveratrol is water soluble, which is favorable for oral bioavailability.

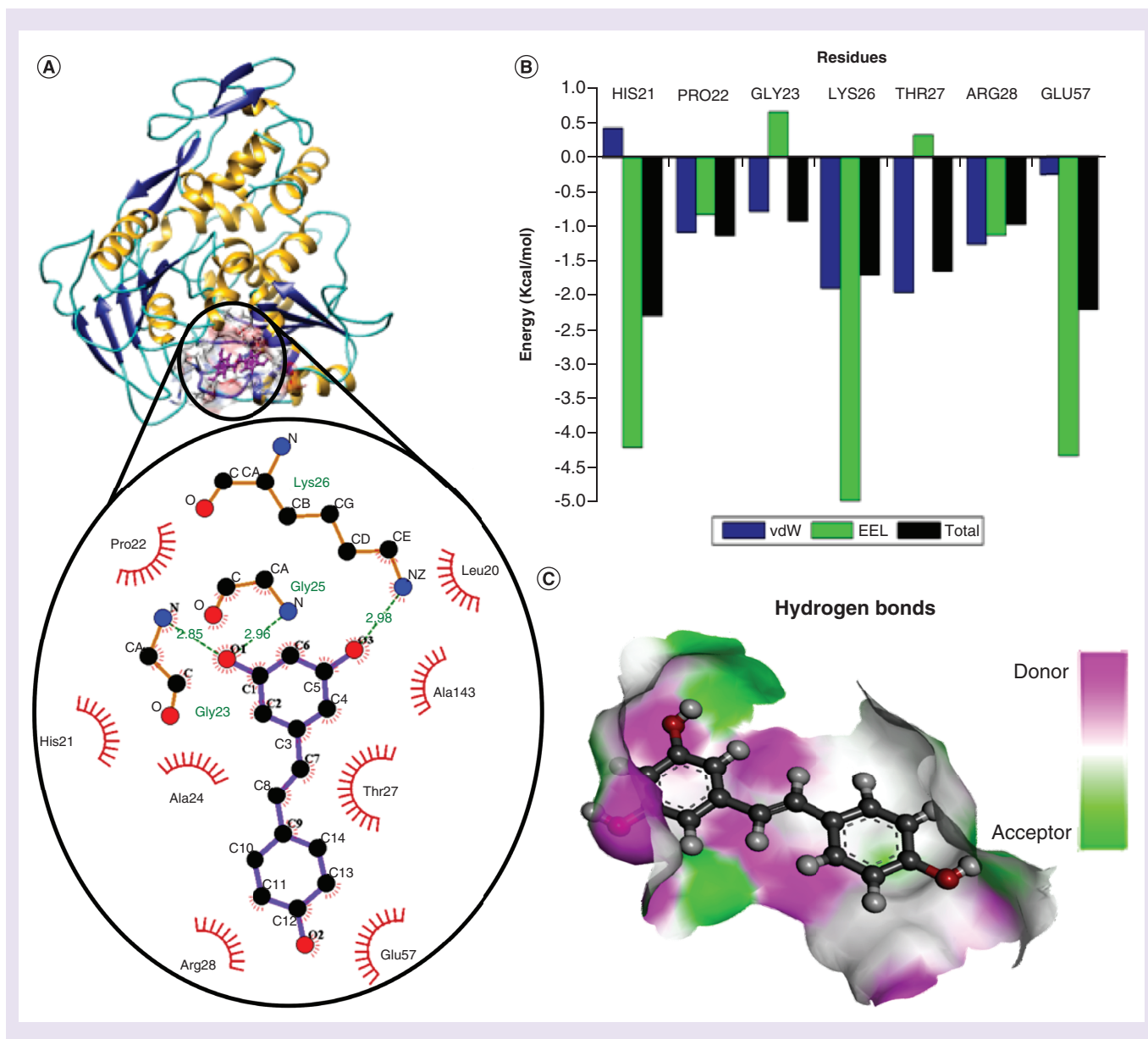


Figure 8. Exploration of the interactions that exist between resveratrol and residues of the Zika virus NS3 helicase. **(A)** Resveratrol within binding pocket of helicase zooming into the hydrophobic interactions and hydrogen bonds between ligand-binding residues and resveratrol. **(B)** Per-residue decomposition analysis of ligand binding residues. **(C)** Hydrogen bonding in ligand binding pocket. EEL: Electrostatic energy; vdW: van der Waals.

Table 2. Druglikeness of resveratrol.

Formula	C ₁₄ H ₁₂ O ₃
Molecular weight	228.24 g.mol ⁻¹
Lipophilicity (LogP)	1.71
Water solubility (Log S)	Soluble
Gastrointestinal absorption	High
BBB permeant	Yes
Lipinski's rules	Yes
Ghose, Veber, Egan, Muegge	Yes

BBB: Blood-brain barrier.

Lipinski's rule of five is used to evaluate druglikeness of a chemical compound [45]. Resveratrol does not violate any of Lipinski's rules, and also adheres to other filters that define druglikeness, including Ghose, Veber, Egan and Muegge. The BOILED-egg diagram of resveratrol generated by SwissADME is represented by Supplementary Figure 2. The physicochemical and pharmacokinetic properties of resveratrol are favorable for drug discovery.

Discussion

The effects of resveratrol have been studied previously for its inhibition of nucleic acid synthesis, gene expression, viral replication and protein synthesis in several viruses. Experimental studies have shown that resveratrol inhibits ZIKV *in vitro*; however, the binding mechanism and binding interactions of resveratrol to the ZIKV NS3 helicase were not elucidated. The 200 ns molecular dynamic simulations of the apo helicase and resveratrol-bound helicase have allowed us to understand the shifts that occur in the enzyme upon binding and the affinity of the helicase for resveratrol.

A 'loose' and expanded structure of the helicase is necessary to accommodate RNA in its binding pocket for viral RNA replication. Resveratrol binding renders the helicase more compact than when unbound, limiting the space within the RNA-binding pocket. The P-loop regulates ATP binding and hydrolysis during ZIKV replication. Resveratrol stabilized the P-loop when compared with the apo and resulted in major shifts and conformational changes in the RNA-binding loop. Since resveratrol binding to the helicase decreases ATP hydrolysis, we speculate that resveratrol binding may also hinder RNA binding and replication due to movements of the RNA-binding loop in front of the entrance of the RNA-binding pocket; however, further experimentation is required to substantiate this theory. Strong binding interactions, including hydrophobic and hydrogen bonding, between resveratrol and residues of the helicase also reduce fluctuations of the enzyme domains, thus explaining the high potency of resveratrol inhibition on the ZIKV NS3 helicase. Conformational ensembles generated from the molecular dynamic simulations in this study match with the experimental data.

Conclusion

To our understanding, this is the first study to have presented data describing the events that occur at a molecular level when resveratrol binds to the ZIKV NS3 helicase enzyme. Since resveratrol is a competitive inhibitor of ATP and stably binds to the ATPase pocket in the helicase, we can speculate that inhibition of ZIKV by resveratrol at an organism level may render the enzyme 'powerless' and may even lead to resveratrol being a potent inhibitor of multiple viruses including other *flaviviruses* such as DENV, West Nile virus and Japanese encephalitis virus. Resveratrol is also a natural antioxidant; therefore, its use as a multipurpose antiviral implies safety, easy availability and accessibility, and cost-effectiveness, particularly in rural communities.

This material refines the knowledge surrounding resveratrol inhibition of the ZIKV NS3 helicase and will aid the search for anti-ZIKV drugs. Additional investigations are vital to substantiate the role of resveratrol in the treatment of ZIKV. Further, analysis will also include the interactions between resveratrol and other members of the *flavivirus* genus of viruses.

Summary points

- The Zika virus (ZIKV) continues to affect pregnant women and their infants without US FDA-approved vaccines or treatments.
- There is still very much to learn about ZIKV before we can effectively treat it.
- Understanding the molecular dynamics behind potential organism level inhibition could help prevent future resistance of ZIKV to drugs.
- Hence, we studied the molecular dynamics of the unbound and resveratrol-bound helicase for 200 ns.
- Molecular dynamic simulations and postdynamic analyses allowed us to pinpoint the precise residues and interactions that are key in the binding of resveratrol to the helicase.
- The movements of loops surrounding RNA and inhibitor binding sites also regulate binding and replication; therefore, we analyzed the shifts in loops surrounding the ATPase pocket and RNA-binding site.
- The druglikeness of resveratrol was also established using computational tools, which led to the conclusion that resveratrol follows all of Lipinski's rules and can pass the blood-brain barrier, making it suitable for the treatment of ZIKV.
- This material demonstrates the structural dynamics of the ZIKV NS3 helicase upon resveratrol binding, which will advance anti-ZIKV drug development.

Financial & competing interests disclosure

This work was financially supported by the German Academic Exchange Service (DAAD) and the National Research Foundation (NRF). Computational support was provided by the Centre for High Performance Computing (CHPC, <http://www.chpc.ac.za>). The authors have no other relevant affiliations or financial involvement with any organization or entity with a financial interest in or financial conflict with the subject matter or materials discussed in the manuscript apart from those disclosed.

No writing assistance was utilized in the production of this manuscript.

Supplementary data

To view the supplementary data that accompany this paper please visit the journal website at: www.futuremedicine.com/doi/full/10.2217/fvl-2018-0170

References

1. Ghosh D. Zika virus – a global emergency. *Curr. Sci.* 114(4), 725 (2018).
2. Dhama K, Karthik K, Tiwari R *et al.* Zika virus/Zika fever: a comprehensive update. *J. Exp. Biol. Agric. Sci.* 6(1), 1–31 (2018).
3. Nandy A, Basak SC. The epidemic that shook the world – the Zika virus rampage. *Explor. Res. Hypothesis Med.* 2(3), 43–56 (2017).
4. Kindhauser MK, Allen T, Frank V, Santhana RS, Dye C. Zika: the origin and spread of a mosquito-borne virus. *Bull. World Health Organ.* 94(9), 675–686 (2016).
5. Ryan SJ, Carlson CJ, Mordecai EA, Johnson LR. Global expansion and redistribution of Aedes-borne virus transmission risk with climate change. *bioRxiv* doi:<https://doi.org/10.1101/172221> (2017) (Epub ahead of print).
6. Jain R, Coloma J, García-Sastre A, Aggarwal AK. Structure of the NS3 helicase from Zika virus. *Nat. Struct. Mol. Biol.* 23(8), 752–754 (2016).
7. Mishra PM, Uversky VN, Giri R. Molecular recognition features in Zika virus proteome. *J. Mol. Biol.* 430(16), 2372–2388 (2017).
8. Wang A, Thurmond S, Islas L, Hui K, Hai R. Zika virus genome biology and molecular pathogenesis. *Emerg. Microbes Infect.* 6(3), e13 (2017).
9. Tian H, Ji X, Yang X *et al.* The crystal structure of Zika virus helicase: basis for antiviral drug design. *Protein Cell* 7(6), 450–454 (2016).
10. Tian H, Ji X, Yang X *et al.* Structural basis of Zika virus helicase in recognizing its substrates. *Protein Cell* 7(8), 562–570 (2016).
11. Devnarain N, Soliman MES. A panoptic uncovering of the dynamical evolution of the Zika virus NS5 methyltransferase binding site loops – zeroing in on the molecular landscape. *Chem. Biol. Drug Des.* 92 (5), 1838–1850 (2018).
12. Pan A, Saw WG, Manimekalai MSS *et al.* Structural features of NS3 of Dengue virus serotypes 2 and 4 in solution and insight into RNA binding and the inhibitory role of quercetin. *Acta Crystallogr. D Struct. Biol.* 73(5), 402–419 (2017).
13. Lee JH, Wendorff TJ, Berger JM. Resveratrol: a novel type of topoisomerase II inhibitor. *J. Biol. Chem.* 292(51), 21011–21022 (2017).
14. Abba Y, Hassim H, Hamzah H, Noordin MM. Antiviral activity of resveratrol against human and animal viruses. *Adv. Virol.* 2015, 1–7 (2015).
15. Saw WG, Pan A, Subramanian Manimekalai MS, Grüber G. Structural features of Zika virus non-structural proteins 3 and –5 and its individual domains in solution as well as insights into NS3 inhibition. *Antiviral Res.* 141(1), 73–90 (2017).
16. Fatima K, Mathew S, Suhail M *et al.* Docking studies of Pakistani HCV NS3 helicase: a possible antiviral drug target. *PLoS ONE* 9(9), 1–12 (2014).
17. Campagna M, Rivas C. Antiviral activity of resveratrol. *Biochem. Soc. Trans.* 38(1), 50–53 (2010).
18. Hausenblas HA, Schoulda JA, Smoliga JM. Resveratrol treatment as an adjunct to pharmacological management in type 2 diabetes mellitus-systematic review and meta-analysis. *Mol. Nutr. Food Res.* 59(1), 147–159 (2015).
19. Xia N, Daiber A, Förstermann U, Li H. Antioxidant effects of resveratrol in the cardiovascular system. *Br. J. Pharmacol.* 174(12), 1633–1646 (2017).
20. Bastianetto S, Ménard C, Quirion R. Neuroprotective action of resveratrol. *Biochim. Biophys. Acta Mol. Basis Dis.* 1852(6), 1195–1201 (2015).
21. Borriello A. Resveratrol in cancer prevention and treatment: focusing on molecular targets and mechanism of action. *Proceedings* 1(10), 976 (2017).
22. Luo D, Vasudevan SG, Lescar J. The flavivirus NS2B-NS3 protease-helicase as a target for antiviral drug development. *Antiviral Res.* 118(1), 148–158 (2015).
23. Lei J, Hansen G, Nitsche C, Klein CD, Zhang L, Hilgenfeld R. Crystal structure of Zika virus NS2B-NS3 protease in complex with a boronate inhibitor. *Science* 353(6298), 503–505 (2016).
24. Rose PW, Prlić A, Altunkaya A *et al.* The RCSB protein data bank: integrative view of protein, gene and 3D structural information. *Nucleic Acids Res.* 45(D1), D271–D281 (2016).

25. Tian H, Ji X, Yang X *et al.* The crystal structure of Zika virus helicase: basis for antiviral drug design. *Protein Cell* 7(6), 450–454 (2016).
26. Kim S, Thiessen PA, Bolton E *et al.* PubChem substance and compound databases. *Nucleic Acids Res.* 44(D1), D1202–D1213 (2016).
27. Yang Z, Lasker K, Schneidman-Duhovny D *et al.* UCSF Chimera, MODELLER, and IMP: an integrated modeling system. *J. Struct. Biol.* 179(3), 269–278 (2012).
28. de Ruyck J, Brysbaert G, Blossey R, Lensink MF. Molecular docking as a popular tool in drug design, an in silico travel. *Adv. Appl. Bioinforma. Chem.* 9(1), 1–11 (2016).
29. Trott O, Olson AJ. AutoDock Vina: improving the speed and accuracy of docking with a new scoring function, efficient optimization and multithreading. *J. Comput. Chem.* 31(1), 445–461 (2010).
30. Alonso H, Bliznyuk AA, Gready JE. Combining docking and molecular dynamic simulations in drug design. *Med. Res. Rev.* 26(5), 531–568 (2006).
31. Munir A, Azam S, Mehmood A. Structure-based pharmacophore modeling, virtual screening and molecular docking for the treatment of ESR1 mutations in breast cancer. *Drug Des. Open Access* 5(137), 1–10 (2016).
32. Meng X-Y, Zhang H-X, Mezei M, Cui M. Molecular Docking: a powerful approach for structure-based drug discovery. *Curr. Comput. Drug Des.* 7(2), 146–157 (2011).
33. Case DA, Cheatham TE, Darden T *et al.* The amber biomolecular simulation programs. *J. Comput. Chem.* 26(16), 1668–1688 (2005).
34. Salomon-Ferrer R, Götz AW, Poole D, Le Grand S, Walker RC. Routine microsecond molecular dynamics simulations with AMBER on GPUs. 2. Explicit solvent particle Mesh Ewald. *J. Chem. Theory Comput.* 9(9), 3878–3888 (2013).
35. Sprenger KG, Jaeger VW, Pfaendtner J. The general AMBER force field (GAFF) can accurately predict thermodynamic and transport properties of many ionic liquids. *J. Phys. Chem. B* 119(18), 5882–5895 (2015).
36. Miner JJ, Cao B, Govero J *et al.* Zika virus infection during pregnancy in mice causes placental damage and fetal demise. *Cell* 165(5), 1081–1091 (2016).
37. Wang J, Wang W, Kollman Pa, Case Da. Antechamber, an accessory software package for molecular mechanical calculations. *J. Chem. Inf. Comput. Sci.* 222(2), U403 (2001).
38. Woods RJ, Chappelle R. Restrained electrostatic potential atomic partial charges for condensed-phase simulations of carbohydrates. *Theochem* 527(1), 149–156 (2000).
39. Genheden S, Ryde U. The MM/PBSA and MM/GBSA methods to estimate ligand-binding affinities. *Expert Opin. Drug Discov.* 10(5), 449–461 (2015).
40. Vanommeslaeghe K, Guvench O, Mackerell AD. Molecular mechanics. *Curr. Pharm. Des.* 20(20), 3281–3292 (2014).
41. Wang H, Guo C, Chen BZ, Ji M. Computational study on the drug resistance mechanism of HCV NS5B RNA-dependent RNA polymerase mutants V494I, V494A, M426A, and M423T to fildesovir. *Antiviral Res.* 113(1), 79–92 (2015).
42. Cele FN, Ramesh M, Soliman MES. Per-residue energy decomposition pharmacophore model to enhance virtual screening in drug discovery: a study for identification of reverse transcriptase inhibitors as potential anti-HIV agents. *Drug Des. Devel. Ther.* 10, 1365–1377 (2016).
43. Daina A, Michielin O, Zoete V. SwissADME: a free web tool to evaluate pharmacokinetics, drug-likeness and medicinal chemistry friendliness of small molecules. *Sci. Rep.* 7, 42717 (2017).
44. Devnarain N, Ramharack P, Soliman ME. Brain grants permission of access to Zika virus but denies entry to drugs: a molecular modeling perspective to infiltrate the boundary. *RSC Adv.* 7(75), 47416–47424 (2017).
45. Lipinski CA. Lead- and drug-like compounds: the rule-of-five revolution. *Drug Discov. Today Technol.* 1(4), 337–341 (2004).